Development a Novel Powered Orthosis System for Hemiplegia Patients

A DISSERTATION SUBMITTED TO THE
GRADUATE SCHOOL OF ENGINEERING AND SCIENCE OF
SHIBAURA INSTITUTE OF TECHNOLOGY

by

NGUYEN THANH TRUNG

IN PARTIAL FULFILLMENT OF THE REQUIREMENTS
FOR THE DEGREE OF

DOCTOR OF ENGINEERING

SEPTEMBER 2015

To my parents for their inspiration and motivation to meet my dreams.

To my wife, Bui Van Anh. Thanks to her love and sacrifice I can keep my mind on my research.

Acknowledgments

First of all, I would like to express my sincere gratitude to my supervisor, Professor Takashi Komeda for his valuable guidance and support throughout my research, as well as my life in Japan. I have learned from him many things related to my research direction. I have also learned from him many other things, especially the professional attitude on working, working plan. Thanks to his kindly support and many instructive comments on the dissertation process, I could complete the disseratation.

Next, I would like to thank all my committee members, Prof. Shinichirou Yamamoto, Prof. Akihiko Hanafusa, Prof. Kazuhisa Ito, and Prof. Tasuku Miyoshi for participating in my defense and their valuable comments. Their suggestions and discussions during my presentations help me to significantly improve my reseach. I aslo would like to thank Mr.Hung, a member of Komeda lab, for his help during my research and experiments.

I would also like to extend my gratitude to the faculty and staff members of Shibaura Institute of Technology for their support. Thanks to all the Komeda Lab members who are very kind to me, I strongly appreciate their helps for my life in Japan.

Finally, I would like to thank all my friends including academic and non-academic ones, who have always been by my side to overcome even the most difficult time. Thank you all for your friendship and

encouragement.

Saitama, September 2, 2015

NGUYEN THANH TRUNG

Abstract

Patients with neurological disorders, such as stroke survivors, can be treated by physical rehabilitation to regain motor control and function. Normally, conventional therapy techniques are labor intensive and non-standardized. This is especially true in gait rehabilitation. In order to overcome the burden for therapists, robotic is now used more and more in a repeatable and measurable fashion.

The focus of this dissertation is ankle rehabilitation for hemiplegia patients who has a half normal body and a half weak body. The Ankle Foot Orthosis (AFO) is attached on the weak lower limb to support it during rehabilitation. In reality, There are number of researches developing the AFOs to support ankle to prevent: foot drop or foot slag, and to control dorsiflexion and plantarflexion. Some of them could control both dorsiflexion and plantarflexion, however they can not generate the propulsion force during terminal stance phase in order to support weak ankle during this time. In this dissertation I propose a novel AFO based on the idea of Center of Pressure (COP) movement during locomotion. Some contributions of the thesis are mentioned as following:

Firstly, I analyzed the movement of COP during human locomotion and then proposed the idea to attack force to two most important points of the COP spline in order to control the phases of walking. The process of mechanical design was presented. In each of mechanism of the system, there are some solutions suggested and analyzed, and then chosen. The possibility of the novel AFO was also proven.

Secondly, the controlling process for the AFO was implemented. These processes included phases detection, controlling solenoids, controlling

ankle joint in case of without wearing and wearing the system on human body.

Besides, relating to DC Servomotor I proposed a method to automatically tune the Fuzzy Logic Controller. The method used Genetic Algorithm (GA) with new method of encoding for membership function as well as an algorithm to automatically tune rule base of the Fuzzy Logic Controller (FLC). The experiment proved the efficiency of the method.

Contents

List of Figures

List of Tables

Acronyms

AFO Ankle Foot Orthosis. iv, 2–4, 19–21, 26–28, 30, 32, 35, 36, 39, 40, 43, 44, 49, 53, 70

BWS Body Weight Support. 35, 70

CD Controlled Dorsiflexion. 27, 43, 52

COM Center of Mass. 13

COP Center of Pressure. iv, 13, 19–21, 51, 52, 55, 70, 71

CP Controlled Plantarflexion. 27, 36, 38, 43, 52

DOF Degree of Freedom. 20, 21

FLC Fuzzy Logic Controller. v, 4, 49, 50, 57, 58, 60, 71

FLCGA Fuzzy Logic Control Genetic Algorithm. 58, 65

GA Genetic Algorithm. v, 6, 57, 59, 60

GC Gait Cycle. 13

GRF Ground Reaction Force. 19, 43, 44

IST Initial Stance. 14, 43, 69, 71

ISW Initial Swing. 14

LR Load Response. 22, 27

MF Membership Functions. 57

MSM Motion Splitting Mechanism. 22, 23, 31, 32

MST Middle Stance. 14, 22, 27

MSW Middle Swing. 14

OG On Ground. 43

POT potentiometer. 46, 47, 50

PP Powered Plantarflexion. 27, 29, 43, 52, 69

SCI Spinal Cord Injury. 1, 16

SCM State Changing Mechanism. 23, 24, 26, 40, 45, 69, 71

SEA Series Elastic Actuator. 3, 4

SW Swing Phase. 27, 29

TST Terminal Stance. 14, 42, 43, 69

TSW Terminal Swing. 14

Chapter 1

Introduction

Standing or walking is something people take it for granted, however, every year thousands of people are prevented from doing it. In a physical and psychological perspective, gait disabilities have a negative impact on people's life, compromising their ability to work, engage in social and leisure activities, or in the worst cases, participate in activities associated with an independent lifestyle [48]. Thus, it is expectable that affected people will tend to become sedentary, fact that will further affect their health condition. Gait disabilities are a serious problem that affects millions of people around the world, and although the existence of many walking aids that directly benefit the affected person, it is clear that with current technology greater benefits are possible to achieve in some pathologies.

Facing various gait disabilities, several approaches of active systems, such as assist people actively with robotic solutions, have been made with the purpose of improve patient's quality of life. It is in this context that the concept of wearable robots has emerged, where the robotic counterparts of current orthoses are referred to as robotic exoskeletons [43]. The function of the exoskeleton has a wide range of applicability, since it can be applied not only to restore and rehabilitate handicapped functions of the body, but also on the improvement and enhancement of normal human body performance. Apply exoskeletons to restore the full walking capacity of a Spinal Cord Injury (SCI) patient is one of the most ambitious objectives that researchers try to achieve.

An AFO is an orthopedic device that can be prescribed to support the ankle function during walking. In general, an orthosis is defined as an externally applied device used to modify the structural or functional characteristics of the neuromuscular system [21]. An AFO is an orthosis that is specifically designed to modify the functioning of the ankle and/or the foot. AFOs are produced in various forms, composed of different materials, and prescribed with a wide variety of aims.

1.1 Motivation

There are millions of individuals who are suffering from some kind of gait disability. Many of these people require either rehabilitation or prosthetic devices. Normally, rehabilitation methods by therapists are very labor intensive. Multiple therapists are often required to perform strenuous physical tasks. There is also a high degree of variability and subjectivity in the current methods.

Robotic therapy has proven effective in rehabilitation. Usage of robotic devices in gait rehabilitation could provide an accurate, repeatable method for assisting lower limb movement. It would also provide an accurate way of recording data for gait analysis and an objective measure of rehabilitation.

The motivation of this research is to improve the gait rehabilitation by using robotic technology. The scope of this dissertation is to design a novel system that would support some or all of the patients' weight while the robotic device assist in lower limb movement, especially for the hemiplegia patient who has a half weak body and a half strong body. The novel AFO device could be used on a treadmill with body weight support system or as an ambulatory device on level platform.

1.2 Literature review

The AFO can be classified into two main groups as either passive, where the human subject transfer forces to move ankle articulation, or active, where ac-

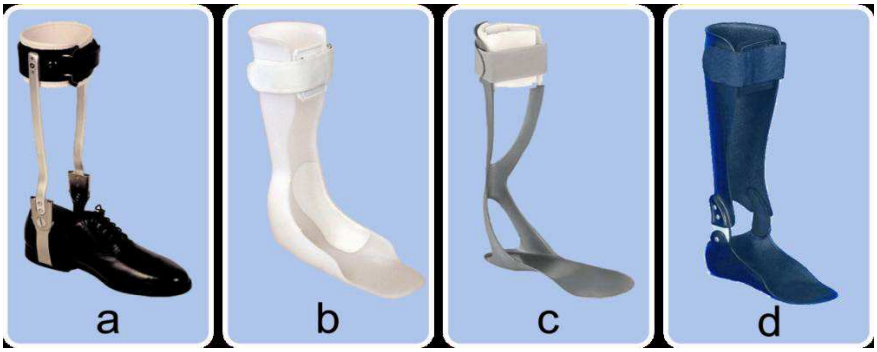

Figure 1.1: Ankle-foot orthosis: (a) Conventional AFO, comprised of a metal frame with leather straps, attached to a shoe, (b) Standard Plastic AFO, (c) prolite Carbon AFO, (d) Plastic Articulated AFO

tuators generate force to control the system. The passive AFOs can be further subdivided by material into metal and leather, thermoplastic composite, and hybrid systems [46], [47]. The Figure 1.1 are some of popular Ankle Foot Orthosis braces that covers the foot, spans the ankle joint an cover the lower limb. The passive systems [5], [30], [1], [36] have some advantages of light weight, economy, being able to provide assistance stiffness from a few Newton meters up to 20 N.m of resistive torque over 30° range of motion. Besides, there are also some limitations for the using of a purely passive device. The passive elements improve gait deficiencies by controlling motion. The control of the passive AFO elements, however, depends on the activation of springs, valves, or switches in open-loop as the individual walks [29]. This control method has limited robustness and does not adapt to changing walking conditions. The other limitation is impossible to provide propulsive force during stance phase.

The active AFOs take advantages of using external actuators to solve both of these limitations. These devices use different external force sources, such as magneto rheological (MR) damper [24], Series Elastic Actuator (SEA) [53], McKibben pneumatic actuator [17] and etc., to control the ankle articulation through the different mechanisms. The system as in Figure 1.2b which was developed by University of Michigan use artificial pneumatic muscles endowing a carbon fiber shank section. By increasing air pressure, the pneumatic muscles (McKibbon muscles) start developing tension and become shortened, allowing the powered

Figure 1.2: (a)Active Ankle-Foot orthosis developed at Massachusetts Institute of Technology, (b) Powered Exoskeleton developed at the University of Michigan, (c) Adjustable robotic tendon robot concept

exoskeleton to provide plantar flexor movement, i.e., artificial soleus muscle activation. Designed for rehabilitation purpose, this system has a mass of approximately 1.1 kg. Other identical system was developed by the same laboratory, which provided both dorsiflexion and plantar flexion control of the ankle joint. Although these active AFOs are able to overcome limitations of the passive one. There are still some points needed to be improved. For the AFO systems using MR damper, they are capable of controlling foot motion, but they cannot generate torque at the ankle joint for use in push-off. To overcome this drawback, the Biomechatronics Group at MIT as Figure 1.2a, Cambridge, U.S uses SEA [27] to develop a new AFO that can assist patients with both plantarflexor and dosirflexor weakness. Nevertheless, the system still did not fully support when push-off phase from mid-stance to push-off. It only minimized the impedance of the AFO to allow full plantarflexor movement. In addition, there was still the impact of body weight on the weaken foot during stance phase of the locomotion.

1.3 Objective

The objective of this work is to develop a novel and autonomous computational system that is capable of providing ankle movement for hemiplegia patient during

rehabilitation process. The process of design for the AFO will be presented and discussed from idea to the 3D model. After that, a completed, real system will be produced and make some experiment to evaluate.

The novel AFO will be an active one, that could be deployed sensing devices that identify the different phases of the gait. An actuator provide ankle movement based on the phase during gait cycle.

Besides, with some systems that are difficult to determine the transfer function or non-linear systems, Fuzzy Logic Controller (FLC) is one of the methods normally used to control. The problem, however, is that the membership functions as well as the rules base of the FLC are determined based on the knowledge of operators about the system. In order to reduce this dependence, this work also develop one tuning method using GA with a novel encoding to reduce the tuning process.

1.4 Structure of this dissertation

This dissertation is structured as following, so that the readers could follow the steps taken in the design process of the AFO:

- Chapter 1 defines and describes the necessary of using robotic technology in the rehabilitaion process. After that, the summary of AFO systems is also presented.
- Chapter 2 is Biomechanical aspects involved in the ankle joint movement, the current problems and idea to develop the new AFO.
- Chapter 3 describes the process of developing the novel AFO that goes from idea to the complete 3D model system. The final model consists of some mechanisms which have different missions during working. Each mechanism is analyzed and chosen from different suggestions. After design, the system was produced and assembled.

- Chapter 4 shows the control aspects that include phases detection, solenoids controlling and actuator controlling.
- Chapter 5 expresses the some experiment results of AFO system in two main cases of hanging on a frame (without load) and wearing the system on a normal individual. Besides, A novel optimization method to tune controller of DC Servo motor was also suggested. The controller that was focused is Fuzzy Logic Controller (FLC), which is suitable for the unidentifiable mathematics model or nonlinear system.
- Chapter 6 describes some conclusions and discussions for the novel AFO system as well as the proposed tuning method for FLC. Some suggestions for future works are also presented.

1.5 Contribution of this dissertation

- Firstly, I analyzed the movement of CoP during human locomotion and then proposed the idea to attack two most important points of the CoP spline in order to control the ankle based on the phases of walking. The process of mechanical design was presented. In each of mechanism of the system, there are some solutions suggested and analyzed, and then chosen. The possibility of the novel AFO was also proven.
- Secondly, the controlling process for the AFO was implemented. These processes included phases detection, controlling solenoids, controlling ankle joint in case of with and without wearing on human body.
- Besides, relating to DC Servomotor I proposed a method to automatically tune the Fuzzy Logic Controller. The method used GA with new method of encoding for membership function as well as an algorithm to automatically tune rule base of the FLC. The experiment proved the efficiency of the method.

Chapter 2

Ankle biomechanics and proposal idea

Biomechanics of human movement can be defined as the interdisciplinary field which describes, analyzes and assesses human movement [59]. Understanding human movement is essential when developing systems capable of assisting the human body, and such requires a close study of its anatomy and physiology. The study of this theme provides essential labels for musculoskeletal structures, joint motions, and function of the different structures [31].

Several key concepts are related with human gait, which is the most common of all human movements [60]. This chapter gives a general overview of the biomechanics involved in human gait, starting in section 2.1 with basic concepts of human anatomy and physiology, and focusing this theme for the ankle-foot orthosis in section 2.2. Human gait is characterized in section 2.3, where its kinematics and kinetics are firstly presented. These important variables are fundamental in the description of the gait cycle. To assist pathological gait, it is first necessary to understand its normal functioning. For that reason, section 2.4 presents the ankle function during gait and its most common pathologies that the devices presented in section 2.5 try to assist.

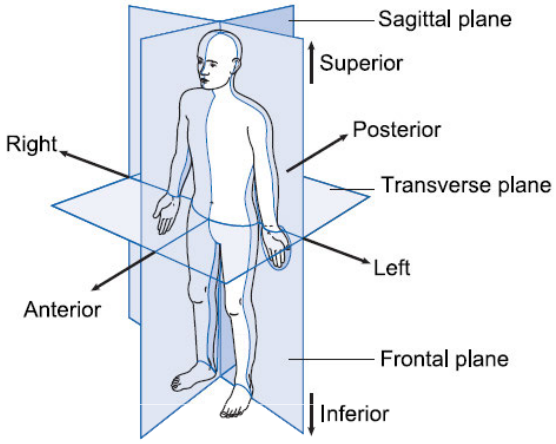

Figure 2.1: The anatomical position, with three reference planes and six fundamental directions with spatial coordinate system used for all data and analysis [58]

2.1 Basic Concepts of anatomy and physical related to gait

Knowledge of biomechanics must be combined with anatomy to accurately determine the musculoskeletal causes or how human movement is created. Anatomy familiarity also provides a common language of human body when communicating with kinesiology and medical professionals [31].

For a correct understanding and later description of human gait, it is necessary to define a reference anatomical position with respect to which reference planes, axis, and other major body movements. The anatomical terms describing the relationships between different parts of the body are based on this anatomical position, in which a person is standing upright, with the feet together and the arms by the side of the body, with the hand palms facing forward. This position, together with the three reference planes (sagittal, frontal and transverse), axis, and six fundamental directions is illustrated in Figure 2.1.

Specific terminology is also used to describe the major rotations of bones at the joints. Most joints can only move in one or two of the three considered planes. Focusing the lower limb system, several movements are possible. Movements in

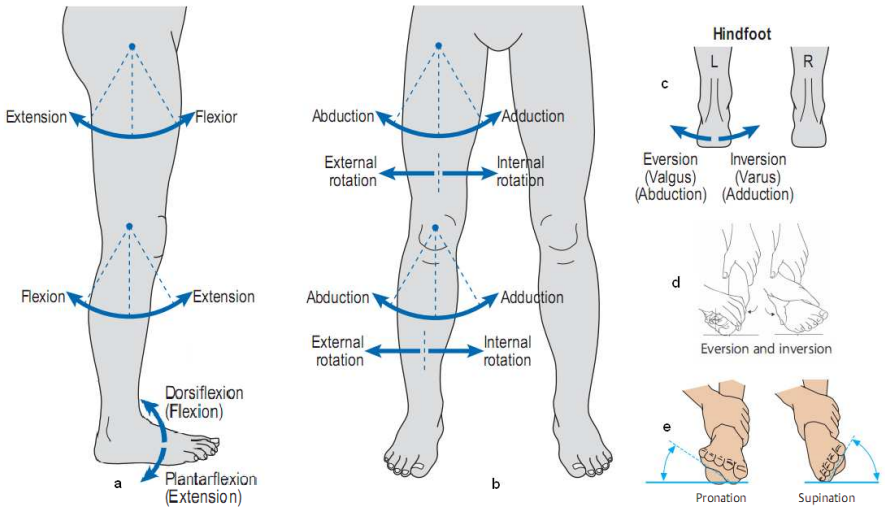

Figure 2.2: (a) Movements about the hip joint (above), knee joint (middle) and ankle joint (below) in sagittal plane [58], (b) Movements about the hip joint (above), knee joint (middle) in frontal and transverse planes [58], (c) Abduction and adduction of the foot [58], (d) Eversion and inversion of the foot [54], (e) Pronation and supination of the foot [20].

the sagittal plane are denominated by flexion and extension, with the exception for the ankle, where these are denominated as dorsiflexion and plantar flexion, respectively Figure 2.2a. Movements about frontal plane are called abduction and adduction, while internal and external rotation take place in the transverse plane Figure 2.2b,c [58]. Other specific movements on the foot are eversion and inversion 2.2d, and pronation and supination Figure 2.2e.

During gait, human body can be approximated by two functional units: passenger and locomotor as in Figure 2.3. In this approximation, the passenger unit is responsible for its own postural integrity, while the locomotor unit carries the body to the desired position. Focusing the locomotor unit during gait, several articulations (joints) are involved in the motion: lumbosacral, bilateral hip, knee, ankle, subtalar, and metatarsophalangeal [42].

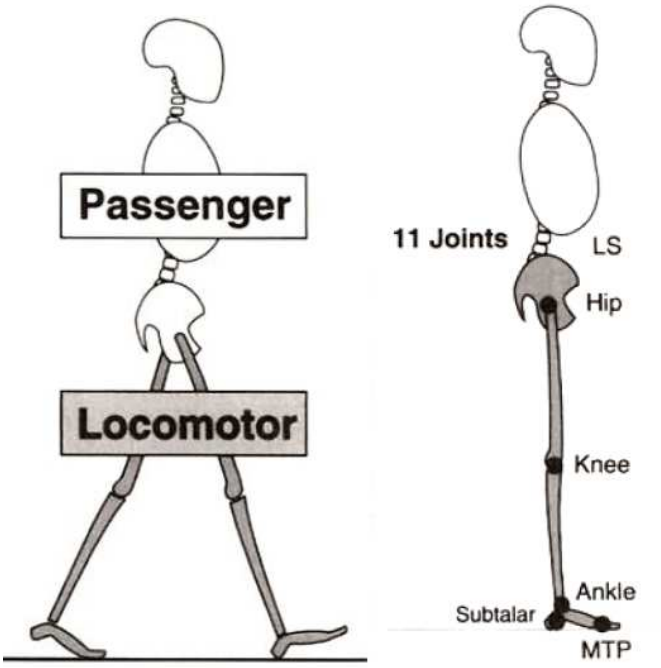

Figure 2.3: Functional division of the body. During walking, the locomotor unit transports the passive passenger unit. The locomotor unit includes the pelvis and both lower limbs, where several joints are involved (lumbosacral, hips, knees, ankles, subtalars, and metatarsal joint) [42].

2.2 Anatomy and physiology of Ankle foot

Leg and foot are part of the locomotor unit, more properly, the free lower limb. The free lower limb is connected to the pelvic girdle by the hip joint and consists of the thigh bone (femur), the leg (crus) including tibia and fibula, and the foot (pes), which includes the ankle (tarsus), metatarsals, and toes (digits) as in Figure 2.4a.

The foot and ankle joint is a complex structure, formed by several joints with different characteristics, that are involved in the motion occurring between the foot and the lower leg. This structure supports and propels the body forward and absorbs the forces of a step, while providing rotation for adaptations on uneven terrains. Foot can also be classified in three elements: forefoot (five metatarsal bones with the phalanges), midfoot (navicular, cuboid and three cuneiform), and

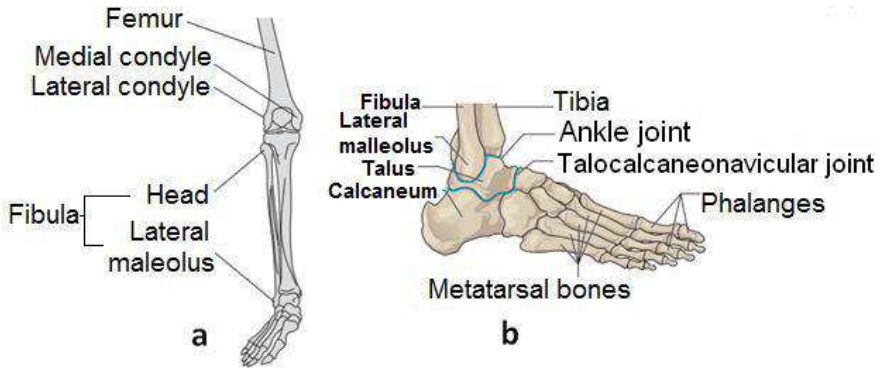

Figure 2.4: Bones and joints of the lower limbs (adapted from Whittle, 2007 p. 6), (b) Bones and joints of the right foot lateral view [20].

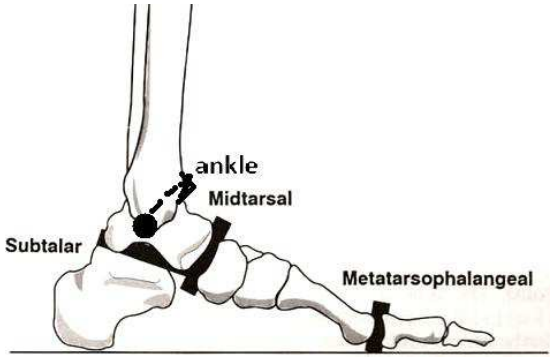

Figure 2.5: Foot and ankle joints with major functional significance during walking (black areas): talocrural, subtalar, midtarsal, and metatarsophalangeal [42].

hindfoot (calcaneus and talus bones).

Four major joints compose the foot and ankle joint complex shown in Figure 2.5: talocrural (true ankle joint), talocalcaneal (subtalar), transverse tarsal (midtarsal), and metatarsophalangeal [23]. The ankle joint is formed by the tibia, fibula and talus, and the movements at this joint are called dorsiflexion and plantar flexion. In the intertarsal joint, the talus articulates with the calcaneus and the 10 navicular bone. The In the subtalar joint, the talus articulates with the calcaneus. In the midtarsal joint, the ball-shaped head of the talus articulates with the calcaneus and the navicular bone. The movements in midtarsal joint are lateral movements, called supination and pronation [20].

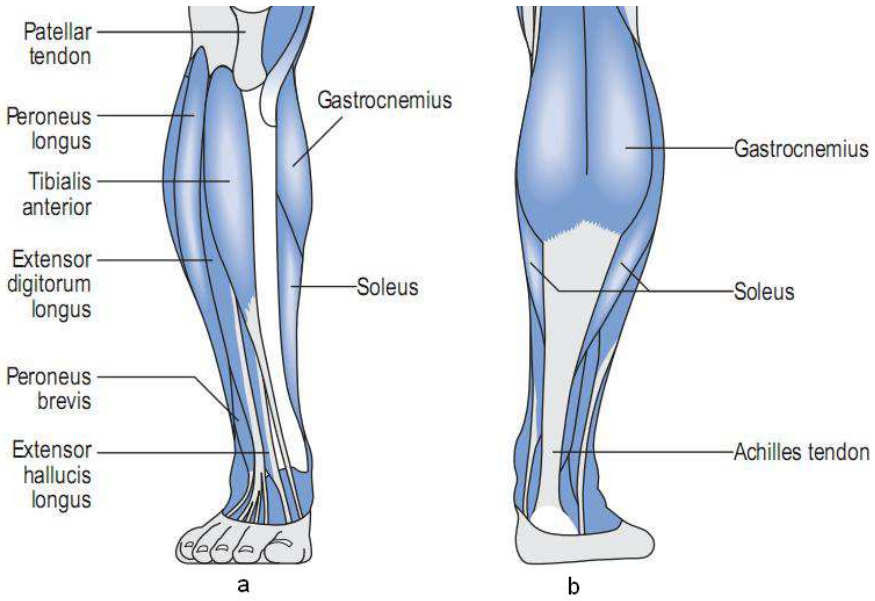

Figure 2.6: Muscles of leg: (a) Anterior view, (b) Posterior view [58].

Aiming for a simpler computational model of the locomotor unit, it was considered an accepted approach of quantifying foot and ankle kinematics during gait as the representation of the entire foot as a single rigid body, with a revolute ankle joint in the sagittal plane [23]. For the same reason, the lumbosacral articulation was considered to be fixed. This way, only movements taken place in sagittal plane are considered, disregarding the movements in the others planes as in Fogire 2.2a.

Muscle forces are the main internal motors and brakes for human movement. The torques created by skeletal muscles are coordinated with torques from external forces, providing the human motion of interest [31].

According to the theme of this dissertation, the muscles of major interest are the ones which provide movement through the ankle joint as in Figure 2.6. As the ankle joint moves in the sagittal plane, all the controlling muscles function are classified either as dorsiflexors or plantar flexors [42].

The anterior tibial group is responsible for the dorsiflexion and supination of the foot, being composed of four muscles: extensor hallucis longus, extensor digitorum longus, peroneus tertius, and tibialis anterior. The two former muscles

are inserted into the toes, which they extend. Peroneus tertius muscle is inserted into the tarsal bones, raising the foot on the lateral side. Tibialis anterior muscle is inserted into the tarsal bones, being the main dorsiflexor muscle and supinator of the foot, while the others muscles are weak dorsiflexors.

Foot plantar flexion is generally acted by a group of seven to eight muscles: soleus, gastrocnemius, tibialis posterior, flexor hallucis longus, flexor digitorum longus, peroneus longus, peroneus brevis, and sometimes the plantaris.

The strongest muscle group in plantar flexion, triceps surae, consists on superficial muscles from the calf, usually composed of two or three muscles, the soleus, the gastrocnemius, and sometimes the plantaris. They join to form the Achilles tendon, which is inserted into the calcaneal tubercle [20]. Five other muscles act as weak plantar flexors. The muscles on the lateral compartment of the calf, peronei longus and brevis, are primarily pronators. Flexor hallucis longus, flexor digitorum longus, and tibialis posterior are posterior calf muscles, assisting primarily as supinators [58].

2.3 Human gait

2.3.1 Kinematic of human gait

Kinematics is the term used in the description of human movement, disregarding the forces, either internal or external, that cause the movement. The evaluated variables are usually linear and angular displacements, velocities, and accelerations [59].

A complete description of spatial coordinate system and its conventions is fundamental when discussing kinematic variables as in Figure 2.7a. Limb angles in the spatial reference system are defined using counterclockwise from the horizontal as positive as in Figure 2.7b. Thus angular velocities and accelerations are also positive in a counterclockwise direction in the plane of movement, which is essential for consistent use in subsequent kinetic analyses. Convention for joint

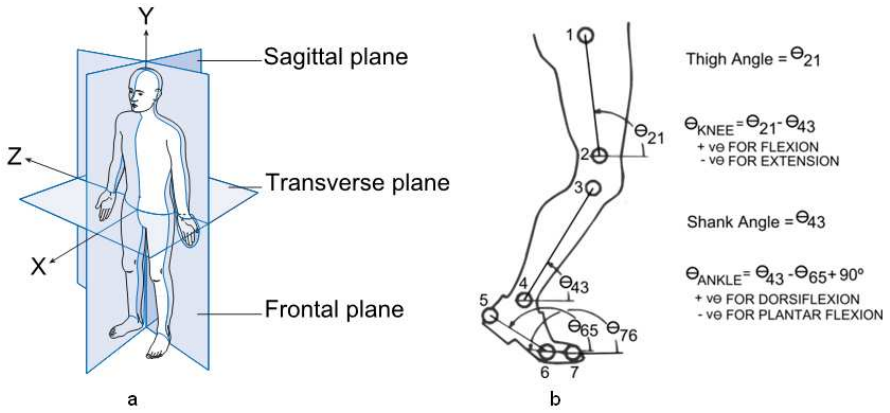

Figure 2.7: (a) Anatomical position with spatial coordinate system used for all data and analysis (adapted from [58]), (b) Marker location and limb and joint angles as defined using an established convention [59]

angles (which are relative) is subject to wide variation among researchers, having the necessity to clarify it [59]. Focusing the movements through the ankle joint, dorsiflexion causes positive ankle joint angles, while plantar flexion causes negative ankle joint angles as in Figure 2.10.

2.3.2 Kinetics of human gait

Kinetics in human gait represents the forces and torques that cause the motion of the body [23], where both internal and external forces are included. Internal forces come from muscle activity, ligaments or friction in the muscles and forces, while external forces come from the ground or from external loads [59].

The future of biomechanics lies in kinetic analyses, since the information acquired allows making definitive assessments and interpretations [59], which are important for the development of systems and methods for assisting pathological gaits.

Comparatively to kinematics, kinetics is more difficult to evaluate, since there are many combinations of muscle forces that can result in the same movement pattern [60], and the measurements cannot be directly observed [48]. The calculation of different variables such as intersegmental moments, work, mechanical

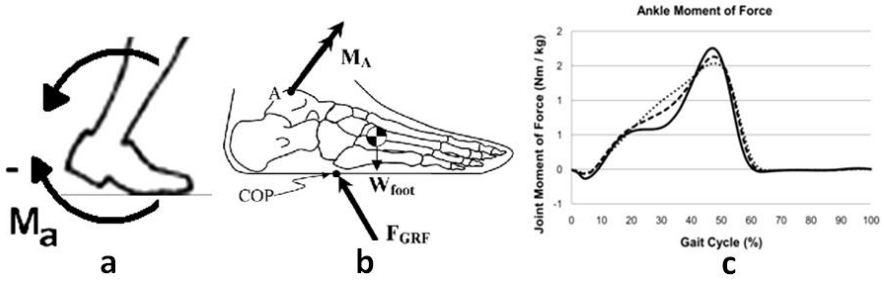

Figure 2.8: (a) Biomechanical convention for moments of force (adapted from [59]), (b) Schematic of the lower leg during gait - free body diagram of the foot showing the ankle moment, weight of the foot (W_{foot}), and ground reaction force (F_{GRF}) [48], (c) Ankle moment of force per body mass during a gait cycle in normal cadence [60]

energy, and power, implies the use of Newton's laws [55] and the law of conservation of energy [55], in order to interpret what is happening at each phase of the gait [60].

In this work, the main focus about kinetic data regards to joint moments. The standard convention for moments of force in the plane of progression is shown in Figure 2.8a. Counterclockwise moments are positive, calculated at the proximal end of each segment, while clockwise moments are negative. Thus, all moments of force in this work are reported in this basis.

Focusing the ankle moment of force, dorsiflexion causes negative moments at the foot, while plantarflexion causes positive moments. In normal gait, the joint angles do not reach their extreme limits, resulting that the net moment is the result of muscle forces only. Focusing the kinetics through the ankle joint, the free body diagram presented in Figure 2.8b exhibits the considered forces applied to the foot during the gait cycle. Thus, the moment of force acting through ankle joint,M_a , becomes

$$M_a = J_a\alpha_a - r_{COM}XW_{foot} - r_{COP}XF_{GRF} \tag{2.1}$$

where J_a is the ankle rotational inertia due to the mass of the foot, α_a the ankle angular acceleration, r_{COM} and r_{COP} the position vectors of the Center of

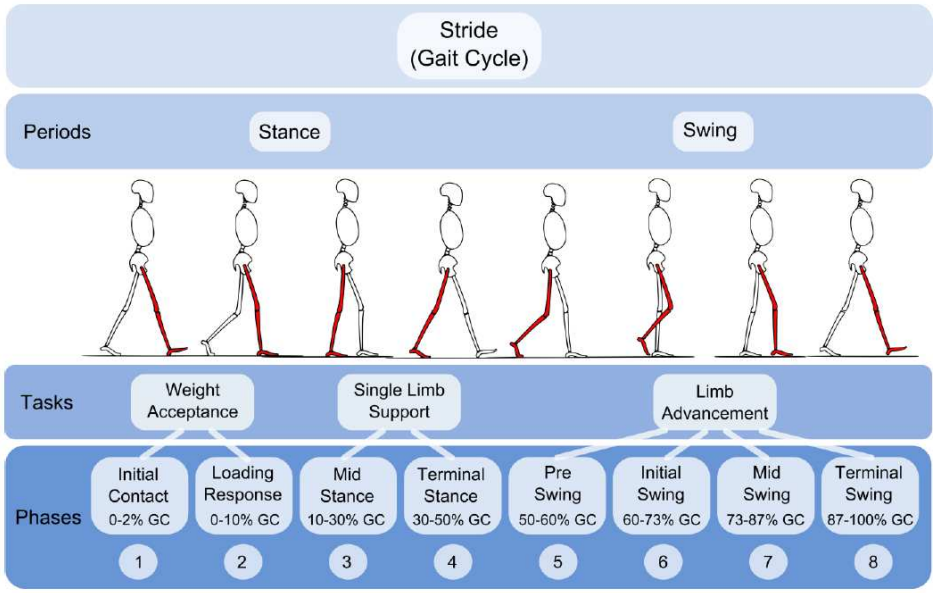

Figure 2.9: Divisions of the gait cycle. Adapted from [42], [48]

Mass (COM) and Center of Pressure relative to ankle joint center, respectively. Generally, the ground reaction forces and the center of pressure, which varies in time, are measured using a force transducer.

2.3.3 Gait cycle

Walking uses a repetitious sequence of limb motions to move the body forward while simultaneously maintaining stance stability. As the body moves forward, one limb serves as a mobile source of support while the other limb advances itself to a new support site. Then the limbs reverse their roles. For the transfer of body weight from one limb to the other, both feet are in contact with the ground. This series of events is repeated by each limb with reciprocal timing until the person's destination is reached. A single sequence of these functions by one limb is called a Gait Cycle (GC) [42].

In gait analysis, the basic unit is the interval between identical positions, i.e. a gait cycle. A step is taken to mean the period of motion of the limb from one initial contact till the next initial contact of the same foot. The gait cycle is

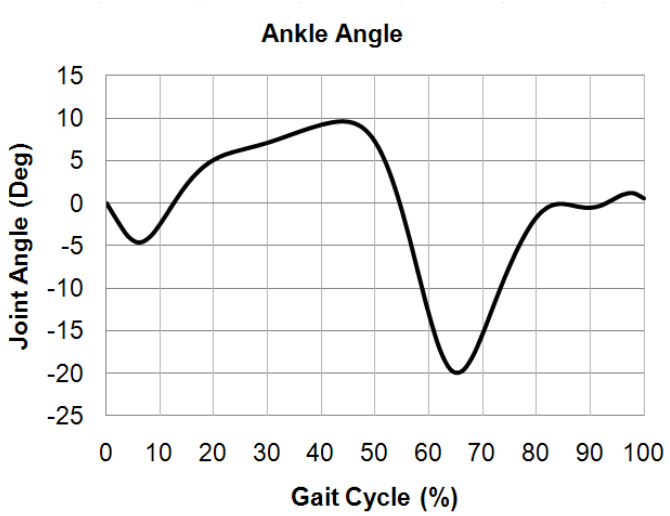

Figure 2.10: Ankle joint angles during a gait cycle in natural cadence [59]

characterized by timing and length [54]. Unfortunately, the nomenclature used to describe the gait cycle varies considerably from one publication to another. The present work attempts to use terms which will be understood by most people working in the field as in Figure 2.9.

The gait cycle can be divided into two periods (phases). First, the stance period /phase, occurs when the foot is in contact with the ground, and the second, the swing period /phase, occurs when the foot is in the air [48]. During walking at a comfortable pace, 60% of the cycle is in the stance period and 40% in the swing period [54]. However, this varies with the walking speed, where the swing period becomes proportionately longer and the stance period shorter as speed increases. The final disappearance of the double support marks the transition from walking to running [58].

Stance period can be subdivided into five phases known as: (1) initial contact, (2) Loading Response (LR), (3) mid stance, (4) terminal stance, and (5) pre-swing. However, we can summarize them into three main sub-phase: Initial Stance (IST), Middle Stance (MST) and Terminal Stance (TST). In addition, swing period into three phases: (6) Initial Swing (ISW), (7) Middle Swing (MSW), and (8) Terminal Swing (TSW).

Considering the five sub-phases of stance period, the first phase, initial con-

tact, begins when the foot just touches the ground. Another term for the onset of stance customarily has been called heel strike. Yet, the heel of a paralytic patient may never contact the ground or do so much later in the gait cycle [42]. The second sub-phase, loading response, is a time of double limb support when both feet are on the ground. During this phase, the limb accepts the weight of the body. Loading response ends when the opposite foot is lifted for swing.

Mid sub-stance is the phase when the center of gravity moves over the foot and the limb fully supports the weight of the body. The fourth sub-phase, terminal stance, is characterized by heel rise and continuous dorsiflexion, while the other foot strikes the ground. The last sub-phase of stance is pre swing, another time of double limb support, when the foot is about to become airborne and the opposite limb progressively accepts more weight.

The last three sub-phases in swing period starts with the initial swing sub-phase. This sub-phase begins when the foot leaves the ground and continues as the knee flexes. Mid swing sub-phase begins with the knee in maximum flexion and ends when the leg is perpendicular to the ground. The last sub-phase, terminal swing, begins with the leg perpendicular to the ground and ends when the foot contacts the ground again [48].

2.3.4 Ankle function and common pathologies

During a gait cycle, the foot and ankle joint are subject to several forces and movements, so the body movement occurs. The ankle movement is crucial to provide correct absorption of forces and limb advancement. Aiming for a system capable of assisting patients with pathological gait, it is first necessary to understand normal gait, since this provides the standard against which the gait of a patient can judged.

At the time of initial contact, the ankle is usually close to its neutral position. With tibia sloping backwards and the foot sloping upward, only the heel contacts the ground. Activated since swing, tibialis anterior maintains the foot dorsiflexed, in preparation for the controlled plantar flexion after initial contact. Loading response phase involves plantar flexion at the ankle caused by external forces at

the heel, which is controlled by the tibialis anterior muscle. This movement is accompanied by internal rotation of the tibia, rolling the body weight forward on the heel, and bringing the forefoot onto the ground. In mid stance, the direction of ankle motion changes to dorsiflexion, as the tibia moves over the stationary foot. Tibialis anterior ceases to contract, while the contraction of the triceps surae begins. Terminal stance is characterized by forward rotation of the tibia about the ankle joint, with the forefoot remaining flat on the ground and the heel rise. Peak ankle dorsiflexion is reached around the final of terminal stance, with triceps surae initially maintaining the ankle angle, while the knee flexes, to later move into plantar flexion. During pre swing, the ankle moves into plantar flexion due to concentric contraction of the triceps surae. Peak ankle angle for plantar flexion occurs just after initial swing. Triceps surae ceases and tibialis anterior begins to contract, with the ankle movement from plantar flexion to dorsiflexion continuing during mid swing. Nevertheless, this contraction is much smaller than the required at the foot lowering after initial contact. In the last phase, terminal swing, ankle position turns close to neutral position. Tibialis anterior continues to contract, holding the ankle in position, but its activity usually increases prior to initial contact, anticipating the greater contraction which will be needed during the loading response [58]. A normal ankle movement during a gait cycle is presented in Figure 2.9.

A large number of diseases or accidents affect the neuromuscular and musculoskeletal systems, which may lead to disorders in the ankle. Among the most important are: Cerebral palsy, Parkinsonism, Muscular dystrophy, Osteoarthritis, Rheumatoid arthritis, Stroke, Head injury, SCI, and Multiple sclerosis [58]. Even with the existence of many walking aids to benefit a person affected by any of these conditions, it is clear that greater benefits are possible in some pathologies than others.

A possible classification of all functional errors at the ankle can be by either considering the existence of excessive dorsiflexion (inadequate plantar flexion), or excessive plantar flexion (inadequate dorsiflexion) [42]. In this work the focus will be placed in patients who have both functional errors, usually patients without motor control at the ankle joint, i.e., ankle palsy. This pathology combines

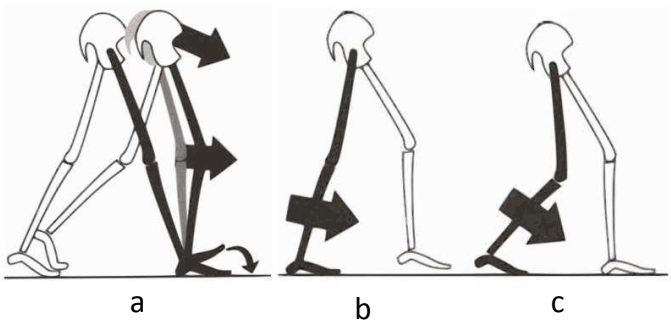

Figure 2.11: (a) Foot slap due to weak dorsiflexion control, (b) Prolonged heel contact due to excessive dorsiflexion, (c) excessive knee flexion combined with heel rise [42].

different functional errors presented in both excessive dorsiflexion and excessive plantar flexion, having different impacts during gait cycle. While excessive dorsiflexion has more functional significance in stance than in swing, excessive plantar flexion has functional significance in both periods. Generally, excessive dorsiflexion is caused by triceps surae weakness, while excessive plantar flexion is caused by pretibial muscles weakness.

In a pathological gait cycle, the normal event of heel strike as initial contact can be replaced by abbreviated heel strike or forefoot contacts [48] due to excessive plantar flexion. The action that accompanies loading the limb varies with the mode of initial contact. Abbreviated heel strike can be followed by instantaneous foot drop due to weak dorsiflexion control as in Figure 2.11a, and in case of forefoot contact, foot rapidly drops onto the heel while the tibia stays vertical [42]. Mid stance with excessive dorsiflexion causes an accelerated rate of ankle dorsiflexion from its initial position of plantar flexion, leading to instability at the onset of single limb support [42]. The lack of plantar flexion allows unrestrained tibial advancement during terminal stance, resulting in flexed knee and a possible loss of heel rise, leading to a prolonged heel contact in pre swing as in Figure 2.11b,c. Generally, heel rise begins when tibia moves forward as result of reaching the ankle's passive range [42]).

During swing, the most compromising functional error is excessive plantar flexion. The inability to dorsiflex the foot during the swing phase causes a func-

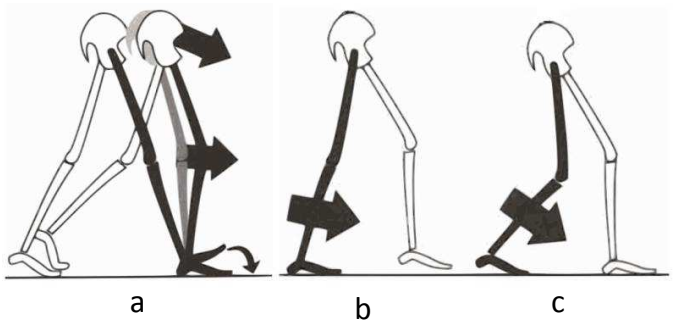

Figure 2.12: (a) Foot slap due to weak dorsiflexion control, (b) Prolonged heel contact due to excessive dorsiflexion, (c) excessive knee flexion combined with heel rise [42].

tional leg length discrepancy, and toe drag is observed when the subject fails to compensate [58]. Unless it is extreme, excessive ankle plantar flexion in initial swing has no clinical influence, since the trailing posture of the tibia tends to minimize the effect increased ankle plantar flexion has on toe drag [42]. Toe drag in mid swing due excessive plantar flexion inhibits limb advancement as in Figure 2.12a result, swing is prematurely terminated unless there is adequate substitution to preserve floor clearance. The most direct substitution for lack of adequate ankle dorsiflexion in swing is increased hip flexion to lift the limb and, hence, the foot Figure 2.12b [42]. In terminal swing, excessive plantar flexion influences the way initial contact occurs, compromising the following phases.

2.4 Hemiplegia disease

Hemiplegia is a more serve case of ***hemiparesis*** which is pathology with half weakened body side. Foot drop or toe slag or both could be seen as the pathology of hemiplegia. Any disease or injury in the motor centers of the brain can cause hemiplegia. It is also necessary to differentiate the hemiparesis/hemiplegia with parapleiga and quaripplegia which are paralysis in both leg below waist and paralysis below neck, respectively.

There are many condition give rise to hemiplegia. Generally, an injury to the

right side of the brain will cause a left-sided hemipleiga while an injury to the left side of the brain will cause a right-sided hemiplegia. The following are some common causes leading hemiplegia disease:

- Stroke: is the commonest cause of hemipleiga. insufficient blood supply to the brain leads to loss of the brain functions. The stroke may be caused by:
  - A clot formed within the blood vessel blocking the blood supply.
  - A thrombus breaks from its site of origin and forms a block elsewhere in the circulation.
  - A bleed from a blood vessel supplying the brain.
- Head injury.
- Brain tumor.
- Diabetes.
- Inflammation of the blood vessel.
- Disease affecting the nerves.

  After affected by injury or insults to the brain cells that control movements in one half of the body, symptoms largely depend on the part of the brain affected. There are some symptoms as: difficult in walking, problems in balance, losses balance when trying to walk, difficult in swallowing, trouble with vision, speech becomes difficult, loss of control over bladder and bowel movement leading to an inability to hold on the tool or urine, unable to perform task like holding objects.

2.5 The gait line and proposal idea

The above Figure 2.13 from [2] depicts the normal Center of Pressure (COP) line (gait line), which is the average vector of all force that act on the bottom of the normal foot as it go through the stance phase. This line goes from heel-strike

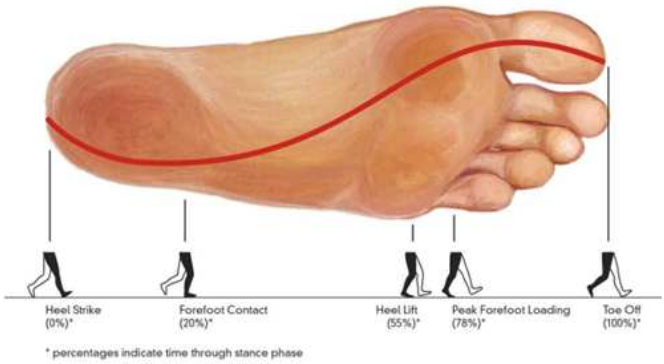

Figure 2.13: Gait line

to toe-off. We can see that, this line is not straight line, this is because during stance phase of locomotion, in addition to the dorsiflexion and plantarflexion in saggital plane the ankle also has inversion/eversion movements in frontal plane as well as the adduction, abduction movements in traverse plane as in [2] and [26].

Relating to the COP movement, according to [25] the Ground Reaction Force (GRF) does not reach the maximum while the heel only in contact with the ground. During the next stage of the stance phase, while the heel still contacts with the ground, the COP continues to move forwards rapidly as force on the heel decreases and force on the metatarsal heads increases. When the heel leaves the ground, the whole load is taken on the forefoot. This is long period relative to the period of heel contact and occur under the metatarsal head.

From CoP analysis, we suggested an idea to develop the novel AFO is that we will use one actuator to attack forces on to the COP points during stance phase in order to control ankle articulation.

Chapter 3

Mechanical design and feasibility analysis

As mentioned in the Chapter 2, the initial idea to develop the novel AFO is using one actuator to attack force following COP during stance phase, from with the the actuator can control the ankle joint. This chapter we will analyze the idea, develop the mechanisms as well as the mechanical structures of the system and finally with feasibility demonstration.

3.1 From biomechanics aspects to idea for the AFO

According to the initial idea, we would like to develop a new AFO that controls both of the COP spline and the ankle joint during locomotion. In order to implement that, normally there are two methods, the first one is to use two different actuators and then cooperate both of them to control two Degree of Freedom (DOF). And the second one is to use a CAM profile for the COP. However, if we used two actuators the system would be very complicated and heavy. Besides, the cooperation between them is one of the most important things. As a results, this solution is not feasible because of complexity and

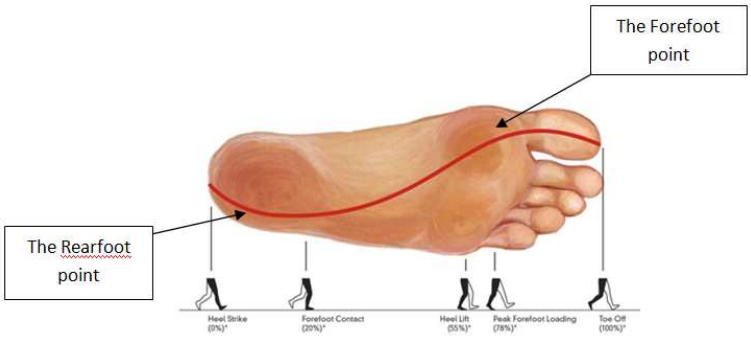

Figure 3.1: Rearfoot and forefoto points to be attacked force.

unnecessariness. And if we used the CAM, because the force transferring points from actuator to the sole of the AFO are on the COP's CAM, the system is still a two DOFs. As a result, it is impossible to use one actuator to control the continuous gait line (COP points).

To overcome the above difficulties, we proposed a solution that is to use one actuator to control two most important points of the COP which are initial and terminal point of the gait line. According to the Chapter 2, this is acceptable because during stance phase the duration of COP almost concentrate on the initial (rearfoot) and terminal (forefoot) part. The movement between the regions is very fast. Based on the gait line in Figure 2.13, the positions of these points are the **lateral heel side** and the **medial forefoot**, respectively.

In summary, after considering the Biomechanics aspects and mechanical evaluation, we finally suggested the novel idea for the AFO is to employ one actuator to control/attack force to the two most important points of the COP which are the lateral heel (rearfoot point) side and the medial forefoot (forefoot point) as in Figure 3.1

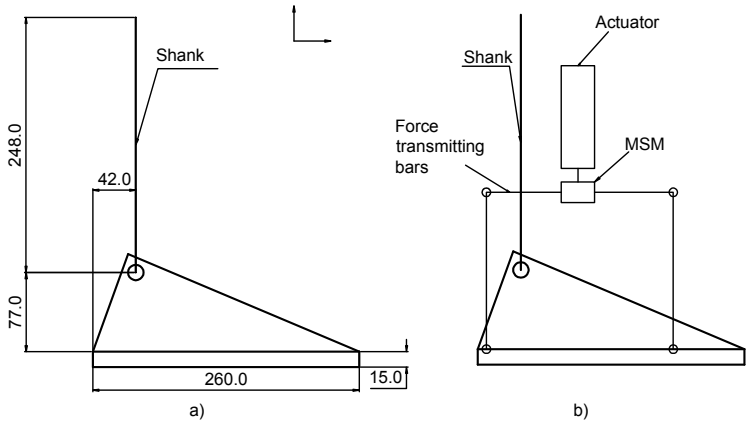

Figure 3.2: a) Basic dimension of human foot, b) Draft position of actuator.

3.2 Mechanism design for the AFO system

3.2.1 Motion splitting mechanism

The Figure 3.2a shows the basic dimension of a human foot. About the position to place actuator, almost of current AFO systems put the actuator at posterior side of foot in order to replace or support for the Gastrocnemius muscle which is most important muscle in generating locomotion. Besides, because this is muscle position which has soft tissues, so that the force transferred from actuator to frame and then to muscles to reduces pain for patient. For the novel AFO, however, because it used one actuator transfer forces to two points, we should place actuator between these points. As a results, the actuator position was chosen at posterior side of lower extremity as in Figure 3.2b. This position is also good when considering safety aspect that will be discussed more in the following part. Relating to reduce the pain and harmfulness for lower limb, the soft material will be padded between the system and the lower limb.

Because there are two points that are attacked forces separately by one actuator as in Figure 3.2b, we have to design a structure to divide motion from the actuator into two flows. That is called Motion Splitting Mechanism (MSM). We proposed to use a bevel gear mechanism to separate motion and a clutch system to change state ON/OFF motion to the left or right side as in Figure

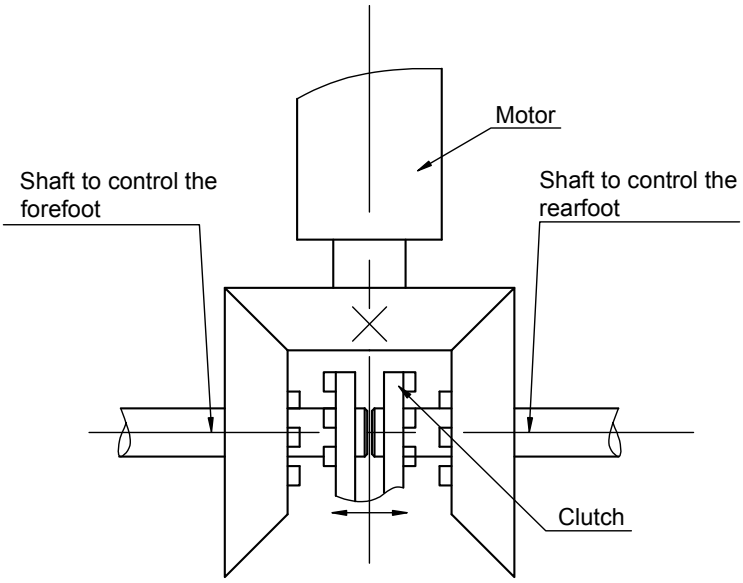

Figure 3.3: Draft MSM mechanism.

3.3. In the scheme of the Figure 3.3, when the clutch moves to the left side the torque/motion generated from the actuator is transmitted to the left bevel gear (the forefoot gear) to attack the forefoot point, the rearfoot has not to be controlled. Whereas, when the clutch moves to the right side, the actuator's torque/motion is transmitted to the right shaft (the rearfoot gear) to attack force to the lateral rearfoot point, the forefoot has not to be controlled. As a result, the system needs two different shafts for the heel bevel gear and the forefoot bevel gear: the heel shaft and the forefoot shaft, respectively. The Table 3.1 shows the role of each attacked point relating to the sub-phase during a gait cycle. The actuator will attack force on rearfoof point in order to control the Load Response (LR) and MST sub-phase of stance phase, whereas the forefoot point will be attacked in the remaining of the gait cycle. From this role table, it can be seen that the role forefoot point is more important than the rearfoot one.

3.2.2 State Changing mechanism

Mission: State Changing Mechanism (SCM) is from attacking force on the rearfoot point to the forefoot point and vice verse.

		Stance phase				Swing phase		
		LR,	MST,	TST,	PSW,	ISW	MSW	TSW
Attacked point	Rearfoot	✓	✓	x	x	x	x	x
	Forefoot	x	x	✓	✓	✓	✓	✓

Table 3.1: Division of gait cycle and attacked part of foot

It is necessary to design a SCM that satisfies some following requirements:

1. Only one state ON exists in each of bevel gears. It means, the changing ON state between the two bevel gears as: the first bevel gear ON – > Neutral – > the second bevel gear ON and vice verse.

2. Quick response.

3. Simple.

4. Reliability.

Results after design the MSM mechanism is shown in Figure 3.3. In this scheme, because the assembly state between the reafoot/forefoot gear with their shafts is loose, the moment flow goes as following:

- *Attack the forefoot point:* Actuator – > Main bevel gear – > Forefoot gear – > Clutch – > Forefoot shaft through clutch or spline between the clutch and the shaft.

- *Attack the rearfoot point:* Actuator – > Main bevel gear – > Rearfoot gear – > Clutch – > Rearfoot shaft through clutch or spline between the clutch and the shaft.

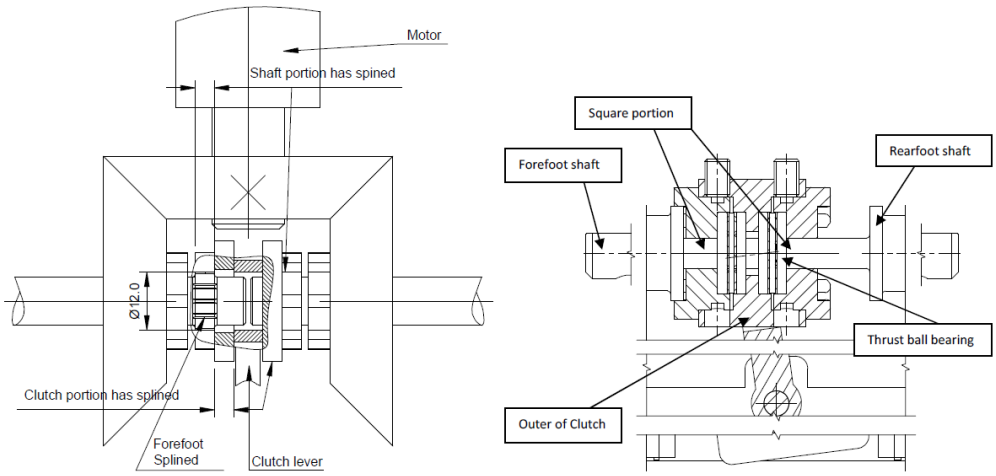

(a) Using Splined (b) Using square shaft and thrust ball bearing

Figure 3.4: Solutions for clurch of CSM.

The SCM includes two main parts: the clutch structure, which is used to transfer force from rearfoot/forefoot gear to rearfoot/forefoot shaft, and controlling clutch mechanism which is used to control the position of clutch to be ON/OFF on the left or right side.

3.2.2.1 Clutch structure of SCM mechanism

We proposed two structures of clutch system and two controlling clutch structures of the SCM. The Figure 3.4 reminded that in the bevel gear system, the motion/torque flow starts from the main actuator goes to the two bevel gears that have loose fit on their shafts. This motion/torque is transferred to the rearfoot shaft or the forefoot shaft when the clutch is closed at the rearfoot gear or forefoot gear, respectively. In the first solution as Figure 3.4a, the system used one clutch which has both clutch ends as well as two portions of splined inside. The forefoot and rearfoot shaft also has portions of splined portions in order to receive torque/motion from the clutches. When the clutch is closed to the forefoot/rearfoot gear, the controlling torque/motion of the forefoot/rearfoot bevel gear is transferred through the clutch to the forefoot/rearfoot shaft in order to control the forefoot/rearfoot point.

When changing the state from controlling the forefoot shaft to controlling the rearfoot shaft, first the clutch must be released from the forefoot gear's clutch, then the remaining forefoot splined portion of the clutch is also freed. During this time the splined portion of the rearfoot shaft and the right splined portion of the clutch are still not yet closed. After disassembling from the splined portion of the forefoot shaft, the clutch continues to assemble to the splined portion of the rearfoot shaft then to clutch on the rearfoot gear. Shortly, for the first solution, in order to change the state from controlling one bevel gear to the other bevel gear the system has to implement 4 times of release/close from/to the gear and shaft.

The second solution is shown in the Figure3.4b. The system uses two clutches separately: the left one is the forefoot clutch and the right one is the rearfoot clutch. These clutches have loose fits with the outer of clutch system. In order to prevent the clutches from axis movement the system used 3 crews for each clutch. By using this mechanism, whenever one clutch is being operating (ON state), which means the clutch is closed on its corresponding gear and shaft, then this shaft is rotated but the other is not rotated even though the clutch on this shaft is on closed state with it. More specifically, it is assumed that, the clutch system is on the left side. The torque/motion from the actuator can be transferred through the forefoot gear to the forefoot shaft by the forefoot clutch. This transmission is actually done by two interlocks of the forefoot clutch on the forefoot shaft and gear. At this instant, because both of the clutches of the clutch system [the forefoot clutch and rearfoot clutch] have loose fit on their clutch system's outer, the torque/motion is not transmitted from the forefoot clutch to the rearfoot shaft even though the rearfoot clutch is closed on its shaft. Thus, when changing the state from closing at the forefoot shaft to the rearfoot shaft, the clutch system firstly is released from the forefoot gear then closed to the rearfoot gear. As a result, in the second solution it needs only two times of release/close to changing the state. The head of the shafts that has interlock fit with the clutches uses square section structure instead of using spline structure in order to ease the manufacturing process.

Comparing the second method with the first one, the second solution has some

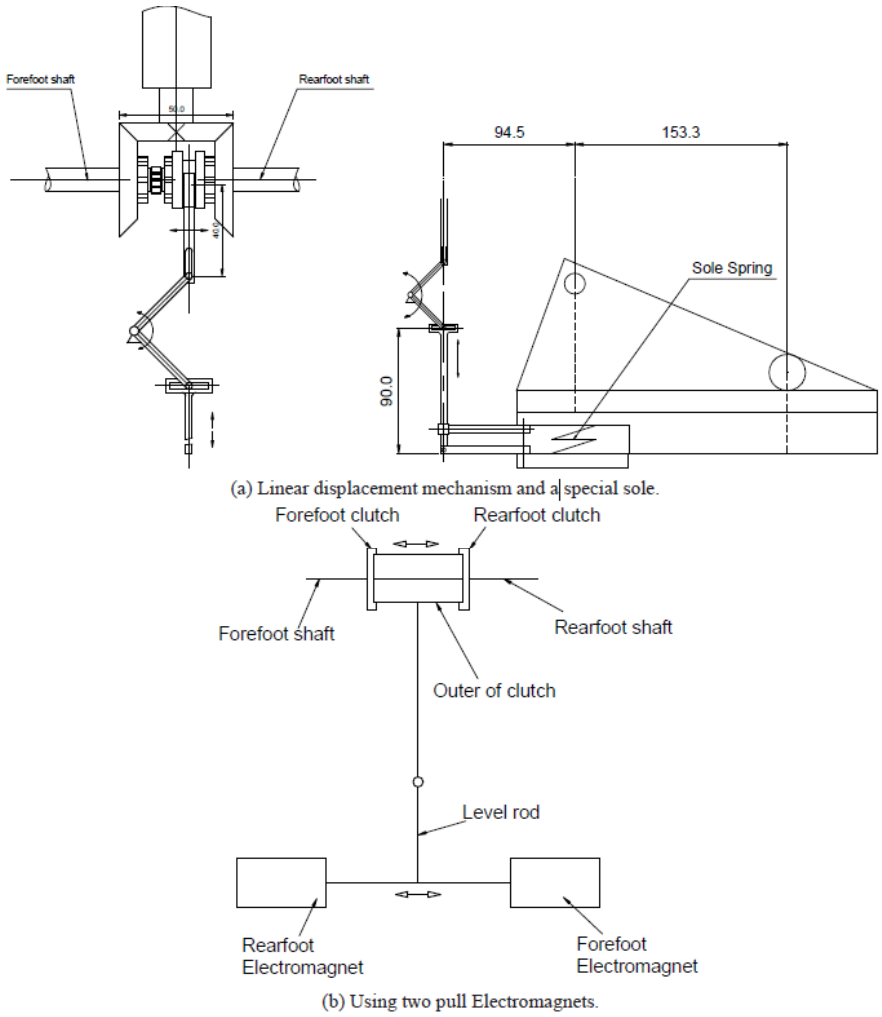

Figure 3.5: Controlling clutch mechanism.

advantages: the structure of the second solution is less complex than the first one which has many splined portions both on the clutch and the shafts. The second method is more reliable than the first one due to having fewer the number of release/close the clutches. As a result, we will chose the second clutch structure.

3.2.2.2 Controlling clutch mechanism of SCM mechanism

In control the position as well as the ON/OFF the clutch on the left or right side, the system need to be equipped with the controlling clutch mechanism.

The Figure 3.5 expresses two solutions for design the controlling mechanism of the clutch system that was demonstrated above. The first one used a linear displacement mechanism and a special sole structure on the shoe as in Figure 3.5a. According to the first solution, the clutch system is a rearfoot normal closed clutch system. Because without outside impact, the swing phase for example, due to the sole's compression spring the clutch system is always on the right side. At the stance phase, under the impact force and the body weight the vertical movement is generated and changed to horizontal movement owing to the linear displacement mechanism to make the clutch system move to the left side.

In the second solution as in the Figure 3.5b the system used 2 pull Solenoids to control the close state of the two clutches on their bevel gears. The ON/OFF state of each Soilenoid is determined by phase state definition and recognition of human gait. For example, at the phase from heel strike to mid-stance, the forefoot solenoid at the right side is on ON state and the rearfoot one is on the OFF state. Comparing the first and the second method has some advantages as: simpler structure, shorter distance from the force generating place to the clutch system.

In summary, after analysis the clutch system in the Figure 3.4 and the controlling mechanism at Figure 3.5. The final solution for the SCM is combination the best solution in each aforementioned structure. The mechanic for each of the mechanism will be discussed on the following parts.

3.2.3 Sole mechanism and crank-connecting mechanism

In order to transfer torques from the forefoot/rearfoot shafts to the sole of the AFO, the system uses the L shape crank-connection structure. The two methods of the sole were also suggested. In the first solution as in the Figure 3.6, the AFO's sole structure looks like the sole of a shoe. The rearfoot structure of the sole is as a piston moving along the sole. There is a spring inside this piston to absorb the impact force during initial contact. This structure has some disadvantages: there are some complex mechanical structures, the sole is easy to be stuck during working, the height of the sole is thick.

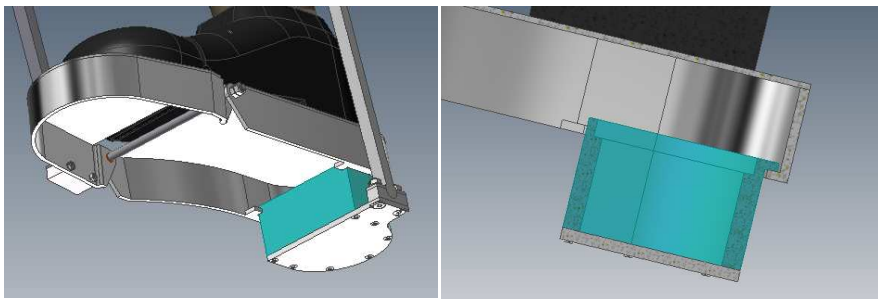

Figure 3.6: First solution for the sole of the AFO.

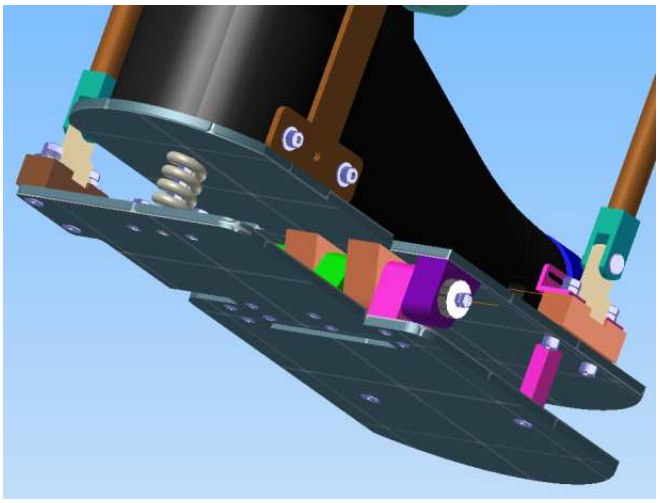

Figure 3.7: Second solution for the sole of the AFO.

The second solution for the AFO's sole is given in the Figure 3.7.(a). This is a hinge structure between the forefoot plates and the rearfoot plates. In order to absorb the initial impact at the heel strike period there is a compression spring assembled between the upper and the lower rearfoot plates. This mechanism has some virtues as: less complex than the first suggestion, more reliable. This is because, for the second method, mechanically, it is easy to produce because the parts composed to system are basis and simple. Besides, in the first suggestion, the movement of rearfoot part like the piston-cylinder movement. This could be dangerous for the patient at trike time because of impact between the movement part with the platform. The stuck problem between the static and the movement part in this rearfoot part is also one issue make this mechanism less feasible than

the second one.

3.3 Feasibility analysis for the system

After deciding the mechanism that focused on operational principle of the system, it is necessary to analyze the feasibility of the system, especially relating to controllabitity for the system. In order to implement this, kinematic analysis will be discuss in this part.

As mentioned in Table 3.1, the controlling process for the AFO could be divided into two main phases: attacking the Rearfoot point during LR, MST sub-phase corresponding with the Controlled Dorsiflexion (CD), Controlled Plantarflexion (CP) as in [3] and attack the forefoot point during the remaining of the gait cycle corresponding with the Powered Plantarflexion (PP) and Swing Phase (SW) as in [3].

3.3.1 Kinematic during CP and CD sub-phase

According to Table 3.1, these sub-phases start from the initial contact and end at the maximum dorsiflexion angle. The system transmits force to the rearfoot point to control the ankle joint. As in Figure 3.8, during this duration the rearfoot part of the AFO always contacts with the ground. Moreover, in the sagittal plane, there are 4 rotational joints of A, B, C, and D. As a result, the ABCD linkage is equal to four-bar mechanism. It is necessary to find out the angle relation between the rearfoot shaft angle θ_3 and the angle at ankle θ_2.

Using complex number to solve this problem from vector formula for four-bar ABCD:

$$\overrightarrow{\mathrm{CD}} + \overrightarrow{\mathrm{DA}} - \overrightarrow{\mathrm{CB}} - \overrightarrow{\mathrm{BA}} = 0 \tag{3.1a}$$

$$\mathrm{a}e^{\mathrm{j}\theta_1} + \mathrm{b}e^{\mathrm{j}\theta_2} - \mathrm{c}e^{\mathrm{j}(180+\theta_3)} - \mathrm{d}e^{\mathrm{j}\theta_4} = 0 \tag{3.1b}$$

After deploying the above mathematic model, we have:

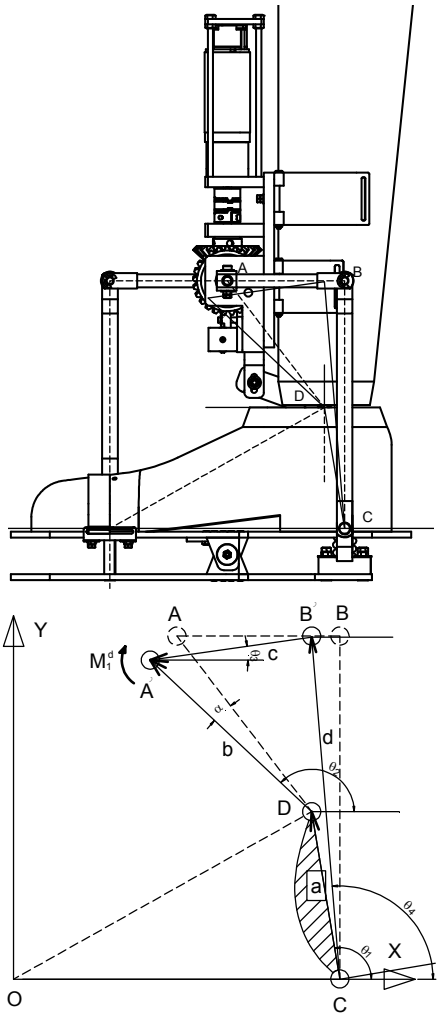

Figure 3.8: Schematic system for CD and CP subphases.

$K_1 \cos\beta_2 + K_2 \cos\beta_3 + K_3 = \cos(\beta_2 - \beta 3)$

where:

$K_1 = -\frac{a}{c}$; $K_2 = \frac{a}{b}$ and $K_3 = \frac{-a^2-b^2-c^2}{2.b.c}$

$\beta_2 = \theta_1 - \theta_2$; $\beta_3 = \theta_1 - \theta_3$

then

$$K_1 \cos\beta_2 + K_2 \cos\beta_3 + K_3 = \cos\beta_2 \cos\beta_3 + \sin\beta_2 \sin\beta 3 \tag{3.2}$$

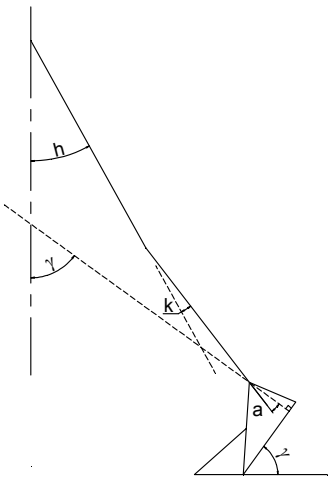

Figure 3.9: Angle between the rearfoot and ground during PP sub-phase.

Besides,
$\sin\beta_3 = \frac{2.\tan(\frac{1}{2}.\beta_3)}{1+\tan^2(\frac{1}{2}\beta_3)}$ and $\cos\beta_3 = \frac{1-\tan^2(\frac{1}{2}.\beta_3)}{1+\tan^2(\frac{1}{2}\beta_3)}$

Replacing to the above equation (3.2):

$$\mathrm{A}\tan^2(\frac{1}{2}\beta_3) + \mathrm{B}\tan(\frac{1}{2}\beta_3) + \mathrm{C} = 0 \tag{3.3}$$

The function (3.3) has two roots as:

$$\theta_3 = \theta_1 - \beta_3 = \theta_1 - 2\tan^{-1}[\frac{-\mathrm{B} \pm \sqrt{\mathrm{B}^2 - 4\mathrm{AC}}}{2\mathrm{A}}] \tag{3.4}$$

The roots (3.4) of angle θ_3 can be calculated by the geometric dimensions of the system as: a, b, c, d and ankle angle. There is a notice that the absolute value of the angle θ_3 is less than 90 degree, then in the two roots (3.4) there is only one value that is sufficient the condition.

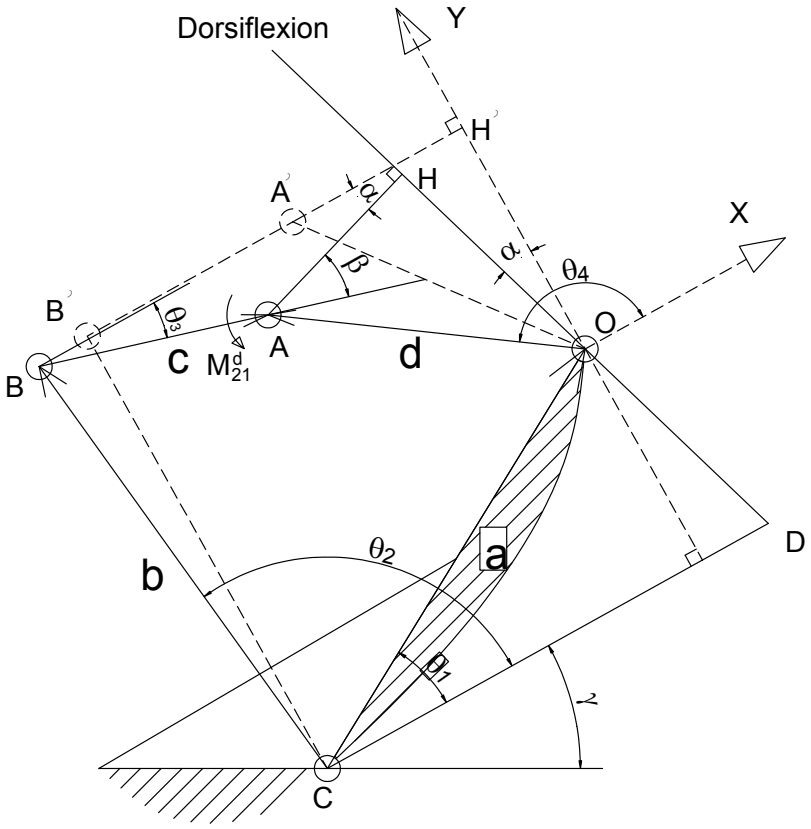

Figure 3.10: Schematic system for PP subphases.

3.3.2 Kinematic during PP and SW sub-phase

The system uses the forefoot point to control PP and SW sub-phases. During the PP duration, the forefoot plate always contacts with the ground and the rearfoot plate does not. However, the angle between the rearfoot and the ground at any instant time is able to be calculated based on the values of hip, knee and ankle value. According to Figure 3.9.

$$\gamma = \mathrm{h} + \mathrm{k} + \mathrm{a} \tag{3.5}$$

Where: h, k and a are angle value of hip, knee and ankle joint, respectively.

As a result, at instant time, in Figure 3.10 the CO linkage can be recognized

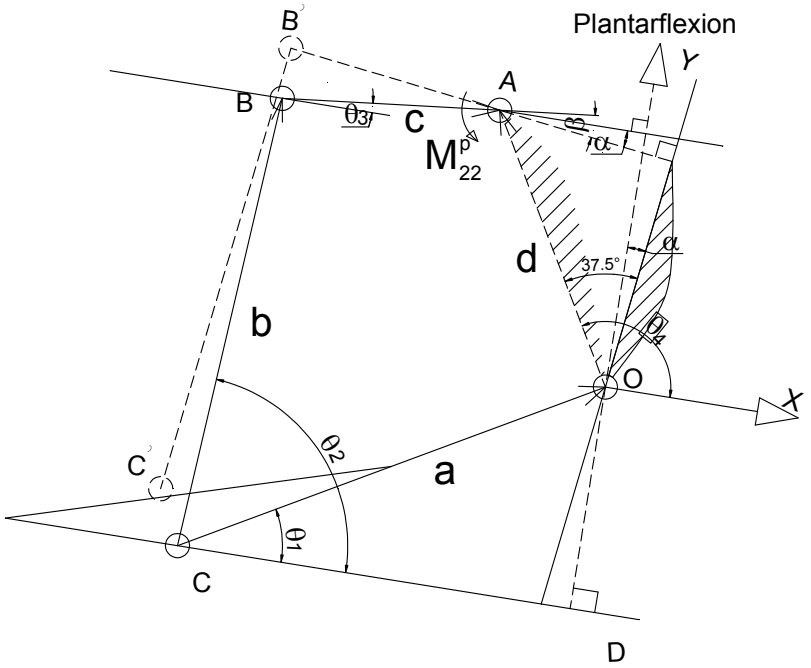

Figure 3.11: Schematic system for SW sub-phases.

as a fixed linkage. Then, the ABCO is equal to four-bar structure and it is similar as the aforementioned calculation. The relationship between the forefoot shaft and ankle value as follow:

$$\beta = \alpha + \theta_3 = \alpha - \theta_1 + 2\tan^{-1}[\frac{-\mathrm{B} \pm \sqrt{\mathrm{B}^2 - 4\mathrm{AC}}}{2\mathrm{A}}] \tag{3.6}$$

where:

$\mathrm{A} = (1 + \mathrm{K}_2)\cos\beta_4 - \mathrm{K}_1 + \mathrm{K}_3$
$\mathrm{B} = -2\sin\beta_4$
$\mathrm{C} = (\mathrm{K}_2 - 1)\cos\beta_4 + \mathrm{K}_1 + \mathrm{K}_3$
$\mathrm{K}_1 = -\frac{\mathrm{a}}{\mathrm{d}}$; $\mathrm{K}_2 = \frac{\mathrm{a}}{\mathrm{c}}$ and $\mathrm{K}_3 = \frac{\mathrm{a}^2+\mathrm{c}^2+\mathrm{d}^2-\mathrm{b}^2}{2\mathrm{cd}}$

For the Swing phase as in Figure 3.11, if the coordination is attached to the shank the AO of the ABCO mechanism is fixed. The relationship between controlled angle of the forefoot shaft and the ankle angle values is described:

$$\beta = \alpha + \theta_3 = \alpha + \theta_1 - 2\tan^{-1}[\frac{-\mathrm{B} \pm \sqrt{\mathrm{B}^2 - 4\mathrm{AC}}}{2\mathrm{A}}] \tag{3.7}$$

where: A, B, C, K_1, K_2 and K_3 are the same as the corresponding values in equation (3.6).

In summary, in both cases of attacking force to the rearfoo/forefoot point we always find out the kinematic relationship between the ankle angle and the angle or motor shaft. And at any time, this relation is unique. As a results, from kinematic aspect, the developing AFO is feasible.

3.4 Mechanical design

After analysis and deciding the mechanism for each structure in the AFO system. It is necessary to design the specific mechanic structure for all the parts as well as choosing electrical modules for the system.

3.4.1 Mechanical design for MSM

In the MSM mechanism, there are some most important parts that are required to determined: bevel gears, type and structure of bearing, and structure of shafts.

3.4.1.1 Gear

In the MSM mechanism, the mission of bevel gears is to change and separate moment from actuator to control reafoot point or forefoot point. Thus, the bevel gear is chosen with ratio of 1:1 and the dimension is decided based on the dimension of the foot. The dimensions and the other parameters of the bevel gear are shown in appendix part. There is only one reminded thing here is that, in order to transfer force from rearfoot/forefoot gear to its corresponding clutch, at the end of the gear also has to have clutch structure as in Figure 3.12.

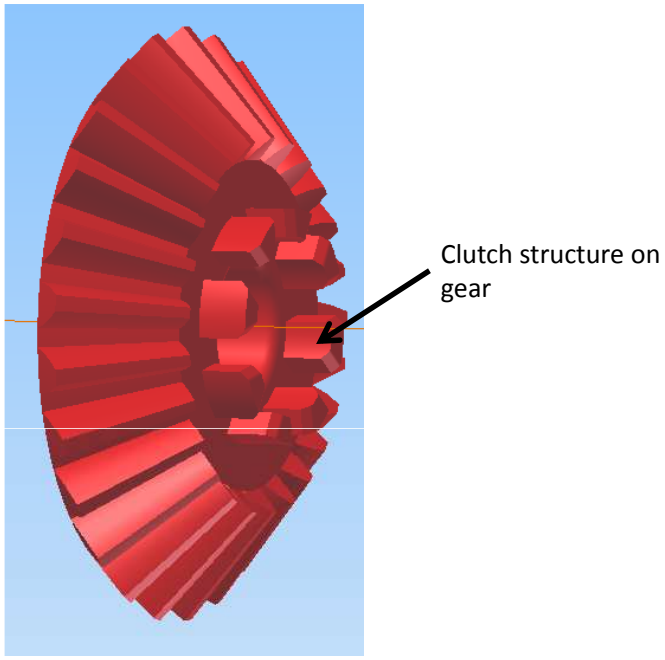

Figure 3.12: Rearfoot or Forefoot gear structure.

3.4.1.2 Bearing

There are many kinds of bearings as in Figure 3.13. With the straight bevel system as aforementioned we chose the angular-contact ball bearing which has medium radial load capability, good axial load capability and medium limiting speed of rotation.

One of most important requirements when choosing the bearings for bevel gear system, especially with the three bevel gears that are assembled perpendicularly is the assembly schema. The following is some points must be reminded when choosing bearings for the system:

- Because each of bevel gear is assembled on its shaft separately: main shaft, reafoot shaft and forefoot shaft. Thus, each of gear has cantilever assembly type on its shaft.
- The structure has to be simple and effective to reduce mass as well as volume for the system.

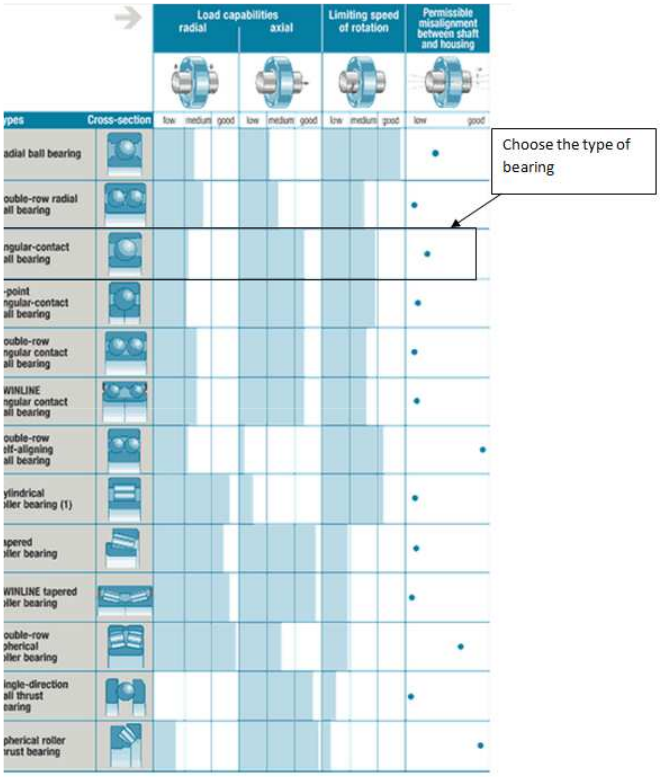

Figure 3.13: Different bearing types and comparison between them.

- Be able to eliminate the axial force on both directions.

Normally with bevel gear having cantilever assembly type, the we often use two array bearing type that are assembled according to "X" or "O" type as in Figuree 3.14. The purpose is to eliminate the axial force in both direction. However if the AFO use this method the system will be very bulky and heavy. I suggest to use only single angular-contact ball bearing for each of gear and its shaft but still meet all above requirements as in Figure 3.15:

- When the axial force has outside direction, the force will be transfer to the base of the system. And when the force has inner direction F_i, this force will be transited from the forefoot shaft to the rearfoot shaft or vice versa because the gap between the two end of the shafts is about 1-2mm. This force when transited to the other shaft will become the outside force F_o at this side and will attack to the base.

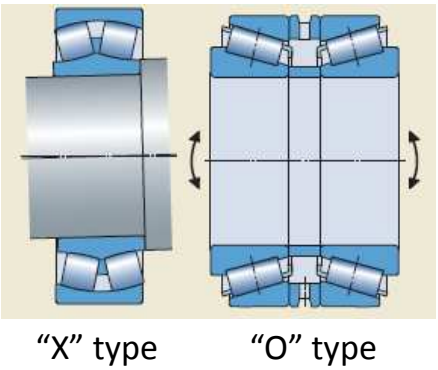

Figure 3.14: Different bearing types and comparison between them.

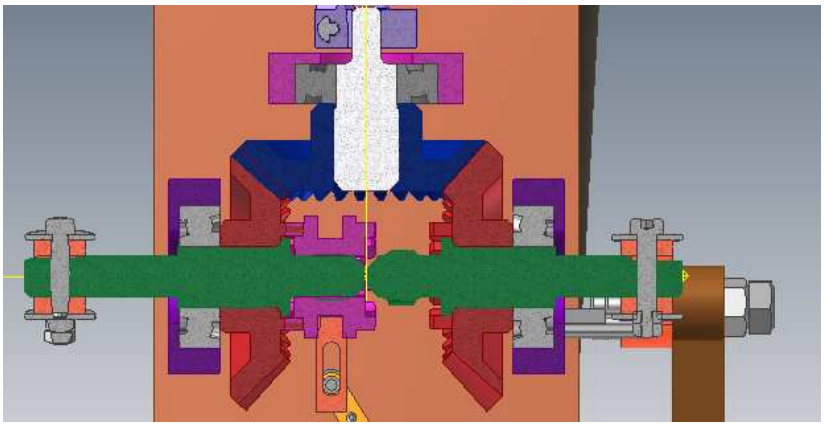

Figure 3.15: The arrangement of angular ball bearing that using single ball bearing but still be able to constraint two direction axis forces.

- Reduce the complexity as well as mass for the system because of using single array bearing.

Finally, we decided to choose Single row angular contact ball bearing M7001 from NSK Ltd company, Japan for all three gears.

3.4.1.3 Shafts

The shafts' structure is decided by the parts that are assembled on its. There is only one thing to remind is that according to the MSM, in stead of using spline structure to transmit moment the head of the shafts that has interlock fit with

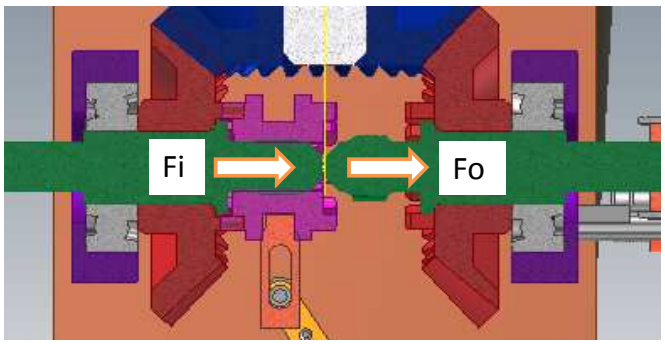

Figure 3.16: Model of transferring force from inner to outer side.

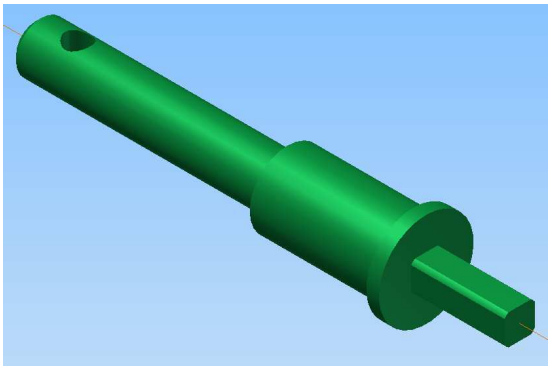

Figure 3.17: Shaft structure.

the clutches uses square section structure to reduce the complexity and be easy to produce as in Figure 3.17.

3.4.2 Patient connection

The connection should be rigid to ensure that the patient moves where the robot does and also to improve controller performance. At the same time, it must not restrict any movement of the patient or cause pain or injury. It is important that the patient interface not apply pressures large enough to restrict blood flow or cause skin damage. This should be more considered especially for the elderly patient. This part will discuss the issues and component design for the connection components to the patient's leg and foot.

The connection would ideally work on either leg and on multiple sizes of

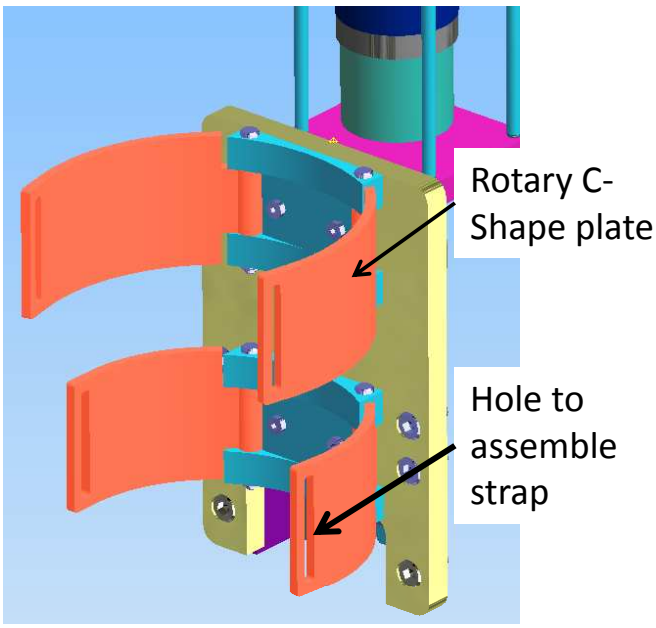

Figure 3.18: Leg connection (Strap not shown).

patients with little or no modifications. It should also be easily attached and removed, taking no longer that 5 minutes.

3.4.2.1 Leg connection

The leg connection piece is an interface between the patient's shank and the plate that the motors and gears mount on. Because this piece bears the weight of nearly the entire device, it is important that it be rigid and connect to the leg in such a way that it will not slide down the leg as the patient walks. To ensure this, a tight connection to the patient is required. It must not, however, apply too much pressure to any part of the leg. For this reason, it was desired to distribute the force as much as possible along the leg.

The Figure 3.18 shows the design of the leg connection. That consists of 4 rotary C-Shape wings. These wings help change the size between the leg and connection depending on the real shank size of patients.

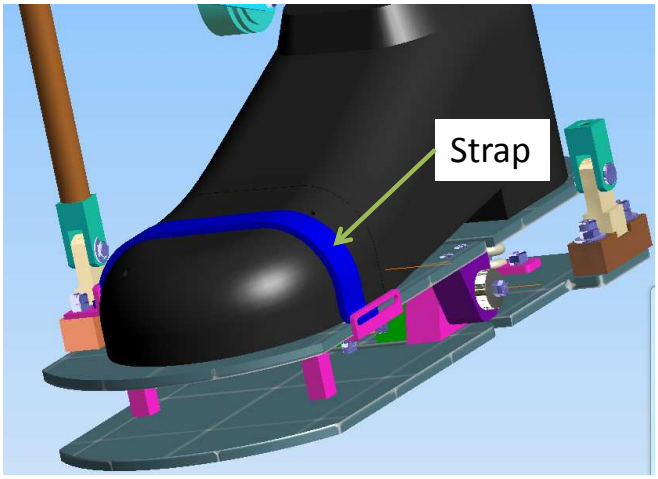

Figure 3.19: Foot connection).

3.4.2.2 Foot connection

Connection between the patient's foot with the system is implemented though the shoe. This shoe is connected to the sole mechanism of the system by a strap at forefoot part as Figure 3.19.

3.4.3 Mechanical design for other structure

Fore the other structure, based on the reality dimension to decide the dimension of them. These structures include: crank-connection, sole. The dimension of them is shown in the appendix.

3.4.4 Actuator

From a mechanical standpoint, the device must provide sufficient force to assist movements. Ankle torques can be very large near the end of stance phase since the body weight is propelled forward (100-200 N-m). Supplying torques of this magnitude would either require large motors, which are heavy, or a large gear reduction, which adds weight and endpoint impedance. The device was designed to supply torques needed to ***position the foot during swing phase and***

provide some assistance during stance phase. Specifically, the device will provide at least 12 N-m of torque to the ankle joint. This value is higher than that required for foot positioning in swing phase for normal subjects [61]. And at stand still, it can support up to 100 N-m. It is anticipated that more torque will be required to position the foot for stroke patients due to increased tone.

For healthy individuals, the maximum necessary power at very slow speed of 0.95 $m.s^{-1}$ is more than twice times compared to their body weight [33] and [51]. In the ongoing development AFO, as mentioned above we develop the system to partly support for hemiparesis patients. As a results, we decided to choose the motor which has 90W of power for the people with 66 Kg weight. This is more acceptable if we use the Body Weight Support (BWS) system during the exercise.

When sizing the motor, there are some aspects that we should remind: power, stall torque of motor, continuous torque, available gear reduction ratio to meet functional requirement, especially we also consider the motor weight.

After consider aforementioned aspect, I decided to choose a Maxon DC Servomtor RE35 which has 0.093Nm of nominal torque, 1.16 N-m of stall torque. The spec of the motor is shown in appendix. The ratio reduction gear head is 120:1.

3.4.5 Sensor

Sensors are needed to give position and possibly force information to the controller and for measurement purposes. A number of options were available for sensing position and force information.

3.4.6 Potentiometer

Because we will directly measure the ankle angle, the potentiomenter is suitable for this mission. The system use potentiometer model CPP-35B. This is shaft precision conductive plastic potentionmeter. This super quality, reliability and performance make it suitable for precision position sensing. This is also high

linear potentiometer, then the calibration is implemented easyly. The spec of the CPP-35B is shown in the appendix.

3.4.7 Force sensor

As mentioned, the AFO system uses one actuator to attack force onto two points in order to control ankle articulation. The changing state from attacking rearfoot point to the forefoot point is done by recognizing the phase. The system uses force sensors which are attached underneath of shoe to measure force as well as recognize the phase during gait cycle.

3.4.7.1 Some criteria for sensor selection

- **Accuracy and Range:** the sensor should be able to measure the full range of the event. During walking, at heel strike stage it can generate a force up to one and a half times body weight. For an average person weighing 660 N, the impact force could be up to 1125 N (253lbs). Besides, for precise calculation the ankle torque, the accuracy of the system must be in range 10 N (2.25lbs).

- **Frequency response or speed:** frequency response of a sensor is a range of frequency over that the sensor gives an accurate response. In normal walking, the amount each cycle walking is normally less than one second. With Controlled Plantarflexion (CP) phase, the heel strike occurs lasts approximately 0.1 seconds. Then, the system has to get the data at a rate greater than 100 Hz.

- **Sensitivity:** is defined as the ratio between change in sensor output corresponding with change in input sensor.

3.4.7.2 Possible force sensors

- **Force sensors:** Force sensor is used to measure the force. It also can be used to measure mass or weight depending on its application. A Force

Sensing Resistor (FSR) is a thin polymer device that exhibit decreasing electrical resistance in response to increasing force-applied perpendicular to the surface of the device. The force versus resistance relationship of FSR is almost logarithmic, nonlinear. One of the major limitations of FSRs is their creep response. It is train or deformation of the mechanical member over time when exposed to a constant force. It is important to remind that FSRs are not appropriate for accurate measurements of force.

- **Pressure sensors:** To measure pressure, an electrical signal is generated in response to a pressure input. The pressure is measured by strain or deflect. The use of these type of sensors was limited, due to their size, same as the force sensor, non linearity signals.

- **Capacitance Force transducers:** These sensors are more accurate and durable than FSR's, but are also larger in size.

- **Strain gauge sensors:** These sensors are used to measure the stress or strain in materials depending on their amount of bending due to applied force. Thus, the bending will be proportional to the change in sensor resistance. Since the gauge is attached on the surface of component, as the component is stressed, its dimension is changed same as of component. This makes change resistance of wire in the gauge. This resistance change is very small and needs to be converted to voltage and amplified before it can be measured. A Wheatstone bridge is used to do this.

- **Flexiforce sensor:** Flexiforce sensor, which is an accurate piezoresistive force sensor, is paper-thin, flexible and be easily integrated into most applications. The sensors are built of two layers of substrate. This substrate is composed of polyester film (or Polyimide in the case of the High-Temperature Sensors). On each layer, a conductive material (silver) is applied, followed by a layer of pressure-sensitive ink. To laminate the two layers, adhesive is used. The silver circle on the top of the pressure-sensitive ink defines the active sensing area. Comparing to strain gauge, the flexiforce sensor has some better points as : Direct force measurement corre-

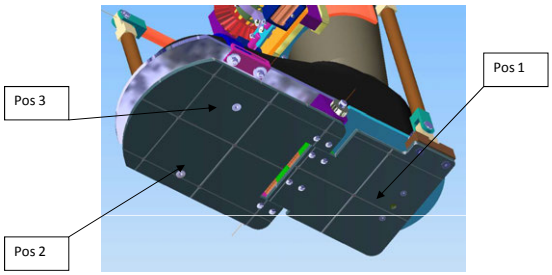

Figure 3.20: Position of sensors.

lating strain movement as in strain gauge, larger dynamic range, simpler electronics, easier to integrate.

As discussed above, it is reasonable to chose Flexiforce sensor for the AFO. Based on the requirements aforementioned. we decided to chose the model A401 from Tekscan, Inc. The specification of this type of sensor is as following: thickness 0.127 mm, length 203mm; width 14mm, sensing area 10mm, force range 0-7000lb.

3.4.7.3 Placement of sensors

The second most important task after choosing sensor is sensor placement on the foot in order to reflect the gait cycle and GRF.

Firstly, we have remind that in our AFO it is necessary to detect the GRF that affect on the patient foot. From this point, the force sensor must be attached right underneath the foot. Thus, we could place them: in-sole shoe or between shoe and the upper plates. Besides, because the orthosis is controlled in the saggital plane, for increasing the reliability of measurement as well as using as least as possible sensors, the sensor should be attached under the shoe.

Secondly, about the number of using sensor and positions of them: Recently, there are number of researches have been focusing on gait monitoring or phase gait detection problem as in references: [40], [63], [4] and [65]. One of most important task in these researches is to find out the best position to attach the force sensors. It can be said that, there more number of used sensors are, there

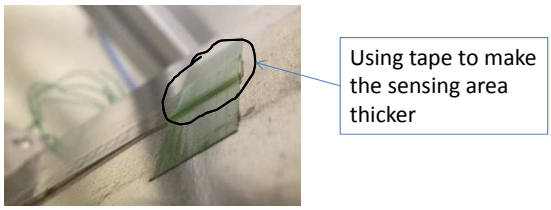

Figure 3.21: Assembly sensors.

more information we can get. This information include amplitude of force in different directions, CP, changing of CP. For our study, we only need the GRF for controlling process, then I decided to choose 3 points to place Flexiforce sensors: one of the Flexiforce sensor was placed underneath of the heel and two underneath of the first and fourth heads of the metatarsal bones. These positions are shown as in Figure 3.20.

Besides, in order to overcome the weak points of using Flexiforce sensors which are small sensing area and only measuring the perpendicular force. On the one hand the sensors was inserted some tapes between the sensor and the sole of the AFO system so that it is thicker and more sensitive to the GRF as in Figure 3.21. On the other hand, the system was also attached two thin plates upon the sensors at the rearfoot and forefoot. The fixed position of the plate is to prevent the shear force from corrugating.

3.5 Conclusions

This chapter presented the completely design process which started from biomechanics aspect to the idea and developed to the 3D as in Figure 3.22. The system consists of three main mechanisms which are Motion splitting mechanism, state changing mechanism, and sole mechanism. During design process, some ideas were suggested for each mechanism. After that, the ideas are analyzed and chosen the better one. The feasibility analysis for the 3D model was also discussed based on the kinematic demonstration. Finally, in order to produce the system, the mechanical parts was chosen based on some criteria.

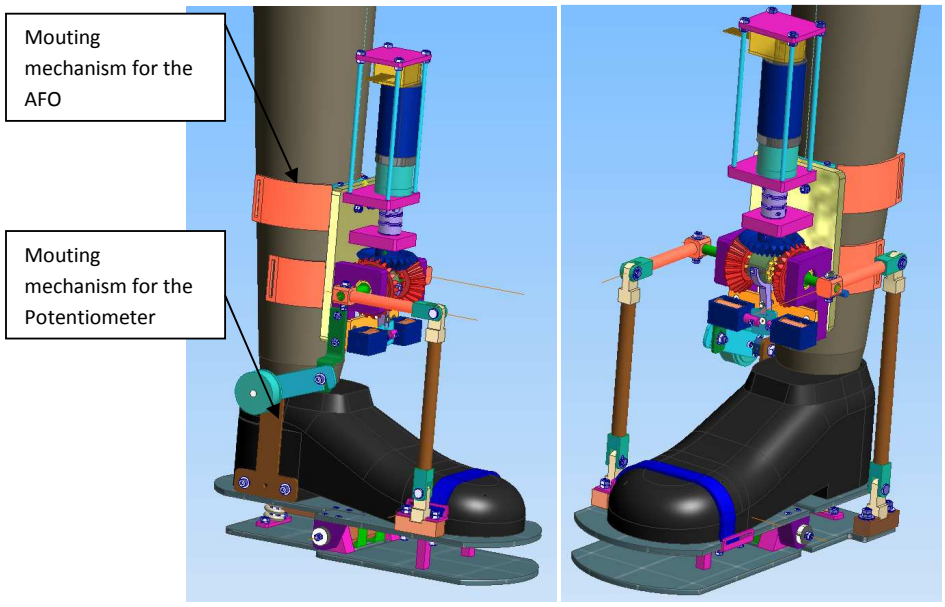

Figure 3.22: Complete 3D AFO model with having patient connection, potentiometer

Chapter 4

Control design

In the previous chapter, the mechanical design was presented, which started from the bimechanics aspect to have the initial idea, after that the mechanical design process was shown. After completing design and producing the AFO, this chapter will present the controller of the system which is used to control a DC Servo motor to attack force on two point of rearfoot and forefoof point. Besides, this controller is also has mission to control two solenoids in order to control the SCM by controlling ON/OFF the clutches. The structure of this chapter is as following: the section 4.1 shows the controller design that contains the controller structure, type of controller. The hardware configuration which show the electrical connection is presented in the section 4.2. The section 4.3 describes the signal processing to overcome the noise. Finally, conclusion is expressed in section 4.4.

4.1 Controller design for the AFO system

Normally, when controlling the orthosis system we often use available trajectory from database to input as a reference based on the gait cycle. However, the biomechanic characteristics of each people are unique. Also, because the AFO is design for the hemiplegia/hemiparesis patients who have a haft strong side and a haft weak side. Thus, it is a suggestion to use the data get from the strong side in order to control the weak one. This principle is described on Figure 4.1.

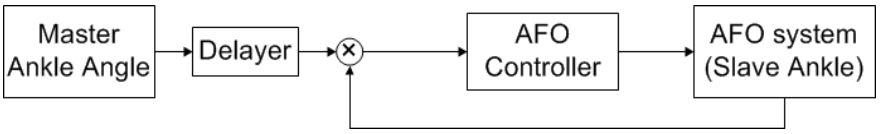

Figure 4.1: Overall controller of the system

The reference signal which is the ankle angle in sagittal plane was collected from the strong ankle. This reference signal was then transmitted though a delayer to become the controlling reference signal for the AFO system.

4.1.1 Choosing control method

The primary mission of robot in general, purpose of orthosis and prosthesis in particular is to execute curtain task in its environments. These tasks can be classified into two main groups: non-contact task and contact tasks [56], [34]. In the case of non-contact tasks, these types of robots, such as spray painting robots, welding robots, performs movements in an unconstrained environment and follows defined position trajectories in free space. However, a wide variety of robot applications requires the contact between end-effector of robot with environment. In such cases, operational-space force control become essential.

For the human locomotion, as mentioned above the gait is divided into two main phases: swing phase and stance phase. Swing phase, which is from toe off to heel strike, is time of non-contact between the lower limb with environment. On the contrary, stance phase, which starts at heel strike and finishes at toe off, has contact time between lower limb and environment. As a result, The proper control method for AFO is fine state control which contains position control for swing phase and force control in stance phase. However, in this AFO system, we only attach the three flexiforce sensors which has small sensing areas. Thus, the received force signal does not truly reflect the actual value. This signal is only used to recognize the phase, sub-phase for the system. As a result, we will use ***Fine-state position-based controller*** for the system.

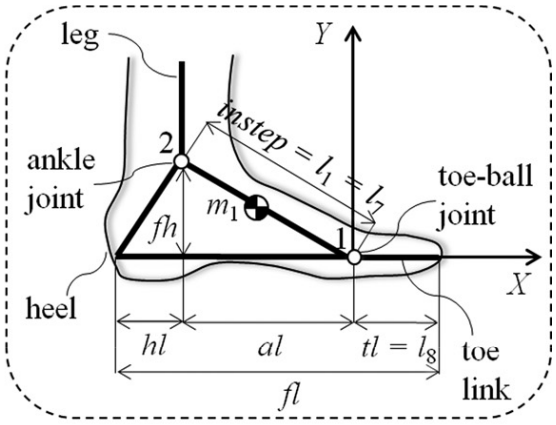

Figure 4.2: Foot model [11]

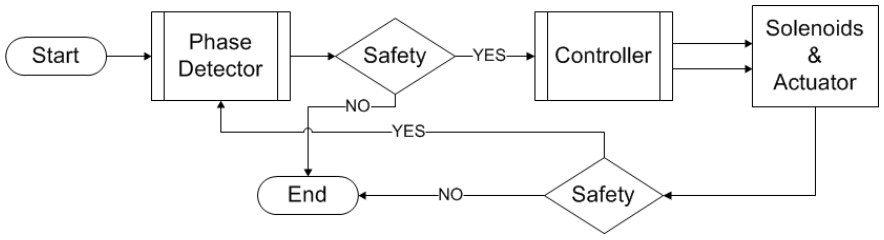

Figure 4.3: Overall AFO controllers.

4.1.2 State definition

As in mechanical design chapter, one of novel points in our AFO is to take metatarsal joint into account by controlling ankle articulation through attacking force at the forefoot point. The metatarsal is a joint that connects the toe-ball and ankle joints. By doing that, the AFO will reduce or limit the body weight on the weak foot during TST sub-phase. This model of containing the metatarsal joint when considering ankle joint is also proper with the new quantitative index which is dynamic gait measure (DGM) suggested by Carlotta [11] The toe segment of stance leg is modeled as an additional link with a negligible mass as in Figure 4.2.

State controller is normally used in the locomotion assistive device because gait is repetitive between strides, and within a stride. For the state controller used in AFO, the ankle angle and GRF will be used to be triggers.

4.1.3 Controller design

The Figure 4.3 present the overall controller structure used to control the system. This process consists of two main stages:

- ***Phase Detector***: to recognize the current phase. At this time the controller also check the safety condition relating to the force value limitation to prevent the wrong measuring.
- ***Controller***: implement to control two solenoid and actuator. This is consecutive process: after controlling the position of solenoids, the system continue to control actuator. In this stage, the safe condition relating to angle value limitation is also checked.

4.1.4 Phase detector

As describing by Palmer [39], characterization of the stance phase of the ankle during level walking could be divided into three parts as in Figure 4.4. The first period of stance phase which was began from foot strike (FS) to the minimum ankle position (foot flat position (FF)) was Controlled Plantarflexion (CP). The second period of the stance phase was Controlled Dorsiflexion (CD), which lasted from FF until the point where the power became positive. And the third period that was Powered Powered Plantarflexion (PP). This began the instant power became positive and lasted until the foot came off the ground (FO).

From the biomechanics aspects mentioned above, incorporating with the mechanical properties of the novel AFO, the controlling cycle for the AFO could be splitted into two phases. The first phase which uses the rearfoot point's role contains the CP and CD stages. The second phase is to control the PP and Swing stage. This controlling period uses the forefoot point to control the AFO. As a result, there are **three states used to control the AFO** :

- **Contact 1** for solving foot slap.
- **Contact 2** for control TST and Swing to deal with toe drag.

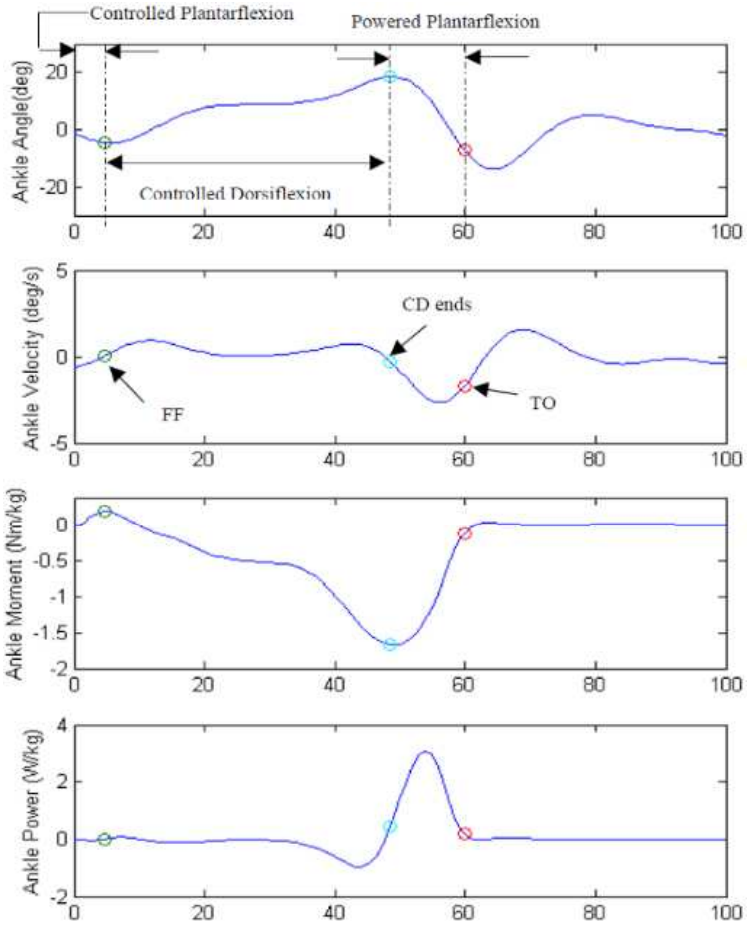

Figure 4.4: Ankle angle, speed, moment and power for one gait cycle of level walking. [11]

- **Safe state** to prevent the foot from dangerous cases.

As in Figure 4.5, contact 1 goes from initial heel strike until middle of mid-stance at neutral position i.e when the shank become perpendicular to the foot and then go on until the COP is changed from the rearfoot to forefoot part. From the Figure 4.6, the Contact 1 starts when the the total vertical GRF is above a constant, On Ground (OG), Which was set at 60 N, as can be seen in Figure 4.5. This was the minimum value that would distinct ground contact from noise during swing. At that time, if the force felt at the forefoot part is less than On Ground (OG)1 (OG1) which is set to be 40 N, the current subphase is IST.

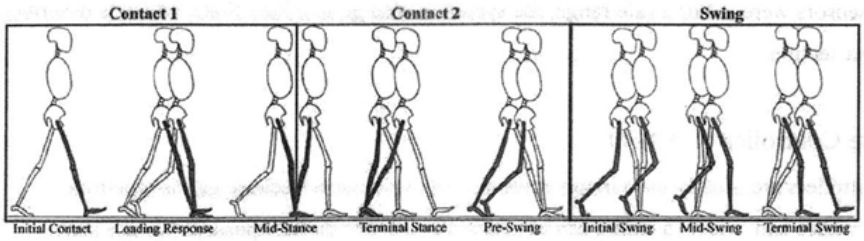

Figure 4.5: Controlled states of a gait cycle [7].

Because the AFO starts to control the second period of the stance phase from the PP stage to propulse the foot, this time is when the COP is already moved to the forefoot portion. The system use a force threshold of On Ground 1 to detect this stage. To change to Contact 2, the total of GRF must be maintained greater than OG and forefoot foot must be greater than the OG1. Contact 2 terminates at the time the GRF is lower than OG. In fact, when the GRF is lower than OG the Swing state is started.

Finally, a Safe State is also created to shut off the system in an unexpected circumstance. This happens when any of force sensor or angle sensor goes out of a specified range. For the force sensors, it was a force greater than 1000 N.

4.1.5 Controller1 and Controller2

According to Figure 4.6, in order to control AFO at Contact1 the system use the Controller 1, and use Controller 2 at Contact2. Each of controller includes two consecutive progresses: control two solenoids, and then control position of ankle articulation.

- ***Solenoid controller:*** Because the solenoids that are being used are the keep solenoid. It means, when the solenoid is at closed position, if we turn off electric, there is still holding force due to permanent magnet. From this reason, we only need supply electric to change the state of solenoids, after that we can turn it off.

  One of the weak point of using solenoids is their temperature increase during working. To reduce the increasing speed in order to last longer working

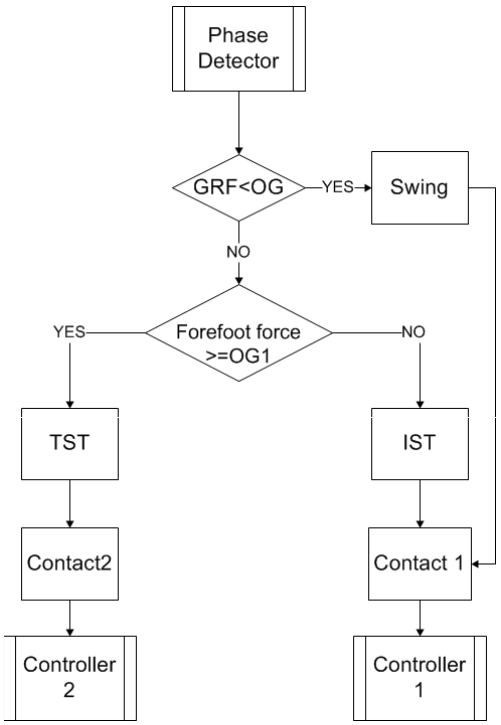

Figure 4.6: Phase detector algorithm.

time for the system, the solenoids are turned on in only short time (T_{on}) of period in each gait cycle. After calibrating, we have $T_{on} = 0.2$ [sec]. If the gait cycle we choose for the AFO T = 3 [sec], then we have the duty cycle for each of solenoid is as following. We can read next section for understanding more detail about the operational principle as well as the solenoids connection of two solenoid.

$$\text{DutyCycle} = \frac{T_{on}}{T_{on} + T_{off}} = 6.67\% \tag{4.1}$$

There is another problem when controlling these solenoids is that, because during the AFO operation there is friction between the clutch of gear and clutch of SCM mechanism. This friction force prevent the SCM's clutch from changing state even there is pull force from solenoid. To overcome this difficulty, in the process of controlling solenoids as in Figure 4.7, during the solenoid is being controlled T_{on}, the controller 1 also reverse the current

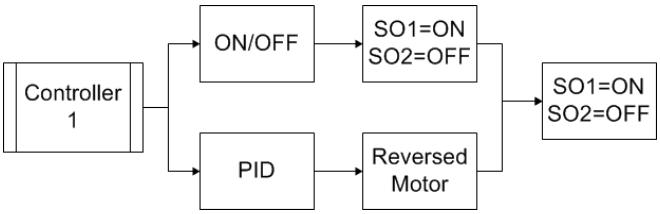

Figure 4.7: Solenoid controller for Contact 1.

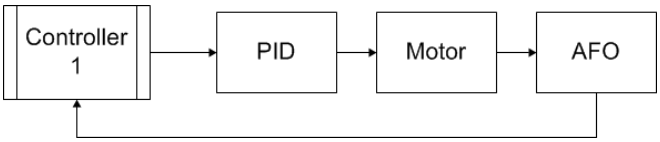

Figure 4.8: Motor controller for Contact 1.

direction of the motor. By doing this, the friction is temporary reduced to zero so that the pull force from the solenoid can pull the SCM's clutch from this state to the other state.

- ***Motor controller:***

  After the SCM's solenoid is changed the state. The controller 1 continues to control motor using PID controller as in Figure 4.8.

  Controller for Contact 2 has similar structure as the Controller 1.

4.2 Hardware configuration

4.2.1 AD/DA Board

The system is using PCI-3523A which is 12-bit analog input/output board. The PCI-3523A provides 8 single-ended analog input channels. The PIC 3523-A has ±10V. The AD conversion time per channel is 10μs for a fixed single channel. Besides, this PCI also provides 4 output channels. It has single output rang of ±10V. The DA settling time per channel is also 10μs . Some other specifications are available in Ref.[12].

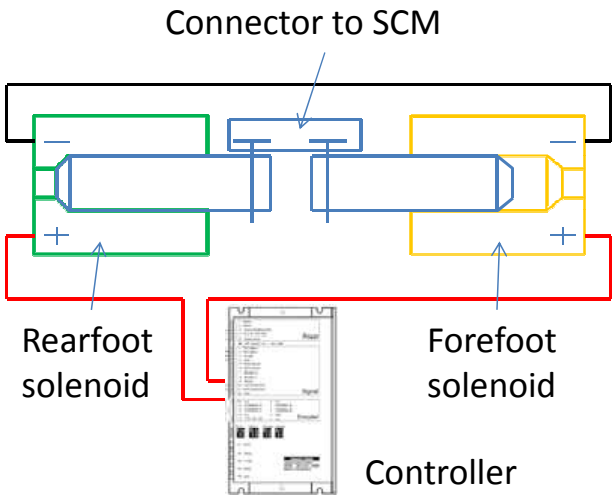

Figure 4.9: Solenoids connection diagram.

4.2.1.1 AD converter

The AFO system uses 7 AD ports as following:

- Ports 1,2,3 used to receive signals from force sensors 1,2,3.
- Ports 4,5 used to receive signals from two Solenoids.
- Port 6 used to receive signal from Slave potentiometer (POT).
- Port 7 used to receive signal from Master POT.

4.2.1.2 DA Converter

In order to control the dc servomotor and two solenoids, the system uses two DA ports. One port is used to control the actuator. And the other one is used to control two solenoids. Because the controlling process of two solenoids is on/off/release process and when one solenoid is being controlled, the other one is turned off. Besides, these solenoids are the keep solenoids and the movements of solenoids coils has mutal relationship. As a results, the solenoid has the connection diagram as in Figure 4.9.

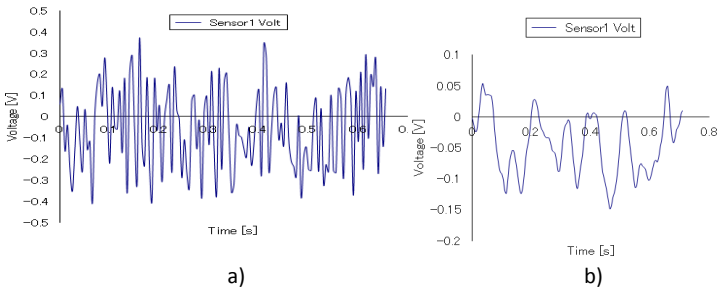

Figure 4.10: Reducing the noise by connecting without through terminal TRM 2401 a) Measured signal using TRM, b) Measured signal without using TRM.

In this connection,two negative polars of the solenoids are connected. Two Positives polars are connected to the controller to be controlled the values of:

- ON +10V
- Release, -10V
- OFF 0V.

Because the solenoids are connected as Figure 4.9, when one solenoid is turned on (+10V) the other one is released (-10V) and when turning off control signal both of them are turned off. Thus, ***the system only need one DA port to control two solenoids.***

4.3 Signal processing

We can classify the signals into two main groups: input and output signals. The input signals are the signals from POTs, encoder and sensors. And the output signals are the control signal from controller.

4.3.1 Input signals

In order to prevent the noise affects to the input signal, we implements some solution as following:

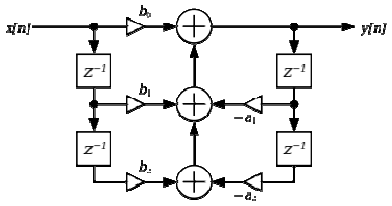

Figure 4.11: Butterworth low pass filter.

- Reduce the connection line between the sensors and PCI board. Normally, connecting between the feedback sensor, POTs to the computer is bridged through an terminal TRM-2401. But by connecting directly from sensors and POTs to Board the noise is reduced partly as in Figure 4.10.

- Using filters: Because the frequency range for human locomotion from 0 to 10 Hz. We choose the sample frequency is 1Khz and cut frequency is 10 Hz. Using the common Butterworth low pass filter as in Figure 4.11. The parameters of b_0, b_1, b_2, a_1, a_2 are 0.02008, 0.0401, 0.02008, 1.561 and -0.641, respectively. After using the filter we have the measured signal as in Figure 4.12. The rise time or can seen as delay time due to using the filter is 0.04[sec] corresponding with 40 samples. In the POT signal, the signal is already calibrated. The relationship between the angle and input voltage is y = –72.961*x + 91.77 with $R^2 = 0.9923$.

- One other method that is also used popular is to use the shielded cable to reduce electric noise from affecting the signals and to reduce electromagnetic radiation that may interfere with other devices.

4.3.2 Output signals

The output signals are the signals from two controllers to control actuator and two solenoids. This signal is also prevented the noise by using the shield cable.

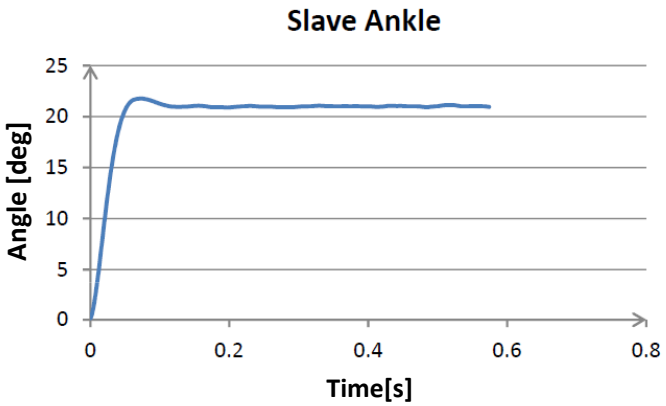

Figure 4.12: Angle Value after using filter

4.4 Conclusion

In in chapter, we presented the controller design for the AFO. These are the Fine-state position-based controllers which use PID controller to control each of phase. The phase detectors and solenoids, motor controller algorithms were also shown. Finally, the process of receiving and transmitting signal for the controller were discussed to ensure these are reliable signals.

Chapter 5

Experiment Results for AFO system and a proposed tuning method for FLC

5.1 Introduction

In the two previous chapters, the design process of mechanic as well as controller for the novel AFO were shown. In this chapter, the experiment to evaluate the system will be presented. Firstly, in order to find out the kinematic ability of the system, some experiment will be done. After that in the next section of 5.3, the phase detection experiment result is shown. The next Sec.5.4 is experiment in case of without load. The system will be hang on a frame, after that it will be made experiment to evaluate the foot drop prevention ability, ability of Changing State Mechanism operation which used the solenoid controller. The experiment on normal human with slow walking speed was done in the Sec.5.5.

Relating to the controlling method, normally for the complex system or the system which is difficult to find the transfer function. One of control methods could be used is Fuzzy Logic Controller (FLC). However, this method depends on the knowledge, experience about the system of the user. Then, with the purpose

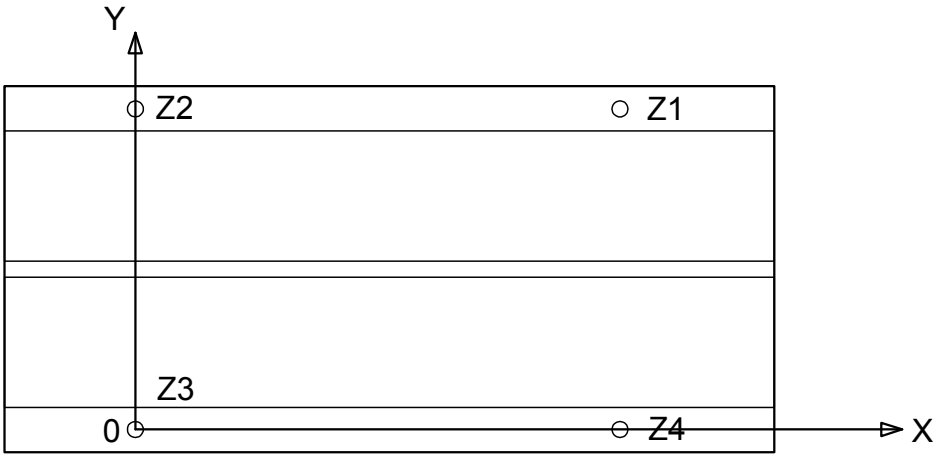

Figure 5.1: Platform of treadmill with four force sensors Z_1, Z_2, Z_3, Z_4 and the co-ordination.

to reduce burden for the user, a novel tuning method for FLC was proposed in the section 5.6. This method proved improvement to reduce the tuning time for DC Servomotor. However, because the possibility dangers as well as the quite longer time consuming comparing to the manual PID tuning, this method was not used in the system.

Finally, some conclusion will be discussed.

5.2 Kinematic and CoP of the AFO system

5.2.1 Description of Experiment

In order to evaluate the range of movement possibility of the AFO, a walking experiment without turning on the actuator was implemented. A wealthy person, who is 66 Kg weight, 167 cm height wearing the system which includes the master shoes and the AFO system at right and left lower limb, respectively. The master shoe has a POT that is used to measure master ankle angle in sagittal plane. This signal can be seen as the standard to compare to the ankle angle at the left side. Due to the limitation of wire connection between the system and computer, the experiment was implemented on the AIRGAIT treadmill. The speed of tread

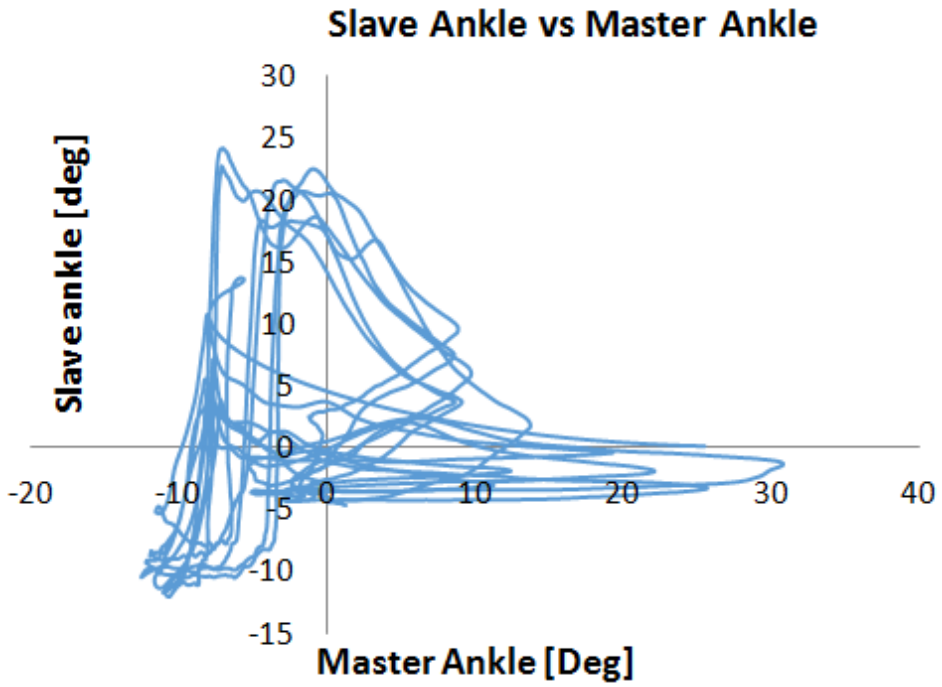

Figure 5.2: Kinematic value of master ankle vs slave ankle without turning on the actuator.

mill is 3 miles/h. Under the platform of the treadmill assembles four force sensor Z_1, Z_2, Z_3, Z_4 as in Figure 5.1. A 2D Cartesian Coordinate system is attached at the Z3 sensor position. The force values from four sensors was used to calculate the location of the CoP points during locomotion based on the following formula:

$$\mathrm{CoP_X} = \frac{Z_1 + Z_4}{Z_1 + Z_2 + Z_3 + Z_4} \quad \text{and} \quad \mathrm{CoP_Y} = \frac{Z_1 + Z_2}{Z_1 + Z_2 + Z_3 + Z_4} \tag{5.1}$$

where Z_1, Z_2, Z_3, Z_4 are the force values of sensors attached at the corresponding locations.

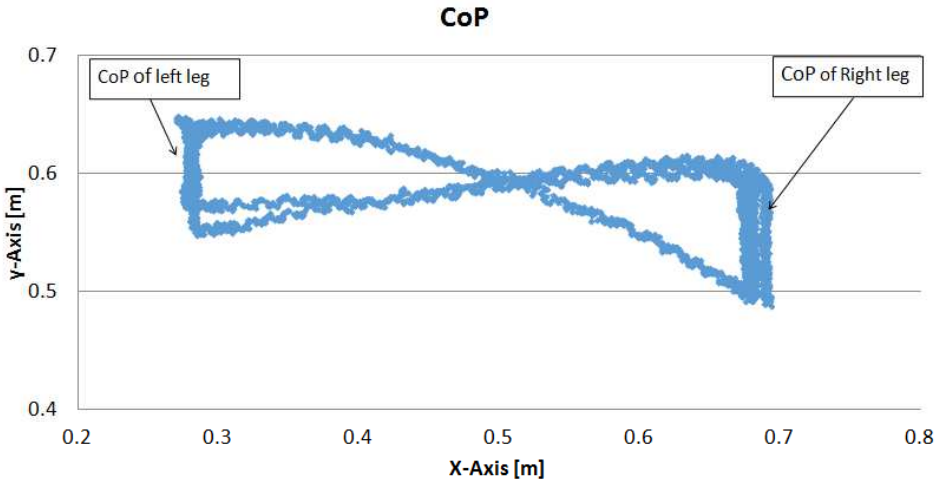

Figure 5.3: CoP movement of human during wearing the system without turning on the actuator.

5.2.2 Results of Kinematic and CoP of the AFO system

The Figure 5.2 describes the ankle angle of slave side compared to master side in case of turning off the motor. The range of weak side is litter reduced compare to the strong side, 35 degree of slave angle compared to 40 degree of master ankle. The minimum dorsiflexion values of two lower limbs are the same as around -10 degree. The maximum platarflexion of weak side, however is little smaller than that value of strong side.

Relating to the CoP movement during locomotion, the Figure 5.3 shows a typical CoP spline for the right (Strong) and left (weak) lower extremity. This CoP spline is a butterfly figure as normal. The spline includes two swings: the right is the COP line of right lower limb and the left is the COP line of the left lower extremity. The lines that connect the left COP and the right CoP are the movement of CoM from left to right and vice verse. It seems that, because the asymmetric between the two side the left lower limb attacks and releases the platform earlier than the strong side. Moreover, the length of CoP line for both right and left are little reduced, 13 cm and 9 cm for the right and left foot respectively. The reduction on CoP line on both lower limb is because the system was attached soles on both foot. These hard sole prevents foot from smoothly

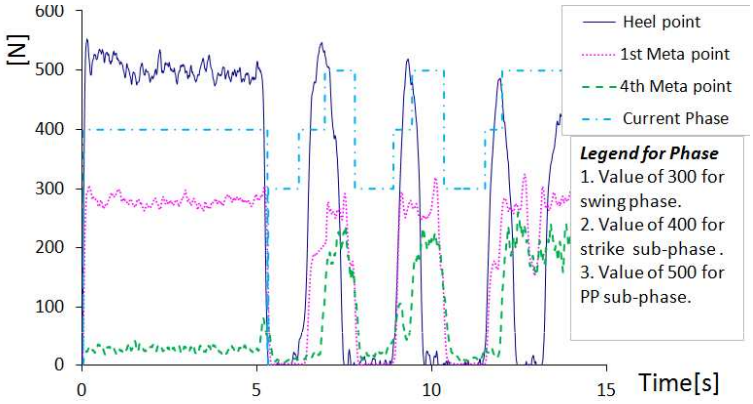

Figure 5.4: Phase detection result.

movement. As a result, instead of point contacting especially at heel strike and foot release, the foot attach the platform by a surface. The harder sole of foot is the shorter the length of CoP of it foot is. Then, the CoP length of the left lower limb is shorter than the CoP length of the right one.

5.3 Phase detection

A normal person who is 66 Kg weight, 167 cm height wore the system on his lower limb. After that he implemented to walk few cycles. The signals were collected and analyzed on Excel.

The result was shown in the Fig.5.4. The force value at heel, first metatarsal point and fourth metatarsal point are shown in continuous, dot and dash lines, respectively. At starting point (stand still), the force value at heel is biggest, then the value at fourth metatarsal and first metatarsal joint. After running the Phase detector algorithm aforementioned, we received the result of sub-phase of gait as is depicted in this graph by dash-dot line. We define the phase and sub-phase line as following: value of 300, 400 and 500 express for swing phase, strike and PP sub-phase, respectively.

The result demonstrated the repeatedly three sub-phases during walking cycles: swing phase then CD, CP Sub-phase and finally with PP sub-phase. During stance phase, the value of first metatarsal force sensor is appear earlier than the

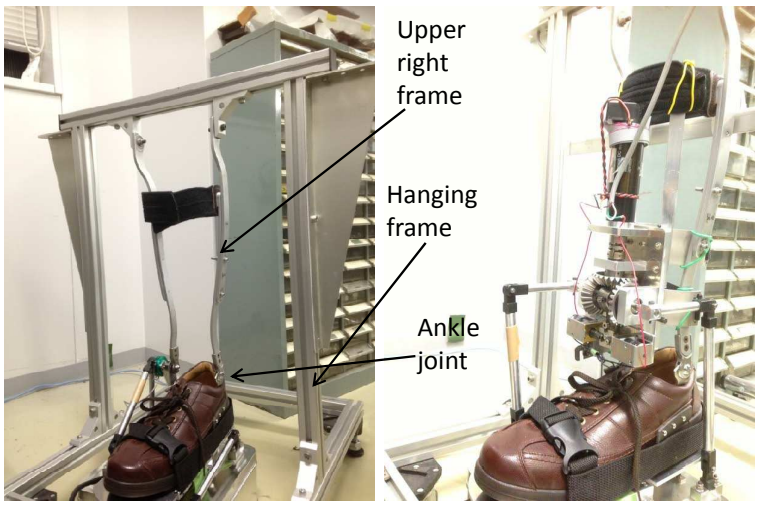

Figure 5.5: Model of without load: a) attach the upper frame at ankle joint, b) attach full AFO system on the frame.

fourth one. This is suitable with the real movement of foot during the stance phase based on COP movement. The duration of stance phase is around 60 % of gait cycle, this partly demonstrate the proper of the algorithm.

5.4 Experiment without load

5.4.1 Experiment model

In order to evaluate the working possibility of the system including mechanic as well as controller, next the system was made experiment in case of without load. The shoe of the system was attached to a upright frame at ankle joint as in Figure 5.5a). After that the complete system was attached on the experiment model as in Figure 5.5b). By fixing the upper right frame on the hanging frame the AFO is only able to move around ankle articulation.

As aforementioned the data was sampled at 1KHz and using Butterworth lower pass filter with cut frequency of 10 Hz for the input signal from force sensors as well as POTs. The data was exported to excel file to analyze. Firstly,

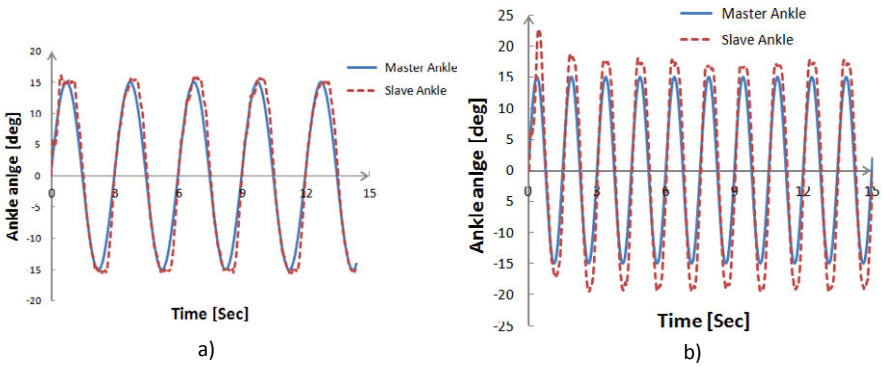

Figure 5.6: Experiment result with sine signal in controlling fore foot to prevent foot drop a) cycle is 3 second, b) cycle is 1.5 second.

the PID tunning was implemented and find out the PID parameter for K_p, K_i and K_d are 0.18, 0.6 and 0.019, respectively. After that some experiments were done.

5.4.2 Experiment results

Firstly, the sine input signals experiments were implemented. The sine signals which have 15° of amptitude, the 1.5 second and 3 second of cycle were imputed as the master ankle signals. The amptitude of 15° was chosen based on the normal range of ankle movement. And the cycle of 1.5 and 3 second were chosen also rely on the slow and very slow cycle time of gait.

The Figure 5.6 shows the results of the control process. In both cases the AFO response (dat dot lines) can follow the input signals (continuous lines) quite well. This can be seen clearly after each cycle time, the slave ankle signal of AFO system meet the input signal from master one. It should remind that the positive ankle values is corresponding to plantarflexion, whereas the negative values is the dorsiflexion angle. In case of cycle is 3 second, the AFO system can well follow the input signal to maximum plantarflexion or minimum dorsiflexion. However, when the AFO reverses direction there is small delay about 0.15 second, and the magnitude is little bigger (about 0.85°) than the input value. These things could have been due to the inertia of the system when it reverse the direction.

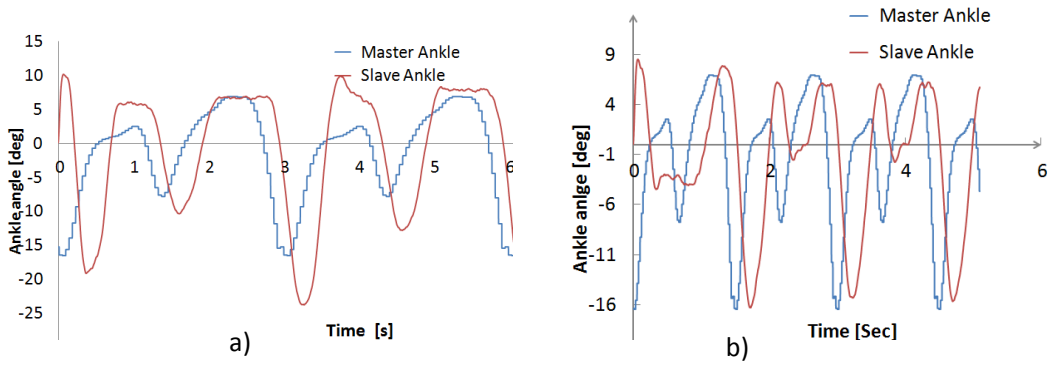

Figure 5.7: Experiment result with normal gait in controlling fore foot to prevent foot drop a) cycle is 3 second, b) cycle is 1.5 second.

It could be seen more apparently in Figure 5.6b) when the cycle signal is reduce to 1.5 second. There is one strange thing here is that it seem the delay time in case of 1.5 second cycle is smaller than the case of 3 [Sec] cycle. Meanwhile, the minimum dorsiflexion values is smaller than in case of 3 [Sec] cycle. This can be explained as following: when cycle is reduced, the changing of input angle and then error as well in a sample of time is increased. As as result, the integral value in PID controller increases corresponding. This make the system move faster and then can reduce the delay time at minimum dorsiflexion as well as in maximum plantar flexion value. However, the bad side of this is the inertia moment of the system increased since faster speed. This leads to the smaller dorsiflexion and bigger plantarflexion values value in 1.5 [Sec] case compare to 3 [Sec]. The absolute deviation in case of dorsiflexion is more than in case of plantarflexion since in platarflexion thank to the forefoot's weight, the required moment needed to control is smaller than in dorsiflexion.

The Figure 5.7 presented the results when input signal of master ankle are normal gait with the gait cycle of 3 [Sec] as Figure 5.7a) and 1.5 [Sec] as Figure 5.7b). The continuous lines are the input signals from master ankle. Meanwhile, the dash and dot lines are the slave responses and error, respectively. Dispite having longer gait cycle (3 [sec]), the absolute aptitude is still bigger than the absolute aptitude in case of 1.5 [s] gait cycle. This could be explained when considering the relation between the inertia moment and time response. In par-

ticular, in the Figure 5.7b) because the time cycle is short then the time response is not fast enough for the output track the input signal. This leads to a big time delay of 0.2 second. At the same time, the integral value in PID has big enough to reverse the direction of the system. As a result, we can see that the trajectory in case of gait cycle 1.5 second is similar to the input gait cycle. This is not similar to the case of Figure 5.7a). Due to having longer gait cycle, the output can track better than and then the delay time is smaller than the previous case. However, The control signal is not strong enough to overcome the inertia moment. Thus, the absolute aptitude in case of 3 second cycle is bigger than 2 second cycle.

5.5 Experiment when wearing the system on human leg

5.5.1 Experiment models

The model is used to make experiment is same as in the experiment to test kinematic and COP of the foot during wearing system without turning on the motor as in Figure 5.8. In this case, the speed of the the treadmill was set to be 1 mile/hour. The delay time between two lower limb is 1.2 second. We implemented two experiments. The first only control the forefoot because this is most important portion during a gait cycle and second experiment is cooperation between the solenoids operation and motor controller.

5.5.2 Experiment results

The Figure 5.9 presented the experiment result when gait cycle is 3 second and the 1.2 second of delay time between the weak and strong lower limb. Figure 5.9 a) includes also the current phases and the slave ankle angle (dash-line) and master ankle angle (continuous line). In the Figure 5.9 b) the delay time was removed to be easy compare between reference and response of the system.

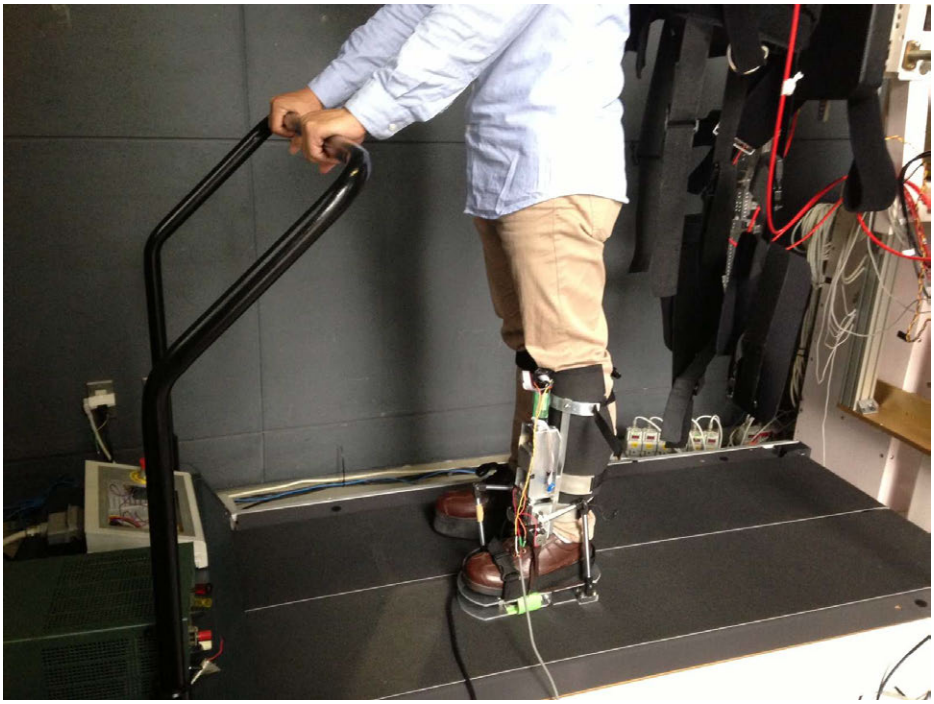

Figure 5.8: Experimental scene

Firstly, we will discuss about the trajectory of the ankle. Each ankle gait cycle has two peak as in Figure 5.9 b). The first peak belongs to the swing phase and the second one belongs to stance phase. After the foot release the ground at terminal stance phase, the ankle angle quickly increase to maximum plantarflexion at first peak. Right after achieving the maximum plantarflexion value, the ankle turns to dorxiflexion to prevent the foot drop during the swing phase. During stance phase, after the heel strike the ankle gets the second peak of plantarflexion, after that it is changed to dorsiflexion. This could be explained by the difficulty in bending the sole of shoe due to its thickness.

Next, in the experiment result as in Figure 5.9 a) as well as Figure 5.9 b) after removing the delay time, the slave ankle can follow the master one quite well. However, the second peak of planterflexion of slave is more delayed since there is more dorsiflexion at terminal swing phase. This doriflexion at AFO system support more possibility for the system to prevent foot drop. One more thing, in the Figure 5.9 a) the phases which composes of swing, strike and terminal stance

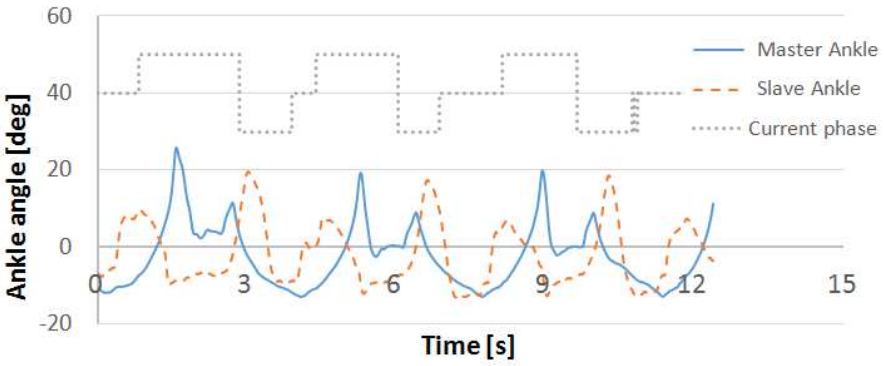

a) Time delay of 1.2 sec.

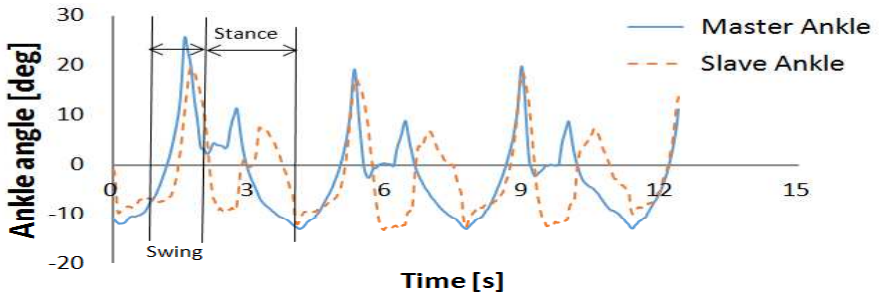

b) Removed time delay.

Figure 5.9: Experiment result with 3 sec of gait cycle.

were recognize well.

Finally, the Figure 5.10 shows the CoP line experiment result in this case. It can be seen that, the CoP line is better than in the Figure 5.3. In particular, it is more symmetric, especially in the Y-Axis. However, because the sole of the AFO is harder than the sole on the right, the length of CoP on the weak lower extremity still is still shorter than the length of CoP on the strong one.

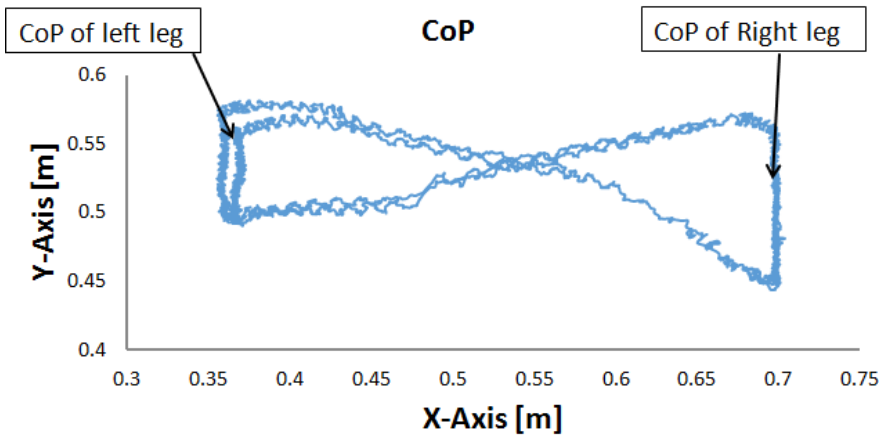

Figure 5.10: CoP line when AFO working with 3 second of gait cycle.

5.6 Optimization of Fuzzy Logic Controller using Motor Speed Profile and Genetic Algorithm in Controlling DC Servomotor

5.6.1 Introduction about the FLC

There are two main kinds of electrical motor that are AC and DC motor. DC motors have better starting moment than AC motors. In addition, DC motors have better performance than AC motors on the traction equipments. DC Servomotor is one kind of DC motor that is being used in many applications in industrial and robotic machines. In the DC Servomotor, the basic continuous feedback control is PID controller. From the view of controlling, nowadays PID controllers have been used very popular because of their simplicity in structure, robust performance in a wide range of operating conditions, and easy implementation [64]. Nevertheless, The PID controllers are not enough adaptation [38] especially when the load is changed or there is noise in the system. In these cases, we should re-tune or re-design the PID controller to be satisfied with the new conditions.

To overcome these weak points of PID controller, in 1965 Lotfi Zadeh first introduced the Fuzzy Logic tool. This is a mathematical method to deal with imprecise data and vague statements by providing a mechanism to present the

linguistic constructs such as "many", "low", "high", etc. [52]. It uses probability theory to measure whether these events will happen or not. Besides, by imitating the rule-of-thumb thought of human beings about the system, the FLC can be replaced for the controller that is built based on precise mathematical computation about the system [45]. Until now, there are many researches have implemented to evaluate the good points of FLC and also compare to the PID controller [45], [19] and [37]. These researches show some advantages of using FLC as follows: the FLC does not need the mathematical model of the system; better possibilities compared to the PID controller in noise rejection, flexibility and sensitiveness to inertia variation.

In addition to the above advantages, the FLC also has disadvantages: because the FLC is built based on the tedious trial and error process, the accuracy and building time depend on the operator's experience on the system. And mostly it is a time-consuming process. In Ref(s). [50], [44], [9], [41], [13], [14] and [35] represent methods of using Genetic Algorithms for auto-tuning FLC to overcome the weak points. GA's are proven to provide robust search in complex space [18]. They are numerical search methods that mimic the process of natural selection. Besides, when implementing optimization or auto-tuning the FLC there are four factors that can be tuned: input scale factor, output scale factor, Membership Functions (MF)s and Control rules (rule-base). Rahul Malhotra et al. [44] employed Genetic Algorithm for tuning MFs and Rule-Base of fuzzy logic controller for speed control of DC motor. The simultaneous optimization of FLC, by using Genetic Algorithm application, shown encouraging results [41]. In addition to using Genetic Algorithm to optimize FLC, there are also other algorithms: Danilo Pelusi used Genetic Algorithm [14] and then combined Genetic Algorithm with Neural Networks [13] to optimize the FLCs that are used in solving the problem of electrical signal frequency driving for signals acquisition experiments, second order control system, respectively. Bouallegue [49] used particle swarm optimization approach to tune PID-type FLC structure and successfully applied on an electrical DC drive speed control. These researches got good results. However, most of them did not take tuned time into account. In fact, the number of generation and chromosomes are quite big. As a result, the required time for tuning

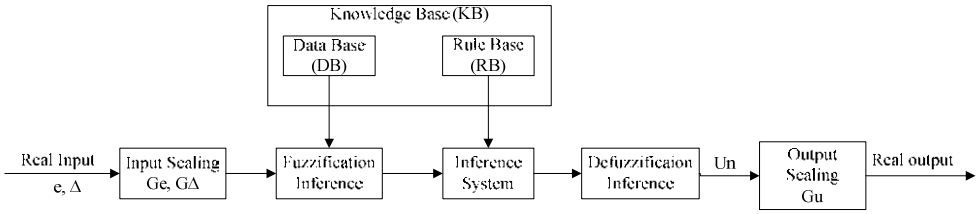

Figure 5.11: Structure of a Mamdani Fuzzy Logic rule-based system.

is long. Moreover, when implementing DC Servo motor sizing, researchers often used some speed profiles [57] such as triangular, trapezoidal profile. Therefore, tuning DC Servomotor based on its speed profile coordinating with using genetic algorithm seem to be a new reasonable approach to optimize the FLC with faster convergence.

This section proposes a new method to auto-tune Fuzzy Logic Controller (FLC) used for control DC Servomotor. This method bases on the motor's speed profile and Genetic Algorithm to tune Rule-Base and Membership Functions, respectively.

The remainder of this chapter is organized as follows: the basic concepts of FLC and GA are described in the section 2. Section 3 explains the proposed Fuzzy Logic Control Genetic Algorithm (FLCGA). Sect. 4 shows the experiment on the DC Servomotor, results and discussion. Finally, Sect. 5 are some conclusions.

5.6.2 The Fuzzy Logic Controller and Genetic Algorithms

5.6.2.1 The components of Fuzzy Logic Controller

The FLC system uses fuzzy logic rules to establish a control mechanism to approximate expert perception and judgment under given conditions. The system is also known as fuzzy inference system or approximate reasoning system or expert system. The structure of FLC can be described in the Figure 5.11. The main parts of FLC include:

- **i)** Input Scaling or normalization: the current physical values of state variables i.e., which are often error (e) and change of error ($\triangle$), are mapped

into normalized values by Scaling factor G_e and $G_{\triangle}$.

- **ii)** Fuzzification: each crisp current process state values (e and $\triangle$) is converted to a fuzzy set to make it compatible with fuzzy set of process variable in the rule-antecedent.
- **iii)** Inferencing (inference engine): The fuzzified input values are transferred to the inference engine to evaluate the control rules stores in rule-based. And the result of this evaluation is a single fuzzy set or several fuzzy sets. Generally, logic rules which are the main facts to compose inference engine use AND (taking minimum value) or OR (taking maximum value) operators.
- **iv)** Deffuzzication: defuzzification converts inference results of all active logic rules into a single crisp value in normalized domain. Defuzzification often use the maximum membership method, center of average method or center of gravity method.
- **v)** Output scaling or denormalization: the defuzzified normalized control output (u_N) is mapped into physical value (u) by the output scaling factor G_u.

GAs are search algorithms which use principles inspired by natural genetics to evolve solutions to problems [15] and [16]. GAs include three major operators: selection, crossover, and mutation, in addition to four control parameters: population size, selection, crossover, and mutation rate [44]. The idea is to maintain a population of chromosomes (representing candidate solutions to the concrete problem being solved) that evolves over time through a process of competition and controller variation. The flow chart as in Figure 5.12 of genetic algorithm is described bellow.

- [**Initial Population**]. GA starts with generating a random population of n chromosomes (suitable solutions for the problem). The population is composed by binary or real coded string chromosomes.

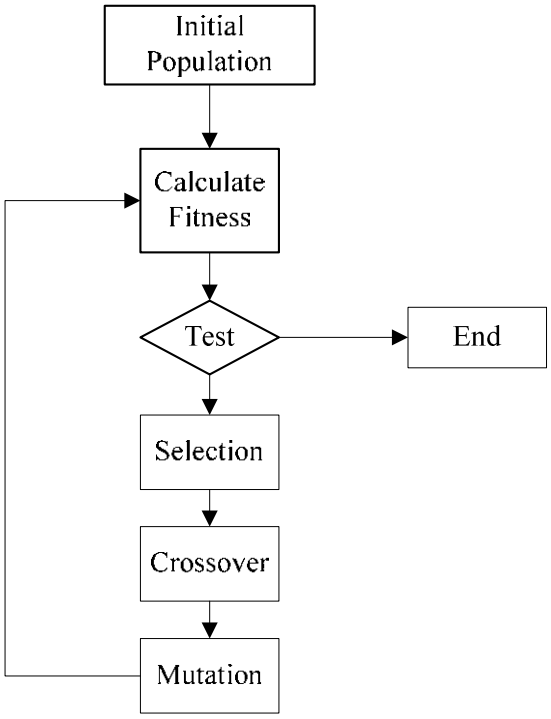

Figure 5.12: The flow chart of genetic algorithm.

- [**Calculate Fitness**]. Evaluate the fitness value of each chromosome in the population.

- [**Test**]. If the end condition is satisfied, Stop, and return the best solution in the current population.

- [**New population**]. If the condition is not satisfied, a population is generated by following the steps below until a new population is complete.
  - **i**)[**Selection**]. Selects two parent chromosomes from a population according to their fitness (the better fitness, the bigger chance to be selected).
  - **ii**)[**Crossover**]. With a crossover probability, cross over the parents to generate new offspring. If no crossover was performed, the offspring is copied exactly the parents.

– **iii**)[**Mutation**]. with a mutation probability, mutate new offspring at each locus.

5.6.3 A new DC motor tuning method - FLCGA Algorithm

In the new tuning method, we implemented to tune the FLC through 2 consecutive steps. First, we tuned rule-base of FLC based on the motor's velocity profile. The goal of this step is to get proper speed profiles of the motor with different reference values. Secondly, we applied genetic algorithm which is coded by a new, simple method, to tune membership functions of the FLC.

For the Mamdani fuzzy logic controller, we use AND operator for inference engine and the centre of gravity defuzzification formula:

$$\mathrm{u} = \frac{\sum_{\mathrm{i}=1}^{\mathrm{m}} \mathrm{m_k} \mu_{\mathrm{Bk}}(\mathrm{u})}{\sum_{\mathrm{i}=1}^{\mathrm{m}} \mu_{\mathrm{Bk}}(\mathrm{u})} \tag{5.2}$$

With mk the centre of fuzzy output set Bk, k = 1, 2...m is the fuzzy output variable. Using the maximum inference engine:

$$\mu_{\mathrm{Bk}} = \max(\mu_{\mathrm{R1}}, \mu_{\mathrm{R2}}, ..., \mu_{\mathrm{Rr}}) \tag{5.3}$$

Where r is the total of candidate rules, Ri is membership function of rule Ri.

5.6.3.1 Rule-Base tuning using DC Servomotor Speed profile

In order to design an optimized FLC, we defined the initial rules of **Table 5.1** in according to with [10]. The linguistic variables are defined as: **NB**: Negative Big, **NM**: Negative Medium, **NS**: Negative Small, **ZE**: Zero, **PS**: Positive Small, **PM**: Positive Medium, **PB**: Positive Big.

The step response is supposed to be divided into 2 stages as in Figure 5.12: the first stage is increasing stage (ST1) of velocity and the other is decreasing stage

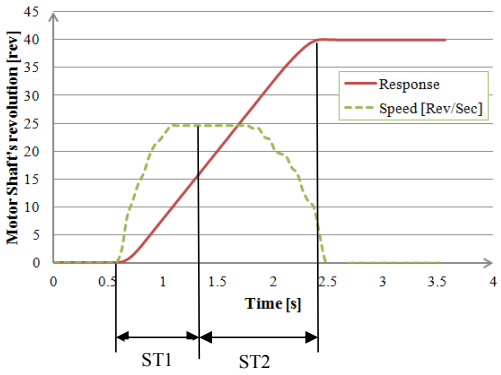

Figure 5.13: Assumption step response

u		Error (e)						
		NB	NM	NS	ZE	PS	PM	PB
Change of Error (ce)	NB	NB	NB	NB	NM	NS	NS	ZE
	NM	NB	NM	NM	NM	NS	ZE	ZE
	NS	NB	NM	NS	NS	ZE	PS	PM
	ZE	NB	NM	NS	ZE	PS	PM	PB
	PS	NM	NS	ZE	PS	PS	PM	PB
	PM	NS	ZE	PS	PM	PM	PM	PB
	PB	ZE	PS	PS	PM	PB	PB	PB

Table 5.1: Initial Rule-Base

Linguistic variables	NB	NM	NS	ZE	PS	PM	PB
Coded value	0	1	2	3	4	5	6

Table 5.2: Coded value of linguistic value

of velocity (ST2) as in Figure 5.13 [28]. In the first stage, the speed of the motor increases to the maximum speed of motor that depends on the load, bearing friction etc. and then stabilize with this speed until the end of this stage. The terminative point of this stage is at around 40% of the reference value, this point can be changed fluctuating around the 40% of the reference value because this point belongs to a fuzzy set of the FLC. The second stage continues to stabilize the motor's maximum speed until the point of around 60% reference value and then reduce to get the stable speed of zero.

The Figure 5.14 shows the Rule-Base tuning algorithm of FLC. The dash line is to tune the first stage and the continuous line is for the second stage. The missions of *GetMinimumVoltage()* function are to get the minimum requirement voltage of the motor to achieve the maximum speed and to count the minimal

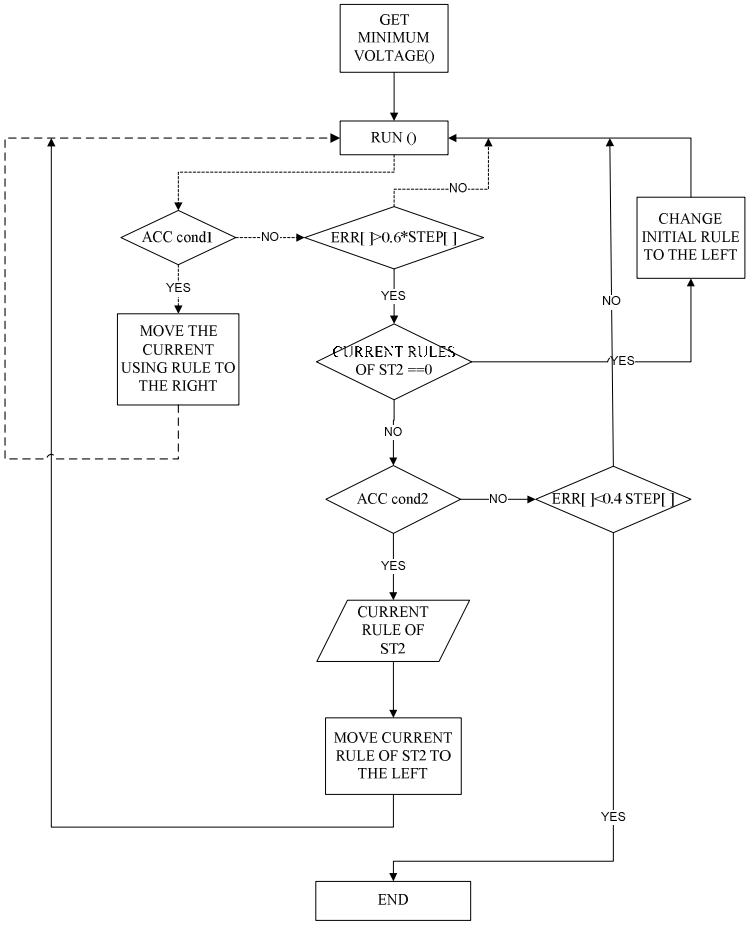

Figure 5.14: Rule-Base tuning algorithm for increasing step.

acceleration time of the motor. The acceleration condition 1 (ACCcond1) is that the motor's acceleration is negative or the acceleration time is more than the minimal acceleration time. In the stage 2, in order to get the reducing speed the ACCcond2 is the acceleration is positive. In this loop, if after some repeated loop but the error is still bigger than 40% of the reference value and the CURRENT RULES OF ST2 equals to "0" (coded value which stands for NEGATIVE BIG (**NB**) in Rule-Base as Table 5.2 we have to CHANGE INITIAL RULE TO THE LEFT (for example the coded value change from "6" to "5", "5" to "4" etc.). This means, some rules that are used at the stage 1 have to move to the left and then the process is implemented again.

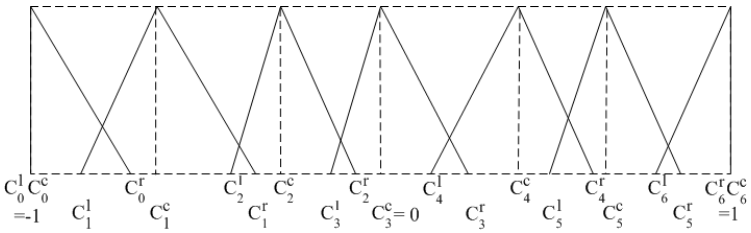

Figure 5.15: Fuzzy sets on a premise.

5.6.3.2 Tuning Membership Function using GA

When implementing a simple genetic algorithm a number of issues must be handled [6], these include the coding procedure, the selection , crossover, mutation.

5.6.3.3 A new encoding method for membership functions

The membership functions show the fuzziess degree in a premise. However, the main feature of membership function is their overlapping capability rather than their shapes precision [41]. Consider a triangle fuzzy member and its parameters are C^{kr}, C^{kc} and C^{kl}, respectively, represent the coordinates of right anchor, cortex and left anchor of k_{th} linguistic degree. In addition, as mention above we divide each universe of discourse into 7 linguistic variables. Therefore, we need 21 parameters to represent each Input or Output premise. Furthermore, without loss of generality, we assume that the first and the last degrees of fuzzy number are left- and right- skewed triangles, respectively. It is noticed that the first, last and center anchor of each universe of discourse are -1,1 and 0 respectively and they need not to be tuned. As a result, to represent each premise we need 16 parameters. Additional constraint are inposed: $C^{kr} \geq C^{kc} \geq C^{kl}$, and the condition to prevent overlapped membership functions [8] we express a typical premise of input or output as Figure 5.15 or as in Formula 5.4.

$$\begin{aligned} C_0^{kl} = C_0^{kc} = -1 \leq C_1^{kl} < C_0^{kr} \leq C_1^{kc} \leq C_2^{kl} < ... \\ \leq C_3^{kc} = 0 \leq ... \leq C_6^{kl} < C_5^{kr} \leq C_6^{kr} = C_6^{kc} = 1 \end{aligned} \tag{5.4}$$

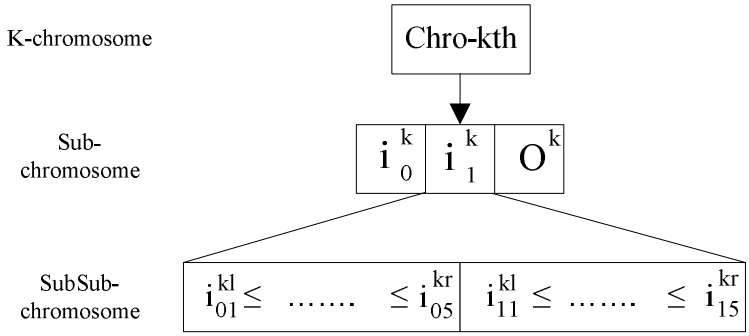

Figure 5.16: Encoding method for Membership functions.

From the condition Formula 5.4, we suggest a simple way to achieve the of parameters' values at initial time to generate the first generation is that in each current range of universe of discourse, [0,1] for example, we randomly select 8 values and rearrange that values following the increasing trend. These increasing values after that are assigned to the parameters form C_1^{kl} to C_5^{kr}. The process of rearrangement is also reperformed after each generation. In addition, in the FLC to control DC Servomotor we choose 2 inputs and 1 output. Therefore, to tune the membership functions, we have to encode 2 input premises and 1 output premise in each chromosome as in Figure 5.16. In the other side, we divide each chromosome into sub- and subsub-chromosome. This method reduces the computational time, time to converge as well compared to the encoding method suggest in Ref(s).[32] and [62].

The Figure 5.16 describes a k − th chromosome structure. Each k − th chromosome includes 3 Sub-Chormosomes which are 2 inputs Sub-Chromosome i_0^k, i_1^k, 1 output Sub-Chromosome o^k. For each Sub-Chromosome, it is partitioned into 2 SubSub-Choromosome that are negative portion: $i_{01}^{kl}...i_{05}^{kr}$ and positive portion $i_{11}^{kl}...i_{15}^{kr}$.

5.6.3.4 GA operators

Crossover and Mutation: The crossover technique used in binary genetic algorithm is a simple crossover technique [22]. The part of this reproduction mecha-

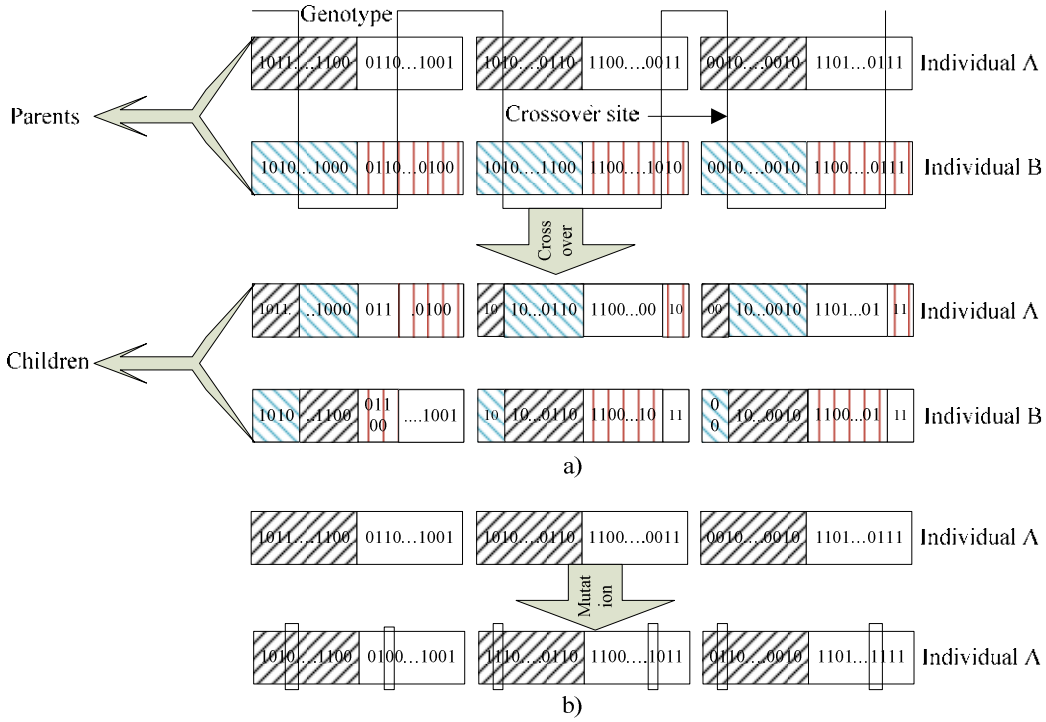

Figure 5.17: Simple crossover operator and mutation operator of the genotypes.

nism is governed by an initiating probability p_1. The crossover process is implemented in each SubSub-Chromosome as in Figure 5.17a.

In order to diversify the genotype strings, mutation operator is performed in each SubSub-Chromosome with mutation probability as in Figure 5.17b.

Selection: The capacity to survive of each individual is evaluated through the cost function. The integral of absolute error (IAE) 5.5 is the cost function which is used to measure the system performance since it is known to give better all round performance indicator of a control system response [50].

$$\mathrm{IAE} = \int_0^\infty |\mathrm{e(t)dt}| \tag{5.5}$$

To evaluate the performance of the DC Servomotor, we compare the minimum value of the cost functions to get the minimal value.

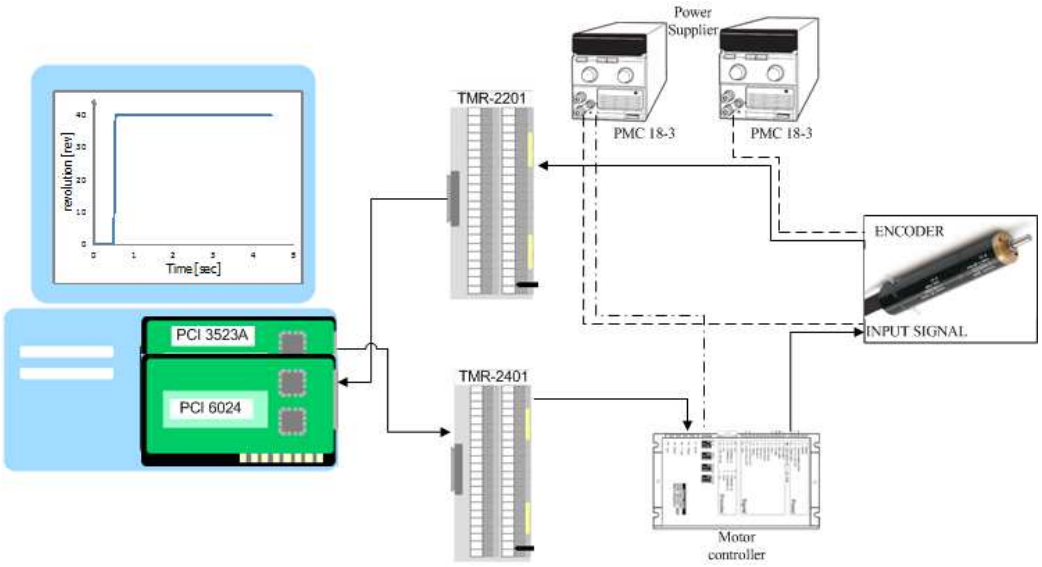

Figure 5.18: Experiment model to control a DC Servomotor.

5.6.4 Experiments and results

5.6.4.1 Experimental setup and method

In order to analyze and verify the FLCGA algorithm, we used the FLCGA to optimize the FLC to control a DC Servomotor. The experimental model is shown in Figure 5.18.In this, the PCI 6024 is a PCI pulse counter board to measure the number of revolutions of motor shaft. And the PCI 3523A is a 12-bit analog Input/Output board that is used to perform AD/DA conversion. The dash or dash-dot lines are the energy transmission for the Encoder HEAL 5540 and the motor controller. The motor RE 35-273752, which is attached a 4.8 :1 reduction ratio Gearhead, is controlled by a Maxon Motor controller of AD 50/5. Two power supplies are PMC 18-3 which are set up based on the specification of the encoder, motor controller and motor. The continuous lines are the signal lines to get the current revolution of the motor shaft and to control the motor.

Firstly, we divided the universe of discourses into 6 equal fuzzy sets and run the first stage of FLCGA. The experiments are implemented in different reference values from 20 to 40 which represent the different fuzzy sets. Next, the second stage of optimization using FLCGA is done to optimize the membership functions

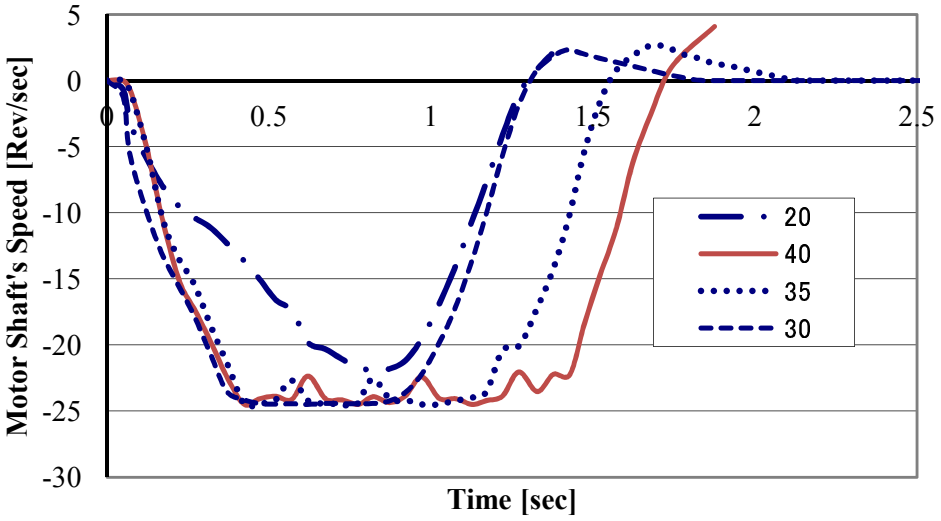

Figure 5.19: Speed response after the 1st stage.

of the FLC.

5.6.4.2 Experiment results by FLCGA

u		Error (e)						
		NB	NM	NS	ZE	PS	PM	PB
Change of Error (ce)	NB	NB	NB	NB	NB	ZE	PM	PM
	NM	NB	NM	NM	NM	NS	PM	PM
	NS	NB	NM	NS	NS	ZE	PS	PS
	ZE	NM	NM	ZE	ZE	NS	PM	PB
	PS	NS	NS	PS	PS	PS	PM	PB
	PM	NS	NB	ZE	PM	PM	PM	PB
	PB	NS	NS	ZE	PB	PB	PB	PB

Table 5.3: Optimized Rule-Base

After running the first stage, we collect the speed responses of the motor as in Figure 5.19 for the different angles of reference values as well as the optimized

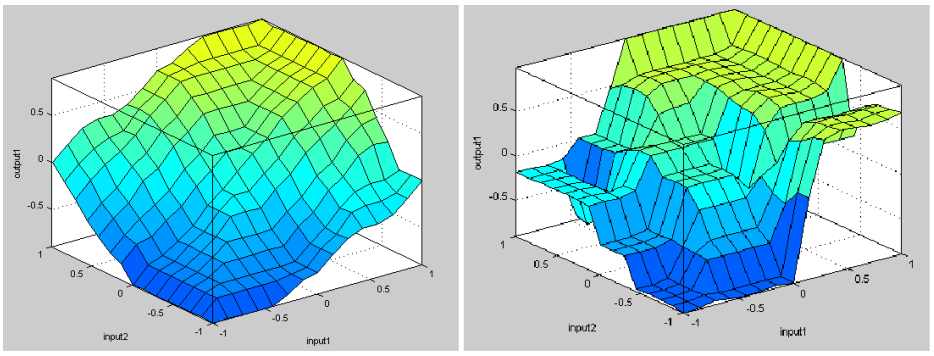

a) b)

Figure 5.20: Fuzzy Rule Base surface at the first (a) and after the second stage (b) generated by the FLCGA.

Rule-Base as in Table 5.3. The maximum speed of the motor in this case is the no load speed:

$$n_0 = \frac{7070}{4,8.60} = 24.5[\text{rev/sec}] \tag{5.6}$$

With 7070[rev/min] is no load speed of motor RE 35-273752.

After completing the first stage, the second optimal stage is performed with a population size is 16 chromosomes, number of generation is 12, gene length is 8 bits, selection rate is 0.5, crossover rate is 0.5 and mutation rate is 0.005. The convergence speed of the proposed FLCGA algorithm is very fast as in Figure 5.22. More specifically, the Table 5.5is the convergence speed comparison between the proposed algorithm with some other algorithms. The Figure 5.20a and Figure 5.20b are respectively the Fuzzy Rule-Base surface at the first stage and after second stage of using FLCGA algorithm, respectively. Figure 5.21 is optimal membership functions .

Next, the Figure 5.23 and Table 5.4 are step response comparison between the FLCGA and PID controller. The proposed FLCGA has better settling time, rise time compared to PID controller. In the Figure 5.23, it can be seen that for both cases of optimized FLC and conventional PID controller the rise times are

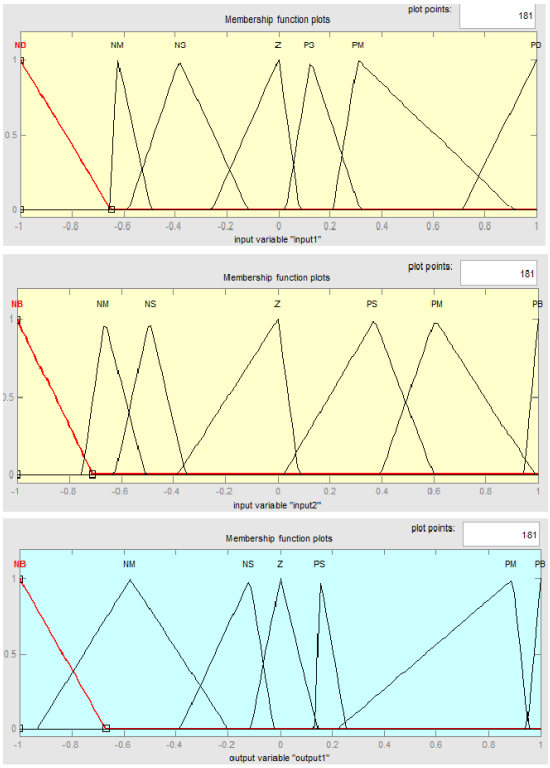

Figure 5.21: The optimized membership functions.

almost the same, because the speed of the actuator in both cases are maximum. However, the optimized FLC has better settling time due to it has finer controller comparing to the PID.

5.6.4.3 Discussion for improving the FLCGA algorithm

It is necessary to improve the accuracy of tunning Rule-Base by properly following the motor speed's profile. In the current research we use the 40% and 60%

	PID	**FLCGA**
Settling time [s]	2.8	2.267
Rise time [s]	1.85	1.767
Overshoot	0.0021	0.00216

Table 5.4: Comparison between PID and FLCGA.

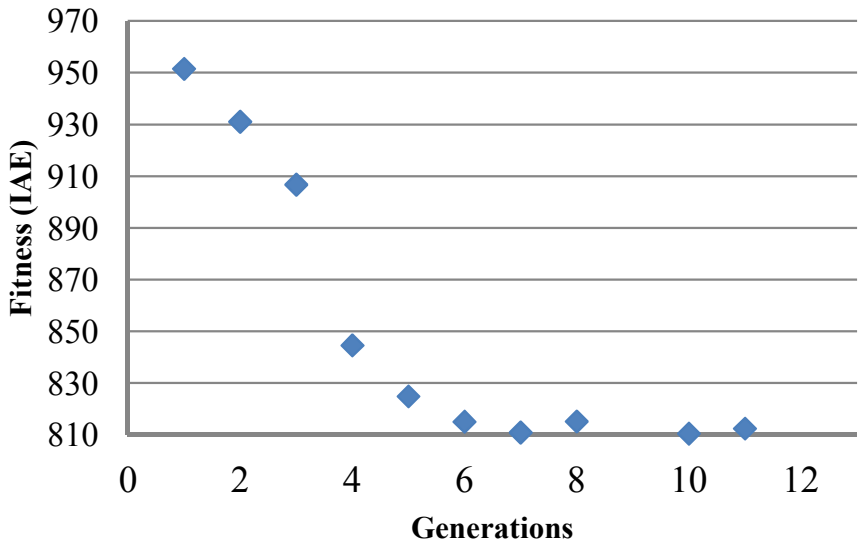

Figure 5.22: Convergence properties of the proposed FLCGA algorithm.

	Algorithm				
	GA [7]	GA [9]	GA [14]	PSO [15]	**FLCGA**
Generations	300	100	100	30	**12**
Chromosomes	30	72	40		**16**

Table 5.5: Comparison the convergence speed between the proposed algorithm with some other algorithms.

reference value to divide the response process into 2 stages. However, it may be better if we divide and tune the speed response into 3 stages which include acceleration, constant speed and deceleration stage. To be able to do this, we need determine the times that are the end of increasing speed and starting point to decrease motor's speed.

5.7 Conclusion

This chapter presented two main mission. The first one is experiment to evaluate the AFO system in some special cases. And the other one is the proposed FLC

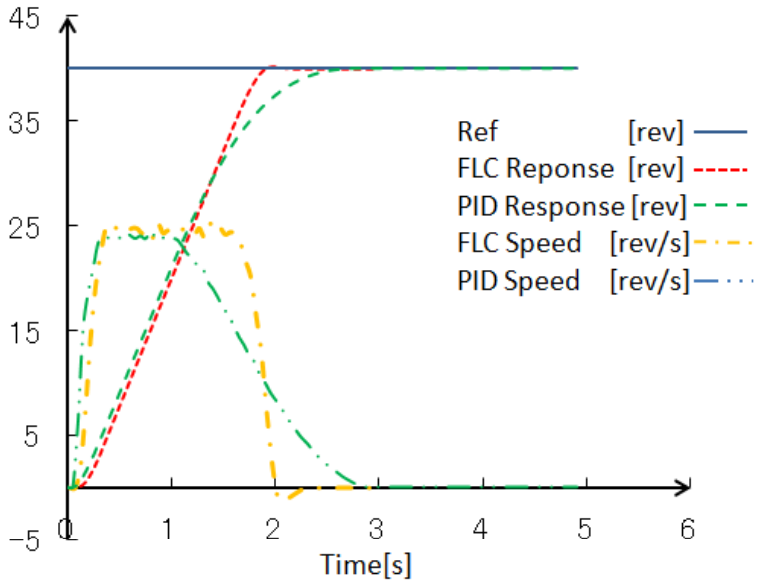

Figure 5.23: Step response of PID and FLCGA.

tuning method to control DC Servomotor.

In order to evaluate the system, firstly it was tested on a frame without load to check as well as to prevent unexpected situations could happen during testing. In this testing, the CSM was closed at forefoot position to check the foot drop prevention possibility since this is most important task for this AFO, besides the process of controlling forefoot point takes longer time compared to the rearfoot one. The test results of the ankle angle showed that the AFO successfully follows the Sine as well as the normal walking input signals. The delay time between the reference and response, however, increases when reducing the gait cycle. Another problem when using testing model is to check the ON/OFF controlling model for the solenoids. By checking and tuning, we suggested to reverse the motor about 200 ms in order to release the clutch from bevel gear during changing state.

The experiments on human test reveal the similar results as in the frame test. The controlling process for ankle joint can be done well from PP of stance phase and swing phase. However, due to the stroke length of ON/OFF clutches as well as the heavy load, the operation of SCM was not stable and need to be improved. Also, the CoP movements results shows some improvement when wearing the

AFO with turning on the motor comparing turning off. Although the novel AFO did not move well at changing state time, it provide force at PP of TST, absorb and energy at IST, and be able to control to prevent foot drop at swing phase.

Relating to control method, this chapter proposed a novel tuning method for FLC which is normally used in complex system, of system which is difficult to find transfer function, nonlinear system... With a novel encoding for membership function as well as the new method that is based on motor's speed profile to tune rule-base, the proposed method proved the improvement in convergence speed as well as the better performance of FLC compared to the PID controller. However, when considering the experimental procedures, the method still need quite long time and was not applied on the system.

Chapter 6

Conclusion and future works

6.1 Conclusion

A novel active ankle orthosis with one DoF was built and tested in this research. The initial idea is based on the COP movement during locomotion, then the system used **one DC Servo motor to attack force on two most important points of CoP: the lateral rearfoot point and the medial forefoot point** in order to control the ankle articulation. The novel AFO works like a exoskeleton, then it could both support to rotate the ankle joint and reduce the impact force during stance phase by transferring force to the ground or the shank. Especially, in this system, by dividing the sole of the AFO to the rearfoot and forefot plate, the system is able to take the metatarsal joint into consideration during the PP sub-phase. A compression spring is used underneath of heel to store and release energy during strike time. The full assembled orthosis weights 3.5 kg, has height 400 mm and a width of 150 mm. Its range of movement is [-20,30°]. The device could provide a support torque of 12 N.m to the ankle joint. This is higher than the requirement for foot positioning during the swing phase of the normal subject. Besides, because of partly supporting the weaken ankle joint during rehabilitation, it is necessary to use the BWS during the practice for the patients.

The process of design for the AFO was presented, this process is started from the initial idea to the competed 3D model with composing mechanisms: motion splitting mechanism, changing state mechanism and sole mechanism. In each of mechanism design process, several proposals were suggested and discussed to choose the suitable one. Finally, AFO experiments were performed on the fabricated orthosis. To evaluate the system, firstly it was tested on a frame without load to check as well as to prevent unexpected situations could happen during testing. In this testing, the CSM was closed at forefoot position to check the foot drop prevention possibility since this is most important task for this AFO, besides the process of controlling forefoot point takes longer time compared to the rearfoot one. The test results of the ankle angle showed that the AFO successfully follows the Sine as well as the normal walking input signals. The delay time between the reference and response, however, increases when reducing the gait cycle. Another problem when using testing model is to check the ON/OFF controlling model for the solenoids. By checking and tuning, we suggested to reverse the motor about 200 ms in order to release the clutch from bevel gear during changing state.

The experiments on human test reveal the similar results as in the frame test. The controlling process for ankle joint can be done well from PP of stance phase and swing phase. However, due to the stroke length of ON/OFF clutches as well as the heavy load, the operation of SCM was not stable and need to be improved. Also, the COP movements results shows some improvement when wearing the AFO with turning on the motor comparing turning off. Although the novel AFO did not move well at changing state time, it provide force at PP of TST, absorb and energy at IST, and be able to control to prevent foot drop at swing phase.

In order to reduce burden for the instructor when controlling the nonlinear, complex or difficult identity the transfer function. A proposed tuning method for FLC was given and make experiments. The new method showed better convergence and better performance comparing PID controller. However, because the operating of the algorithm is based on the principle of optimizing then running and optimizing then the total time to optimizing still long and due to the possibility that could happen for the human with during such quite long of time.

Then this method was not applied in the system.

6.2 Future work

As a proof-of-concept prototype, several limitations exist in this design. Future work will address weight and size reduction and improve the mechanical performance.

The first and foremost is to optimize the system to make it work more stably and more naturally. Although the results of the frame test (no-load experiments) showed that the orthosis ankle has a good response, stability and repeat-ability, the experiments when wearing the system on human subject tests revealed that there are still some space to improve. In particularly, some mechanisms need to be optimized: the sole mechanims should be reduced the height then the movements from both lower limbs will be more natural, the movements of CoP will be near as the CoP of normal walking. Moreover, the tooth of clutch should be recalculated to reduce the stroke movement as well as the release, close force when changing state.

After optimizing the structure, the second work is to optimize the dimension and material to reduce the mass and dimension of the system. There are several ways to reduce the overall weight of the design orthosis. The majority of weight is located in the stainless steel components and the base to assemble the components. It is proved that some of them are unnecessary. For instance, the dimension of bevel gear now was decided since requirement space for the clutch inside them. However, after optimizing to reduce tooth as well as the stroke movement of the clutch, this space can be decreased. Also, because the rotation of gears is repeated and not full round. As a result, we do not need full of gears.

The second orthosis iteration should take torque, force evaluation into consideration. This is done by increase the number of force sensors or using force plate underneath of the AFO system. The force information is very important because it can be used both in the controlling process such as phase detection, force controller.. and used to evaluate and compare the efficiency of the system

to the other AFO. Besides, in order to avoid the broken problem, some motion simulation should be done. A stronger but smaller and lighter should be built in the next generation.

References

[1] Tamarack Variable Assist Joint. [Online]. Available:http://www.tamarackhti.com.

[2] Gait line. [Online]. Available: http://www.wefixfeet.ca/images/pdf/biomechanics.pdf.

[3] S. Aua and H. Herr. Powered ankle-foot prosthesis to assist level ground and stair descent gaits. *Neural networks Journa*, **4**(21):654–666, 2008.

[4] J. Bae, K. Long, N. Byl, and M. Tomizukai. A mobile gait monitoring system for abnormal gait diagnosis and rehabilitation: A pilot study for parkinson disease patients. *Journal of Biomechanical Engineering*, **133**(4):1–11, 2011.

[5] MI Becker Orthopedic, Troy. 2009, 2003.

[6] Titel F. Belarbi K., Bourebia W., and Benmahammed K. Design of mamdani fuzzy logic controllers with rule base minimisation using genetic algorithm,. *Engineering Applications of Artificial Intelligence,*, pages 875–885, 2005,.

[7] .J. A. Blaya. Force-controllable ankle foot orthosis (AFO) to assist drop foot gait, Master thesis at MIT, 2003.

[8] Chen C., Hong T., and Tseng V.S. A comparison of different fitness functions for extracting membership functions used in fuzzy data mining,. In *IEEE Symposium on foundations of computational intelligence*, pages 550–555, 2011.

[9] Liu C., Li B., and Yang X. Fuzzy logic controller design based on genetic algorithm for dc motor,. In *IEEE International Conf. On Electronics, Communications and Control (ICECC)*, pages 2662–2665, 2011.

[10] Mitra R. Chopra S. Fuzzy controller: choosing an appropriate and smallest rule set,. *International journal of computational cognition*, **3**(4):73–79, 2005,.

[11] C.Mummolo, L. Mangialardi, and J.H.Kim. quantifying dynamic characteristic of human walking for comprehensive gait cycle,. *Journal of Biomechanical engineering,*, **135**(9):4–10, 2013,.

[12] Interface company. User's manual PCI-3523A, Ver. 1.1.

[13] Pelusi D. Genetic-neuro-fuzzy controllers for second order control systems,. In *5th European Symposium on Computer Modeling and Simulation*, pages 12–17, 2011.

[14] Pelusi D. Improving settling and rise times of controllers via intelligent algorithms,. In *14th International Conference on Modelling and Simulation,*, pages 187–192, 2012.

[15] Goldberg D.E. Genetic Algorithms in search, optimization, and machine learning, Addison-Wesley, Reading, MA, 1989.

[16] Goldberg D.E. The Design of competent Genetic Algorithms: Steps towards a computational theory of innovation, Kluwer Academic Publishers, Dordrecht, 2002.

[17] D.P.Ferris, J. M.Czerniecki, and B.Hannaford. An ankle-foot orthosis powered by artificial pneumatic muscles. *J. Appl. Biomech.*, **21**(2):189–197, 2005.

[18] Herrera F., Lozano M., and Verdegay J.L. Tuning fuzzy logic controllers by genetic algorithms,. *International Journal of Approximate Reasoning,*, pages 299–315, 1995,.

[19] Rahmat M. F. and Ghazaly M. M. Performance comparison between pid and fuzzy logic controller in position control system of dc servomotor. *Journal Of Technology*, pages 1–7, 2006.

[20] A. Faller and M. Schuenke. " The Human Body: An Introduction to Structure and Function" [Book]. - Stuttgart : Thieme, 2004.

[21] S. Fatone. Challenges in lower-limb orthotic research. *Prosthet Orthot Int.*, **34**(3):235–241, 2001.

[22] Gilbert Syswerda G. Uniform crossover in genetic algorithms,. In *Proceedings of the 3rd International Conference on Genetic Algorithms,*, pages 2–9, 1989.

[23] G. Harris, P. Smith, and R. Marks. "Foot and Ankle Motion Analysis: Clinical Treatment and Technology:, [Book]. - New York : Taylor & Francis Group, 2008.

[24] H.Naito, Y.Akazawa, K.Tagaya, T.Matsumoto, and M.Tanaka. An ankle-foot orthosis with a variable-resistance ankle joint suing a magnetorheological-fluid rotary damper. *Jour. Of Biomechanical Sience and Engineering*, **4**(2):182–191, 2009.

[25] A. E. Hunta, R. M. Smithb, M. Torodeb, and A. Keenanc. An investigation of the centres of pressure under the foot while walking. *J Bone Joint Surg Br.*, **57**(1):98–103, 1975.

[26] A. E. Hunta, R. M. Smithb, M. Torodeb, and A. Keenanc. Inter-segment foot motion and ground reaction forces over the stance phase of walking. *jour. of clinical biomechanics*, **16**(7):592–600, 2001.

[27] S. Hwang, J. Kim, and Y. Kim. Development of an active ankle-foot orthosis for hemiplegic patients. In *1st Int. Convention Rehabil. Eng. Assistive Technol.: Conjunction 1st Tan Tock Seng Hospital Neurorehabil. Meet.*, pages 110–113, 2007.

[28] Jamaludin J., Rahim N.A., and Hew W.P. Development of a self-tuning fuzzy logic controller for intelligent control of elevator systems,. *Engineering Applications of Artificial Intelligence,*, pages 1167–1178, 2009,.

[29] K.A.Shorter, J.Xia, Elizabeth, T. Hsiao-Wecksler, and Geza F. Kogler. Technologies for powered ankle-foot orthotic systems: Possibilities and challenges. *IEEE/ASME Transactions on Mechatronics*, **8**(1):337–347, 2013.

[30] H. B. Kitaoka, X. M. Crevoisier, K. Harbst, B. Kotajarvi D. Hansen, and K. Kaufman. The effect of custom-made braces for the ankle and hindfoot on ankle and foot kinematics and ground reaction forces. *Archives Phys. Med. Rehabil.*, **87**(1):130–135, 2006.

[31] D. Knudson. "Fundamentals of Biomechanics", 2nd Edition [Book]. - New York : Springer, 2007.

[32] Baron .L, Achiche .S, and Balazinski .M. Fuzzy decision support system knowledge base generation using a genetic algorithm,. *International journal of approximate reasoning,*, **24**(2-3):125–148, 2001,.

[33] S. J. Lee and J. Hidler. Biomechanics of overgorund vs. treadmill walking in healthy individuals. *J Appl Physiol*, **104**(3):747–755, 2007.

[34] F. L. Lewis., D. M. Dawson, and C. T. Abdallah. Robot Manipulator Control Theory and Practice.

[35] Ozturk N. and Celik E. Speed control of permanent magnet synchronous motors using fuzzy controller based on genetic algorithms,. *International journal of Electrical Power and Energy Systems,*, **43**(1):889–898, 2012,.

[36] T. F. Novacheck, C. Beattie, A. Rozumalski, G.Gent, and G.Kroll. Quantifying the spring-like properties of ankle-foot orthoses (afos). *J. Prosthetics Orthotics*, **19**(4):98–103, 2007.

[37] Gundogdu O. and Erenturk K. Fuzzy control of a dc motor driven four-bar mechanism. *Mechatronics Journal*, pages 423–438, 2003.

[38] Wahyunggoro O. and Saad N. B. Ieee intl. conf. on control, automation, robotics and vision. In *IEEE Proc. Of American Control Conference*, pages 1545–1550, 2008.

[39] M. Palmer. Sagittal plane characterization of normal human ankle function across a range of walking gait speeds, Masters Thesis, Massachusetts Institute of Technology, 2002.

[40] Ion P. I. Pappas, Milos R. Popovic, T. Keller, V. Dietz, and M. Morari. A reliable gait phase detection system. *IEEE transactions on neural systems and rehabilitation engineering*, **9**(2):113–125, 2001.

[41] Shill P.C., Pal K.K., Md. Amin M.F., and Murase K. Genetic algorithm based fully automated and adaptive fuzzy logic controller,. In *IEEE International Conference on Fuzzy Systems,*, pages 1572–1579, 2011.

[42] J. Perry. " Gait Analysis: Normal and Pathological Function", [Book Section]. - New Jersey : SLACK Inc., 1992.

[43] J. Pons. "Wearable Robots: Biomechatronic Exoskeletons" [Book]. -[s.l.] : John Wiley & Sons, Ltd, 2008.

[44] Malhotra R., Singh N., and Singh Y. Design of embedded hybrid fuzzy-ga control strategy for speed control of dc motor: A servo control case study,. *International Journal of Computer Applications,*, **6**(5):37–46, 2010,.

[45] Malhotra R. and Kaur T. Dc motor control using fuzzy logic controller. *International journal of advanced engineering sciences and technologies*, **8**(2):291–296, 2011.

[46] J. B. Redford and O.Etcetera. 1986.

[47] G. K. Rose. Williams and Wilkins, 1986.

[48] J. Rose and G. J. Human. "Human Walking," 3rd Edition [Book]. - [s.l.] : Lippincott Williams & Wilkins, 2006.

[49] Boualegue S., Haggege J., Ayadi M., and Benrejeb M. Pid-type fuzzy logic controller tuning based on particle swarm optimization,. *Engineering Applications of Artificial Intelligence,*, pages 483–493, 2013,.

[50] Khan S. and et al. Design and implementation of an optimal fuzzy logic controller using genetic algorithm,. *Journal of Computer Science,*, **4**(10):799–806, 2008.

[51] Z. Safaeepour, A. Esteki, F. T. Ghomshe, and N. A. A. Osman. Quantitative analysis of human ankle characteristics at different gait phases and speeds for utilizing in ankle-foot prosthetic design. *BioMedical Engineering*, **13**(1):19–26, 2014.

[52] Sumathi S. Sivanandam S. N. and Deepa S. N. Introduction to Fuzzy Logic using MATLAB, Springer, 2007.

[53] W. Svensson and U. Holmberg. Ankle-foot-orthosis control in inclinations and stairs. In *in Proc. IEEE Int. Conf. Robot., Autom. Mechatronics*, pages 1301– 306, 2008.

[54] M. Szendroi. " Orthopedics", [Book]. - Budapest : Semmelweis Publisher, 2008.

[55] P. Tipler and G. Mosca. "Physics for Scientists and Engineers", 5th edition [Book]. - New York : W. H. Freeman and Componany, 2004.

[56] M. Vukobratovic. DYNAMIC AND ROBUST CONTROL OF ROBOT-ENVIRONMENT INTERACTION.

[57] Voss W. Copperhill Technologies Corporation, 2007.

[58] M. Whittle. " Gait Analysis: An Introduction", [Book]. - Philadelphia : Elsevier, 2007.

[59] D. Winter. "Biomechanics and Motor Control of Human Movement", Hoboken, NJ, USA : John Wiley & Sons, Ltd, 2004.

[60] D. Winter. "The Biomechanics and Motor Control of Human Gait: Normal, Elderly and Pathological" [Book]. - Waterloo, Ontario, Canada : University of Waterloo Press, 1991. - 2 ed.

[61] D.A. Winter, J. J. Eng, and M. G. Ishac. " Gait Analysis: Theory and Application", 1995.

[62] Chiou Y. and Lan L. Genetic fuzzy logic controller: an iterative evolution algorithm with new encoding method,. *Fuzzy Sets and Systems,*, **152**(3):617–635, 2005,.

[63] H. Yu, D. Wang, C. Yang, and K. Lee. A walking monitoring shoe system for simultaneous plantar-force measurement and gait-phase detection. In *IEEE/ASME International Conference on Advanced Intelligent Mechatronics*, pages 207 – 212, 2010.

[64] J. Zhang, Wang N., and S. Wang. A developed method of tuning pid controllers with fuzzy rules for integrating process. In *IEEE Proc. Of American Control Conference*, pages 1109–1114, 2004.

[65] E. Zheng, B. Chen, X. Wang, Y. Huang, and Q. Wang. On the design of a wearable multi-sensor system for recognizing motion modes and sit-to-stand transition, 2014.

List of Publications

[P.1] T. Ngueyn, T. Komeda, "Using Motor Speed Profile and Genetic Algorithm to Optimize the Fuzzy Logic Controller for Controlling DC Servomotor, International Journal of Computer Applications," *International Journal of Computer Applications*, Vol.94, No.14, pp. 1-8, 2014.

[P.2] T. Nguyen, H. Dao, T. Komeda, " A Novel Active Ankle Orthosis System: Idea and Design, Applied Mechanics and Materials Journal" *Applied Mechanics and Materials Journal*, waiting for publication.

[P.3] T. Nguyen, L. Ota, T. Miyoshi, T. Komeda, " The Powered Gait Training System Using Feedback from Own Walking Information," *The 4th IEEE BioScience and BioRobotic Conference (BRC2013)*, 18-20 Feb 2013.

[P.4] T. Nguyen, L. Ota, T. Miyoshi, T. Komeda, "A newly physical modeling tool in matlab and apply to initially model a powerd gait training system," *7th SEATUC Symposium,* 4-6 Mar, 2013.

[P.5] T. Nguyen, L. Ota, T. Miyoshi, T. Komeda, " A new tool to model physical system: Application to the powered gait orthosis system for hemiplegic patients," *e 24th IASTED International Conference on Modeling and Simulation (MS2013),* 17-19 Jul. 2013.

[P.6] T. Nguyen, H. Dao, T. Komeda, "Design and Model a Novel Ankle Foot Orthosis," *The 26th European Modeling and Simulation Symposium,* 10-12 Sep. 2014.

[P.7] T. Nguyen, H. Dao, T. Komeda, " A Novel Active Ankle Orthosis System: Idea and Design," *2014 International Conference on Mechatronics and Mechanical Design,* 26-28 Dec, 2014.

Drawings of AFO system

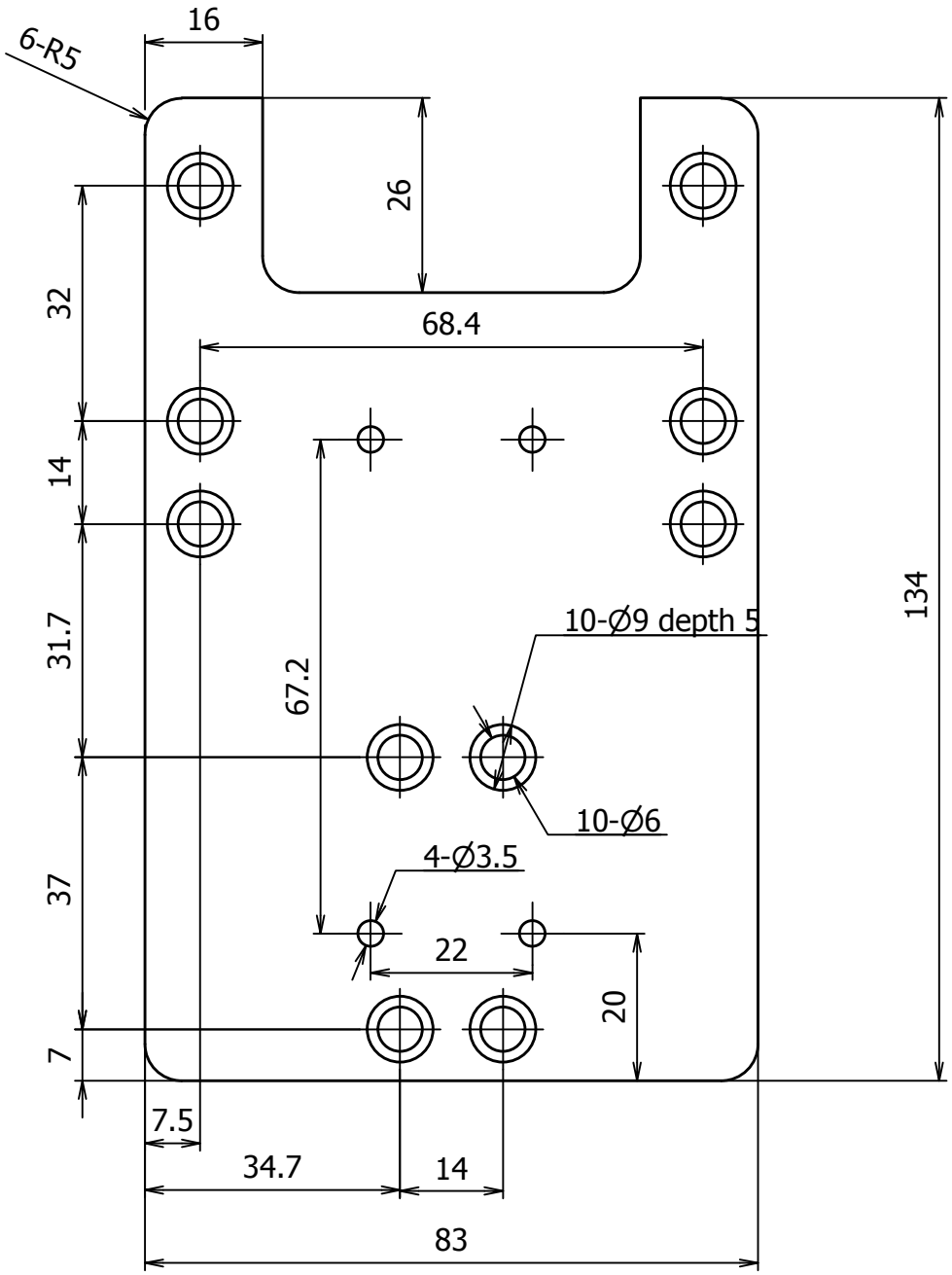

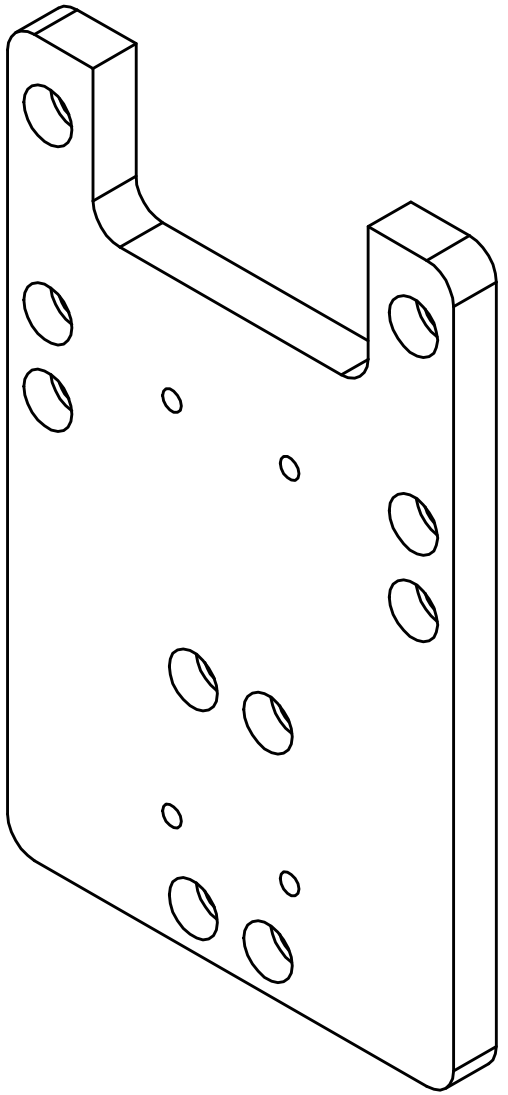

Note:
t = 8

ANKLE ORTHOSIS			SCALE 1:1	REF. DRAW. 35, 38		KOMEDA LAB	
						BASE	
Rev	Date	Description	TRUNG Author	Checked	Approved		
			MASS [Kg] 0.211	MATERIAL Aluminum-6061		PART NUMBER: 01	1 / 38
			Number of part 1				A4

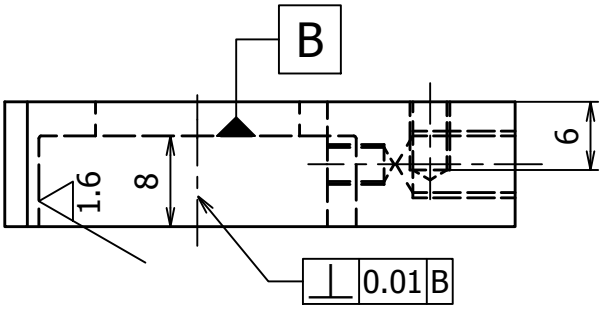

AP-AP (1.5 : 1)

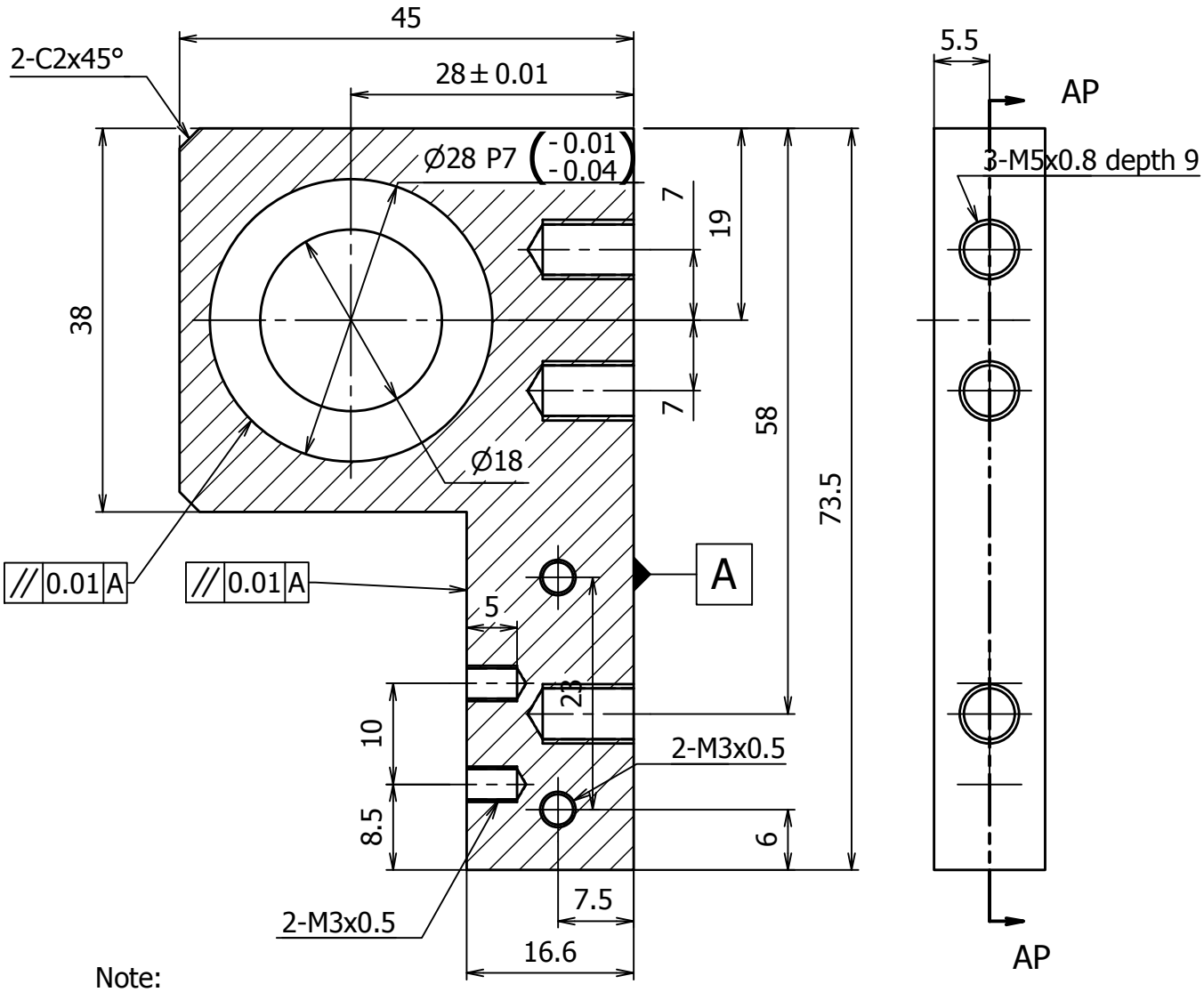

Note:

1. Hole Ø28 is assemble bearing P_03

ANKLE ORTHOSIS			SCALE 2:1	REF. DRAW. 35, 38, 46		KOMEDA LAB
						FLANGE OF REARFOOT BEVEL GEAR
Rev	Date	Description	TRUNG Author	Checked	Approved	
			MASS [Kg] 0.03	MATERIAL Aluminum-6061		PART NUMBER: 04
			Number of part 1			A4

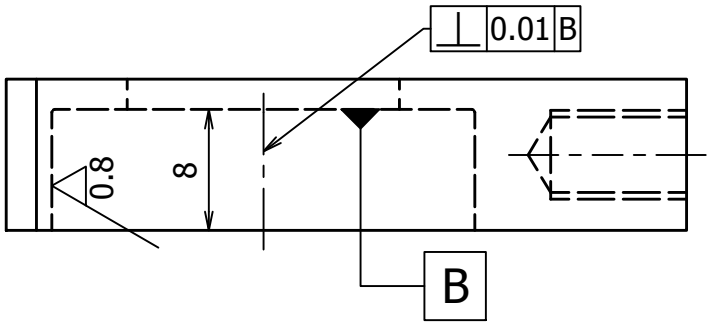

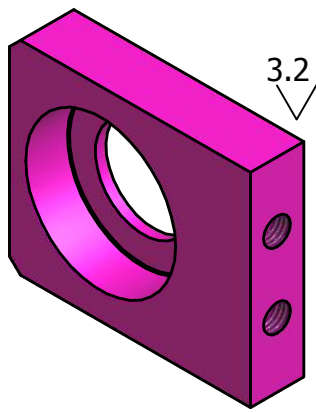

Isometric
1:1

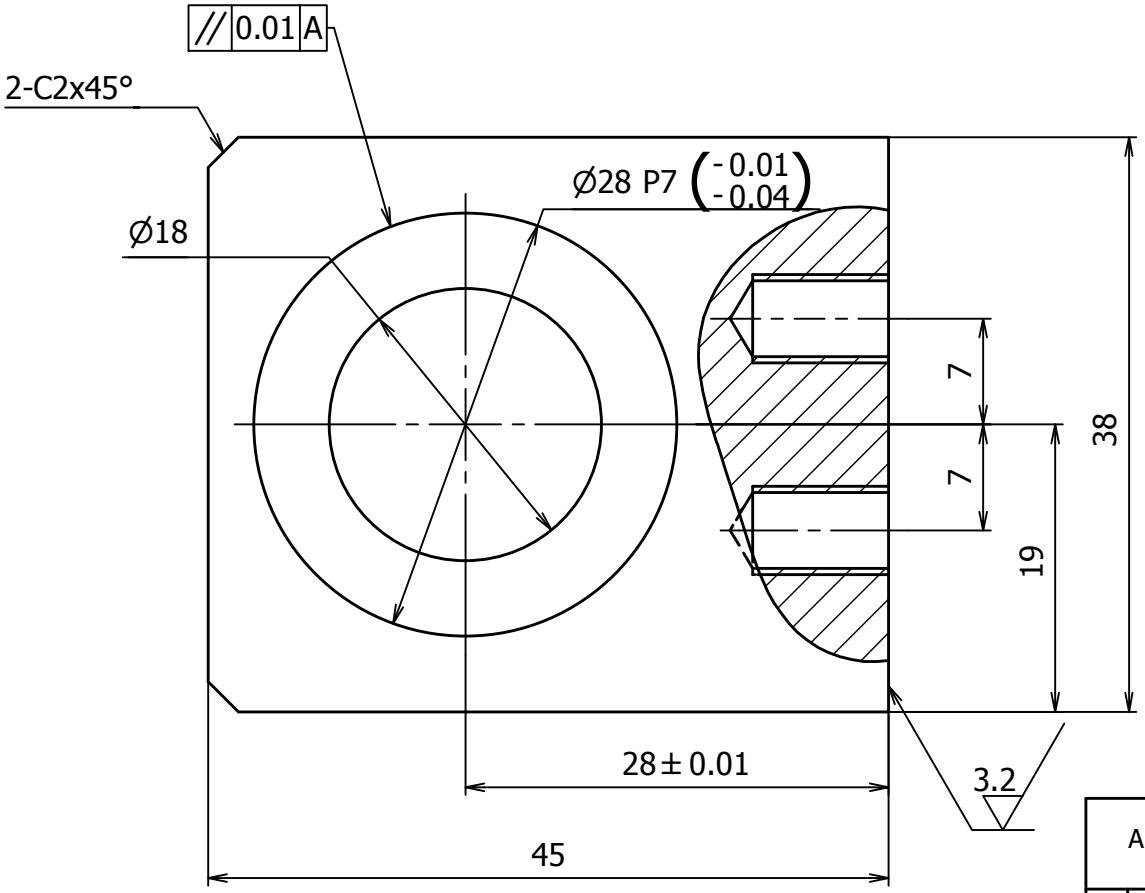

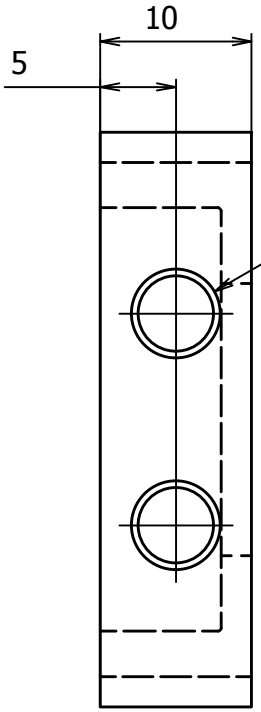

Note:

1. Hole Ø28 is assemble bearing P_03

ANKLE ORTHOSIS			SCALE 2:1	REF. DRAW. 35, 38		KOMEDA LAB	
						FLANGE OF COUPLING	
Rev	Date	Description	TRUNG Author	Checked	Approved		
			MASS [Kg] 0.0305	MATERIAL Aluminum-6061		PART NUMBER: 03	3 / 38
			Number of part 1				A4

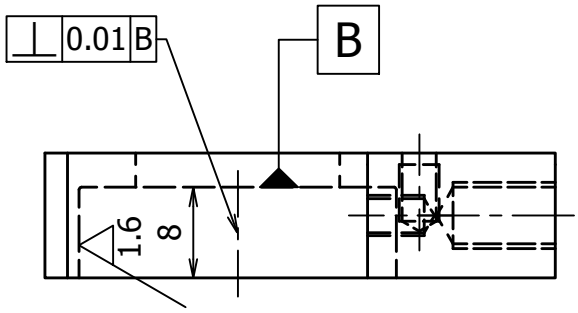

AT-AT (1.5 : 1)

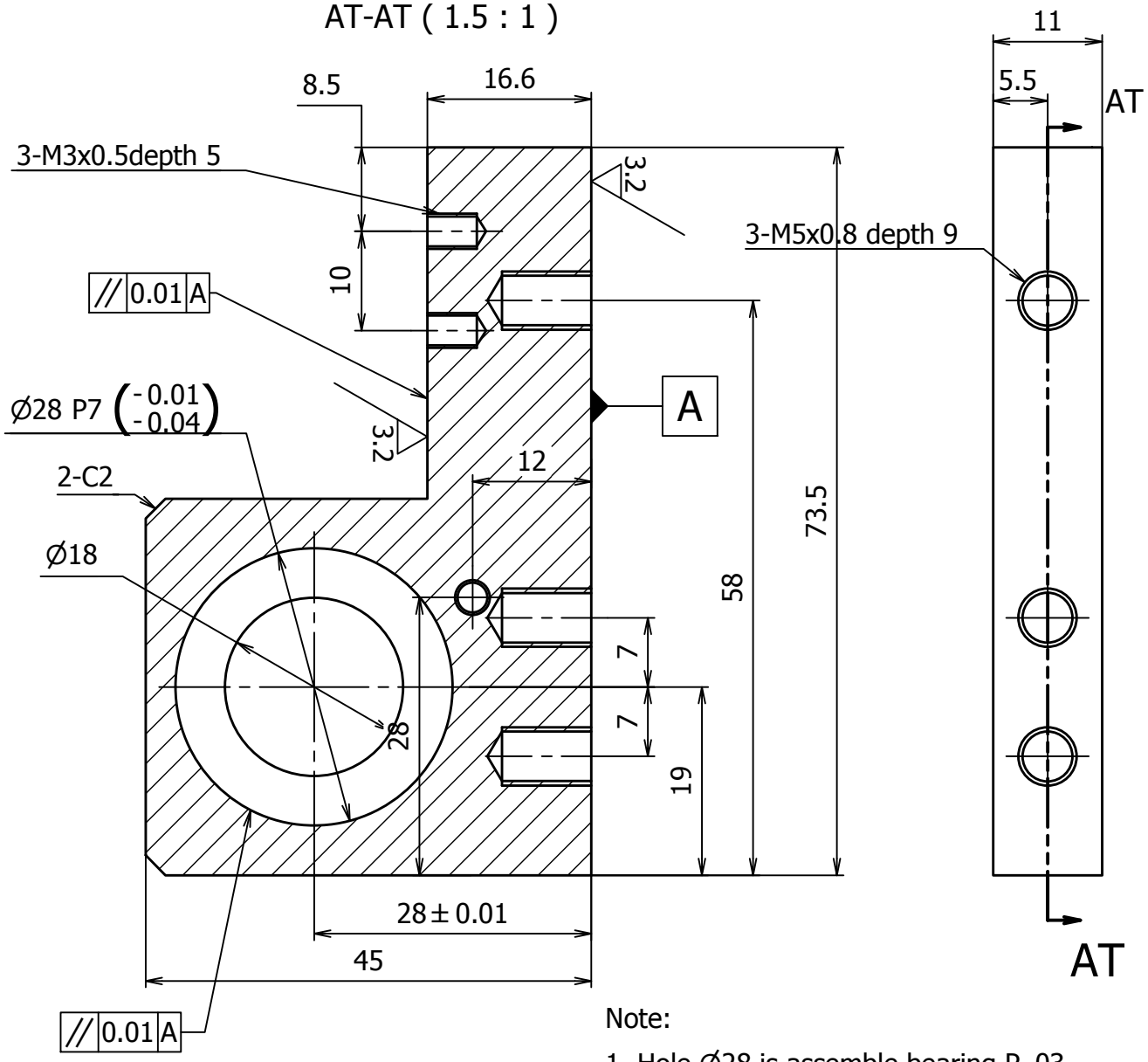

Note:

1. Hole Ø28 is assemble bearing P_03

ANKLE ORTHOSIS			SCALE 1.5:1	REF. DRAW. 35, 38		KOMEDA LAB	
						FLANGE OF FOREFOOT BEVEL GEAR	
Rev	Date	Description	TRUNG Author	Checked	Approved		
			MASS [Kg] 0.046	MATERIAL Aluminum-6061		PART NUMBER: 02	4 / 38
			Number of part 1				A4

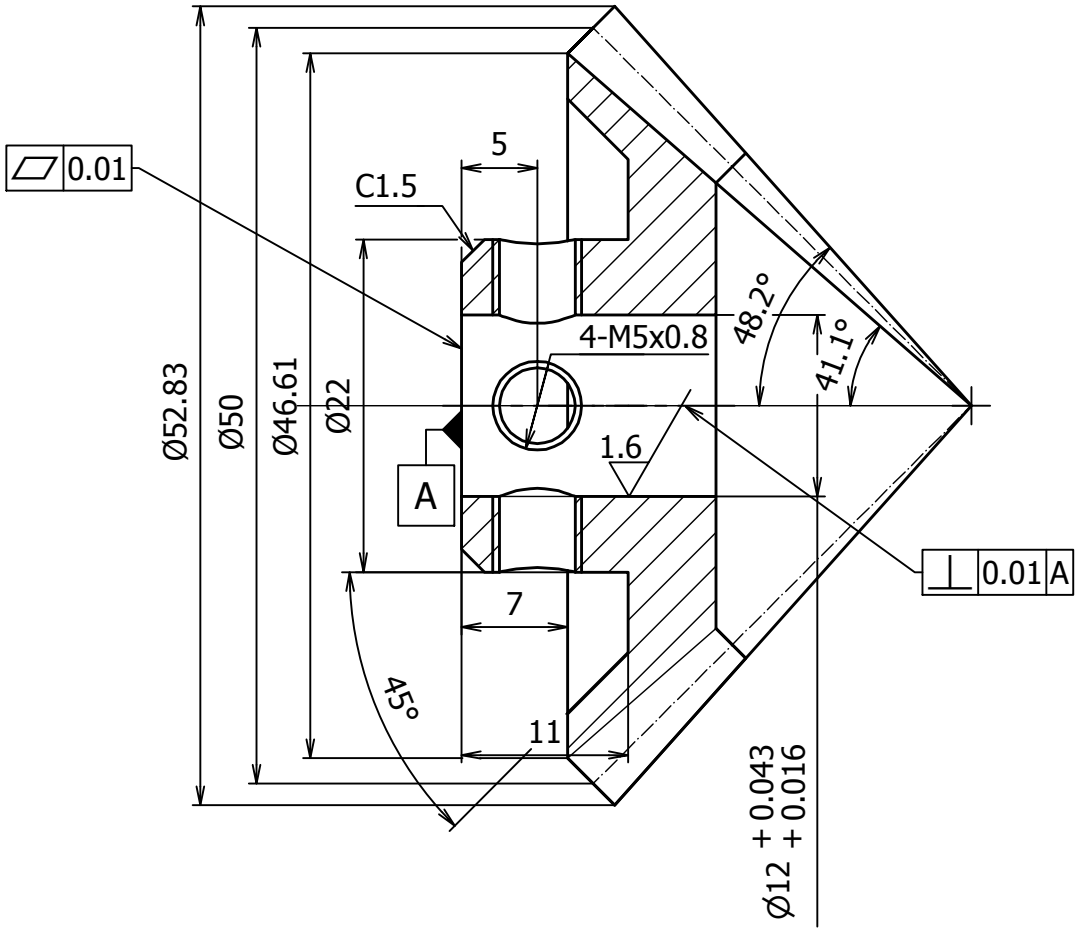

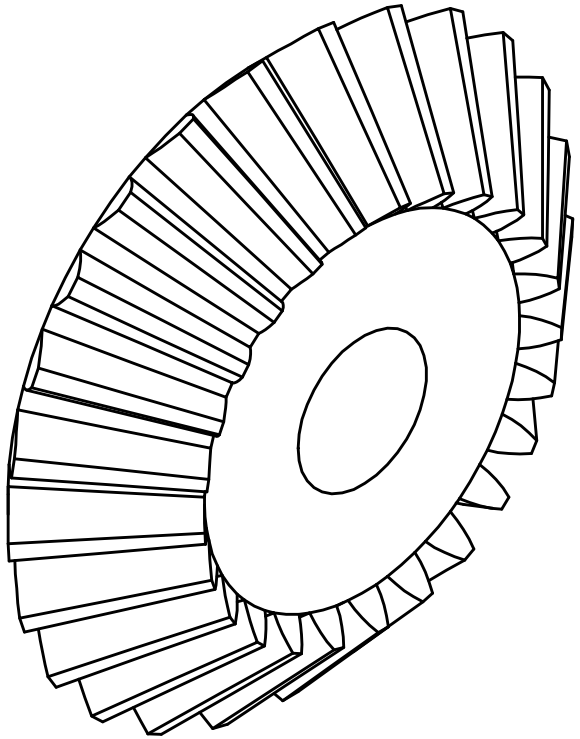

TABLE			
No.	Item	Symbol	Value
1	Shaft angle	Σ (Deg)	90
2	Module	m (mm)	2
3	Pressure angle	a (Deg)	20
4	Number of teeth	z	25
5	Face width	b (mm)	13

Note: The angle between two consecutive thread hole M5x0.8 is 90°

ANKLE ORTHOSIS	SCALE 2:1	REF. DRAW. 35, 38		KOMEDA LAB	
				MAIN BEVEL GEAR	
Rev | Date | Description	TRUNG Author	Checked	Approved		
	MASS [Kg] 0.093	MATERIAL Steel		PART NUMBER: 06	5 / 38
	Number of part 1				A4

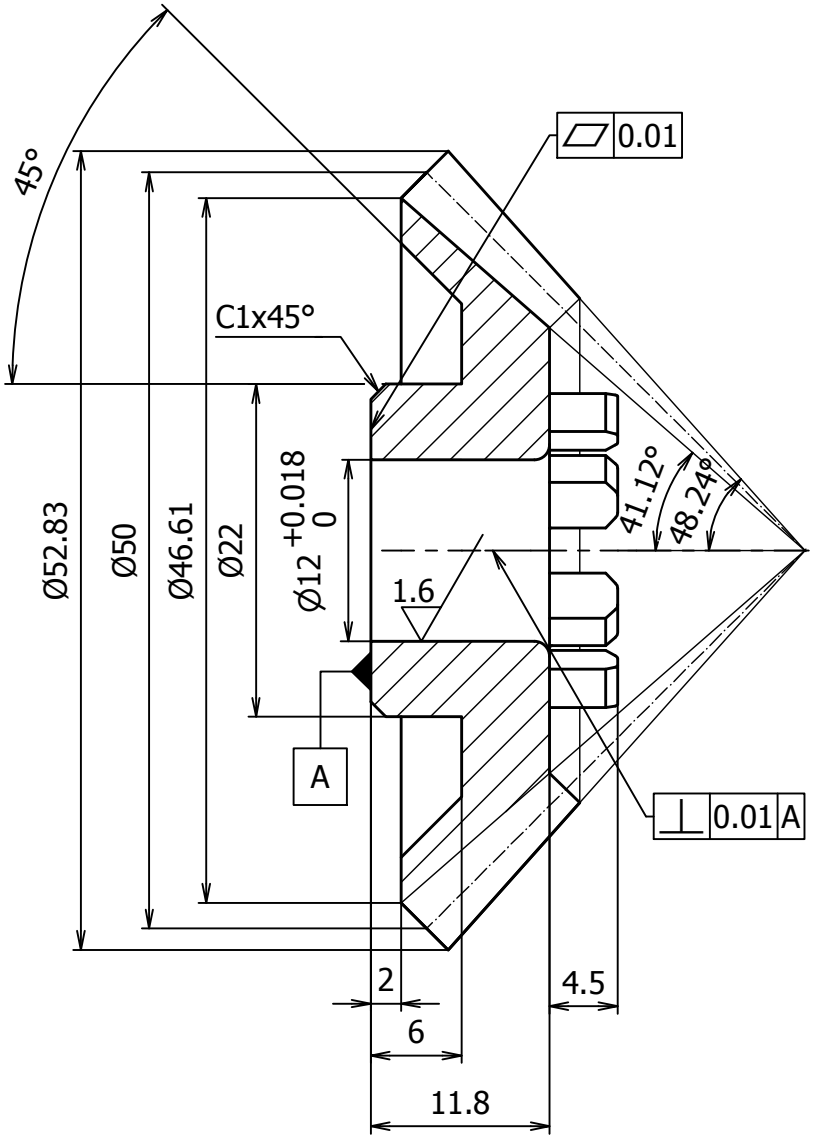

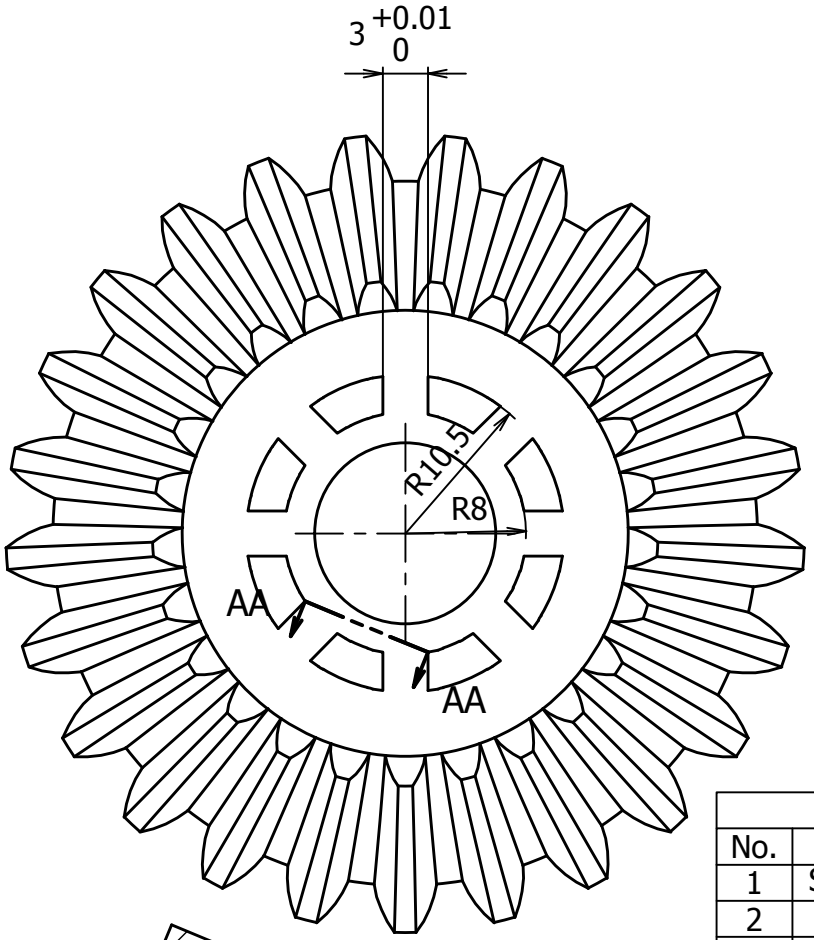

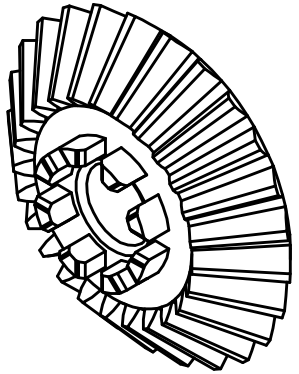

Isometric
1:1

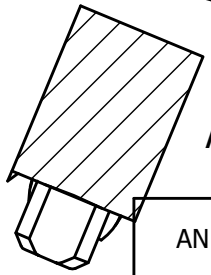

AA-AA (2 : 1)

TABLE			
No.	Item	Symbol	Value
1	Shaft angle	Σ (Deg)	90
2	Module	m (mm)	2
3	Pressure angle	a (Deg)	20
4	Number of teeth	z	25
5	Face width	b (mm)	13

Note:
Edges of shoulder to assemble clutch are chanfered with width of 0.8 mm and angle 45°

ANKLE ORTHOSIS	SCALE 2:1	REF. DRAW. 35, 38		KOMEDA LAB	
				REARFOOT BEVEL GEAR	
Rev / Date / Description	TRUNG Author	Checked	Approved		
	MASS [Kg] 0.089	MATERIAL Steel		PART NUMBER: 07	6 / 38
	Number of part 2				A4

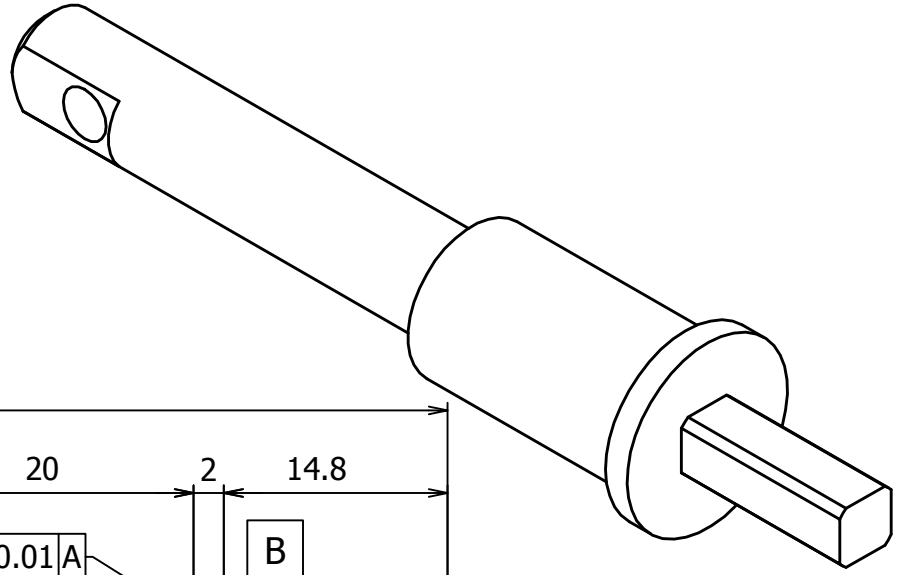

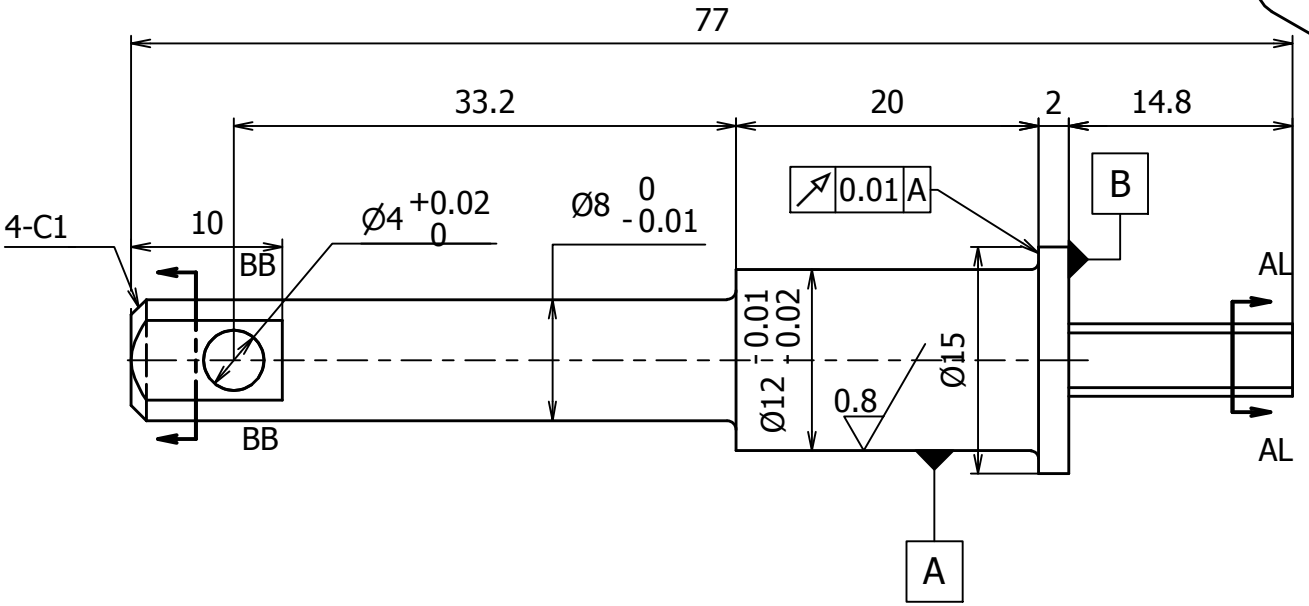

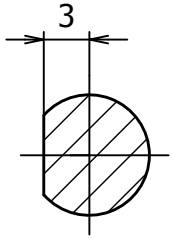

BB-BB (2 : 1)

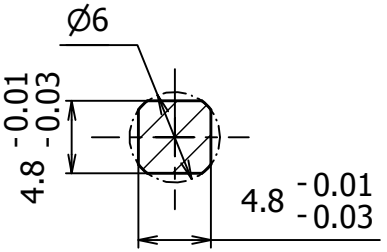

AL-AL (2 : 1)

Note:
Shaft shoulder A is used to assemble bearing and bevel gear.

ANKLE ORTHOSIS			SCALE 1:1	REF. DRAW. 34		KOMEDA LAB	
						SHAFT OF FOREFOOT BEVEL GEAR	
Rev	Date	Description	TRUNG Author		Checked	Approved	
			MASS [Kg] 0.038	MATERIAL Steel		PART NUMBER: 08	7 / 38
			Number of part 1				A4

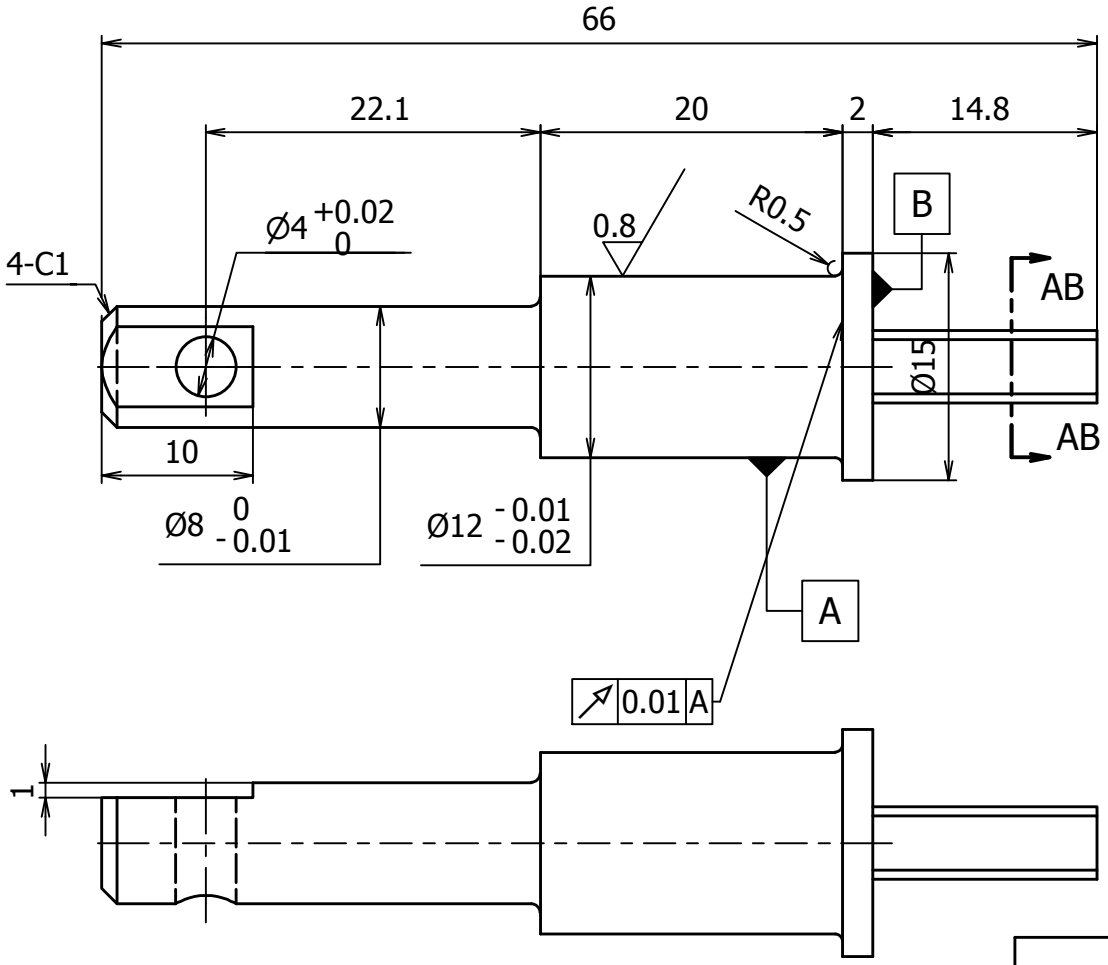

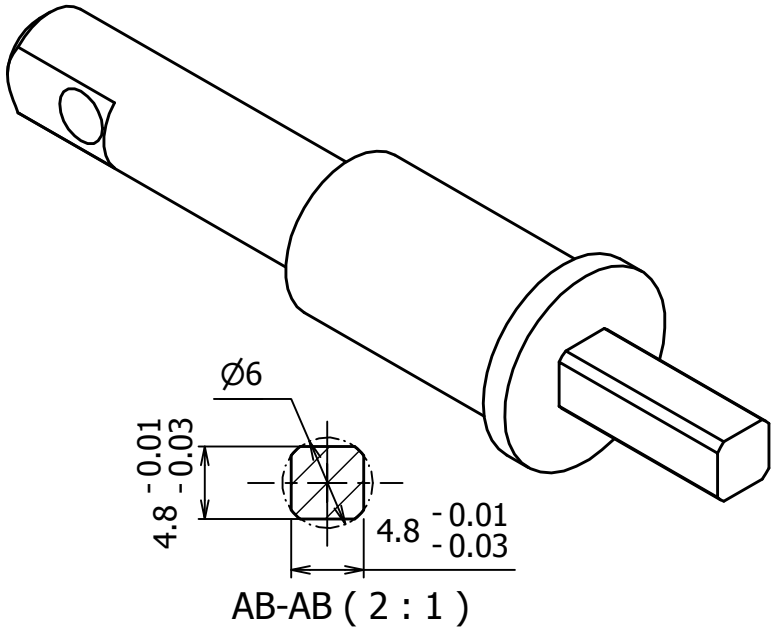

AB-AB (2 : 1)

Note:
Shaft shoulder A is used to assemble bearing and bevel gear.

ANKLE ORTHOSIS			SCALE 1:1	REF. DRAW. 34, 35		KOMEDA LAB	
						SHAFT OF REARFOOT BEVEL GEAR	
Rev	Date	Description	TRUNG Author	Checked	Approved		
			MASS [Kg] 0.034	MATERIAL Steel		PART NUMBER: 09	8 / 38
			Number of part 1				A4

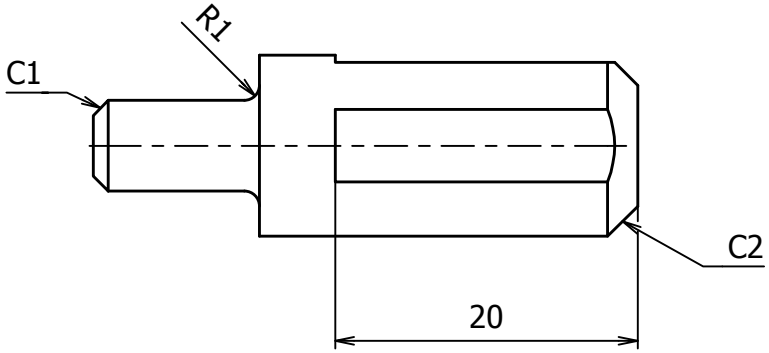

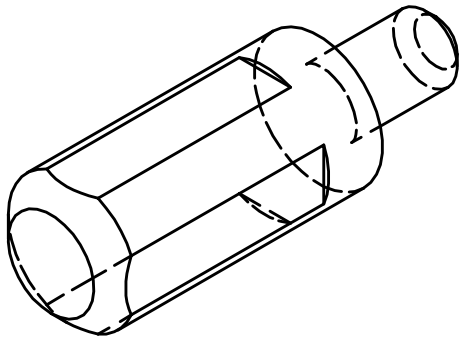

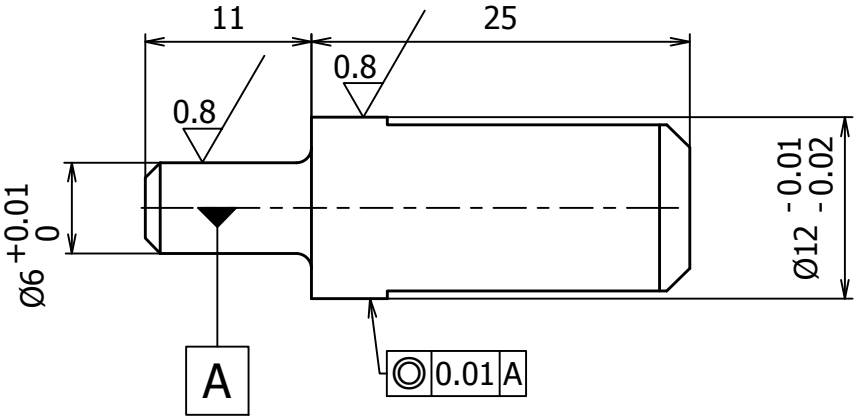

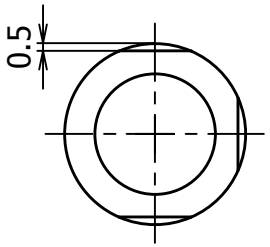

ANKLE ORTHOSIS			SCALE 2:1	REF. DRAW. 35		KOMEDA LAB	
						SHAFT OF MAIN BEVEL GEAR	
Rev	Date	Description	TRUNG Author	Checked	Approved		
			MASS [Kg] 0.026	MATERIAL Steel		PART NUMBER: 10	9 / 38
			Number of part 1				A4

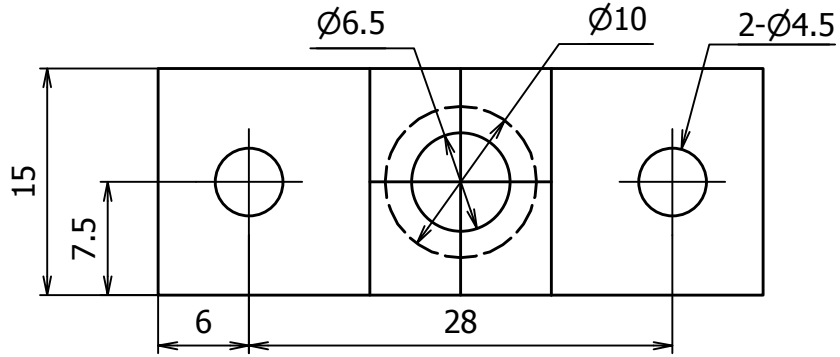

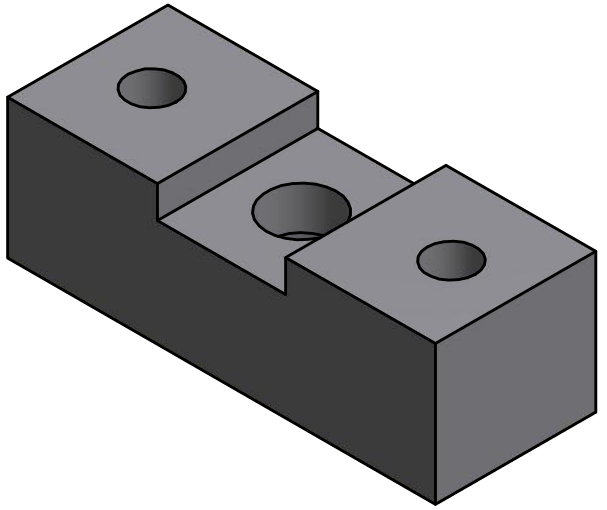

Isometric
2:1

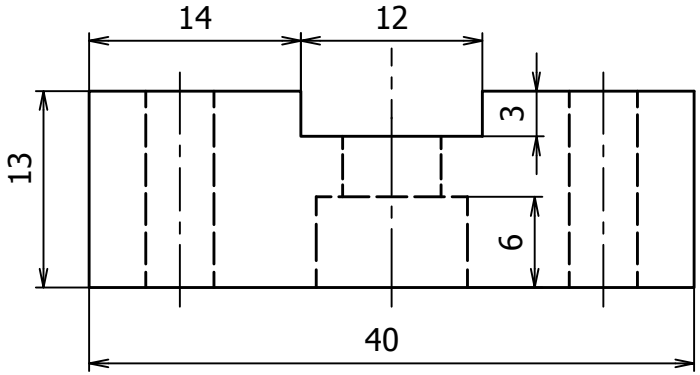

ANKLE ORTHOSIS			SCALE 2:1	REF. DRAW. 36, 38		KOMEDA LAB
						BASE FOR ROTARY JOINTS AT REARFOOT AND FOREFOOT
Rev	Date	Description	TRUNG Author	Checked	Approved	
			MASS [Kg] 0.031	MATERIAL Steel		PART NUMBER: 11
			Number of part 2			10 / 38 A4

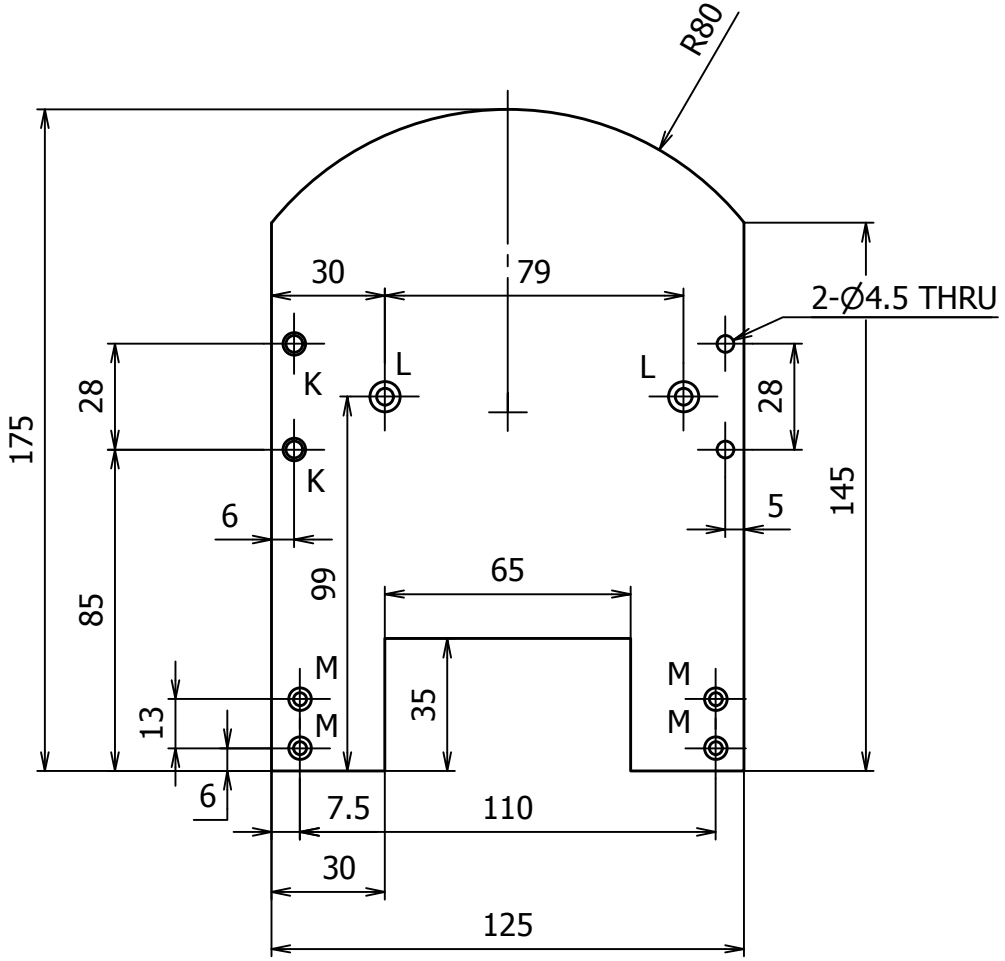

K (2 : 1)

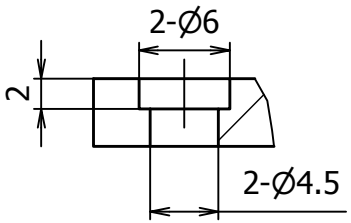

L (2 : 1)

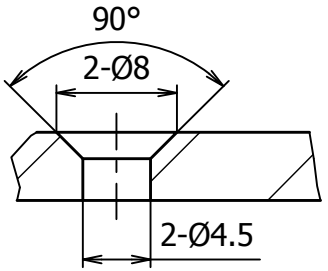

M (2 : 1)

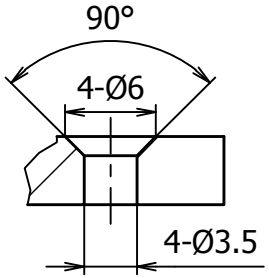

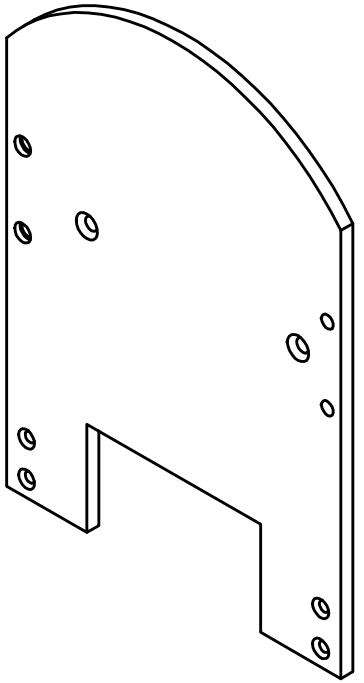

Note:
t=4.5

ANKLE ORTHOSIS			SCALE 2:1	REF. DRAW. 36, 38		KOMEDA LAB	
						UPPER FOREFOOT PLATE	
Rev	Date	Description	TRUNG Author	Checked	Approved		
			MASS [Kg] 0.149	MATERIAL Aluminum-6061		PART NUMBER: 12	11 / 38
			Number of part 1				A4

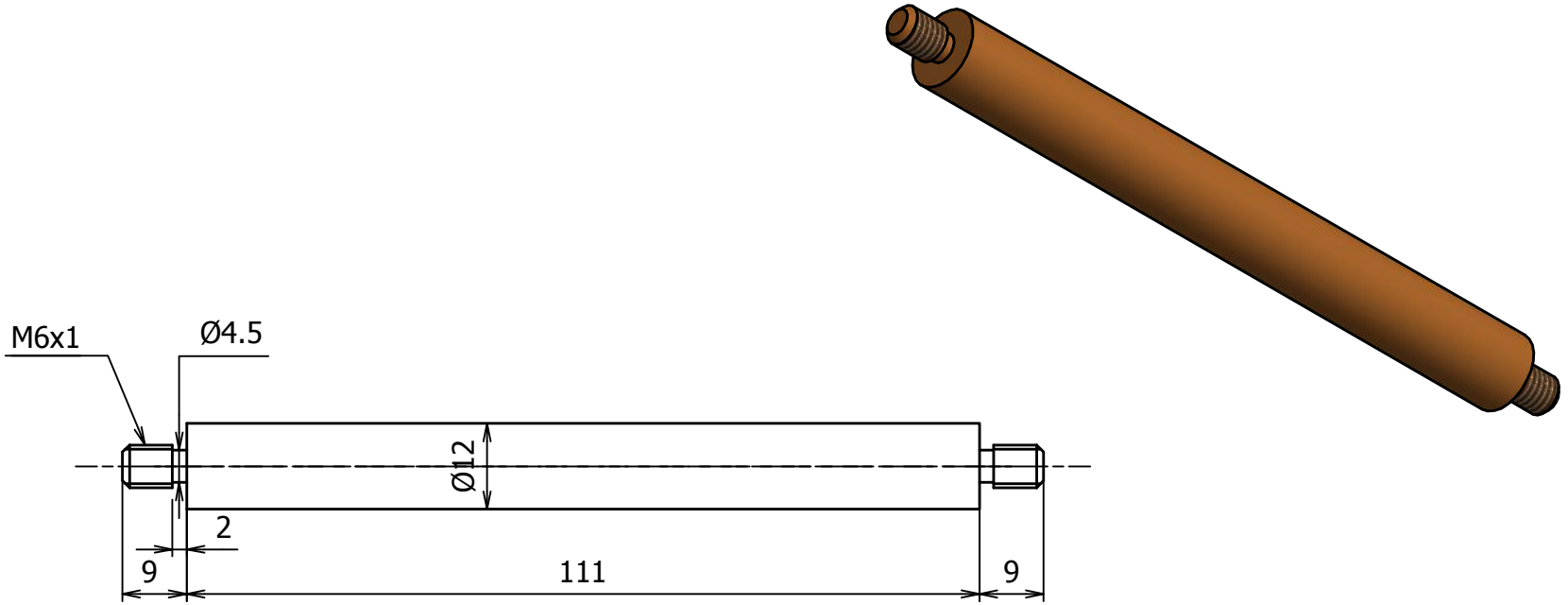

ANKLE ORTHOSIS			SCALE 1:1	REF. DRAW. 36, 38		KOMEDA LAB
						FOREFOOT VERTICAL ROD
Rev	Date	Description	TRUNG Author		Checked	Approved
			MASS [Kg] 0.097	MATERIAL Aluminum-6061	PART NUMBER: 13	12 / 38
			Number of part 1			A4

3.2

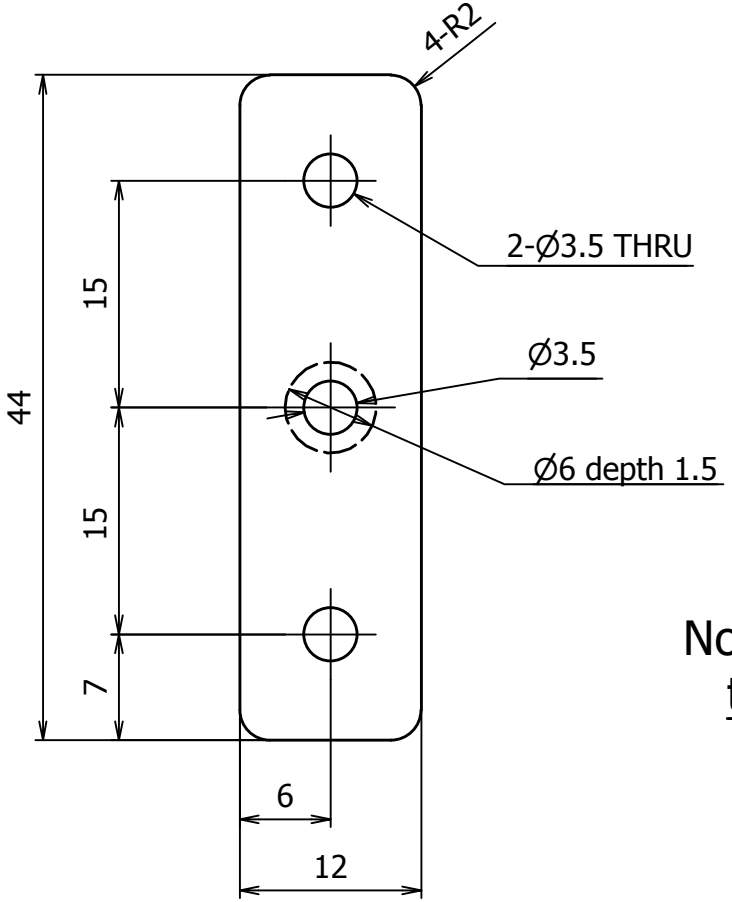

Note:
t = 3

ANKLE ORTHOSIS			SCALE 2:1	REF. DRAW. 36, 38		KOMEDA LAB
						GUILDING PART FOR REARFOOT SPRING
Rev	Date	Description	TRUNG Author	Checked	Approved	
			MASS [Kg] 0.011	MATERIAL Steel		PART NUMBER: 14
			Number of part 1			13 / 38 A4

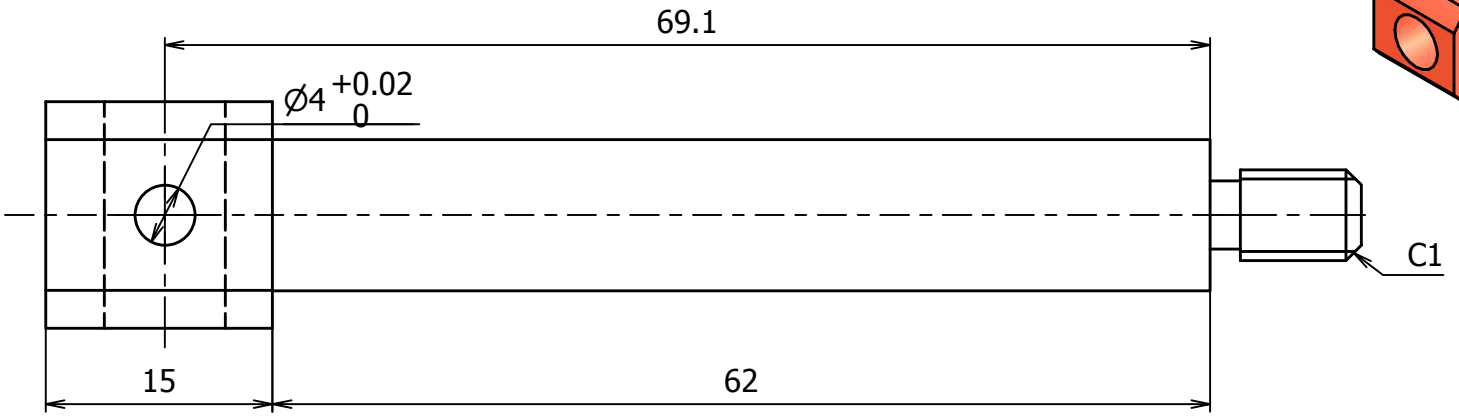

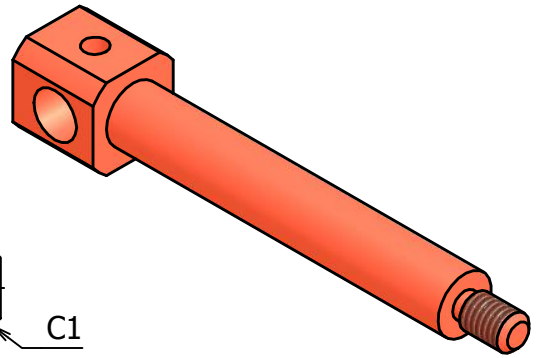

Isometric
1:1

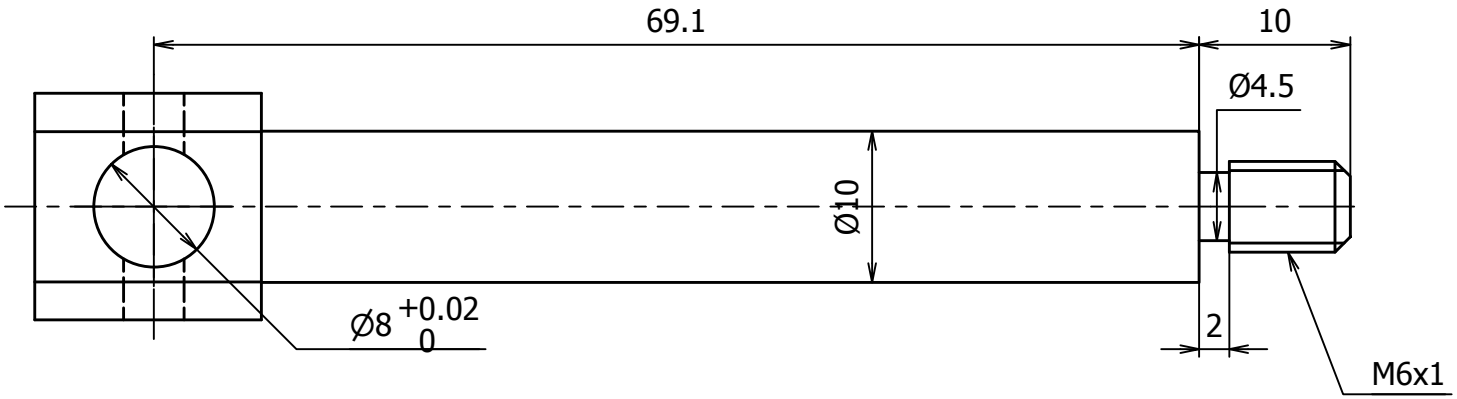

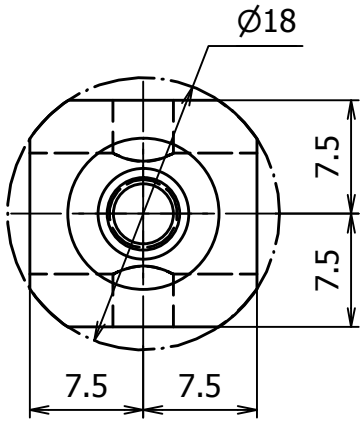

ANKLE ORTHOSIS			SCALE 2:1	REF. DRAW. 36, 38		KOMEDA LAB
						FOREFOOT HORIZONAL ROD
Rev	Date	Description	TRUNG Author		Checked	Approved
			MASS [Kg] 0.02		MATERIAL Aluminum-6061	PART NUMBER: 15
			Number of part 2			A4

14 / 38

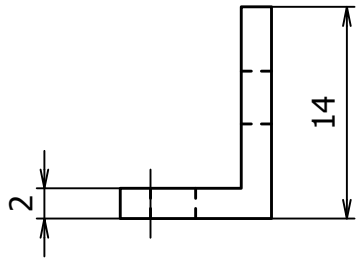

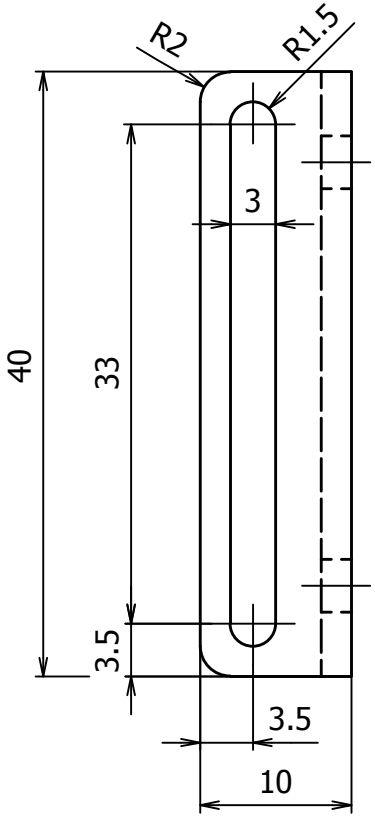

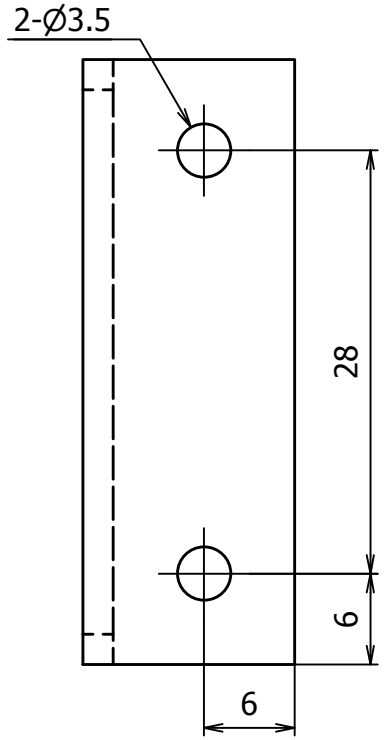

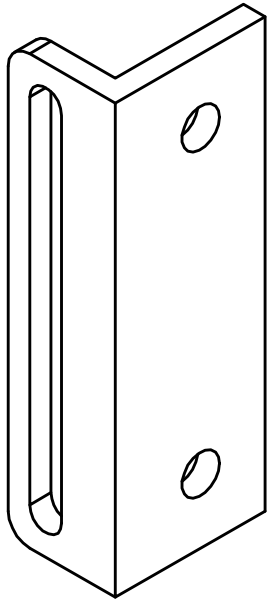

ANKLE ORTHOSIS			SCALE 2:1	REF. DRAW. 36, 38		KOMEDA LAB
						LEFT HINDGE OF FOREFOOT STRAP
Rev	Date	Description	TRUNG Author	Checked	Approved	
			MASS [Kg] 0.004	MATERIAL Aluminum-6061		PART NUMBER: 17
			Number of part 1			15 / 38 A4

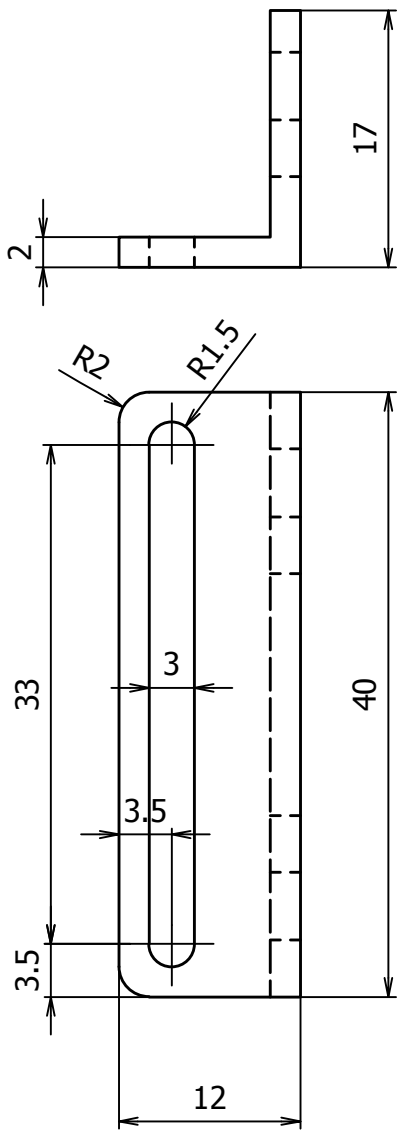

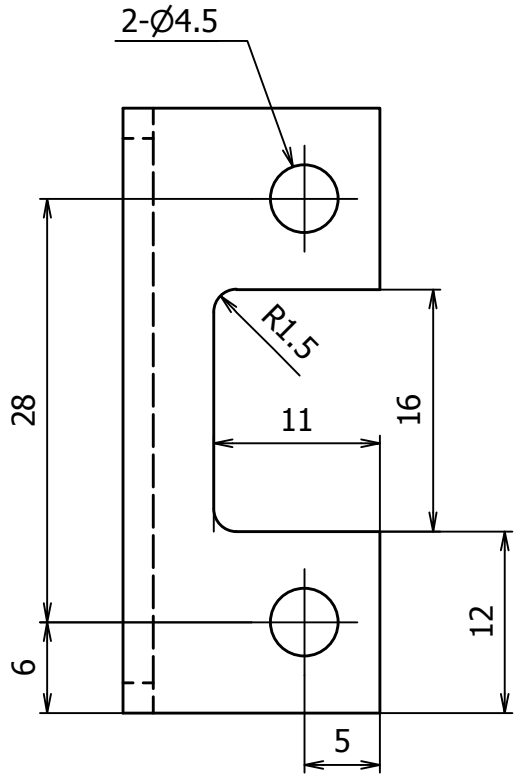

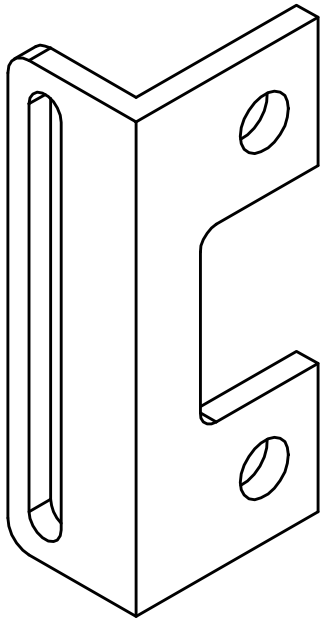

ANKLE ORTHOSIS			SCALE 4:1	REF. DRAW. 36, 38		KOMEDA LAB	
						RIGHT HINDGE OF FOREFOOT STRAP	
Rev	Date	Description	TRUNG Author	Checked	Approved		
			MASS [Kg] 0.004	MATERIAL Aluminum-6061		PART NUMBER: 18	16 / 38
			Number of part 1				A4

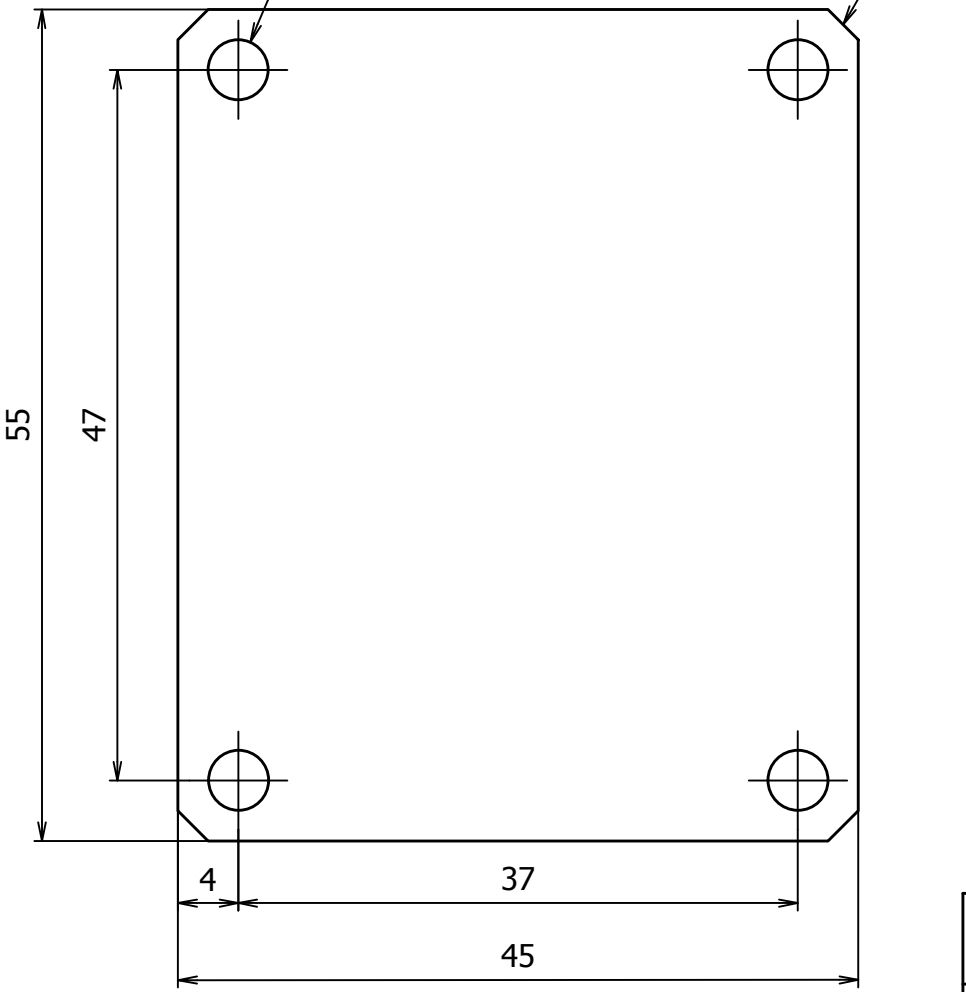

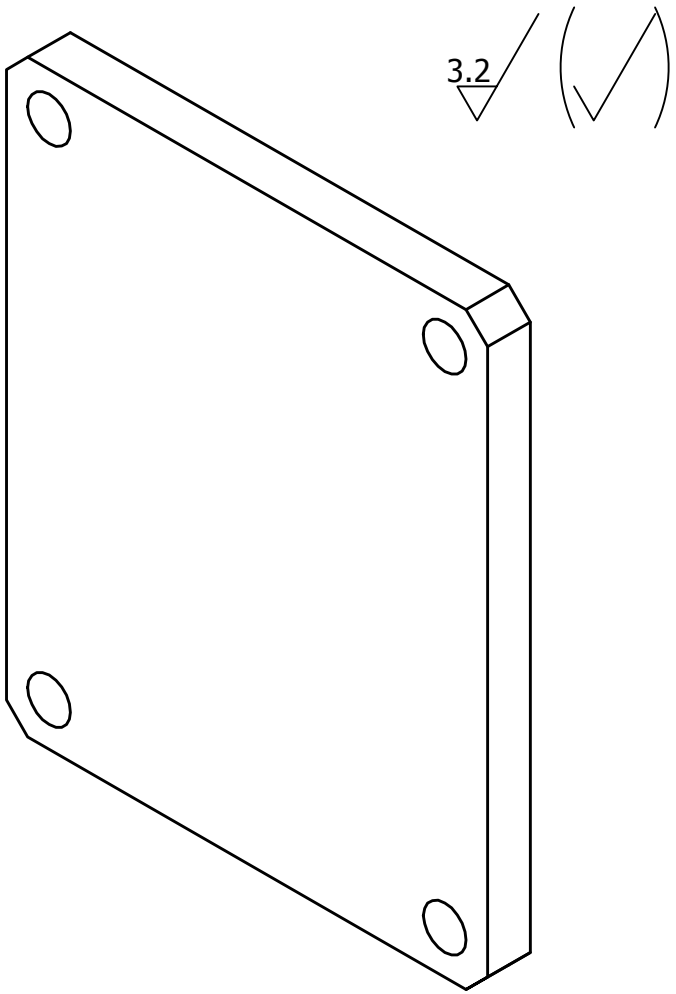

Note:
t=4

ANKLE ORTHOSIS			SCALE 2:1	REF. DRAW. 38		KOMEDA LAB	
						COVER FOR MOTOR PROTECTION FRAME	
Rev	Date	Description	TRUNG Author	Checked	Approved		
			MASS [Kg] 0.02	MATERIAL Aluminum-6061		PART NUMBER: 19	17 / 38
			Number of part 1				A4

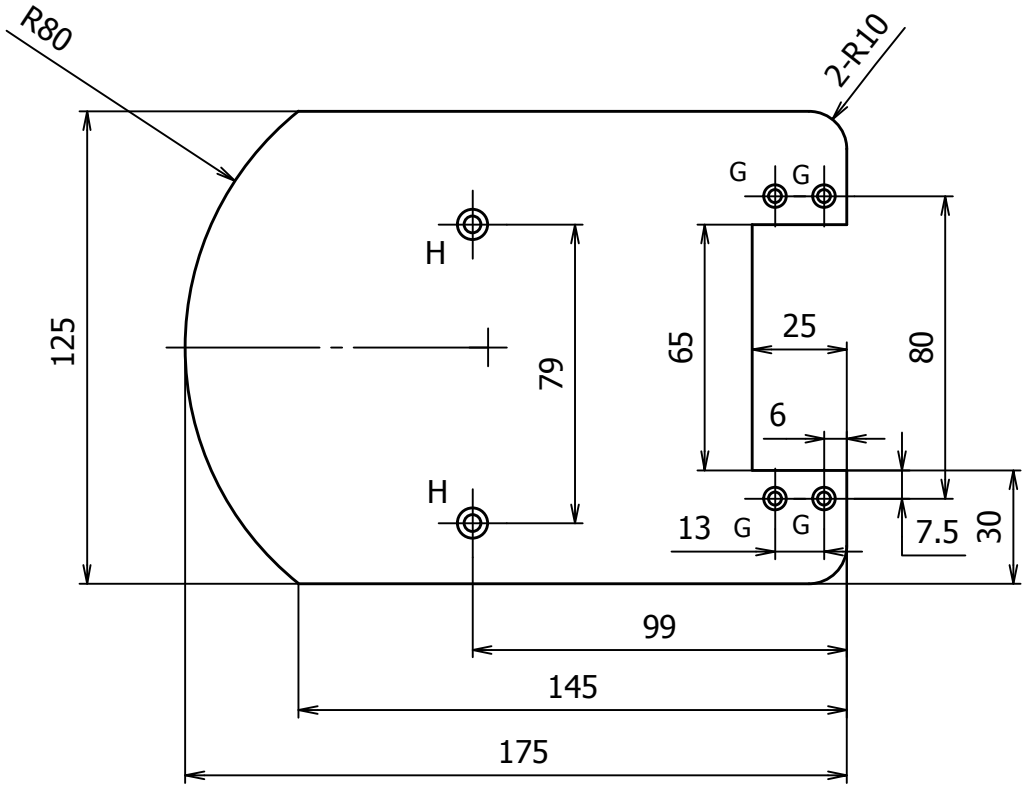

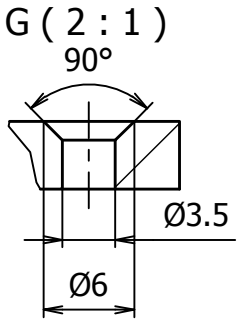

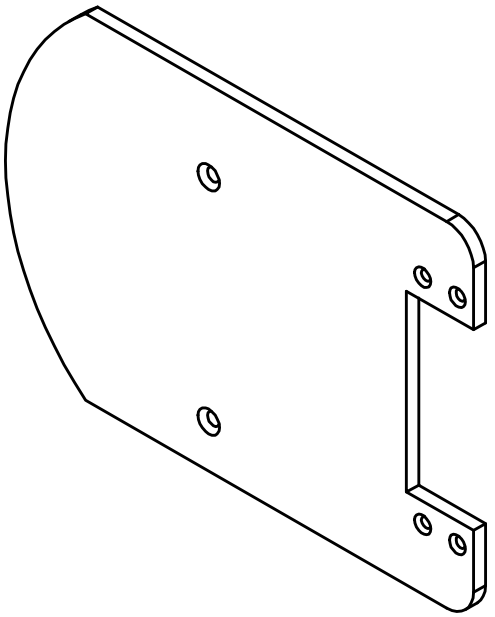

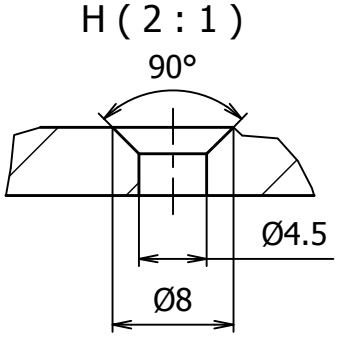

Note:
t=4.5

ANKLE ORTHOSIS			SCALE 1:2	REF. DRAW. 36, 38		KOMEDA LAB	
						LOWER FOREFOOT PLATE	
Rev	Date	Description	TRUNG Author	Checked	Approved		
			MASS [Kg] 0.447	MATERIAL Aluminum-6061		PART NUMBER: 20	18 / 38
			Number of part 1				A4

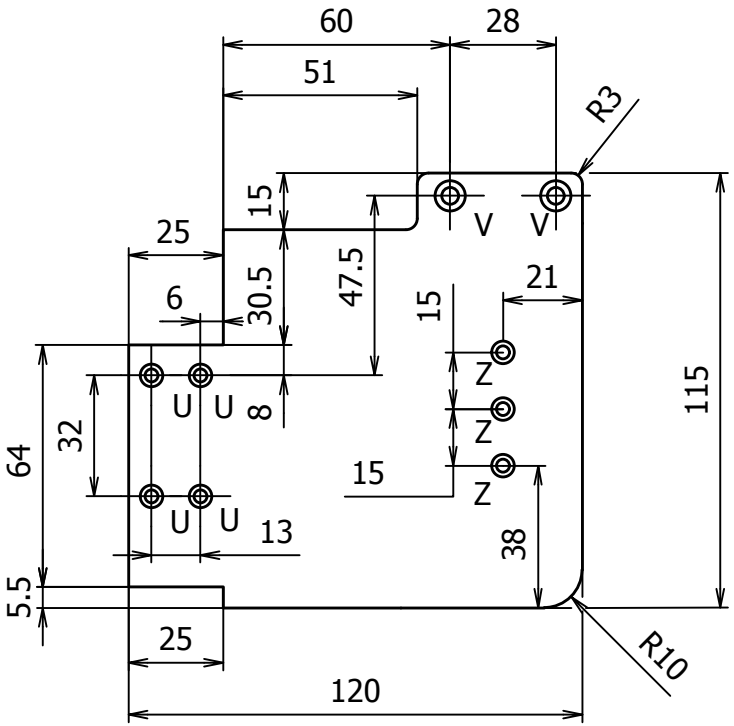

U (2 : 1)

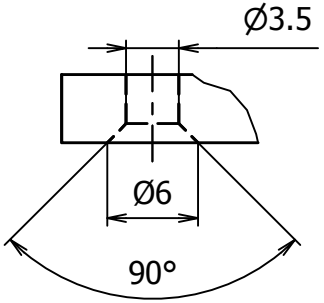

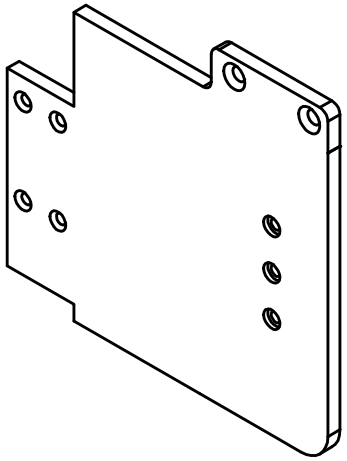

V (2 : 1)

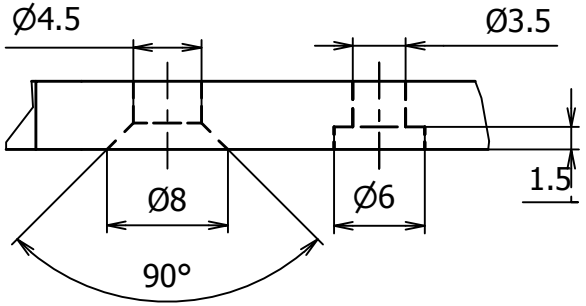

Note:
t=3.5

ANKLE ORTHOSIS			SCALE 1:2	REF. DRAW. 36, 38		KOMEDA LAB	
						LOWER REARFOOT PLATE	
Rev	Date	Description	TRUNG Author	Checked	Approved		
			MASS [Kg] 0.094	MATERIAL Aluminum-6061		PART NUMBER: 21	19 / 38
			Number of part 1				A4

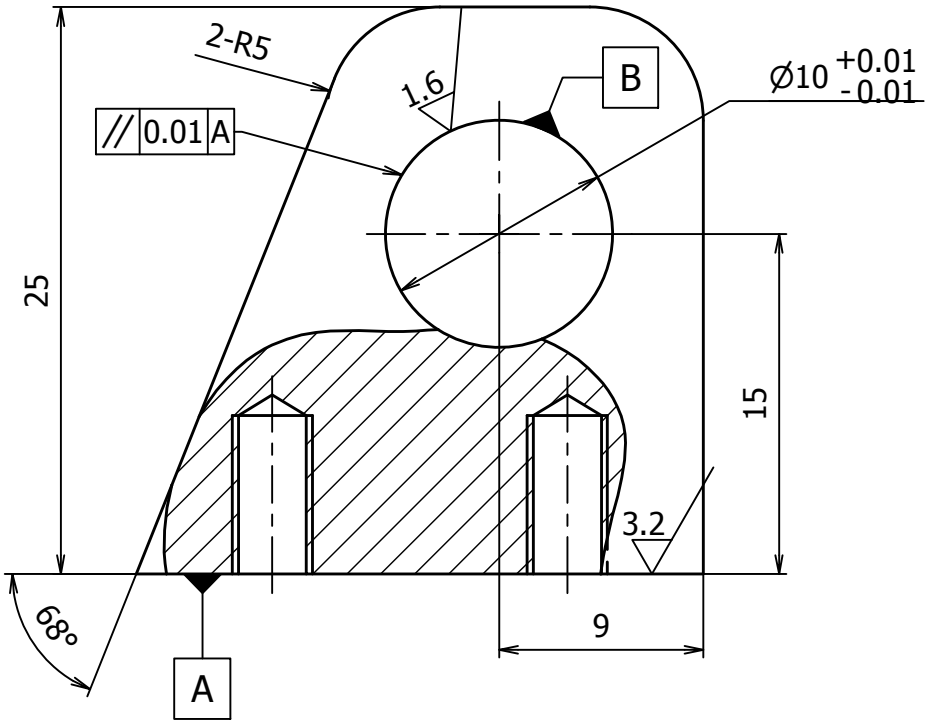

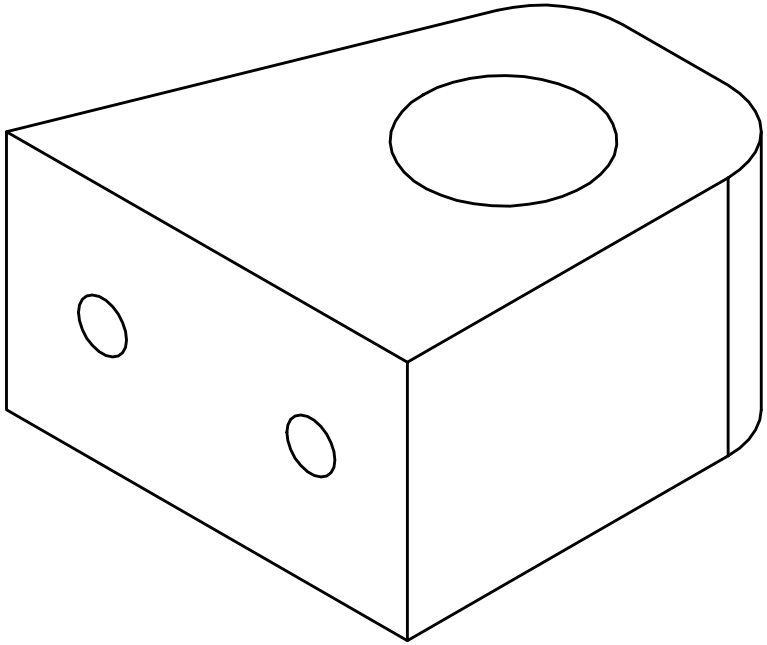

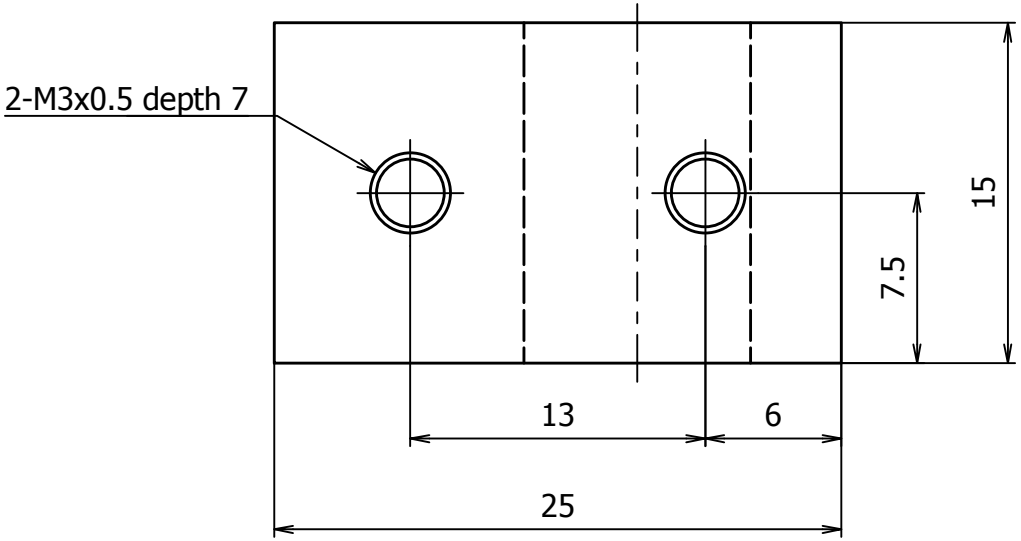

Note:

1. Hole B is assemble bushing P_06
2. Assemble hindges part number: 22,23,24,25 between plate parts 12,20,21,27 and ensure the concentricity requirement of B holes so that we can assemble bushing and shaft P_52.

ANKLE ORTHOSIS			SCALE 3:1	REF. DRAW. 36,38, 21-23, 11 18, 19, 24		KOMEDA LAB	
						RIGHT HINDGE OF LOWER FOREFOOT PLATE	
Rev	Date	Description	TRUNG Author	Checked	Approved		
			MASS [Kg] 0.017	MATERIAL Aluminum-6061		PART NUMBER: 22	20 / 38
			Number of part 2				A4

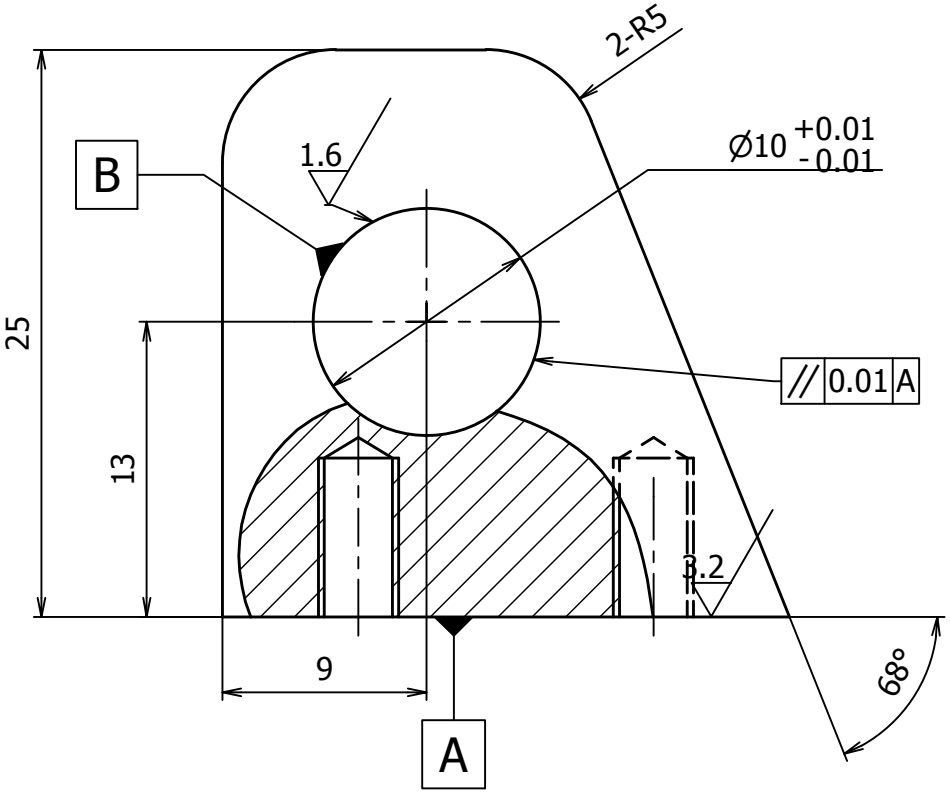

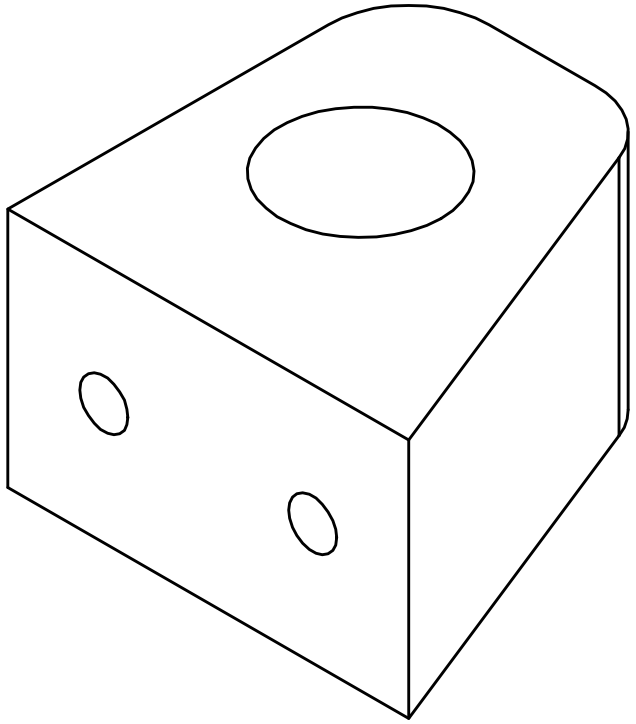

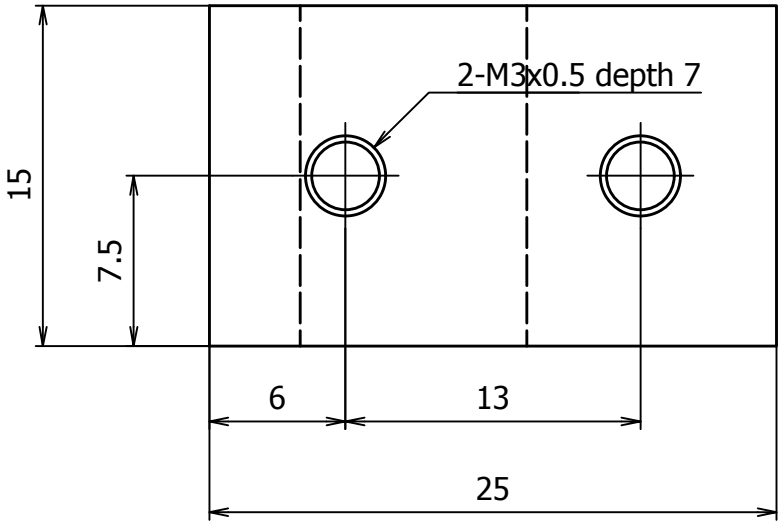

Note:

1. Hole B is assemble bushing P_06
2. Assemble hindges part number: 22,23,24,25 between plate parts 12,20,21,27 and ensure the concentricity requirement of B holes so that we can assemble bushing and shaft P_52.

ANKLE ORTHOSIS			SCALE 3:1	REF. DRAW. 36,38, ,20, 22, 23, 11, 18, 19, 24		KOMEDA LAB
						RIGHT HINDGE OF UPPER FOREFOOT PLATE
Rev	Date	Description	TRUNG Author	Checked	Approved	
			MASS [Kg] 0.017	MATERIAL Aluminum-6061		PART NUMBER: 23
			Number of part 2			21 / 38 A4

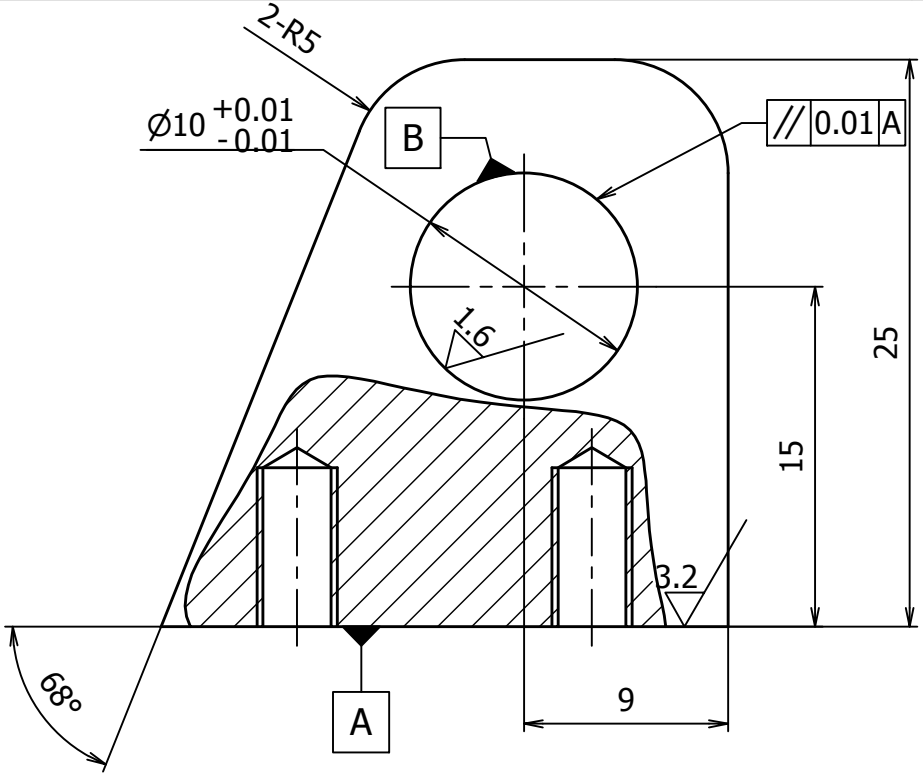

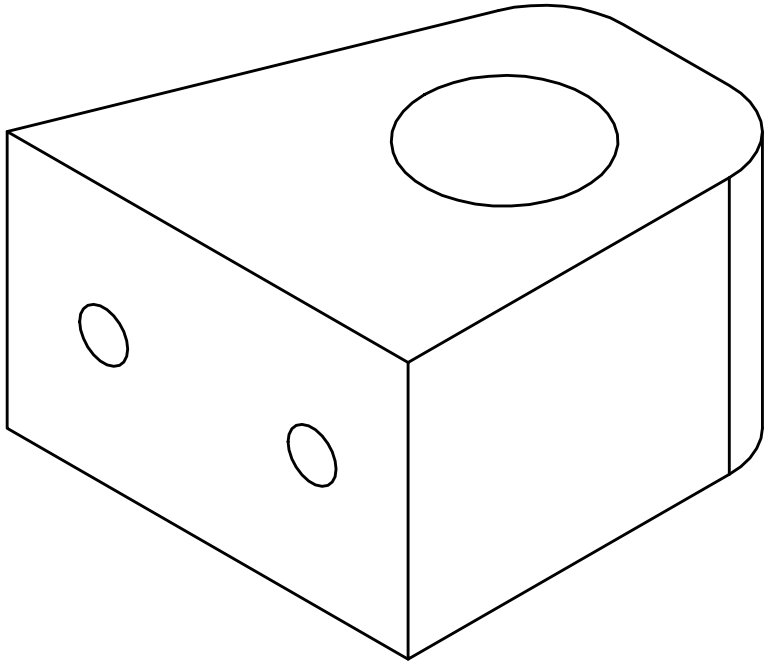

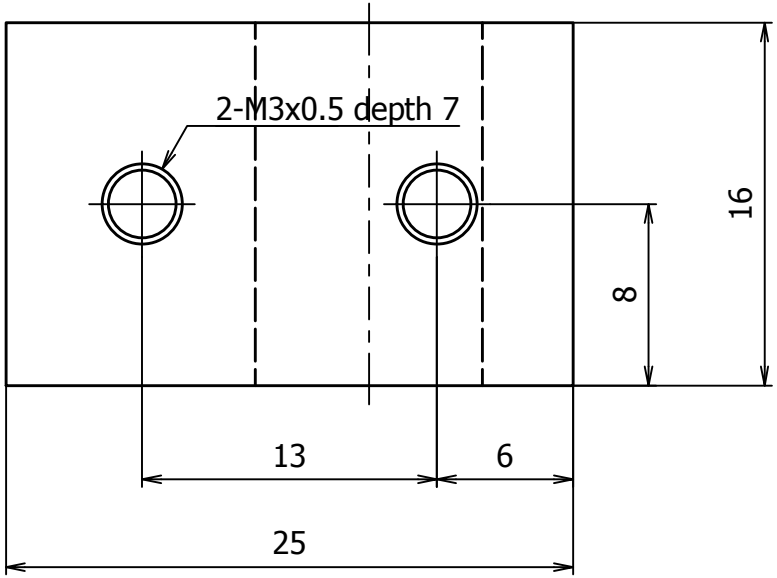

Note:

1. Hole B is assemble bushing P_06
2. Assemble hindges part number: 22,23,24,25 between plate parts 12,20,21,27 and ensure the concentricity requirement of B holes so that we can assemble bushing and shaft P_52.

ANKLE ORTHOSIS			SCALE 3:1	REF. DRAW. 36,38, 20, 21, 23, 11, 18, 19, 24		KOMEDA LAB
						LEFT HINDGE OF LOWER REARFOOT PLATE
Rev	Date	Description	TRUNG Author	Checked	Approved	
			MASS [Kg] 0.018	MATERIAL Aluminum-6061		PART NUMBER: 24
			Number of part 2			A4

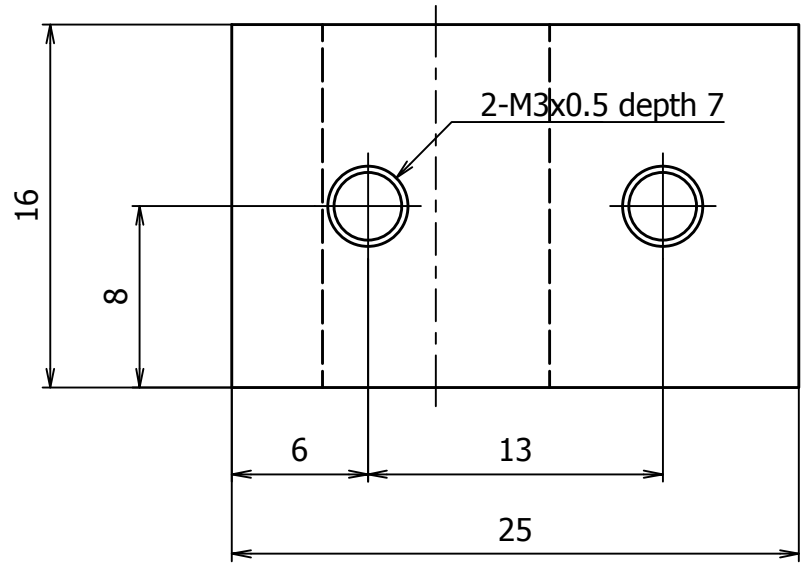

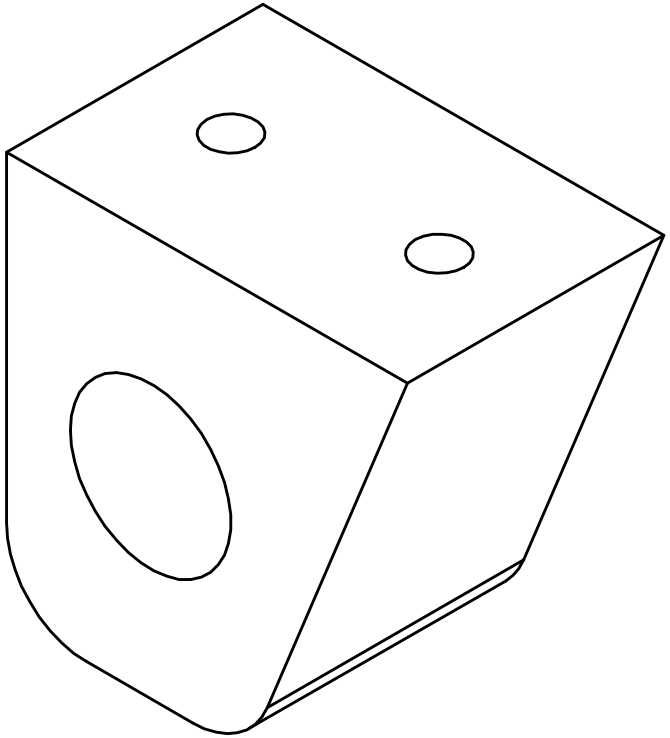

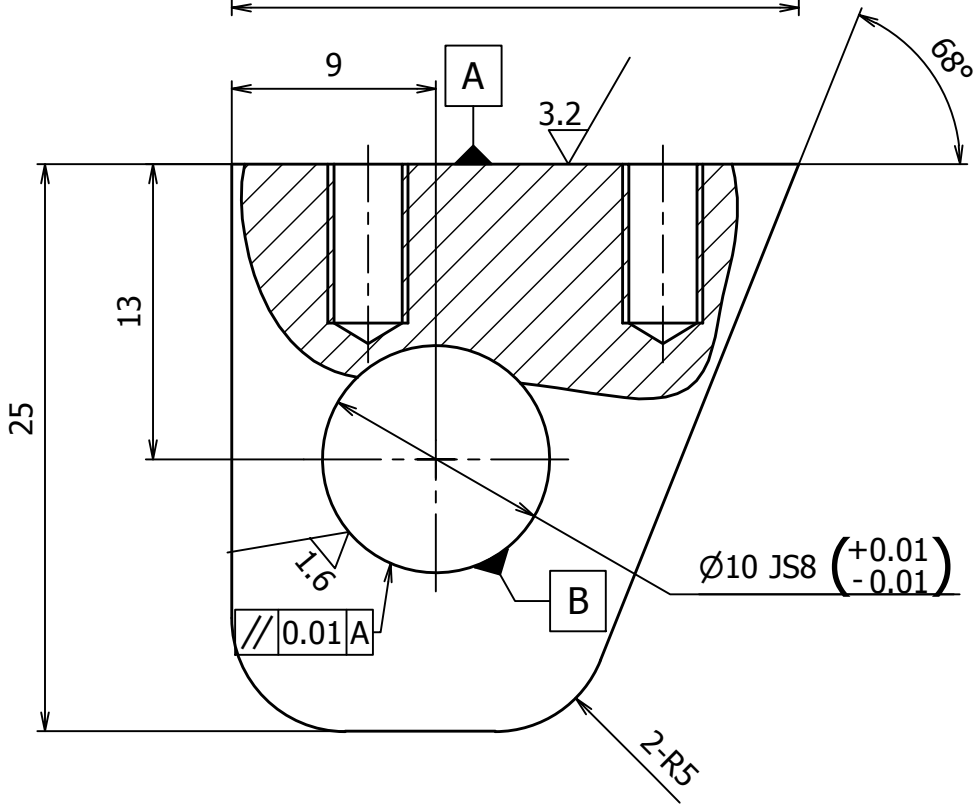

Note:

1. Hole B is assemble bushing P_06
2. Assemble hindges part number: 22,23,24,25 between plate parts 12,20,21,27 and ensure the concentricity requirement of B holes so that we can assemble bushing and shaft P_52.

ANKLE ORTHOSIS			SCALE 2:1	REF. DRAW. 36,38, ,20-22, 11, 18, 19, 24		KOMEDA LAB
						LEFT HINDGE OF UPPER REARFOOT PLATE
Rev	Date	Description	TRUNG Author	Checked	Approved	
			MASS [Kg] 0.018	MATERIAL Aluminum-6061		PART NUMBER: 25
			Number of part 2			A4

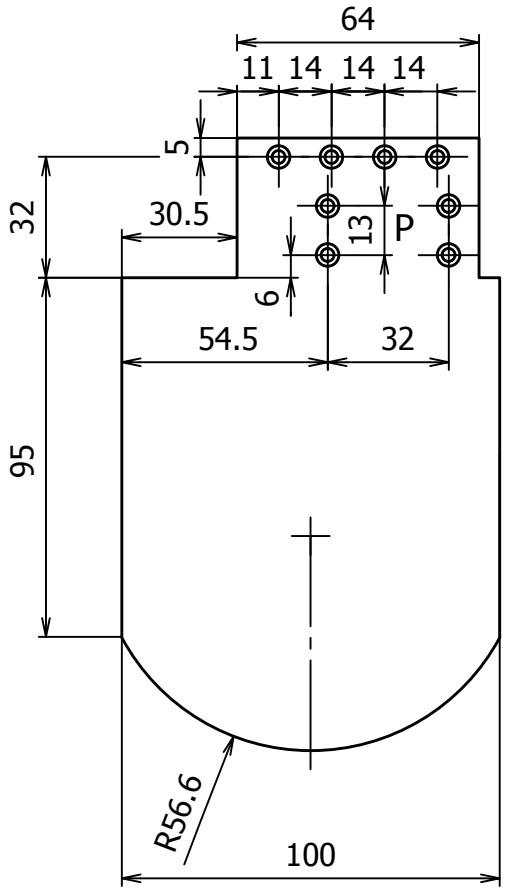

P (2 : 1)

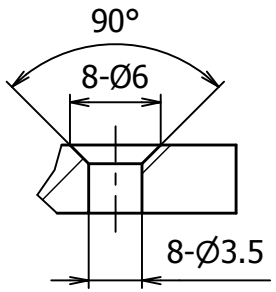

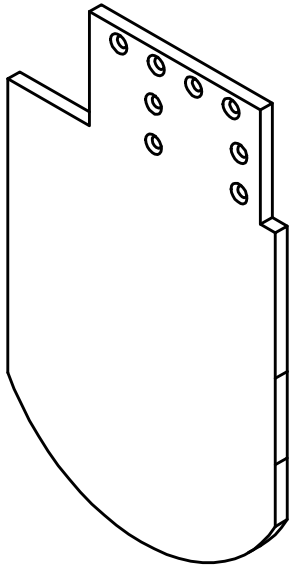

Note:
t=4.5

ANKLE ORTHOSIS			SCALE 1:2	REF. DRAW. 36, 38		KOMEDA LAB
						UPPER REARFOOT PLATE
Rev	Date	Description	TRUNG Author	Checked	Approved	
			MASS [Kg] 0.113	MATERIAL Aluminum-6061		PART NUMBER: 27
			Number of part 1			A4

M6x1

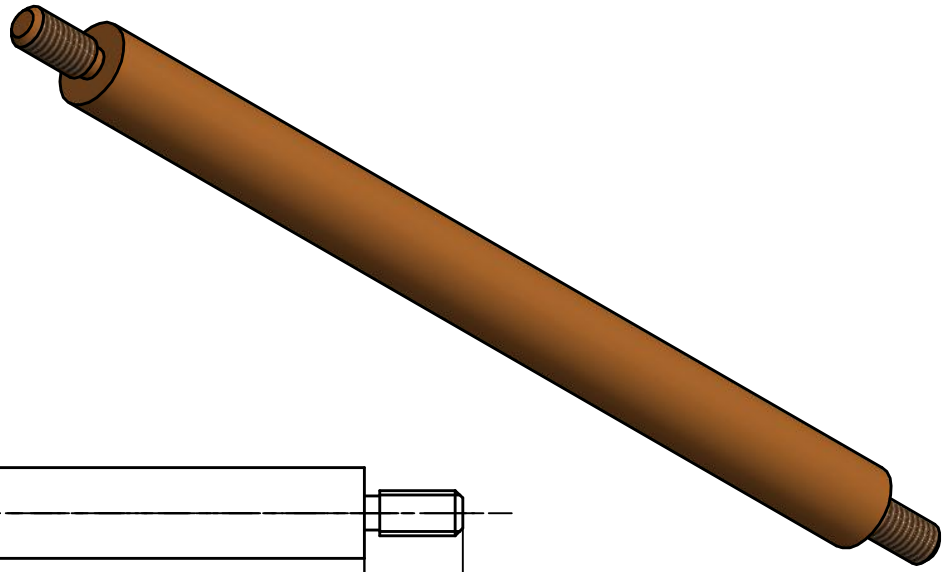

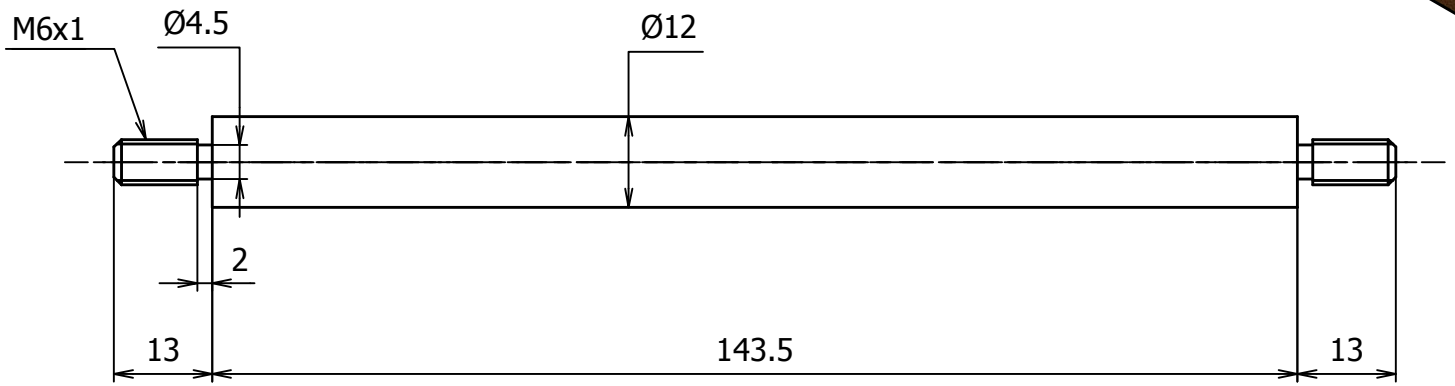

M6x1

ANKLE ORTHOSIS			SCALE 1:1	REF. DRAW. 36, 38		KOMEDA LAB
						REARFOOT VERTICAL ROD
Rev	Date	Description	TRUNG Author		Checked	Approved
			MASS [Kg] 0.125	MATERIAL Steel	PART NUMBER: 28	25 / 38
			Number of part 1			A4

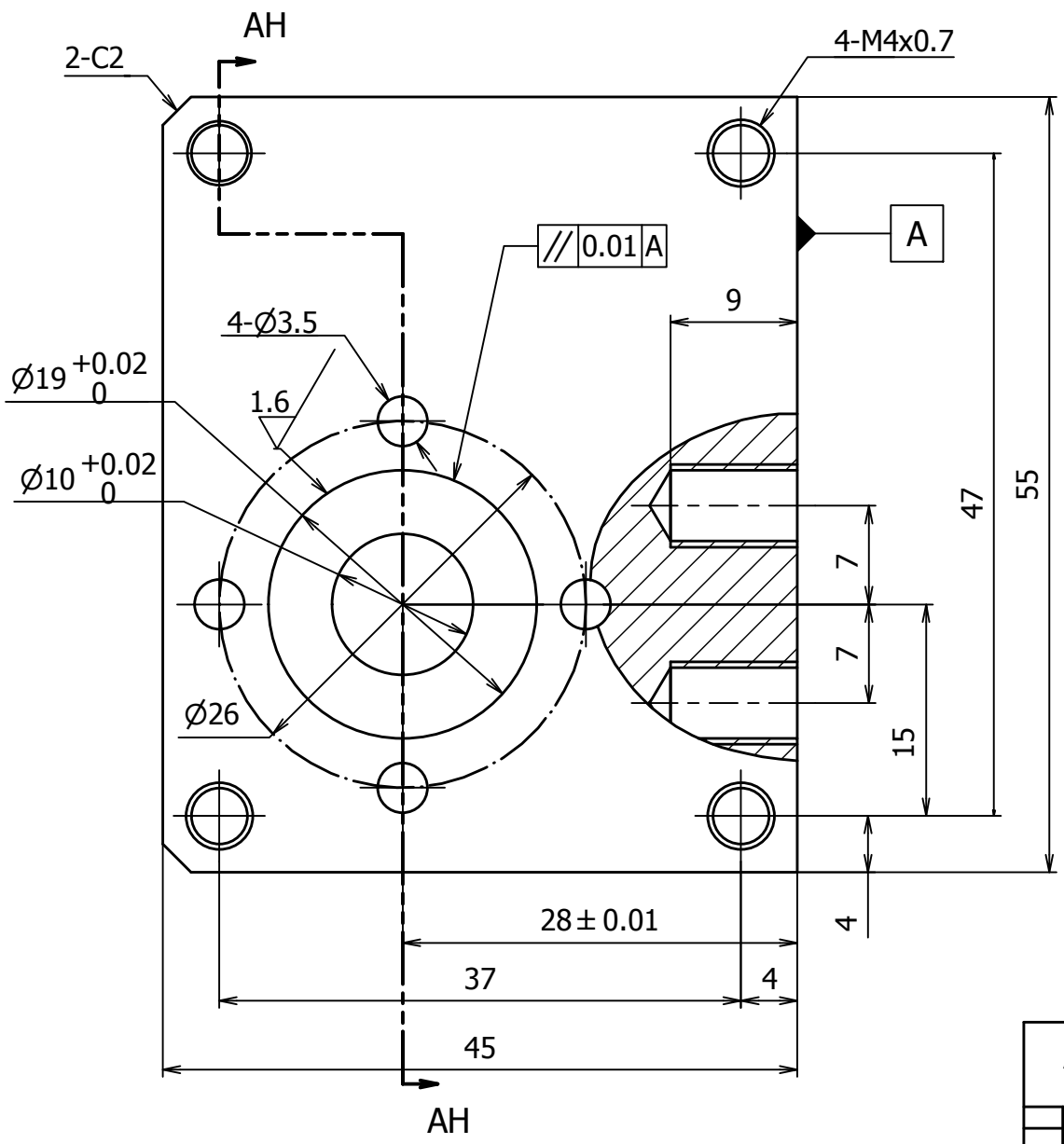

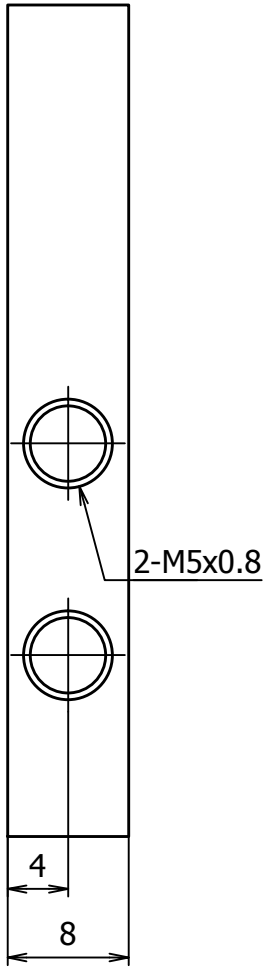

AH-AH (2 : 1)

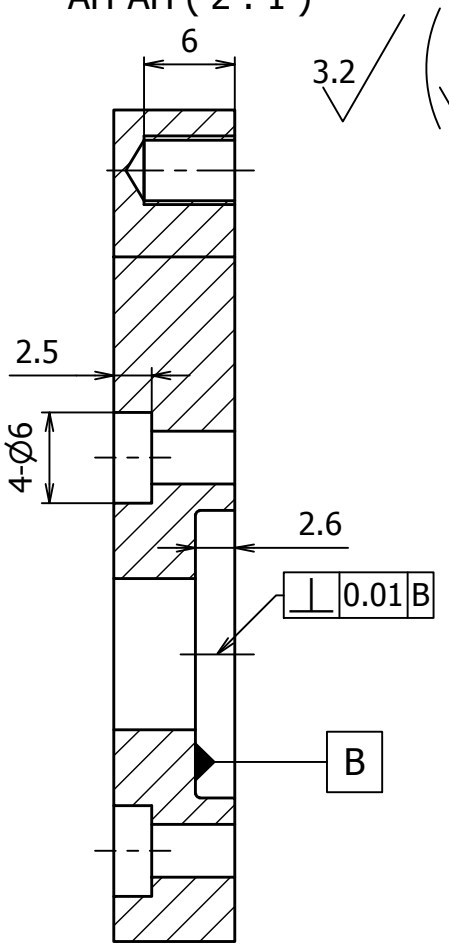

ANKLE ORTHOSIS			SCALE 2:1	REF. DRAW. 35		KOMEDA LAB
						FLANGE OF MOTOR
Rev	Date	Description	TRUNG Author	Checked	Approved	
			MASS [Kg] 0.047	MATERIAL Aluminum-6061		PART NUMBER: 29
			Number of part 1			26 / 38 A4

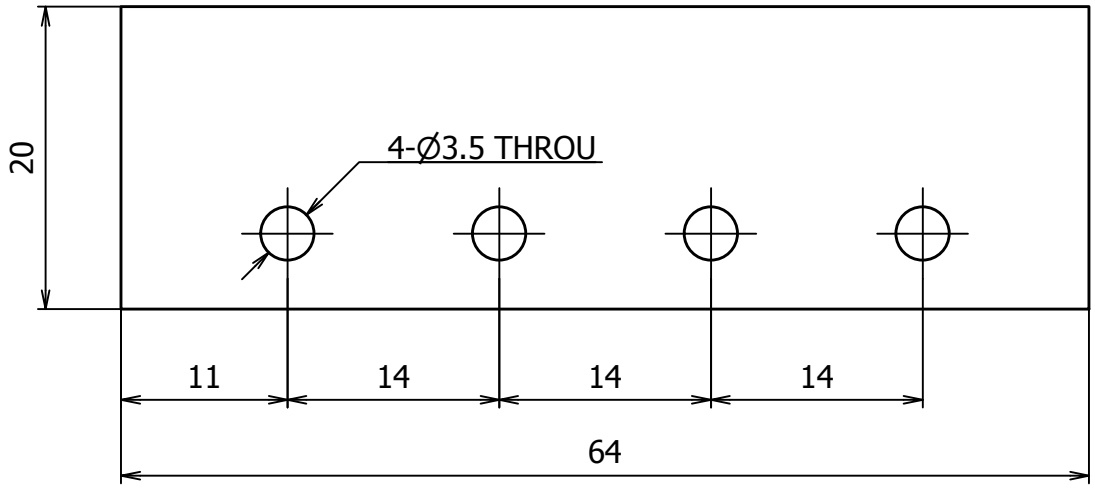

Note:
t = 3

ANKLE ORTHOSIS			SCALE 2:1	REF. DRAW.		KOMEDA LAB	
						PLATE OF FIXING REARFOOT TO FOREFOOT	
Rev	Date	Description	TRUNG Author		Checked	Approved	
			MASS [Kg] 0.01		MATERIAL Aluminum-6061	PART NUMBER: 30	27 / 38
			Number of part 1				A4

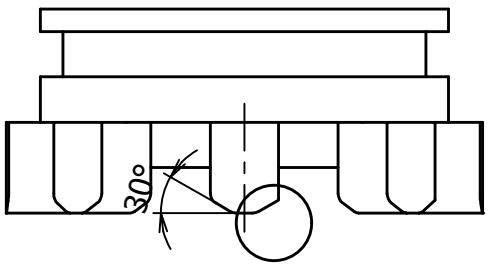

BC

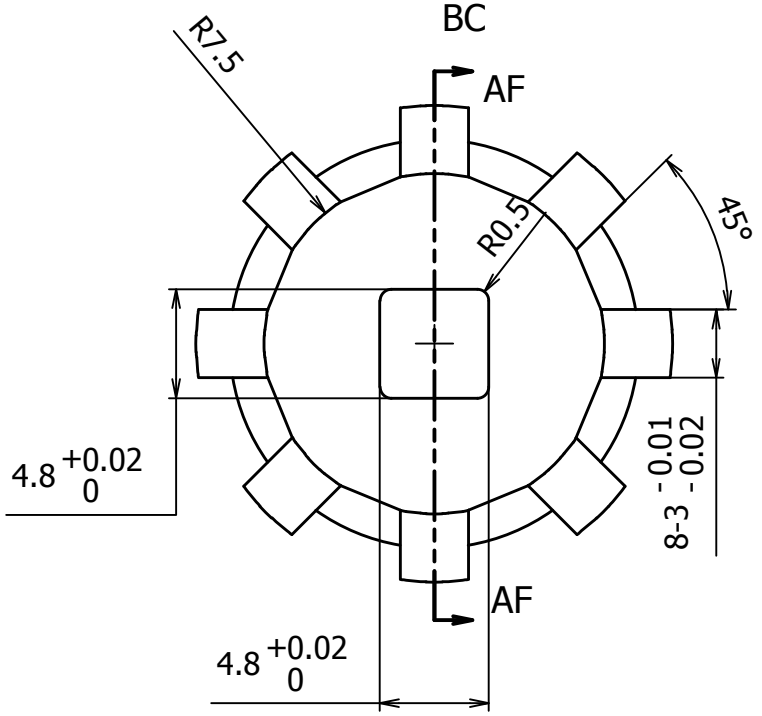

BC (6 : 1)

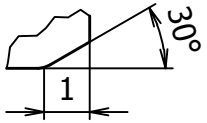

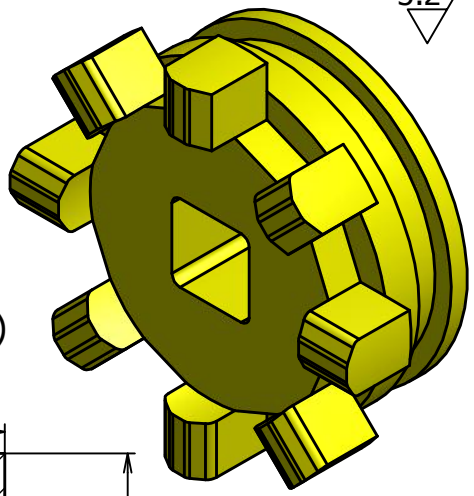

3.2

AF-AF (3:1)

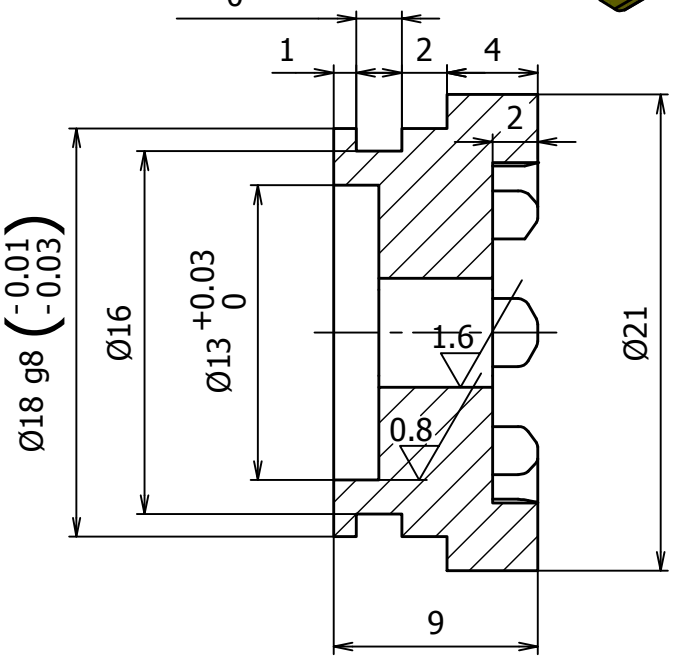

Note:

1. Ø18 has loose fit assembly with outer clutch 34.
2. Hole Ø13 is assembled with thrust ball bearing.
3. Square hole 4.8 has loose fit assembly with shaft 8, 9.

ANKLE ORTHOSIS			SCALE 2:1	REF. DRAW. 34, 35, 7, 8		KOMEDA LAB	
						JAW CLUTCH	
Rev	Date	Description	TRUNG Author	Checked	Approved		
			MASS [Kg] 0.011	MATERIAL Steel		PART NUMBER: 31	28 / 38
			Number of part 2				A4

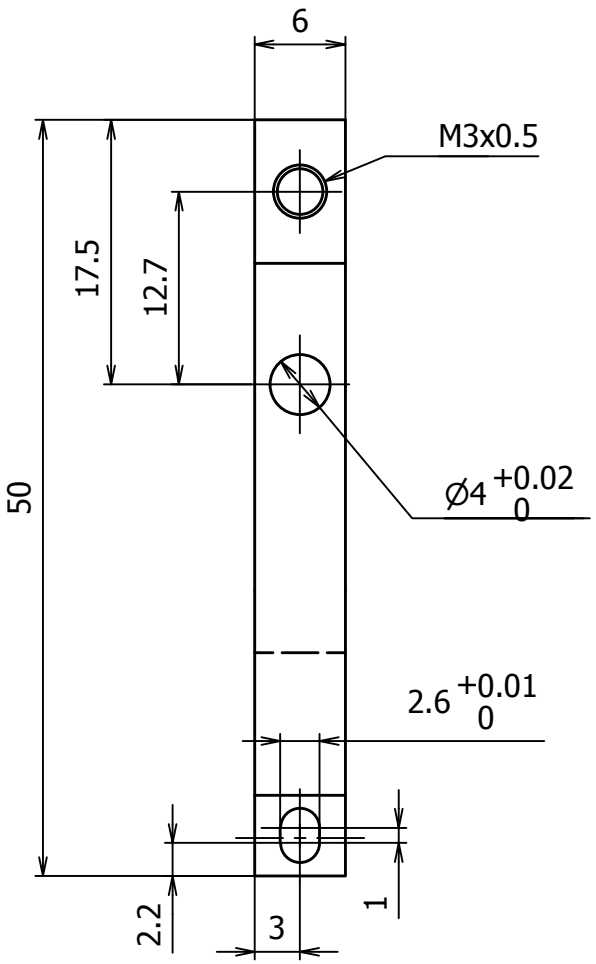

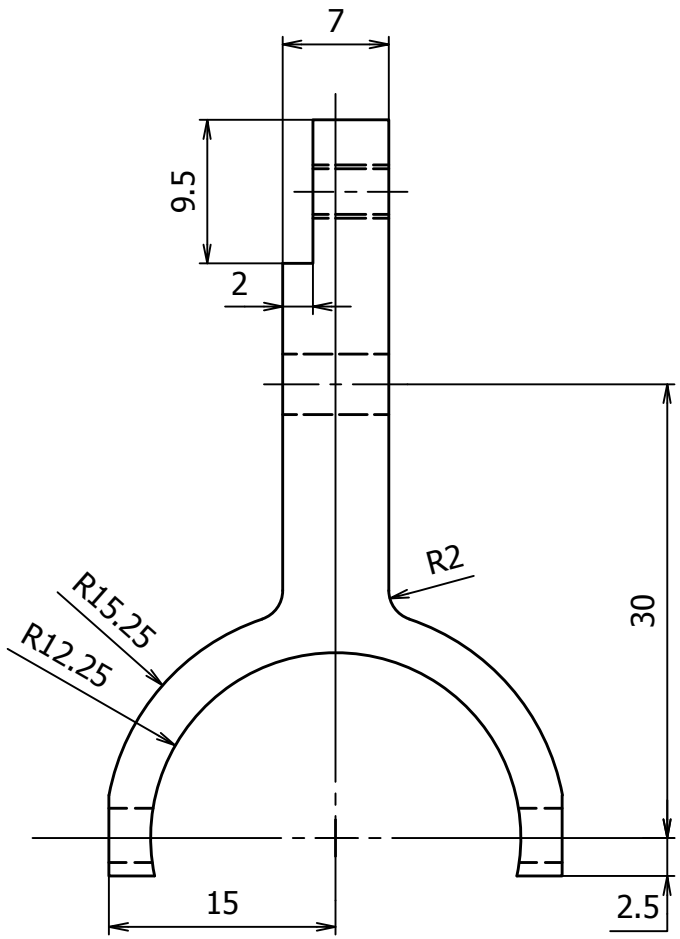

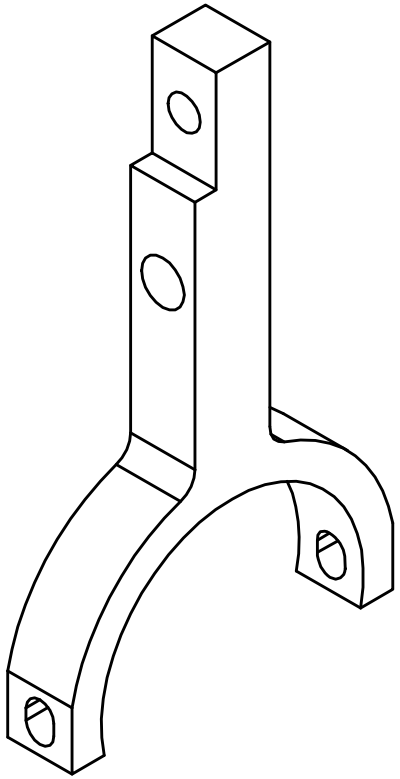

ANKLE ORTHOSIS			SCALE 3:1	REF. DRAW. 34, 35		KOMEDA LAB	
						LEVEL ROD	
Rev	Date	Description	TRUNG Author	Checked	Approved		
			MASS [Kg] 0.034	MATERIAL Steel		PART NUMBER: 33	29 / 38
			Number of part 1				A4

AE-AE (2 : 1)

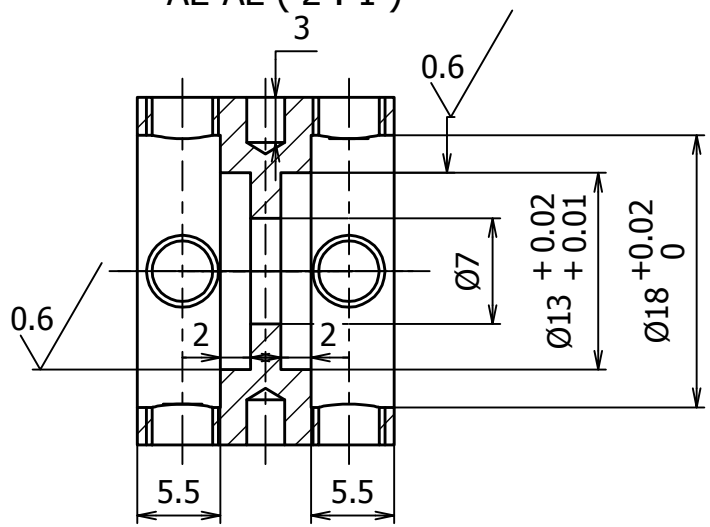

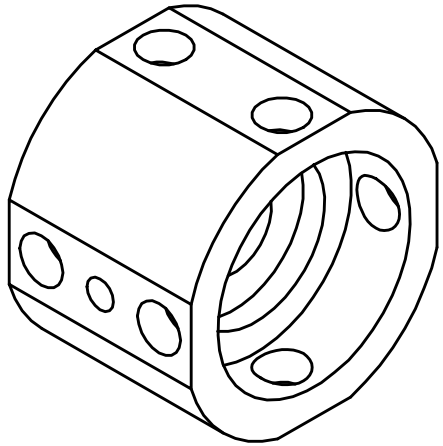

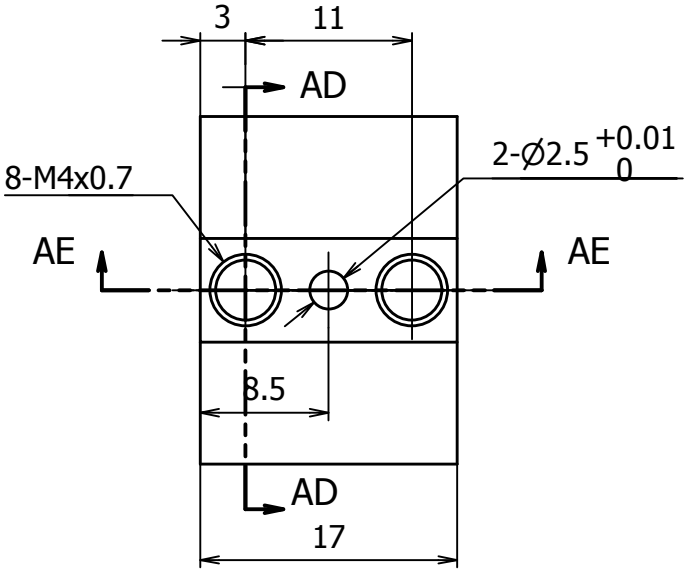

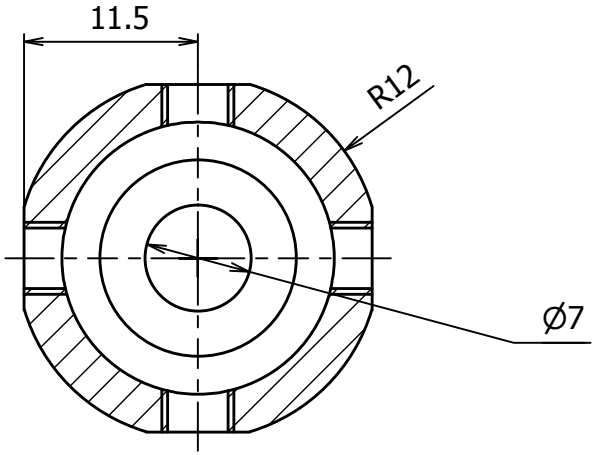

AD-AD (2 : 1)

Note:

1. Holes A and B are used to assembled thrust ball bearing.
2. Hole Ø18 has loose fit with Thrust ball bearing.
3. 2 holes Ø2.5 has inference fit with locating pins P_17

ANKLE ORTHOSIS			SCALE 2:1	REF. DRAW. 34, 35		KOMEDA LAB
						OUTER OF CLUTCH
Rev	Date	Description	TRUNG Author	Checked	Approved	
			MASS [Kg] 0.011	MATERIAL Steel		PART NUMBER: 34
			Number of part 1			30 / 38 A4

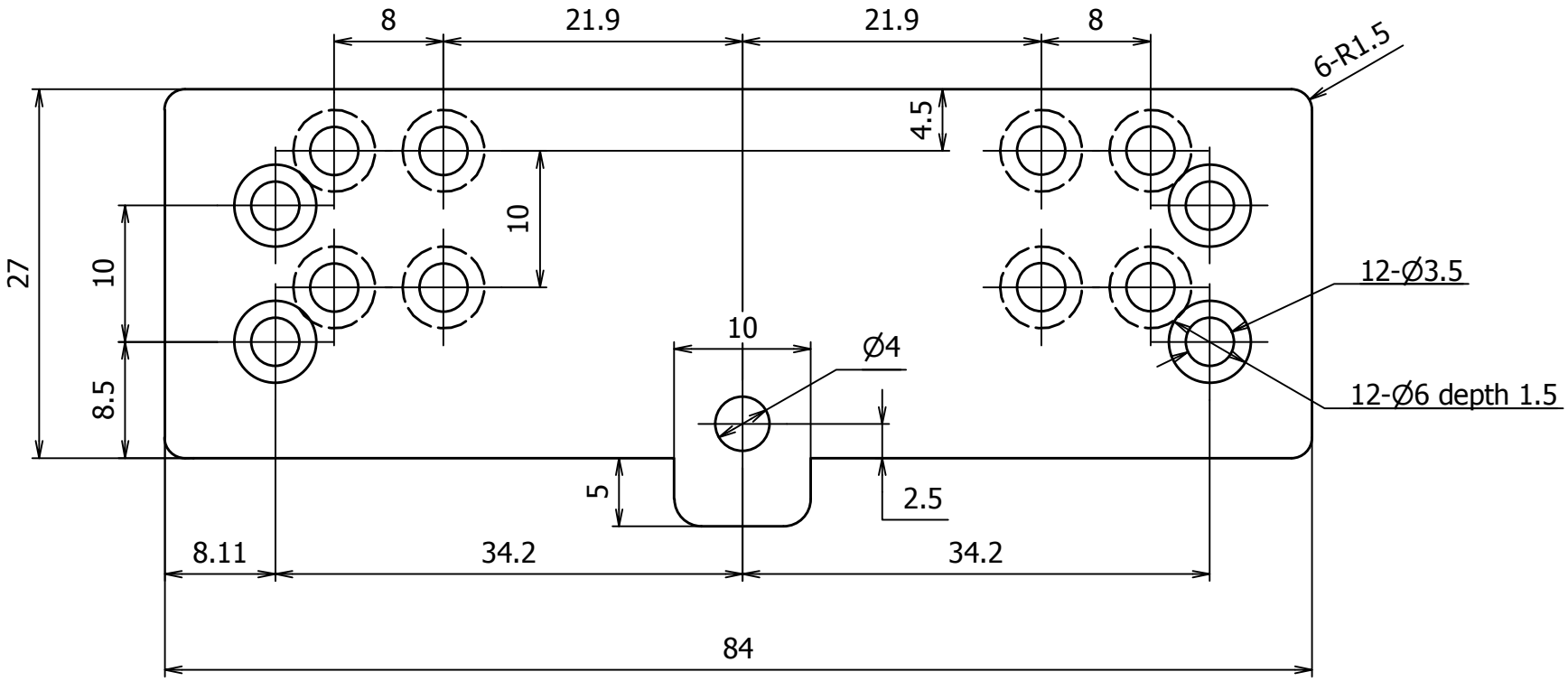

Note:
t=4

ANKLE ORTHOSIS			SCALE 2:1	REF. DRAW. 35		KOMEDA LAB
						BASE PLATE FORE EM
Rev	Date	Description	Trung Author	Checked	Approved	
			MASS [Kg] 0.01	MATERIAL Aluminum-6061		PART NUMBER: 39
			Number of part 1			A4

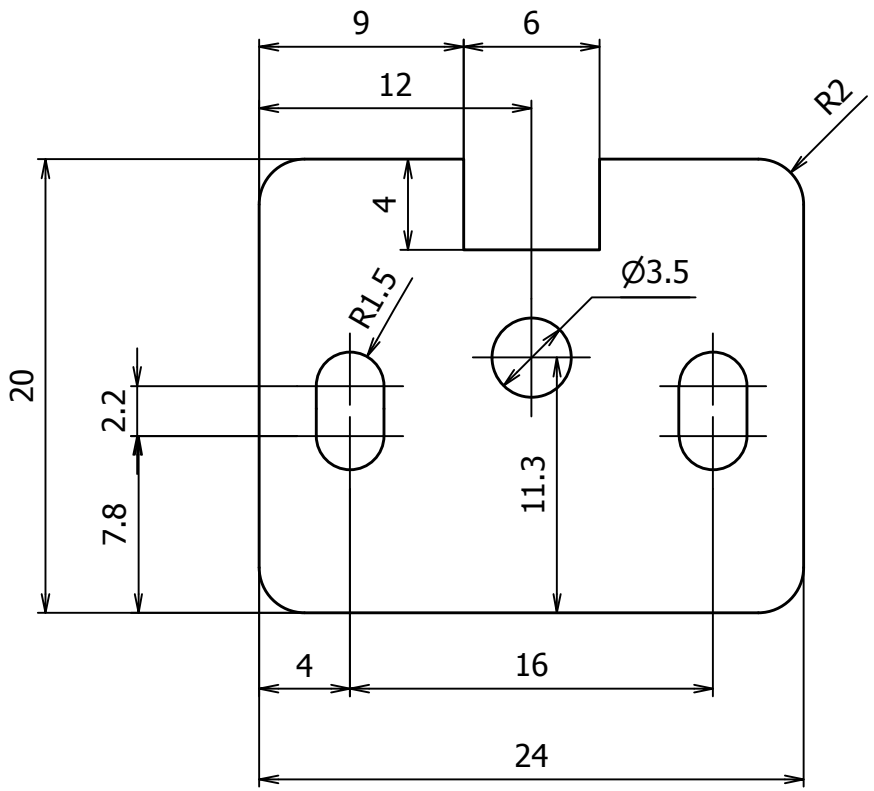

Note:
t = 2.1

ANKLE ORTHOSIS			SCALE 2:1	REF. DRAW. 34, 35		KOMEDA LAB	
						FORCE LINKAGE PLATE	
Rev	Date	Description	Trung Author	Checked	Approved		
			MASS [Kg] 0.002	MATERIAL Aluminum-6061		PART NUMBER: 26	32 / 38
			Number of part 1				A4

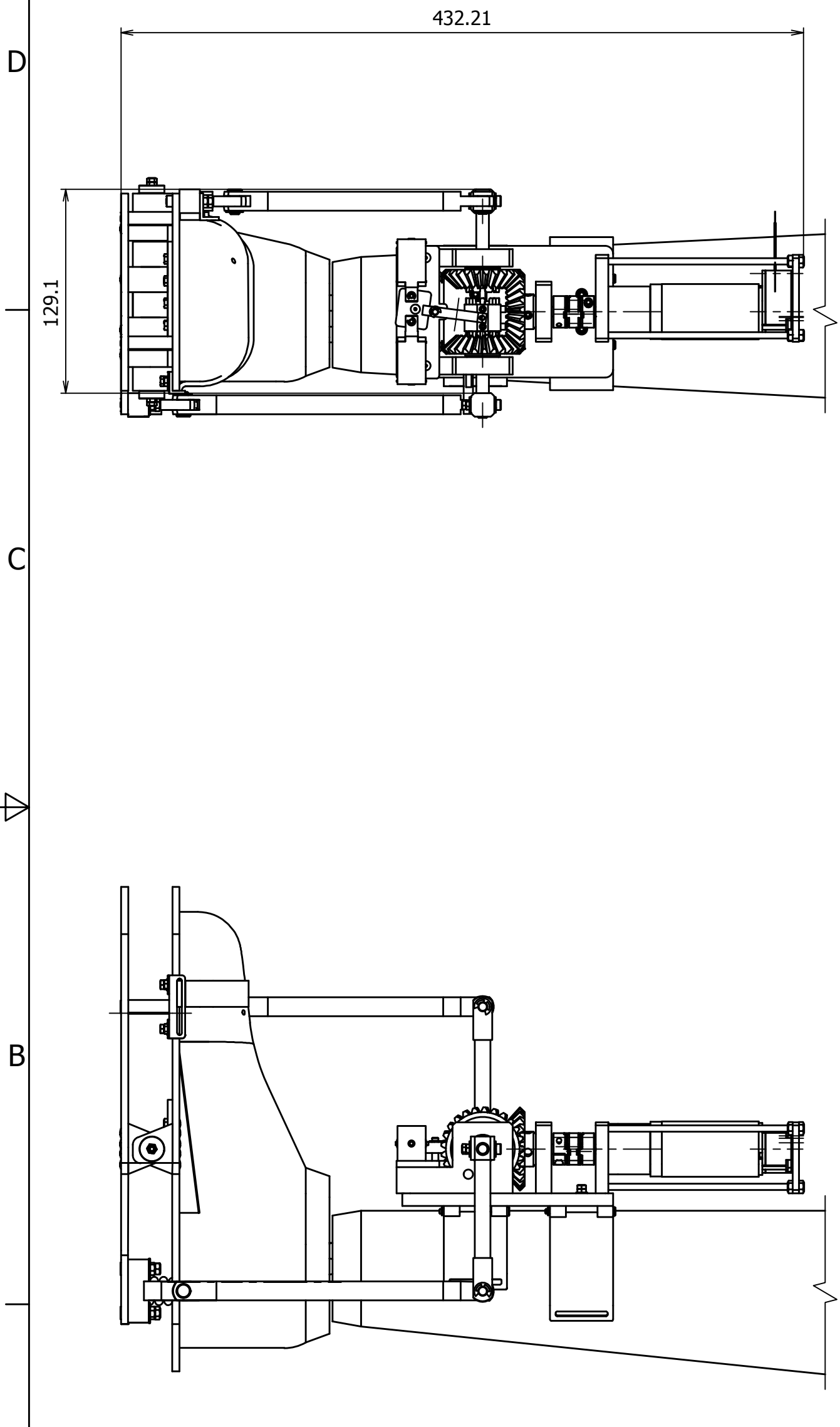

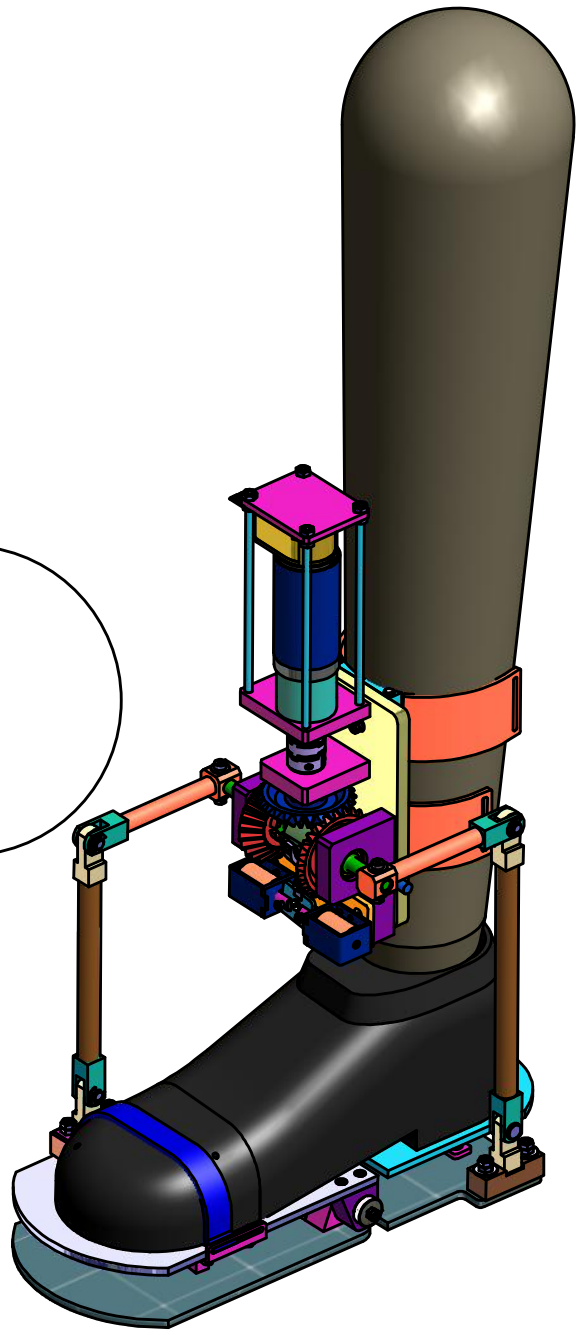

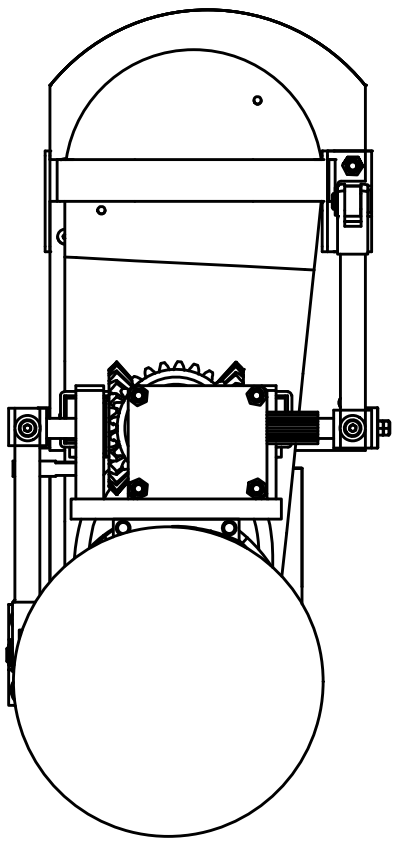

ANKLE ORTHOSIS			SCALE 1:3	REF. DRAW.		KOMEDA LAB	
			TRUNG				
Rev	Date	Description	Author	Checked	Approved		
			MASS [Kg]	MATERIAL		PART NUMBER: 3D ASSEMBLE	33 / 38
			Number of part				A3

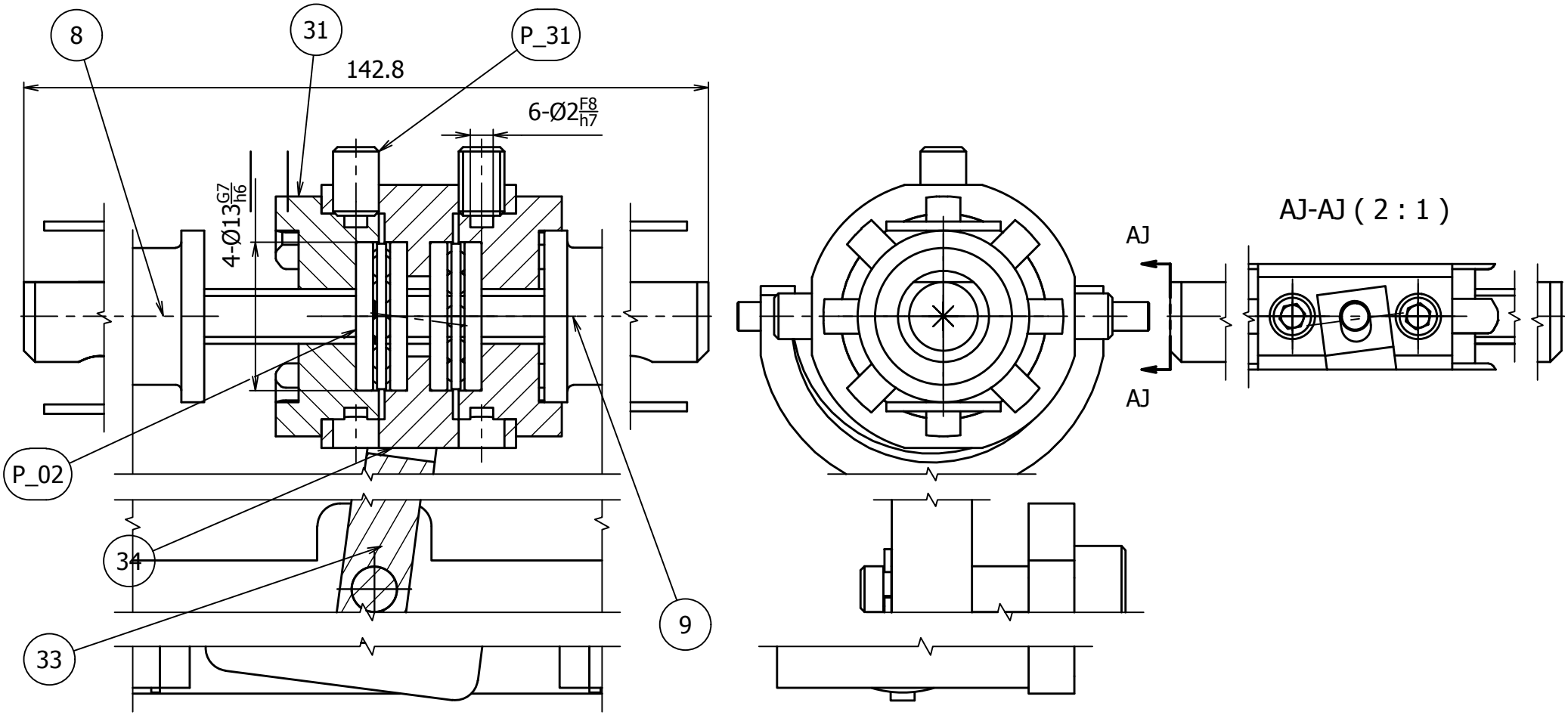

PARTS LIST	
PART NUMBER	TITLE
33	LEVEL ROD
34	OUTER OF CLUTCH
P_02	BEARING FOR CLUTCH
P_31	SCREW TO LIMIT AXIS MOVEMENT

PARTS LIST	
PART NUMBER	TITLE
08	SHAFT OF FOREFOOT BEVEL GEAR
09	SHAFT OF REARFOOT BEVEL GEAR
10	SHAFT OF MAIN BEVEL GEAR
31	JAW CLUTCH

ANKLE ORTHOSIS			SCALE 2:1	REF. DRAW. 35		KOMEDA LAB
						CLUTCH MECHANISM
Rev	Date	Description	TRUNG Author	Checked	Approved	
			MASS [Kg]	MATERIAL		34 / 38
			Number of part			A4

PARTS LIST		
PART NUMBER	QTY	TITLE
29	1	FLANGE OF MOTOR
31	2	JAW CLUTCH
33	1	LEVEL ROD
34	1	OUTER OF CLUTCH
39	1	BASE PLATE FORE EM
P_07	1	COUPLING
P_08	2	ELECTROMAGNET
P_13	1	Planetary Gearhead
P_14	1	MAXON MOTOR
P_19	1	STOPPING PIN FOR REARFOOT

PARTS LIST		
PART NUMBER	QTY	TITLE
01	1	BASE
03	1	FLANGE OF COUPLING
04	1	FLANGE OF REARFOOT BEVEL GEAR
05	2	FOREFOOT BEVEL GEAR
06	1	MAIN BEVEL GEAR
08	1	SHAFT OF FOREFOOT BEVEL GEAR
09	1	SHAFT OF REARFOOT BEVEL GEAR
10	1	SHAFT OF MAIN BEVEL GEAR
19	1	COVER FOR MOTOR PROTECTION FRAME
26	1	FORCE LINKAGE PLATE

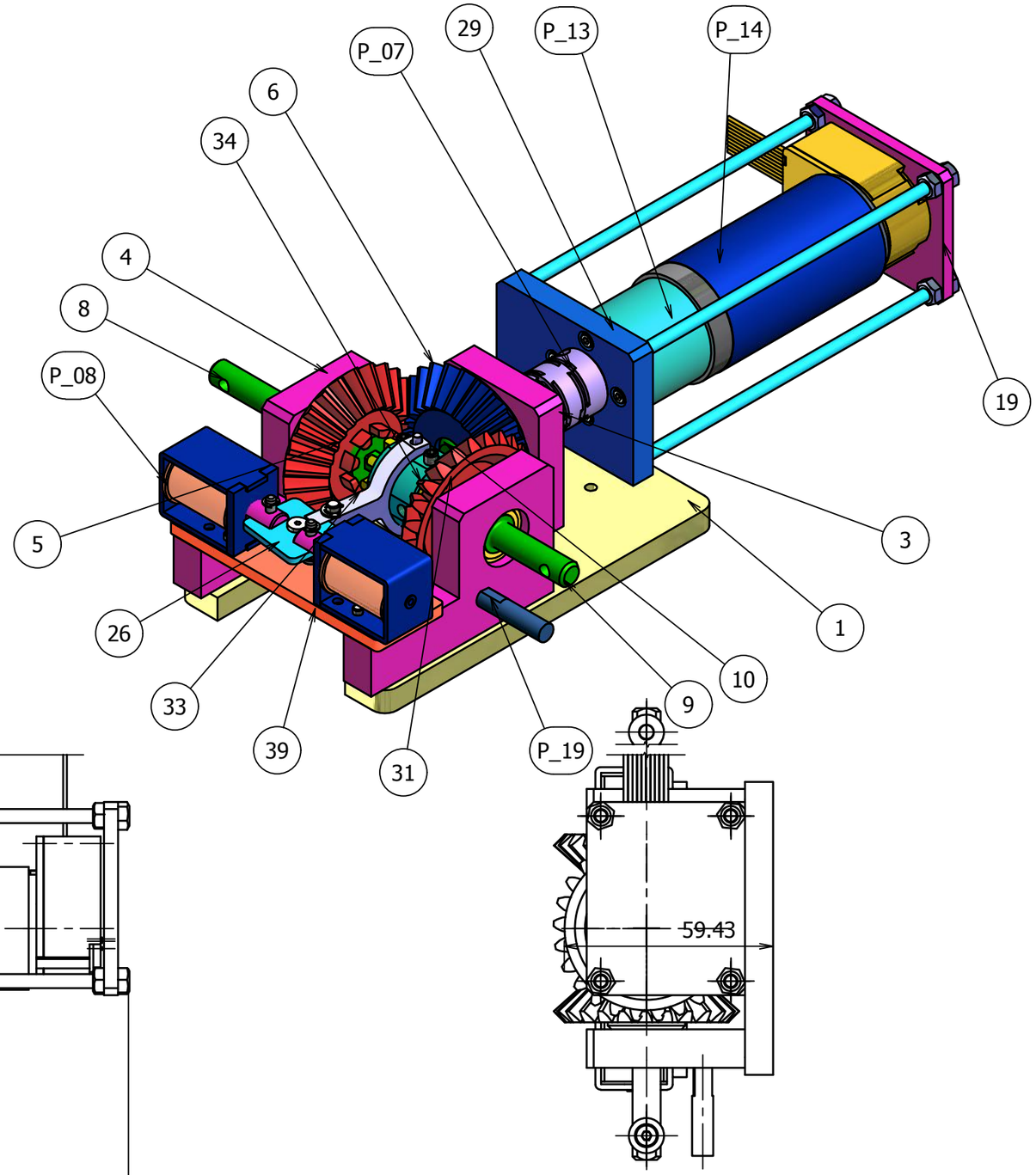

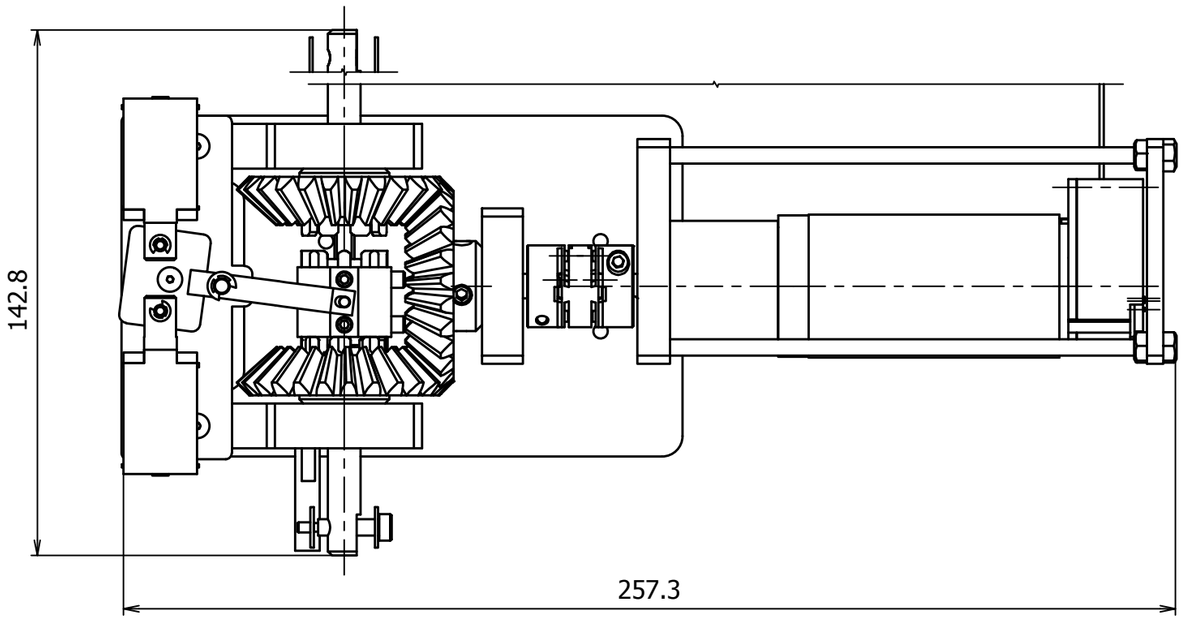

ANKLE ORTHOSIS			SCALE 1:1	REF. DRAW. 34, 38		KOMEDA LAB
						POWER GENERATING STRUCTURE
				TRUNG		
Rev	Date	Description	Author	Checked	Approved	
			MASS [Kg] 1.95	MATERIAL		35 / 38
			Number of part			A3

PARTS LIST		
PART NUMBER	QTY	TITLE
27	1	UPPER REARFOOT PLATE
28	1	REARFOOT VERTICAL ROD
P_06	8	BUSHING
P_11	4	ROTARY JOINT
P_20	2	POST BETWEEN UPPER AND LOWER FOREFOOT PLATE
P_52	1	ROTARY SHARFT BETWEEN REARFOOT AND FOREFOOT PLATE
P_53	1	SPRING

PARTS LIST		
PART NUMBER	QTY	TITLE
10	1	SHAFT OF MAIN BEVEL GEAR
11	2	BASE FOR ROTARY JOINTS AT REARFOOT AND FOREFOOT
12	1	UPPER FOREFOOT PLATE
13	1	FOREFOOT VERTICAL ROD
16	2	REARFOOT HORIZONAL ROD
18	1	RIGHT HINDGE OF FOREFOOT STRAP
20	1	LOWER FOREFOOT PLATE
21	1	LOWER REARFOOT PLATE
22	2	RIGHT HINDGE OF LOWER FOREFOOT PLATE
23	2	RIGHT HINDGE OF UPPER FOREFOOT PLATE
24	2	LEFT HINDGE OF LOWER REARFOOT PLATE

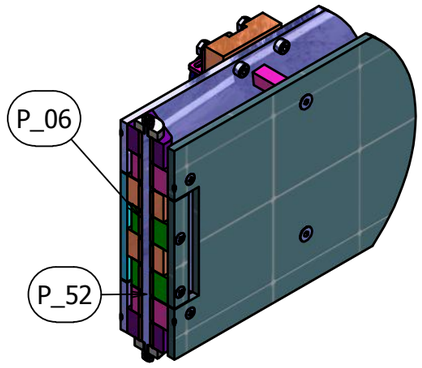

Slide view through the rotary shaft between rearfoot an forefoot plate (1:3)

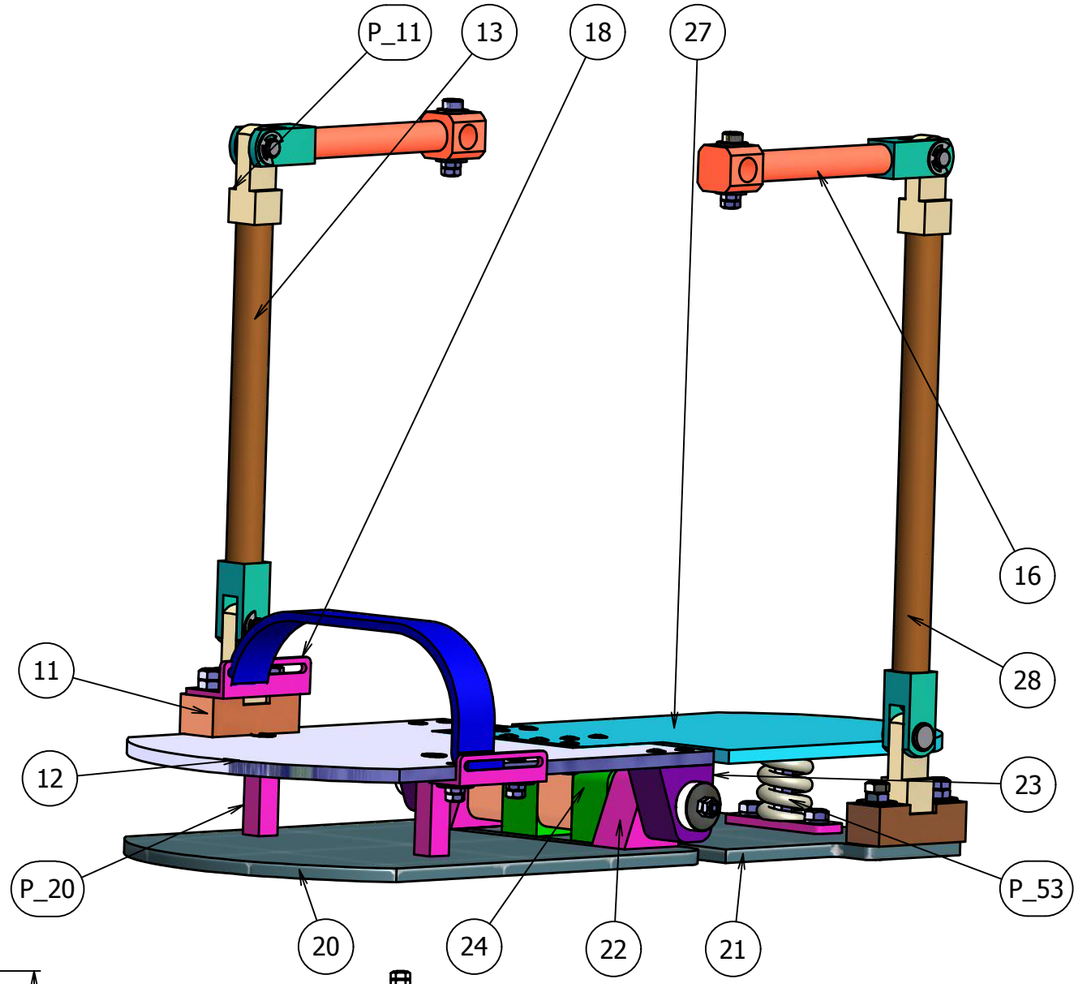

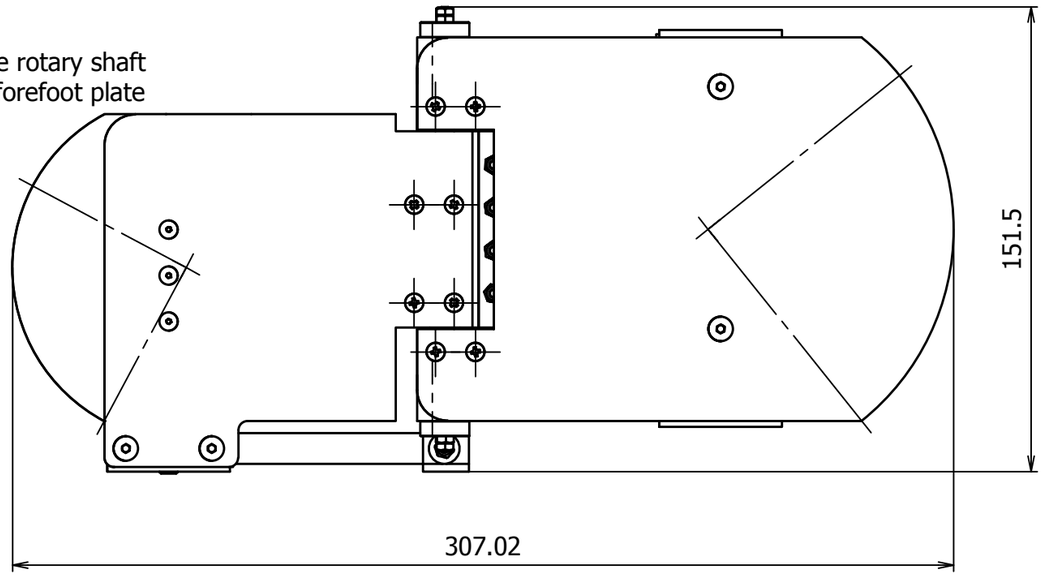

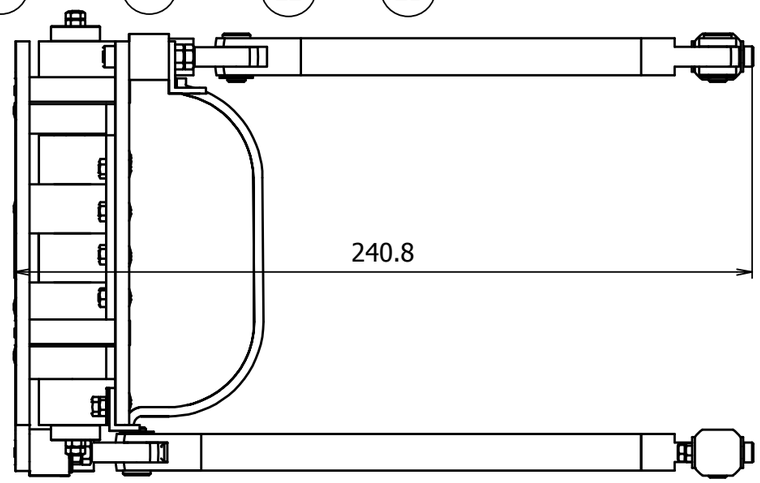

ANKLE ORTHOSIS			SCALE 1:2	REF. DRAW.		KOMEDA LAB
						SOLE AND CRANK-CONNECTION MECHANISM
Rev	Date	Description	TRUNG Author		Checked	Approved
			MASS [Kg] 1.66		MATERIAL	36 / 38
			Number of part			A3

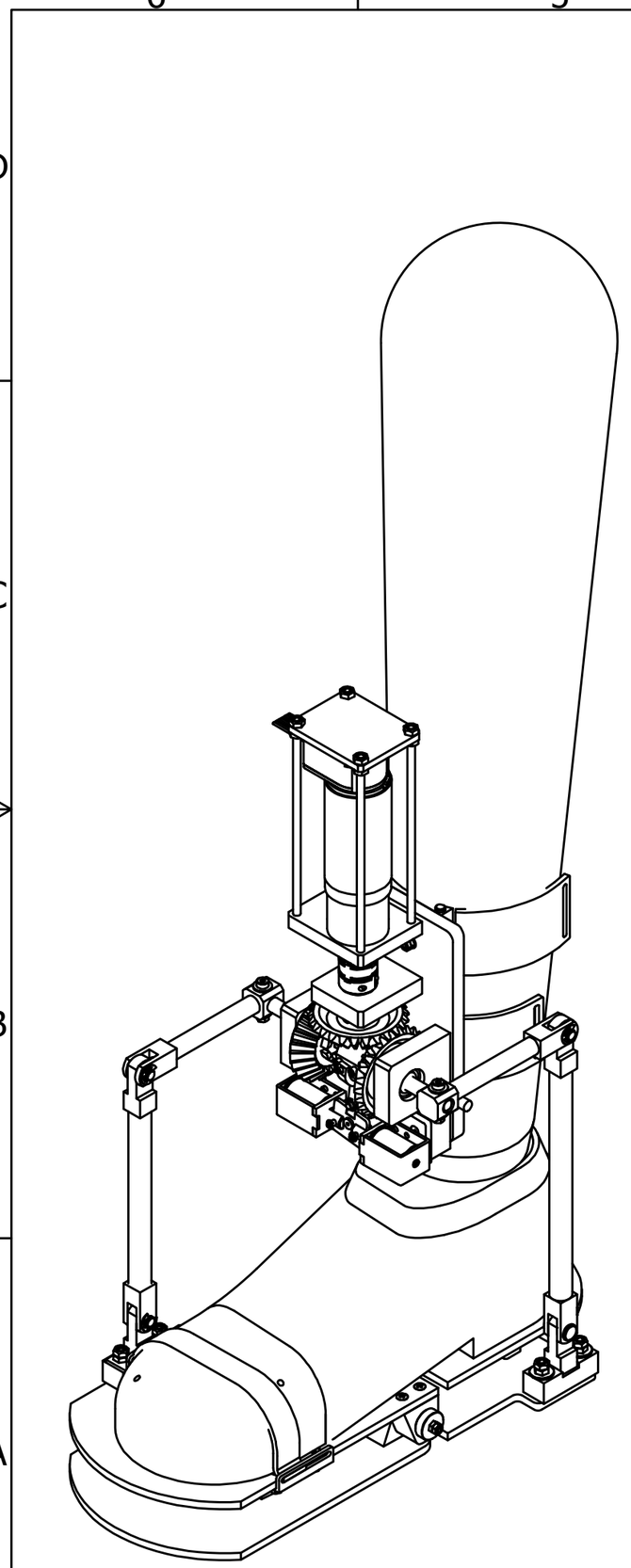

PARTS LIST

PART NUMBER	STOCK NUMBER	QTY	DESCRIPTION
P_31	SBPP4_6	6	Hexagon Socket Set Screws - Soft Point
P_32	CBS3-16	4	CBS, CBSST - Hexagon Socket Low Head Cap Screws
P_33	CBSS3-6	9	Hexagon Socket Extra Low Head Cap Screws
P_34	FB4_10	4	Hexagon Socket Head Cap Screws
P_37	CB4-25	2	CB - Hexagon Socket Head Cap Screws
P_38	CB2.5-10	4	Hexagon Socket Head Cap Screws
P_39	CBSS3-10	5	Hexagon Socket Extra Low Head Cap Screws
P_40	VIS3-10	20	Ornamental Screws
P_41	FWB4-130-E7-F10	4	Screws - Both Ends Right-Hand Screw
P_42	ACB3-25	2	Hexagon Socket Head Cap Screws
P_43	MSSF5-5	2	Hexagon Socket Set Screws
P_44	CB5-10	10	Hexagon Socket Head Cap Screws
P_45	LSBRK6-25	1	Hexagonal Posts - Both Ends Tapped - Standard L
P_46	CBALW4	4	Washers - Standard/Precision
P_47	CBALW3	4	CBALW, CBALWB - Aluminum Washers
P_49	WSSB12-3-1	2	Washers - Standard/Precision
P_50	R6.5-16	4	Washers - Standard/Precision
P_51	SLW4	2	Spring Washers
P_52	SFRM6-125.0-F10.0-B5-P3-T10.0-S5-Q3	1	Both Ends Threaded
P_53	SWL18_35	1	Compression spring
P_54	NETW2	6	1.0 - Retaining Rings - E
P_55	CB6-12	2	CB - Hexagon Socket Head Cap Screws
P_56	FB4-25	2	FB - Hexagon Socket Head Cap Screws

PARTS LIST

PART NUMBER	STOCK NUMBER	QTY	DESCRIPTION
P_01	HCCG6-12.2D	4	Precision Pivot Pins - Standard with Head and Retaining Ring Grooves - Configurable L Dimension
P_02	AST_Bearings_F7-13M	2	Thrust ball bearing
P_03	B7001	3	Angular Ball Bearings
P_06	MPBZ6-15	8	Copper Alloy - Straight Bushing
P_07	D_MCGLC20-6-6	1	Disc Clamping - Double Discs
P_08	CE0830	2	TAKAHA EM
P_09	110514	1	Encoder HEDL 5540, 500 CPT, 3 Channels, with Line Driver RS 422
P_10	NJTW2body	4	NJTW-body - Knuckle Joints - Standard - Concave
P_11	NJT2	4	Knuckle Joints - Standard - Convex
P_12	NETW5	4	1.2 - Retaining Rings - E
P_13	166156	1	Planetary Gearhead GP 32 A Ø32 mm, 0.75 - 4.5 Nm
P_14	273752_01	1	DC ServoMotor
P_16	AJP4-16	1	AJP, AJPB - Adjusting Pins
P_17	SPPTP-D2.51-L9.5	2	Locating Pins - Small Diameter - Configurable Straight Tolerance
P_18	HCDG3-10D	2	Standard with Head and Retaining Ring Grooves - Standard L Dimension
P_19	STPAB6_L25_00	1	Locating Pins for Jigs -Flat
P_20	NLRFB8_28_M4	2	Both Ends Tapped
P_22	NETW3	1	1.0 - Retaining Rings - E
P_23	CBALN4	12	Aluminum Nuts
P_24	CBTN3	20	CBTN - Titanium Nuts
P_25	CBALN3	4	Aluminum Nuts
P_29	CBTN4	6	Titanium Nuts
P_30	MSB4-15	2	Stripper Bolts - Shaft Diameter Tolerance e9

ANKLE ORTHOSIS			SCALE 1:1	REF. DRAW.		KOMEDA LAB
						LIST OF PURCHASED PARTS
			TRUNG			
Rev	Date	Description	Author	Checked	Approved	
			MASS [Kg]	MATERIAL		37 / 38
			Number of part			A3

PARTS LIST

PART NUMBER	QTY	TITLE	MATERIAL
19	1	COVER FOR MOTOR PROTECTION FRAME	Aluminum-6061
20	1	LOWER FOREFOOT PLATE	Aluminum-6061
21	1	LOWER REARFOOT PLATE	Aluminum-6061
22	2	RIGHT HINDGE OF LOWER FOREFOOT PLATE	Aluminum-6061
23	2	RIGHT HINDGE OF UPPER FOREFOOT PLATE	Aluminum-6061
24	2	LEFT HINDGE OF LOWER REARFOOT PLATE	Aluminum-6061
25	2	LEFT HINDGE OF UPPER REARFOOT PLATE	Aluminum-6061
26	1	FORCE LINKAGE PLATE	Aluminum-6061
27	1	UPPER REARFOOT PLATE	Aluminum-6061
28	1	REARFOOT VERTICAL ROD	Steel
29	1	FLANGE OF MOTOR	Aluminum-6061
30	1	PLATE OF FIXING REARFOOT TO FOREFOOT	Aluminum-6061
31	2	JAW CLUTCH	Steel
33	1	LEVEL ROD	Steel
34	1	OUTER OF CLUTCH	Steel
39	1	BASE PLATE FORE EM	Aluminum-6061

PARTS LIST

PART NUMBER	QTY	TITLE	MATERIAL
01	1	BASE	Aluminum-6061
02	1	FLANGE OF FOREFOOT BEVEL GEAR	Aluminum-6061
03	1	FLANGE OF COUPLING	Aluminum-6061
04	1	FLANGE OF REARFOOT BEVEL GEAR	Aluminum-6061
05	2	FOREFOOT BEVEL GEAR	Steel
06	1	MAIN BEVEL GEAR	Steel
08	1	SHAFT OF FOREFOOT BEVEL GEAR	Steel
09	1	SHAFT OF REARFOOT BEVEL GEAR	Steel
10	1	SHAFT OF MAIN BEVEL GEAR	Steel
11	2	BASE FOR ROTARY JOINTS AT REARFOOT AND FOREFOOT	Steel
12	1	UPPER FOREFOOT PLATE	Aluminum-6061
13	1	FOREFOOT VERTICAL ROD	Aluminum-6061
14	1	GUILDING PART FOR REARFOOT SPRING	Steel
15	1	FOREFOOT HORIZONAL ROD	Aluminum-6061
16	2	REARFOOT HORIZONAL ROD	Steel
17	1	LEFT HINDGE OF FOREFOOT STRAP	Aluminum-6061
18	1	RIGHT HINDGE OF FOREFOOT STRAP	Aluminum-6061

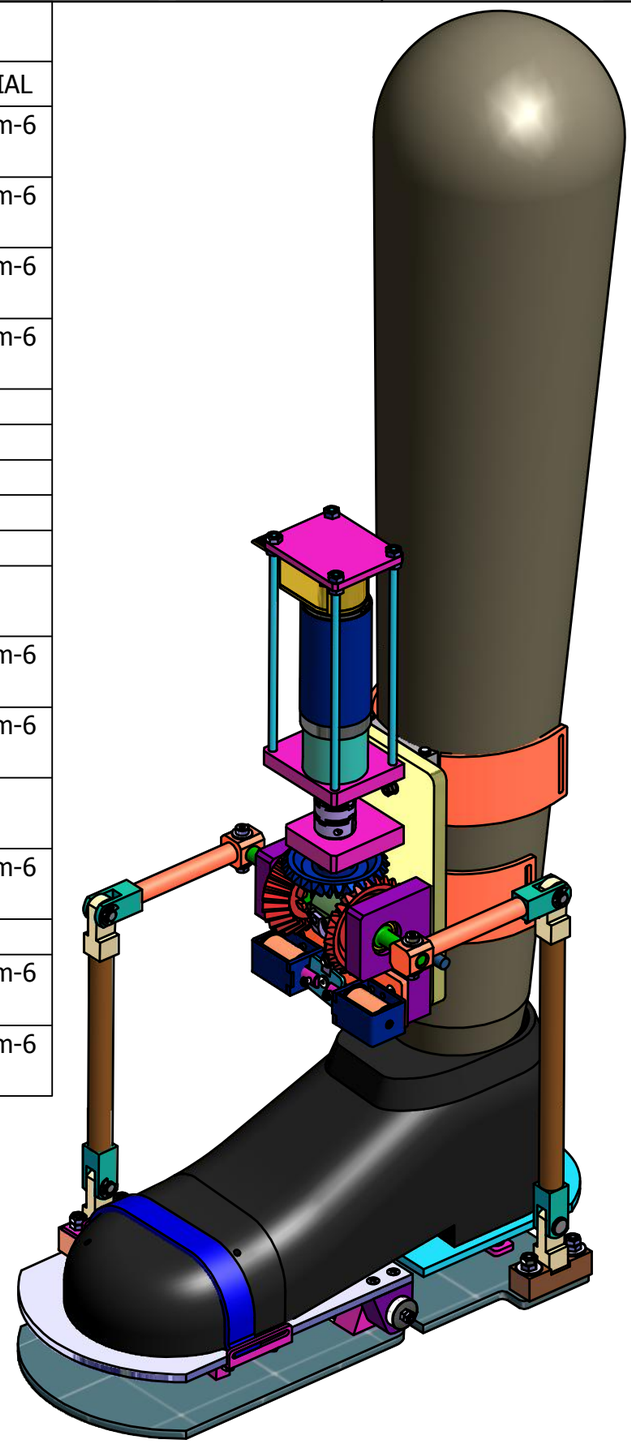

ANKLE ORTHOSIS		SCALE 1:1	REF. DRAW.		KOMEDA LAB
					LIST OF MANUFACTURED PARTS
Rev	Date	Description	TRUNG Author	Checked	Approved
			MASS [Kg]	MATERIAL	38 / 38
			Number of part		A3

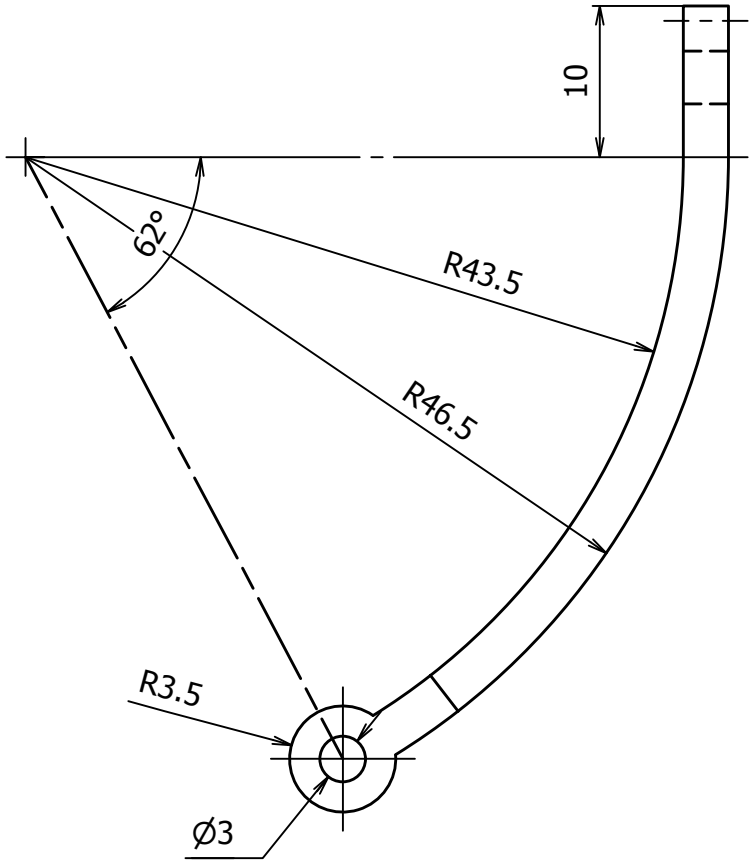

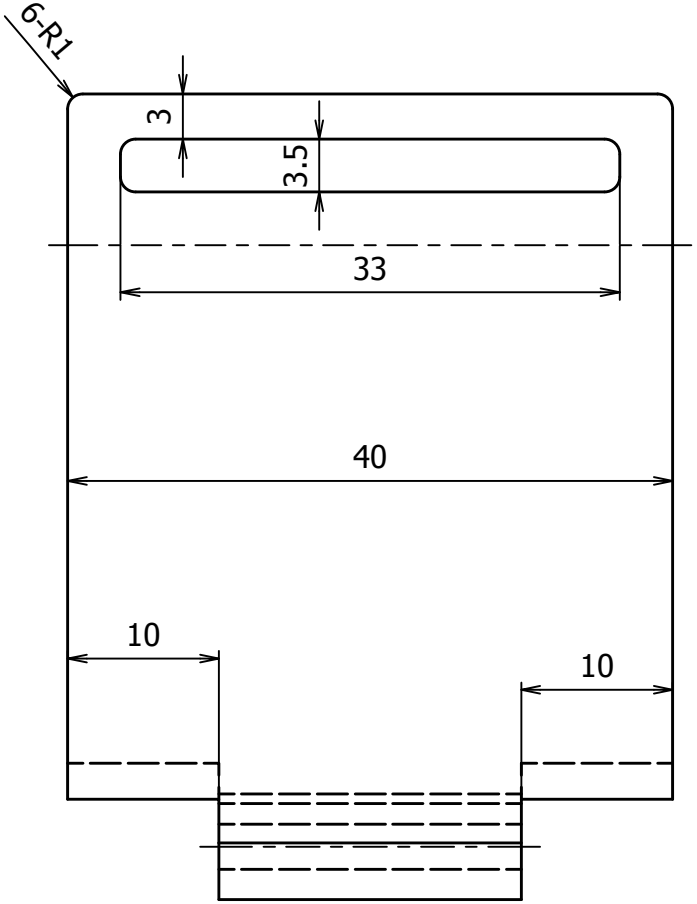

ANKLE ORTHOSIS			SCALE 2:1	REF. DRAW. 46		KOMEDA LAB	
						MOVABLE JAW OF LOWER CUFF	
Rev	Date	Description	TRUNG Author		Checked	Approved	
			MASS [Kg] 0.018	MATERIAL Aluminum-6061		PART NUMBER: 38	38 / 46
			Number of part 2				A4

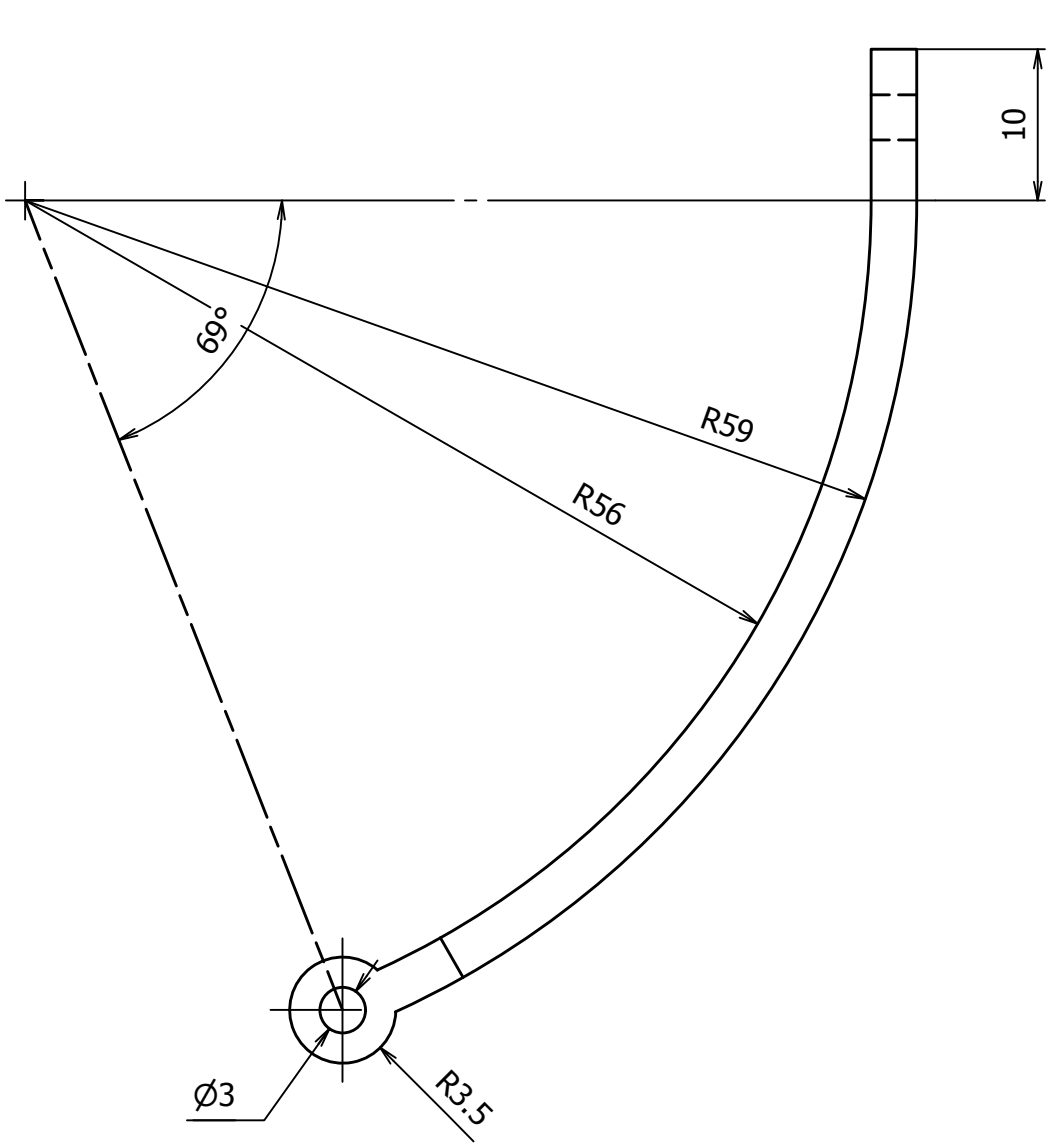

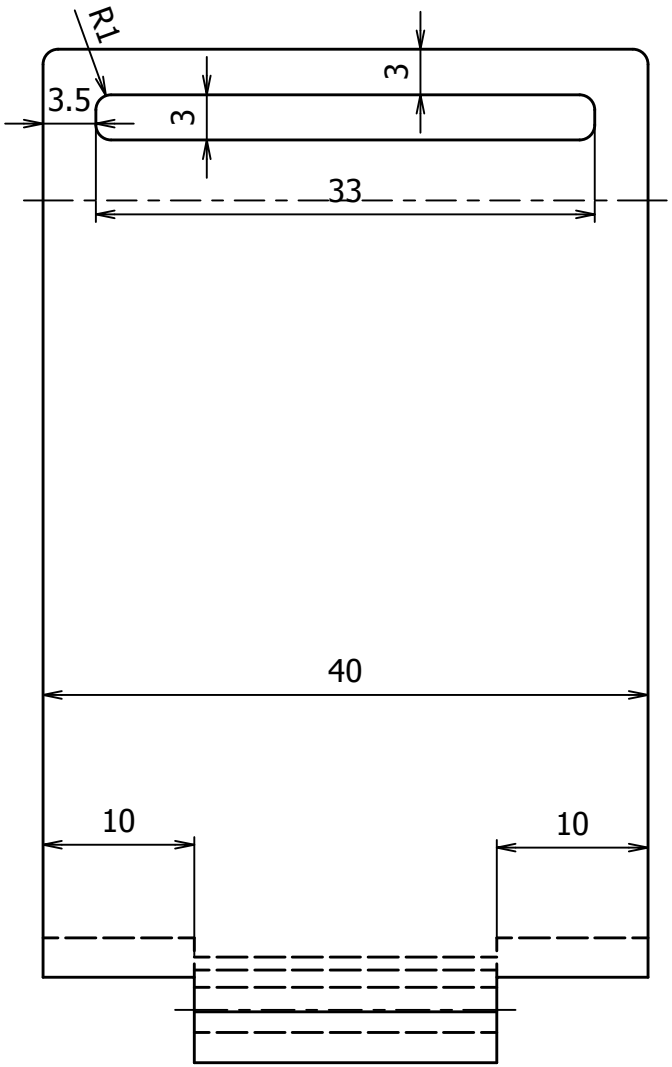

ANKLE ORTHOSIS			SCALE 2:1	REF. DRAW. 46		KOMEDA LAB	
						MOVABLE JAW OF UPPER CUFF	
Rev	Date	Description	TRUNG Author		Checked	Approved	
			MASS [Kg] 0.025		MATERIAL Aluminum-6061	PART NUMBER: 37	37 / 46
			Number of part 2				A4

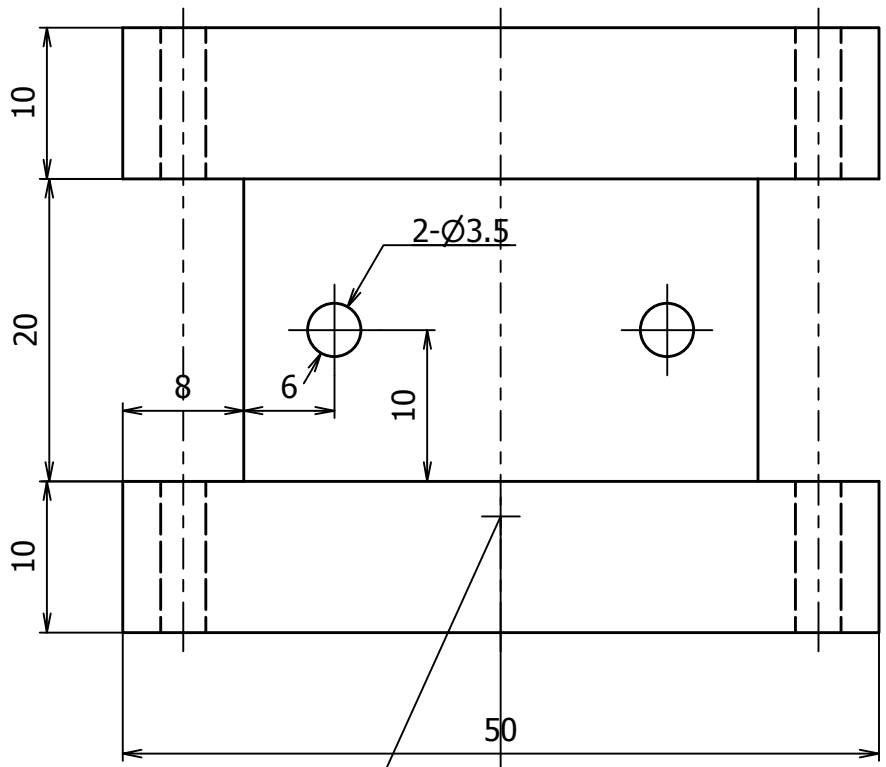

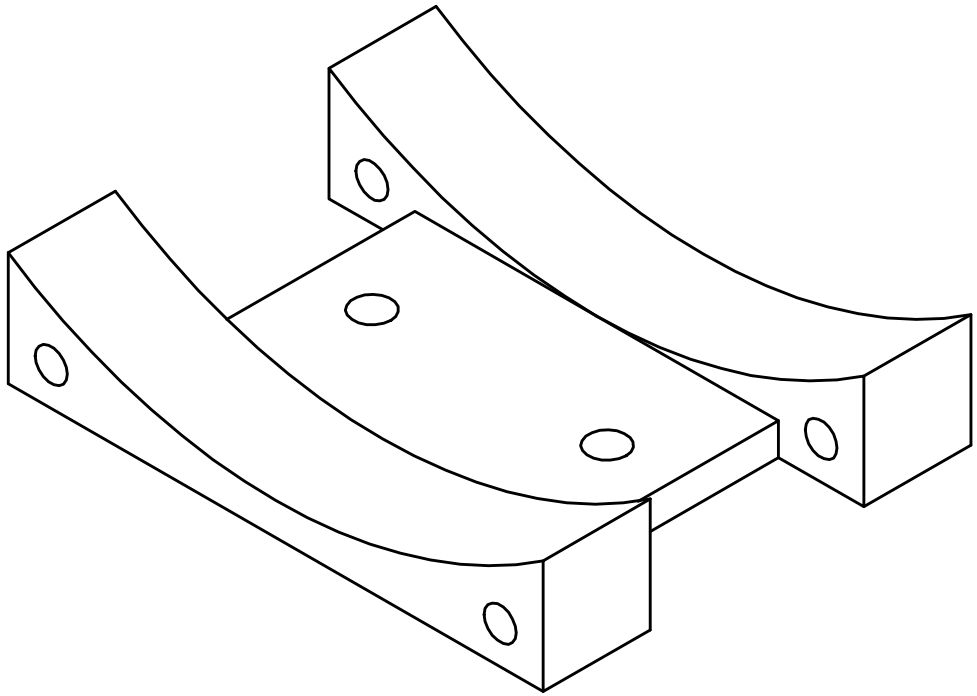

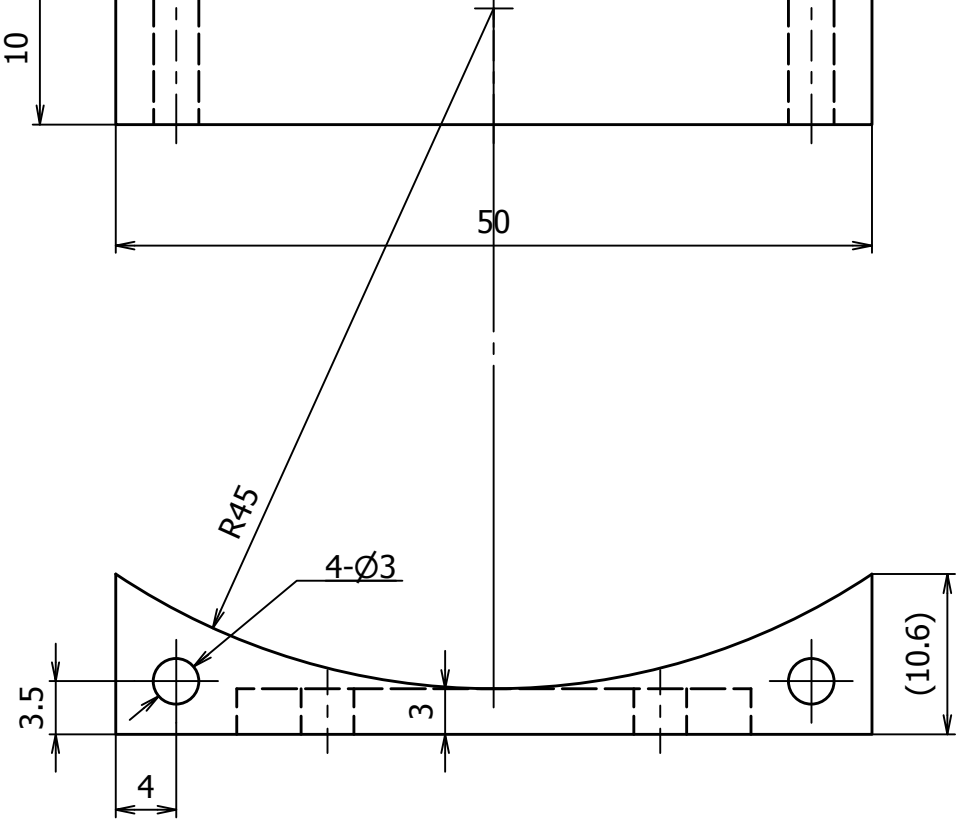

ANKLE ORTHOSIS			SCALE 2:1	REF. DRAW. 46		KOMEDA LAB
						LOWER BASE CUFF
Rev	Date	Description	TRUNG Author	Checked	Approved	
			MASS [Kg] 0.019	MATERIAL Aluminum-6061		PART NUMBER: 36
			Number of part 1			A4

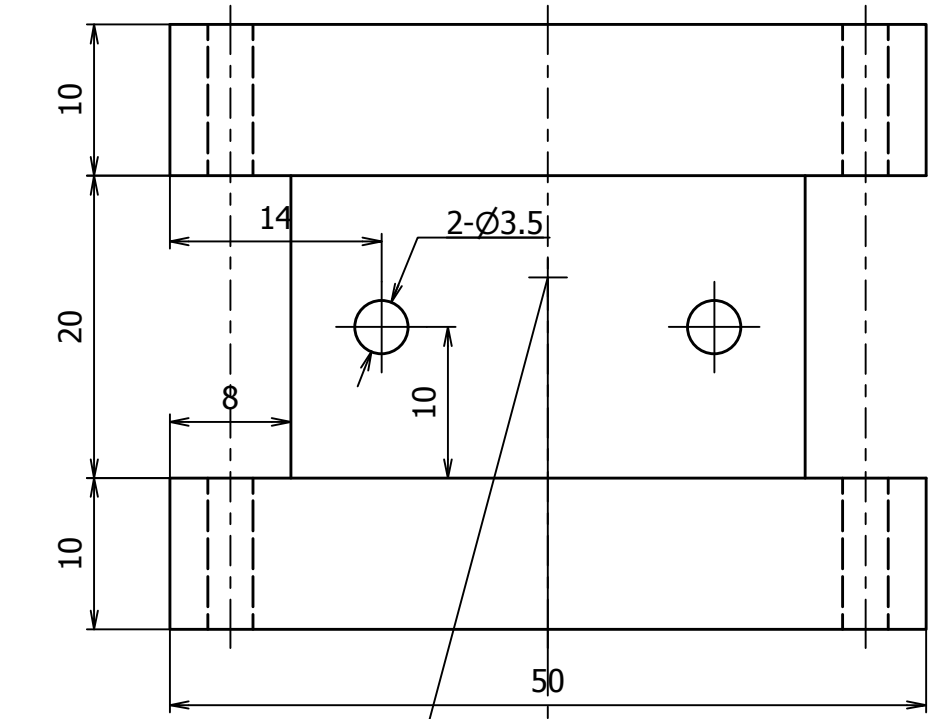

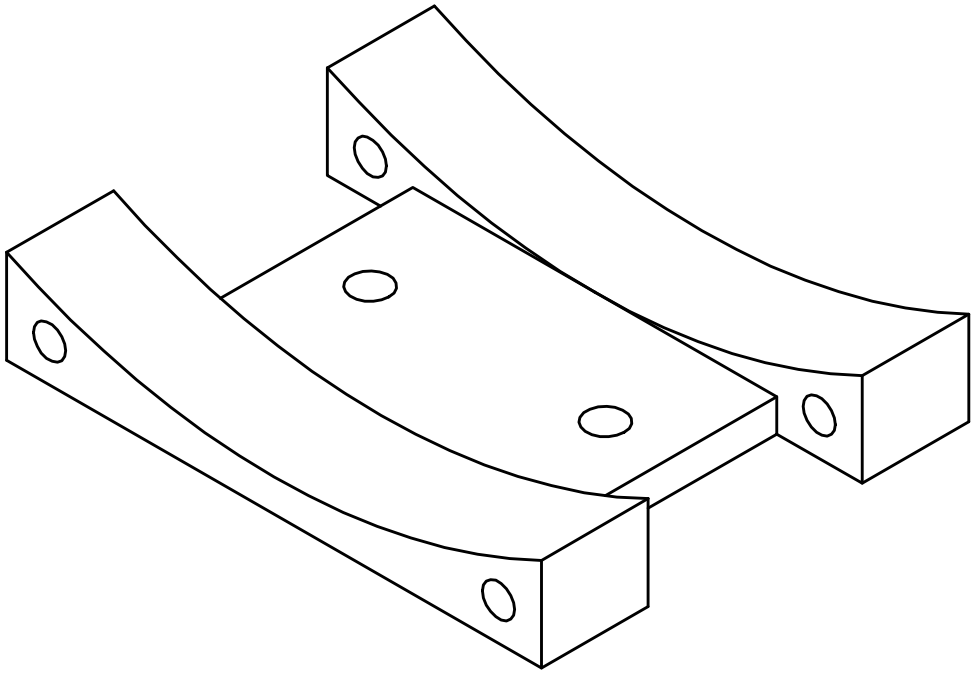

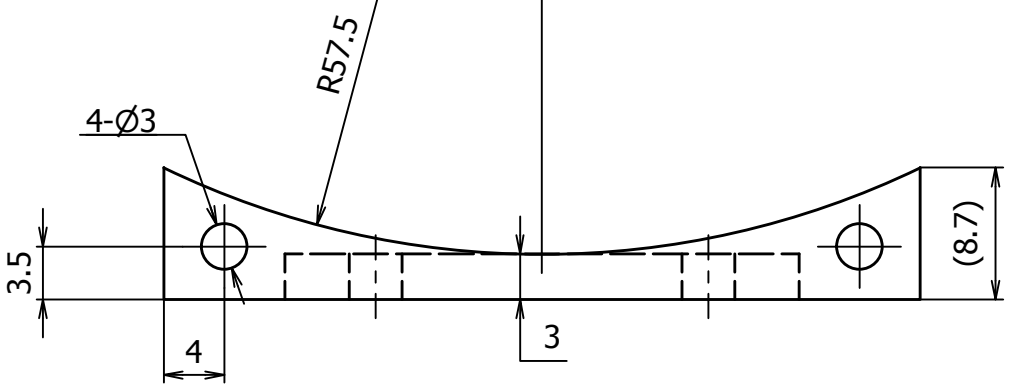

ANKLE ORTHOSIS			SCALE 2:1	REF. DRAW. 46		KOMEDA LAB	
						UPPER BASE CUFF	
Rev	Date	Description	TRUNG Author		Checked	Approved	
			MASS [Kg] 0.018		MATERIAL Aluminum-6061	PART NUMBER: 32	35 / 46
			Number of part 1				A4

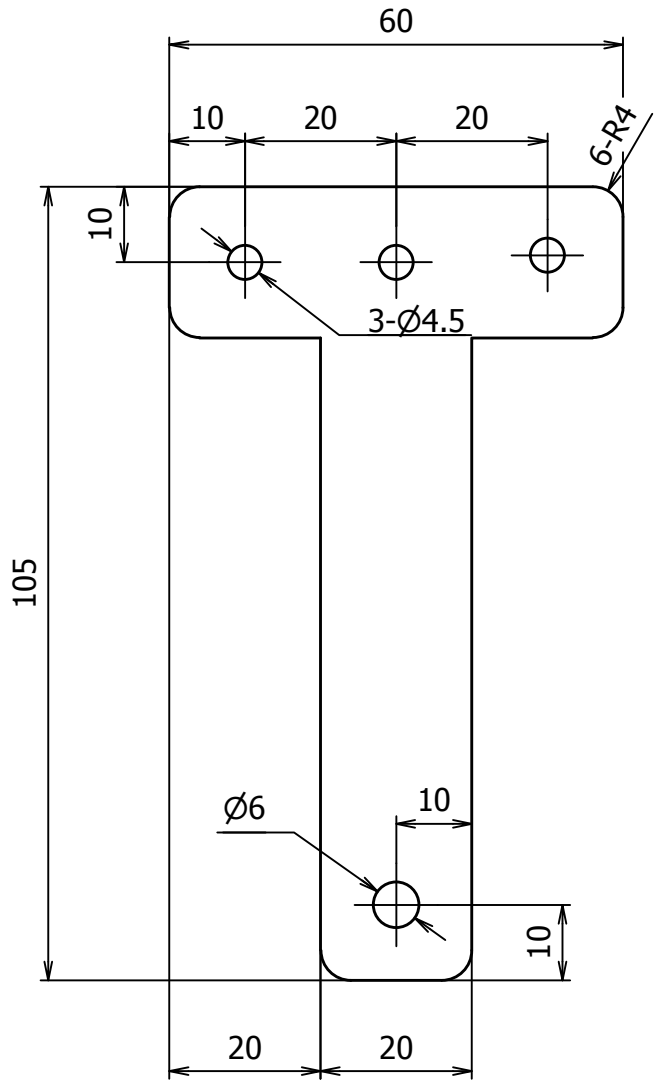

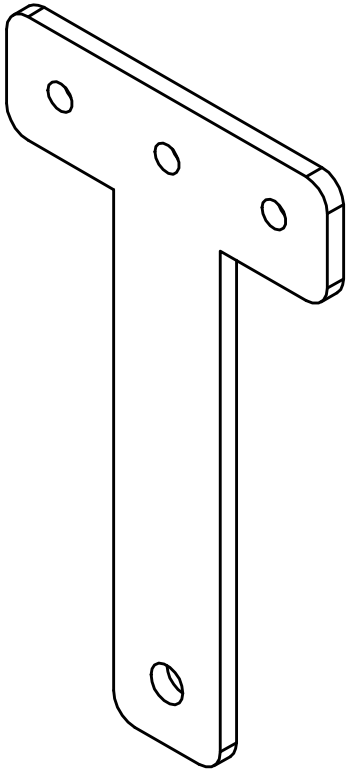

Note:
t=3 mm

ANKLE ORTHOSIS			SCALE 1:1	REF. DRAW. 46		KOMEDA LAB	
						ATTACHED ROD ON HEEL	
Rev	Date	Description	TRUNG Author	Checked	Approved		
			MASS [Kg] 0.023	MATERIAL Aluminum-6061		PART NUMBER: 40	41 / 46
			Number of part 1				A4

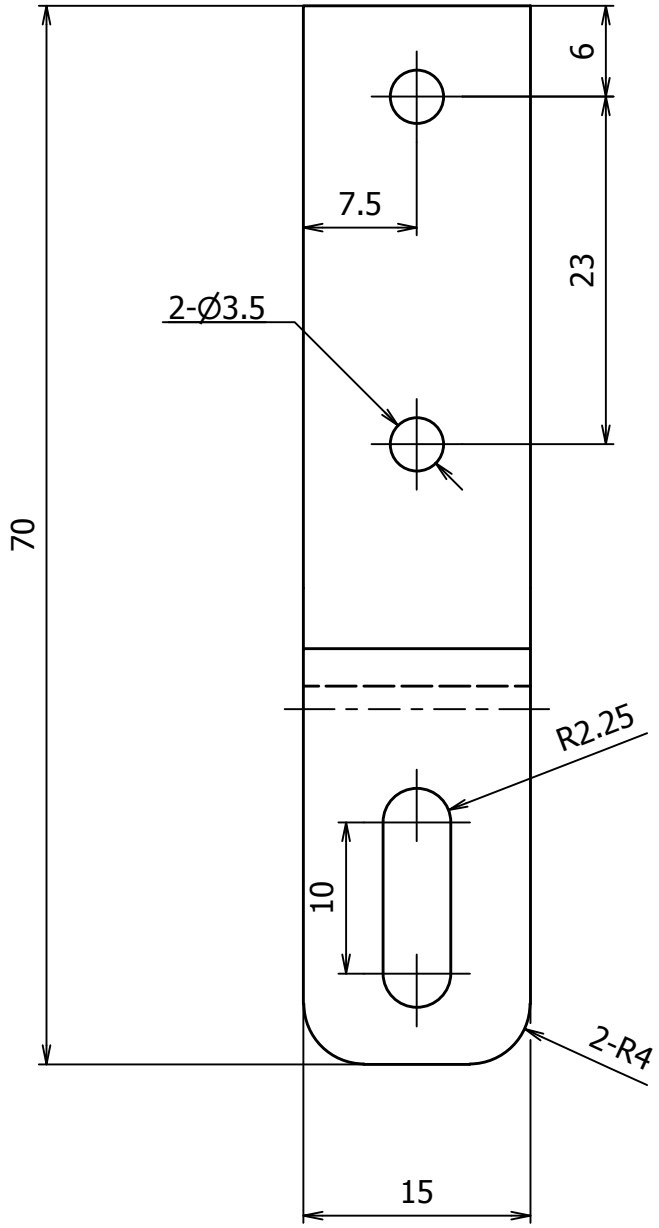

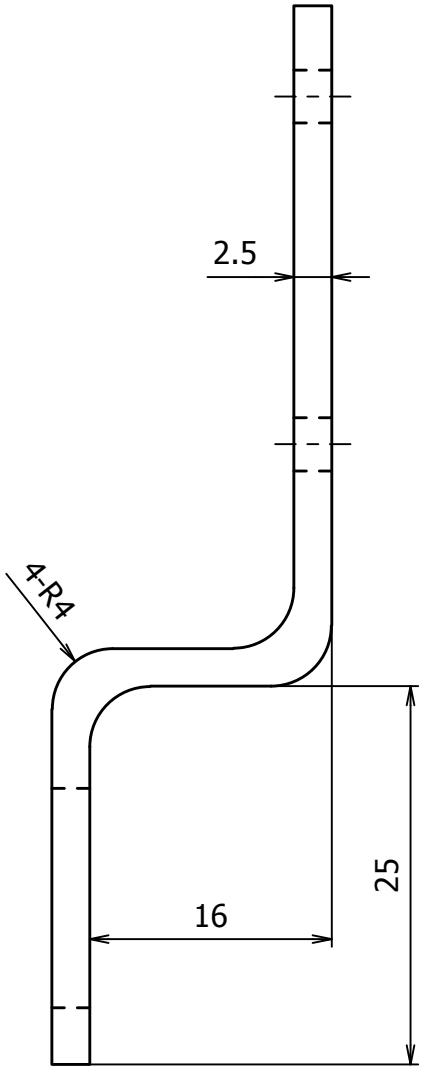

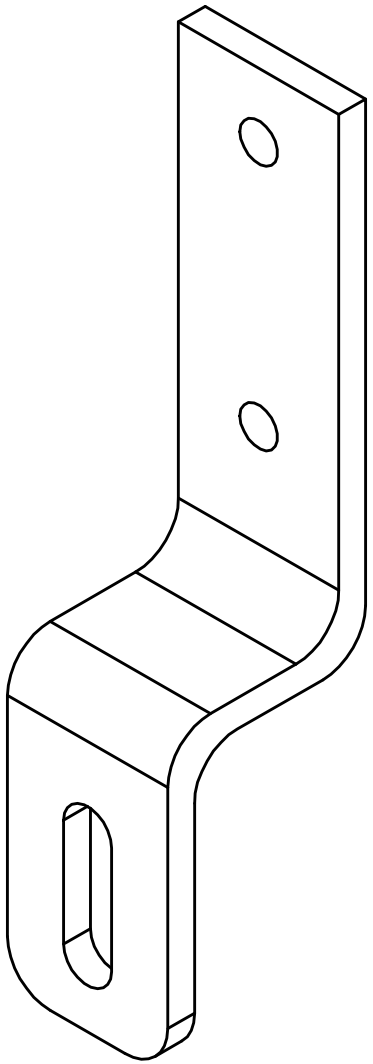

ANKLE ORTHOSIS			SCALE 2:1	REF. DRAW. 46		KOMEDA LAB	
						VERTICAL CONNECTOR FOR POT AT SHANK	
Rev	Date	Description	TRUNG Author	Checked	Approved		
			MASS [Kg] 0.024	MATERIAL Steel		PART NUMBER: 42	39 / 46
			Number of part 1				A4

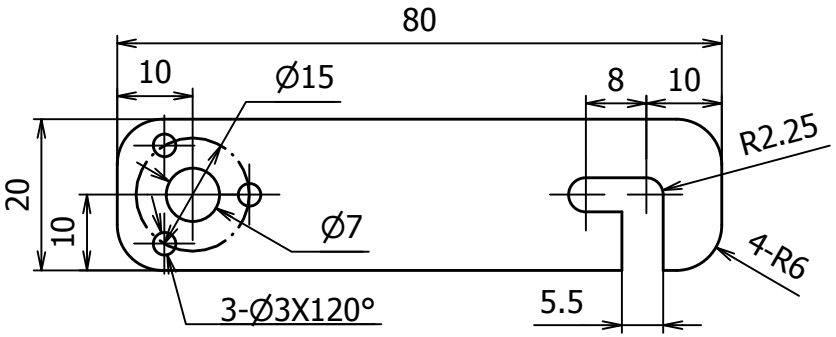

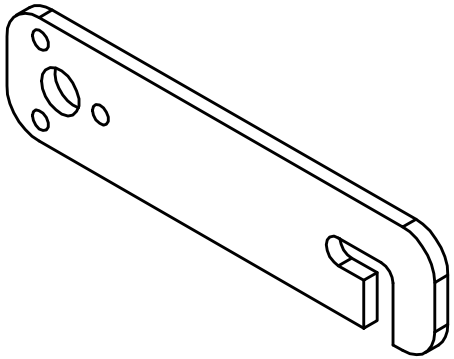

Note:
t=2.5 mm

ANKLE ORTHOSIS			SCALE 1:1	REF. DRAW. 46		KOMEDA LAB
						HORIZONAL CONNECTOR FOR POT AT SHANK
Rev	Date	Description	TRUNG Author	Checked	Approved	
			MASS [Kg] 0.01	MATERIAL Aluminum-6061		PART NUMBER: 41
			Number of part 1			40 / 46 A4

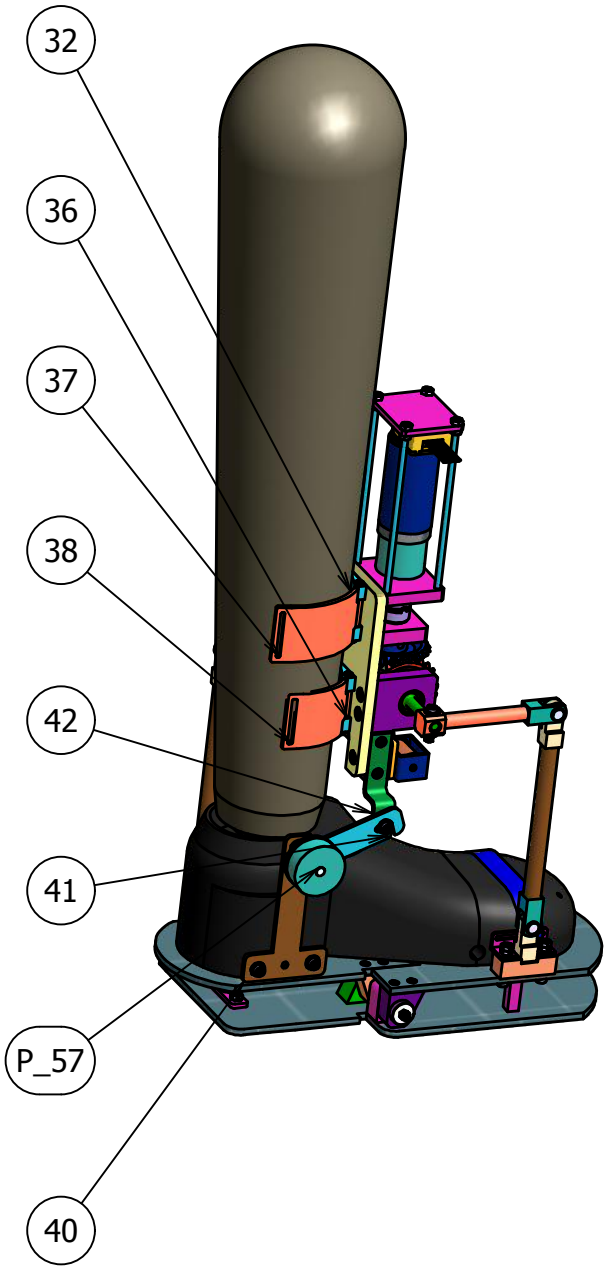

PARTS LIST		
ITEM	PART NUMBER	TITLE
32	32	UPPER BASE CUFF
36	36	LOWER BASE CUFF
37	37	MOVABLE JAW OF UPPER CUFF
38	38	MOVABLE JAW OF LOWER CUFF
40	40	ATTACHED ROD ON HEEL
41	41	HORIZONAL CONNECTOR FOR POT AT SHANK
42	42	VERTICAL CONNECTOR FOR POT AT SHANK
P_57	P_57	POTENTIOMETER

ANKLE ORTHOSIS		SCALE	REF. DRAW.		KOMEDA LAB
Rev	Date	Description	TRUNG Author	Checked	Approved
			MASS [Kg]	MATERIAL	PART NUMBER: 3D ASSEMBLE
			Number of part		A4

RE 35 ∅35 mm, Graphite Brushes, 90 Watt

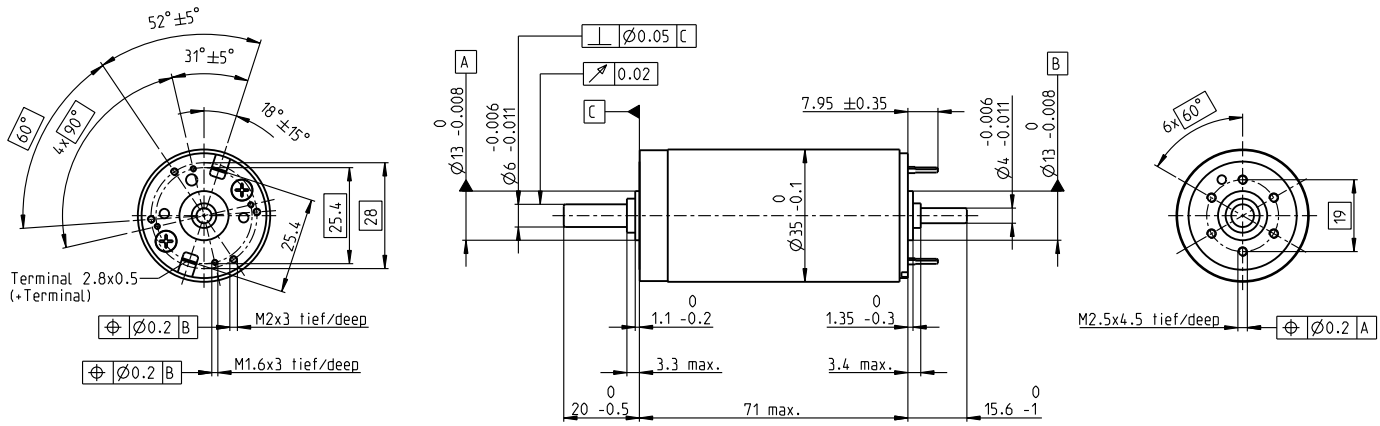

M 1:2

Stock program
Standard program
Special program (on request)

			Order Number												
	according to dimensional drawing		273752	323890	273753	273754	273755	273756	273757	273758	273759	273760	273761	273762	273763
	shaft length 15.6 shortened to 4 mm		285785	323891	285786	285787	285788	285789	285790	285791	285792	285793	285794	285795	285796
Motor Data															
	Values at nominal voltage														
1	Nominal voltage	V	15.0	24.0	30.0	42.0	48.0	48.0	48.0	48.0	48.0	48.0	48.0	48.0	48.0
2	No load speed	rpm	7070	7670	7220	7530	7270	6650	5960	4740	3810	3140	2570	2100	1620
3	No load current	mA	245	168	123	92.7	77.3	68.7	59.7	44.7	34.2	27.1	21.6	17.2	12.9
4	Nominal speed	rpm	6270	6910	6420	6770	6490	5860	5150	3920	2970	2280	1710	1220	732
5	Nominal torque (max. continuous torque)	mNm	73.2	93.3	92.4	97.7	96.5	98.2	98.8	102	105	105	105	104	104
6	Nominal current (max. continuous current)	A	4.00	3.36	2.50	1.95	1.63	1.51	1.36	1.12	0.915	0.752	0.621	0.503	0.391
7	Stall torque	mNm	874	1160	949	1070	967	878	766	613	493	394	320	253	194
8	Starting current	A	45.0	39.7	24.4	20.3	15.5	12.9	10.1	6.43	4.16	2.74	1.83	1.18	0.704
9	Max. efficiency	%	81	84	84	86	85	85	84	83	82	80	79	77	74
	Characteristics														
10	Terminal resistance	Ω	0.334	0.605	1.23	2.07	3.09	3.72	4.75	7.46	11.5	17.5	26.2	40.5	68.2
11	Terminal inductance	mH	0.085	0.191	0.340	0.620	0.870	1.04	1.29	2.04	3.16	4.65	6.89	10.3	17.1
12	Torque constant	mNm / A	19.4	29.2	38.9	52.5	62.2	68	75.8	95.2	119	144	175	214	276
13	Speed constant	rpm / V	491	328	246	182	154	140	126	100	80.5	66.4	54.6	44.7	34.6
14	Speed / torque gradient	rpm / mNm	8.43	6.79	7.76	7.16	7.62	7.67	7.89	7.85	7.84	8.08	8.19	8.46	8.55
15	Mechanical time constant	ms	5.97	5.60	5.50	5.40	5.38	5.38	5.39	5.38	5.37	5.38	5.39	5.39	5.41
16	Rotor inertia	gcm²	67.6	78.7	67.6	72.0	67.4	67.0	65.2	65.4	65.5	63.6	62.8	60.8	60.4

Specifications

Thermal data

17	Thermal resistance housing-ambient	6.2 K / W
18	Thermal resistance winding-housing	2.0 K / W
19	Thermal time constant winding	30 s
20	Thermal time constant motor	1050 s
21	Ambient temperature	-30 ... +100°C
22	Max. permissible winding temperature	+155°C

Mechanical data (ball bearings)

23	Max. permissible speed	12000 rpm
24	Axial play	0.05 - 0.15 mm
25	Radial play	0.025 mm
26	Max. axial load (dynamic)	5.6 N
27	Max. force for press fits (static)	110 N
	(static, shaft supported)	1200 N
28	Max. radial loading, 5 mm from flange	28 N

Other specifications

29	Number of pole pairs	1
30	Number of commutator segments	13
31	Weight of motor	340 g

Values listed in the table are nominal.
Explanation of the figures on page 49.

Option
Hollow shaft as special design
Preloaded ball bearings

Operating Range

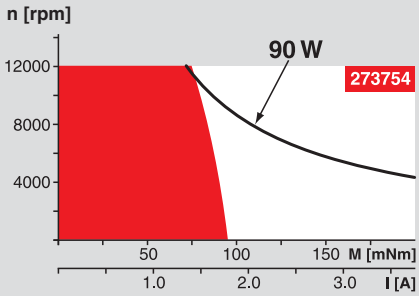

Comments

Continuous operation
In observation of above listed thermal resistance (lines 17 and 18) the maximum permissible winding temperature will be reached during continuous operation at 25°C ambient.
= Thermal limit.

Short term operation
The motor may be briefly overloaded (recurring).

Assigned power rating

maxon Modular System

Overview on page 16 - 21

Planetary Gearhead
∅32 mm
0.75 - 6.0 Nm
Page 229 / 231 / 232

Planetary Gearhead
∅32 mm
4.0 - 8.0 Nm
Page 234

Planetary Gearhead
∅42 mm
3 - 15 Nm
Page 237

Spindle Drive
∅32 mm
Page 249 / 250 / 251

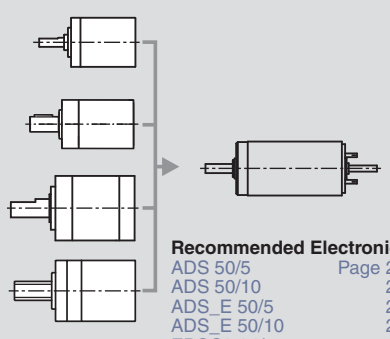

Recommended Electronics:

ADS 50/5	Page 282
ADS 50/10	283
ADS_E 50/5	283
ADS_E 50/10	283
EPOS2 24/5	305
EPOS2 50/5	305
EPOS2 P 24/5	308
Notes	**18**

Encoder MR
256 - 1024 CPT,
3 channels
Page 263

Encoder HED_ 5540
500 CPT,
3 channels
Page 266 / 268

DC-Tacho DCT
∅22 mm
0.52 V
Page 276

Brake AB 28
24 VDC
0.4 Nm
Page 318

10734 REF. NO: MPCL CAT. P64

REVISION					
C.O.N	SYM	DESCRIPTION	DATE	DRAWN	APPR'D
	A	1) ±0.2% ADDED.	8/19/04	TSUGAWA	

GENERAL:

MODEL CPP-35B IS 36.5mm(1.44")O.D., 6mm(0.236")DIA. SHAFT PRECISION CONDUCTIVE PLASTIC POTENTIOMETER. ITS SUPERB QUALITY, RELIABILITY AND PERFORMANCE MAKE CPP-35B SUITABLE FOR PRECISION POSITION SENSING APPLICATIONS.

ELECTRICAL SPECIFICATIONS:

ELECTRICAL ANGLE:	340°
TOTAL RESISTANCE:	0.5, 1, 2, 5, 10K OHMS
TOTAL RESISTANCE TOLERANCE:	±20%
LINEARITY (INDEPENDENT):	±1% (±0.15%, ±0.2% AVAILABLE) (A1)
REPEATABILITY:	0.003%
POWER RATING:	2 WATTS @70°C
INSULATION RESISTANCE:	100 meg OHMS MIN. @ 1,000 Vdc
DIELECTRIC STRENGTH:	1,000 Vrms @50/60 Hz for 1 MINUTE

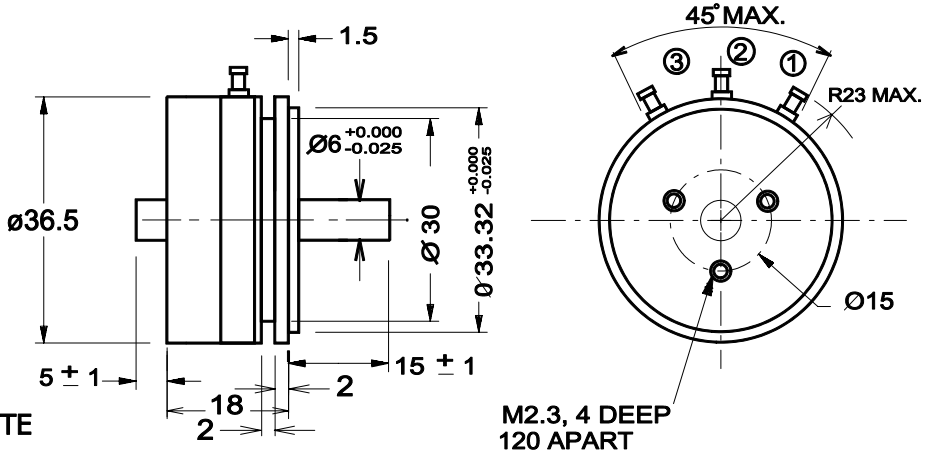

FIGURE 1 OUTLINE DIMENSION

MECHANICAL SPECIFICATIONS:

MECHANICAL ANGLE:	360°
TORQUE:	14 g-cm MAX. (0.2 oz-in MAX.)
WEIGHT:	APPROX. 40 g (1.4 oz)
LIFE:	10 MILLION CYCLES MIN.
GANGING:	UP TO 6 SECTIONS

ENVIRONMENTAL SPECIFICATIONS:

OPERATING TEMPERATURE:	-40°C to +120°C
VIBRATIONS:	15 Gs, 2,000 Hz
SHOCK:	50Gs, 11 mS

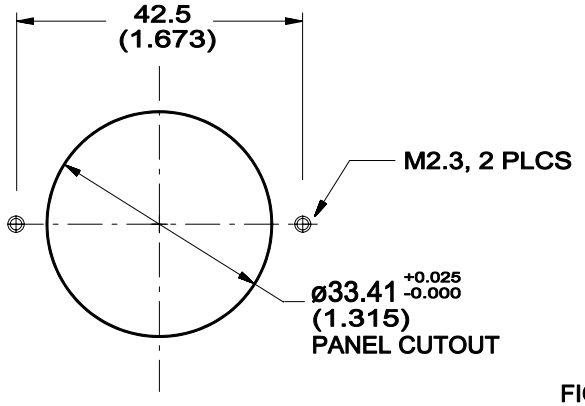

FIGURE 2 MOUNTING DIMENSION

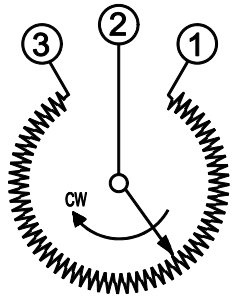

FIGURE 3 WIRING DIAGRAM

UNLESS OTHERWISE SPECIFIED,DIMENSIONS ARE IN mm(In). TOLERANCES: ANGLES ±1.5° <10 mm: ±0.25 <100 mm: ±0.5 >100 mm: ±1	DRAWN T.TSUGAWA	DATE 5/25/94	SPECIFICATION DWG FOR MODEL CPP-35B POTENTIOMETER	Midori America Corporation FULLERTON, CA
	CHECKED	DATE		
	APPROVED	DATE		
	APPROVED	DATE		A-MAC-B45 A
	SCALE:		FILE: CPP-35B	1 OF 1

CD1037

DIMENSIONS ARE INCHES / MILLIMETERS

Pull : Red Wire (+) Black Wire (-)

Release : Red Wire (-) Black Wire (+)

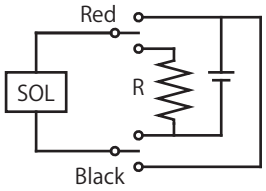

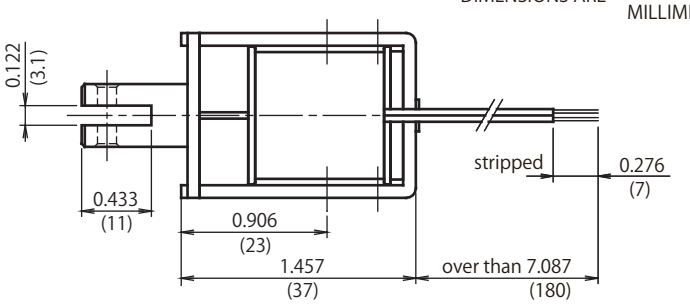

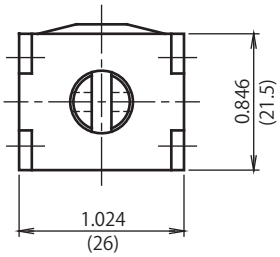

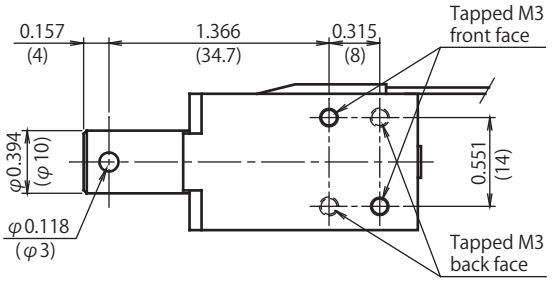

Adsorbed position

Duty Cycle

Insulation Class A 105℃(221ºF)

Part Number	Coil Resistance	Rated DC6V	Rated DC12V	Rated DC24V
CD10370120	12 Ohms	100%	25%	6%
CD10370190	19 Ohms		40%	10%
CD10370480	48 Ohms	-	100%	25%
CD10370960	96 Ohms	-	-	50%

Holding force (N)
16.0

Graph Release power consumption - load

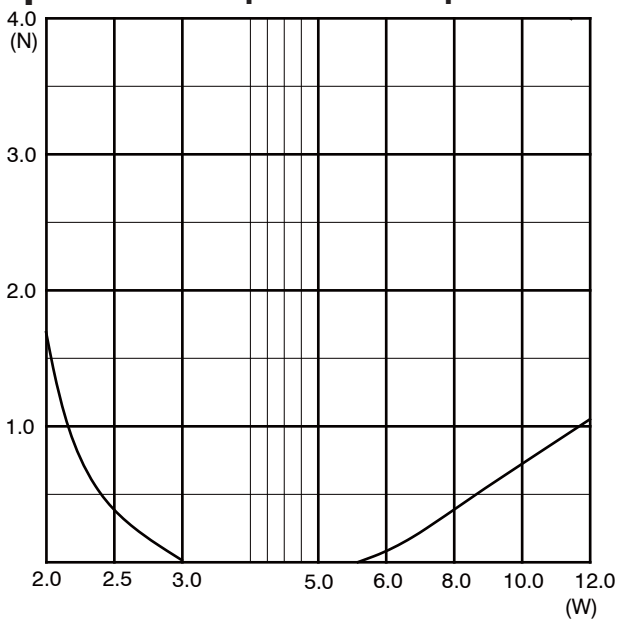

Graph Force - Stroke

DC24V 20℃(68ºF)